

**ENGINEERING STUDY OF
VAPOR CYCLE COOLING EQUIPMENT FOR ZERO-GRAVITY
ENVIRONMENT**

EDITED BY KYMUS GINWALA

NORTHERN RESEARCH AND ENGINEERING CORPORATION

JANUARY 1961

**FLIGHT ACCESSORIES LABORATORY
CONTRACT No. AF 33(616)-6783
PROJECT No. 0(15-6146)
TASK No. 60998**

**WRIGHT AIR DEVELOPMENT DIVISION
AIR RESEARCH AND DEVELOPMENT COMMAND
UNITED STATES AIR FORCE
WRIGHT-PATTERSON AIR FORCE BASE, OHIO**

Contrails

FOREWORD

This report contains the findings and conclusions of the work entitled, "Engineering Study of a Vapor Cycle for Zero-Gravity Environment" which was performed for the Wright Air Development Division* by the Northern Research and Engineering Corporation of Cambridge, Massachusetts. The project was under the administration of the Environmental Control Branch of the Aeronautical Accessories Laboratory, under Contract No. AF 33(616)-6783, Project No. O(15-6146), Task No. 60998. The study, which lasted from October 1, 1959 to August 31, 1960, was conducted by Messrs. Thomas Blatt, Kymus Ginwala, Willem Jansen, Ghassan Khabbaz, and Seymour Shenkman, with Kymus Ginwala acting as Project Engineer. The authors are indebted to Professor R. J. Nickerson for his assistance in the condensation studies.

The authors would like to thank Lt. T. D. Moseley, who administered the program initially, and Lt. N. P. Jeffries, the subsequent project administrator, for their cooperation.

*Presently designated Aeronautical Systems Division

Contrails

ABSTRACT

This report discusses the results of an analytical and experimental study of space vehicle vapor cycle cooling systems operating in a zero-gravity environment. The evaporator temperature varies from 40 degrees F to 55 degrees F, and the condenser temperature varies between 150 degrees F and 250 degrees F; the evaporator cooling load varies from 400 BTU/min to 4000 BTU/min. The ultimate heat dissipation is by radiation to space. The study considers some of the problems encountered in the operation of a vapor cycle in a zero-gravity environment and presents solutions to these problems. Emphasis has been placed on the vapor-liquid separation problems in evaporation and condensation.

The vortex evaporator is presented as a solution to the zero-gravity evaporation problem. Its volume is less than that of a conventional plate-fin evaporator operating under a one-g environment, but its weight is greater. The spiral condenser is presented as a solution to the zero-g condenser problem; its volume is several times larger than the smallest tube-fin unit (operating at one-g) for the same conditions. An analysis for and design of a rotating condenser is also shown. Wick materials are well suited to zero-gravity evaporators. The experimental work conducted in this study must be extended before any reliable design and construction of a wick evaporator is possible. Film condensation under zero gravity in the laminar region is also analyzed. For vapor cycles operating at large differences in condenser and evaporator temperature, the substitution of an expansion engine for the throttle valve results in a significant improvement in the cycle performance.

PUBLICATION REVIEW

The publication of this report does not constitute approval by the Air Force of the findings or conclusions contained herein. It is published only for the exchange and stimulation of ideas.

FOR THE COMMANDER:


WILLIAM C. SAVAGE
Chief, Environmental Branch
Flight Accessories Laboratory

Contrails

TABLE OF CONTENTS

Section		Page
I	Introduction	1
II	Thermodynamic Selection of Refrigerant	9
III	Vapor-Liquid Separation Study	29
IV	Vapor-Liquid Separator Study	31
V	Vortex Evaporator Study	37
VI	Rotating Condenser Study	83
VII	Spiral Condenser Study	107
VIII	Film Condensation Under Zero Gravity	127
IX	Expander Study	143
X	Wick Materials Study	155
XI	Compressor Study	187
XII	Conclusions and Recommendations	193
	Appendices	
	1. Evaporator Design Methods and Calculations	197
	2. Design Methods and Calculation Procedures for the Rotating Condenser	209
	3. Design Procedure and Sample Calculation for Spiral Condensers	225
	4. Derivation of Equations for Film Condensation Under Zero Gravity	241
	5. Minimum Condensation Heat Transfer Coefficient Analysis	247

Contrails

LIST OF ILLUSTRATIONS

Figure		Page
1	Schematic of Vapor Cycle	5
2	Temperature-Entropy and Pressure-Enthalpy Diagrams for Ideal Vapor Cycles	6
3	Temperature-Entropy and Pressure-Enthalpy Diagrams for Actual Vapor Cycles	7
4	Diagrams for Vapor Cycle with Superheater-Subcooler	8
5	Coefficient of Performance of Freon Refrigerants	18
6	Refrigeration Effect per Unit Volume for Freon Refrigerants	19
7	Ratio of Condenser Pressure to Evaporator Pressure for Freon Refrigerants	20
8	Freon 11 Centrifugal Compressor Minimum Speed for Specific Speed of 0.06	21
9	Freon 113 Centrifugal Compressor Minimum Speed for Specific Speed of 0.06	22
10	Schematic of Vapor Cycle with Separators	34
11	Vapor-Liquid Separator	35
12	Regimes of Boiling	69
13	Comparison of Volumes of Freon 11 Plate Fin, Vortex Tube and Plain Fin-Tube Evaporators	70
14	Comparison of Volumes of Freon 11 Plate Fin, Vortex Tube and Plain Fin-Tube Evaporators	71
15	Comparison of Volumes of Freon 11 Plate Fin, Vortex Tube and Plain Fin-Tube Evaporators	72
16	Comparison of Volumes of Freon 11 Plate Fin, Vortex Tube and Plain Fin-Tube Evaporators	73
17	Comparison of Volumes of Freon 11 Plate Fin, Vortex Tube and Plain Fin-Tube Evaporators	74
18	Comparison of Volumes of Freon 11 Plate Fin, Vortex Tube and Plain Fin-Tube Evaporators	75
19	Comparison of Volumes of Freon 11 Plate Fin, Vortex Tube and Plain Fin-Tube Evaporators	76
20	Comparison of Volumes of Freon 11 Plate Fin, Vortex Tube and Plain Fin-Tube Evaporators	77
21	Comparison of Volumes of Freon 11 Plate Fin, Vortex Tube and Plain Fin-Tube Evaporators	78
22	Comparison of Weights of Freon 11 Plate Fin, Vortex Tube and Plain Fin-Tube Evaporators	79

Contrails

LIST OF ILLUSTRATIONS

Figure		Page
23	Comparison of Weights of Freon 11 Plate Fin, Vortex Tube and Plain Fin-Tube Evaporators	80
24	Comparison of Weights of Freon 11 Plate Fin, Vortex Tube and Plain Fin-Tube Evaporators	81
25	Rotating Condenser	98
26	Flow Diagram	99
27	Rotating Condenser - Gap Design	100
28	Rotating Condenser Configuration	100
29	Rotating Condenser Configuration	100
30	Condenser System Dead Weight vs. Number of Discs (Condenser Angular Velocity and System Capacity are the Parameters)	101
31	Condenser System Dead Weight vs. Number of Discs (Condenser Angular Velocity and Evaporation Temperature are the Parameters)	102
32	Condenser System Dead Weight vs. Number of Discs (Condenser Angular Velocity and Condensation Temperatures are the Parameters)	103
33	Total Power Requirement vs. Number of Discs (Condenser Angular Velocity and System Capacity are the Parameters)	104
34	Total Power Requirement vs. Number of Discs (Condenser Angular Velocity and Evaporation Temperature are the Parameters)	105
35	Total Power Requirement vs. Number of Discs (Condenser Angular Velocity and Condensation Temperature are the Parameters)	106
36	Diagram of a Spiral Condenser (Fluids in Counterflow)	121
37	Volumes of Small Freon 11 Tube-Fin Condensers Operating at One-G	122
38	Comparison of Volumes of Freon 11 Spiral Condenser (Zero-G) with Large Tube-Fin Condensers (One-G)	123
39	Volume and Pressure Drop for Freon 11 Spiral Condenser	124
40	Variation of Freon 11 Spiral Condenser Volume and Pressure with NaK-Side Hydraulic Diameter	125
41	Condensate Velocity Distribution	140
42	Wetted-Wall Tube Friction Factor Data of Bergelin, Kegel, Carpenter, and Gazley	141
43	Plot of Numerical Results	142
44	Constant-Enthalpy Expansion vs. Constant-Entropy Expansion in a Vapor Cycle	150

Contrails

LIST OF ILLUSTRATIONS

Figure		Page
45	Effect of Replacing the Isenthalpic Process by an Isentropic Process in a Vapor Cycle	151
46	Coefficient of Performance of Vapor Cycle with Separate Expander and Heat Exchanger	152
47	Coefficient of Performance of Vapor Cycle vs. Heat Exchanger Effectiveness	153
48	Liquid Rise in Wick Materials as a Function of Time	172
49	Rate of Weight Decrease of Soaked Wick Materials as a Function of Time (Continuous Liquid Supply Through Bottom of the Specimens by Capillary Action Only)	173
50	Rate of Weight Decrease of Soaked Wick Materials as a Function of Time (No Liquid Supply to the Specimens)	174
51	Schematic of Apparatus to Test Capillary Flow	175
52	Flow Through Capillary Tube	176
53	Flow in Capillary Tubes	177
54	Schematic of Apparatus to Test Capillary Flow in Wick Materials	178
55	Decrease of Flow Rate with Time (Silica Batt)	179
56	Decrease of Flow Rate with Time (Silica Batt)	180
57	Decrease of Flow Rate with Time (cellulose Sponge)	181
58	Decrease of Flow Rate with Time (Am. Felt Co. No. 7544)	182
59	Decrease of Flow Rate with Time (Am. Felt Co. No. 7545)	183
60	Decrease of Flow Rate with Time (Am. Felt Co. No. 7546)	184
61	Actual Flow Rate Drop in Wick Materials	185
62	Schematic of Wick Heat Exchanger (Reference 7)	186

Contrails

LIST OF TABLES

Table		Page
1	Refrigerant Properties	15
2	Physical Properties of Suitable Refrigerants	16
3	Summary of Properties of Selected Refrigerants	17
4	Range of Optimum Specific Speeds	17
5	Surface Tension of Liquids (Against Air)	29
6	Design Characteristics of Plate-Fin Evaporators	66
7	Design Characteristics of Vortex Evaporators	67
8	Freon 11 Side Pressure Drop in Evaporators	68
9	Minimum Ratios for Condensing-Side to Radiating-Side Heat Transfer Coefficients for Integral Radiator-Condensers . .	117
10	Design Characteristics of Small Tube-Fin Condensers	118
11	Design Characteristics of Large Tube-Fin Condensers	119
12	Total Volume and NaK Pressure Drop For Counterflow Spiral Condensers	120
13	Expander Study - Summary of Numerical Results	147
14	Vapor Cycle System with Expansion Machine Increase in COP with Varying Expander Efficiencies	148
15	Vapor Cycle with Throttle Valve and Superheater Increase of COP with Varying Superheater Effectiveness	149
16	Physical Properties and Absorption Characteristics of Wick Materials	168
17	Physical Properties and Absorption Characteristics of Wick Materials	169
18	Physical Data for Capillary Flow Wick Material Specimens	171
19	Film Condensation Under Zero Gravity - Summary of Numerical Results	245

Contrails

SECTION I

INTRODUCTION

From the standpoint of environmental control systems, earth satellites and space vehicles differ from aircraft in several important aspects. One of the more significant factors is the almost continuous gravity-absent environment in which the former vehicles and their associated equipment must operate. Although aircraft may encounter a reduced-gravity or a zero-gravity environment, this condition is, at most, a transient one, allowance for which may be made either in the control system of the affected equipment or by some simple equipment modification. In space vehicles and satellites, however, the zero-gravity environment is a permanent condition which requires the redesign of equipment which would be affected adversely by this environment.

In any given space vehicle system, the environmental control problem is defined accurately. Proper atmosphere control, pressurization and temperature levels must be maintained to ensure the specified performance of the equipment and the inhabitants which are on board the vehicle. For a vehicle mission of any extended duration, dissipation of heat by radiation to space appears to be the most feasible method of maintaining the temperature levels within the vehicle. For such extended-duration missions, vapor cycles in conjunction with radiant heat sinks appear to offer many advantages (such as low system weight and power requirements) over other heat pumps.

However, as indicated above, a major problem in the application of vapor cycle systems to the conditioning of a space vehicle is the absence of the gravity force field. In the design of a conventional vapor cycle (that is, one operating within the gravity field), certain body forces are of primary importance to the mechanisms which take place in the vapor cycle--such as evaporation, boiling, and condensation. Normally these body forces are neglected, since, up to the present time, vapor cycles have always operated in the presence of the gravity field. The absence of the gravity field and, consequently, of the body forces associated with gravity affects the design and operation of a vapor cycle in two ways: first, through the heat transfer mechanisms which depend on the forces; and second, through the specific design features in the cycle which use the effects of buoyancy and hydrostatic pressure. The satisfactory operation of a vapor cycle in a gravity-absent field requires an understanding and analysis of the specific effects of these body forces on the design and operation of the cycle, allowance for the absence of the body forces, and specific new design concepts which will overcome these problems. A major difficulty in the undertaking is the inability to simulate the zero-gravity environment in the laboratory for a length of time which would enable a study of the effect of the absent body forces in the steady-state condition.

Manuscript released by the author 23 January 1961 for publication as a WADD Technical Report.

VAPOR CYCLE COOLING SYSTEMS - GENERAL CONSIDERATIONS

A vapor cycle cooling system consists mainly of components whose function is to cool some fluid outside the system by heat exchange with a primary fluid which is the refrigerant. The refrigerant circulates through the components of the vapor cycle, but does not leave the cycle which is a closed system. A schematic of a simple vapor cycle is presented in Figure 1, and the thermodynamic processes occurring within an ideal cycle are shown on the temperature-entropy diagram in Figure 2(a) and on the pressure-enthalpy diagram in Figure 2(b).

The liquid refrigerant is evaporated (1-2) at essentially constant temperature and pressure and removes heat from the fluid to be cooled. The saturated refrigerant vapor is then compressed isentropically (2-3) to the high side condenser pressure. Condensation of the vapor takes place (3-4) at the higher pressure; heat dissipation may occur either directly by radiation or indirectly by a heat transport fluid and then by radiation. The saturated refrigerant liquid leaving the condenser is then expanded isenthalpically (4-1) through a throttle valve from condenser (high) to evaporator (low) pressure, and the process continues.

The Carnot cycle is the most efficient cooling cycle attainable, and differs from the ideal vapor cycle described above in two steps—condensation and expansion, which are isothermal and isentropic in a Carnot cycle, and are shown by dotted lines in Figure 2. The coefficient of performance (COP) of a Carnot cycle is given by

$$\text{COP}_{\text{Carnot}} = \frac{T_E}{T_C - T_E}$$

and is a function of the evaporator and condenser temperatures only, and is not dependent on the thermodynamic properties of the refrigerant. In order to convert the ideal vapor cycle into a Carnot cycle, isentropic compression of a vapor-liquid mixture is necessary so that saturated and not superheated vapor enters the compressor. The condensation process then becomes both isothermal and isobaric. In addition, the constant enthalpy expansion process is made isentropic, and the work output of the expander is used to reduce the work of compression. Wet compression, however, is not feasible since it may cause severe erosion in the compressor; isentropic expansion with work utilization presents some difficulties, but is not an insurmountable problem.

An actual vapor cycle differs from an ideal vapor cycle due to friction losses in lines and components. Figure 3 shows some of these losses in an actual vapor cycle. The vapor leaving the evaporator is usually superheated to ensure that no liquid enters the compressor. In an actual vapor cycle, the refrigerant must enter the evaporator at a higher pressure than that in an ideal cycle to allow for the pressure drop in the evaporator; this increases the evaporator size. The pressure loss in the suction line of the compressor increases the compressor size. Compressor discharge pressure must be slightly higher than for an ideal cycle to allow for the discharge line pressure drop. The most important factor which reduces the COP of an actual cycle is the compression process which is nonisentropic for an actual cycle.

Contrails

Many variations are possible with practical vapor cycles. For example, the vapor leaving the evaporator is usually superheated to some extent to prevent liquid intake into the compressor and to operate the constant-superheat expansion valve.* The superheat may be obtained in the evaporator or in a separate heat exchanger which may be used to subcool the condenser discharge in order to ensure only liquid intake into the throttle valve, and to increase the cooling effect obtained in the evaporator. Figures 4(a), 4(b), and 4(c) show a schematic, a temperature-entropy, and a pressure-enthalpy diagram respectively for a vapor cycle with a superheater-subcooler.

Another variation is to subcool the major portion of the high-pressure condenser exit stream with a small portion of the same stream which has been expanded through a throttle valve, evaporated in the subcooler, and then fed either to the first or some intermediate stage of the compressor.

Where the difference between evaporator and condenser temperatures is very large, compound cycles with multi-stage compression are necessary. As with simple cycles, many variations with these cycles, such as intercooling, subcooling, and superheating, are possible.

SCOPE OF THE RESEARCH PROGRAM

The purpose of this study was to investigate the design characteristics and operation performance and reliability of a vapor cycle environmental cooling system using a radiant heat sink in a zero-gravity environment. For this study the following parameters were specified:

Evaporator temperature: from 40 deg F to 55 deg F

Condenser temperature: from 150 deg F to 250 deg F

Cooling capacity: from 400 BTU/min to 4000 BTU/min

The purpose of the program was to study analytically the effects of zero gravity on the performance and reliability of the various components and to determine how and what components would be adversely affected. The affected components would then be investigated further to establish design methods or operating techniques which would solve or circumvent the zero gravity-problem. The designs for the new components would be compared to conventional vapor cycle component designs on the basis of minimum component or system volume, weight and power, and for ease of testing to ensure performance and reliability under zero-gravity conditions. Where the above criteria were insufficient, new criteria would be developed for comparison of zero-gravity and conventional systems and components.

Wicking materials were to be considered for use in both the evaporator and condenser where liquid feed and liquid removal, respectively, were possible problems. Simple laboratory experiments were to be conducted where necessary.

*This valve is a refrigerant flow control, metering the correct refrigerant into the evaporator, according to demand.

Contrails

The research program was divided into the following major sections, some of which were divided into several studies:

1. Literature Survey
2. Selection of Refrigerant
3. Investigation of Potential Vapor-Liquid Separation Techniques
4. Investigation of Potential Compressors
5. Heat Exchanger Studies
6. Expander Studies
7. Vapor Cycle Component and System Comparisons

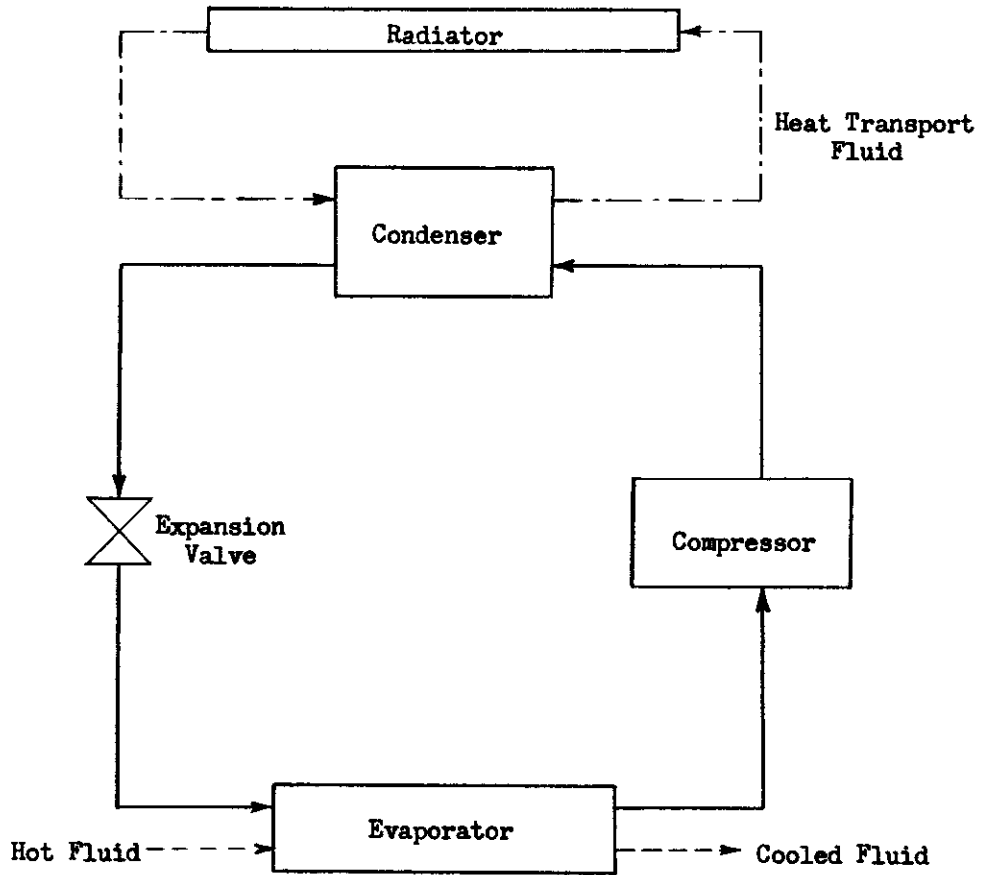


FIGURE 1: SCHEMATIC OF VAPOR CYCLE

Contrails

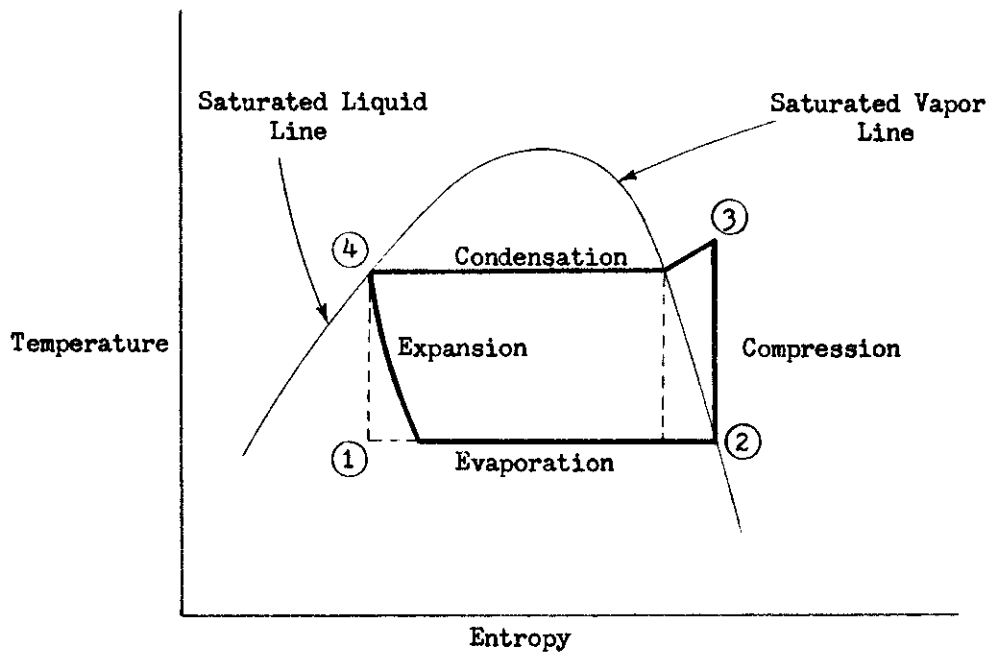


Figure 2 (a)

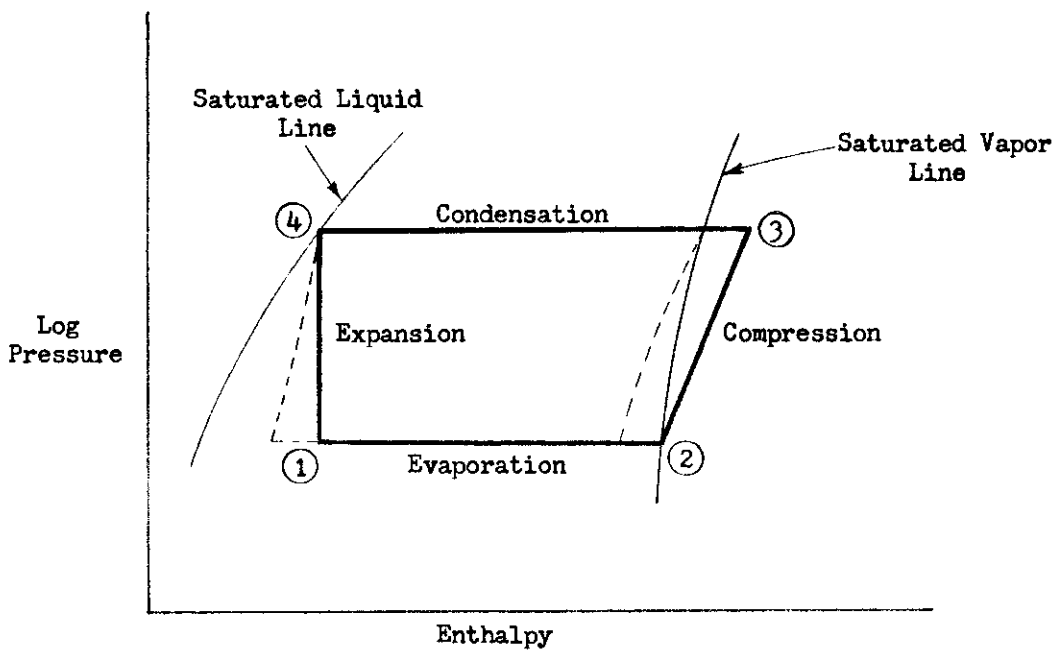


Figure 2 (b)

FIGURE 2: TEMPERATURE-ENTROPY AND PRESSURE-ENTHALPY DIAGRAMS FOR IDEAL VAPOR CYCLES

Contrails

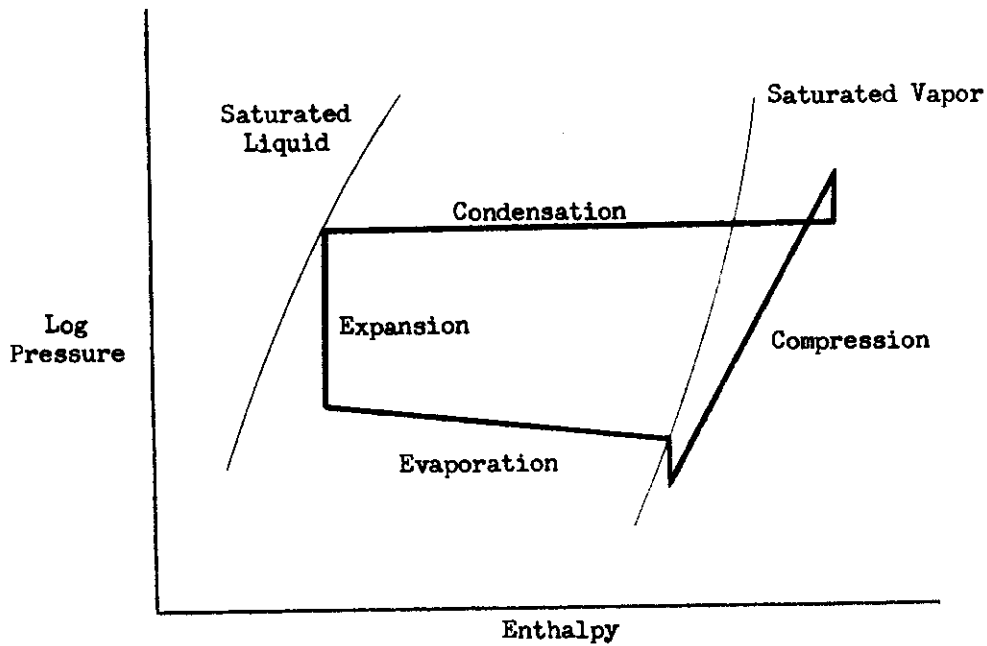
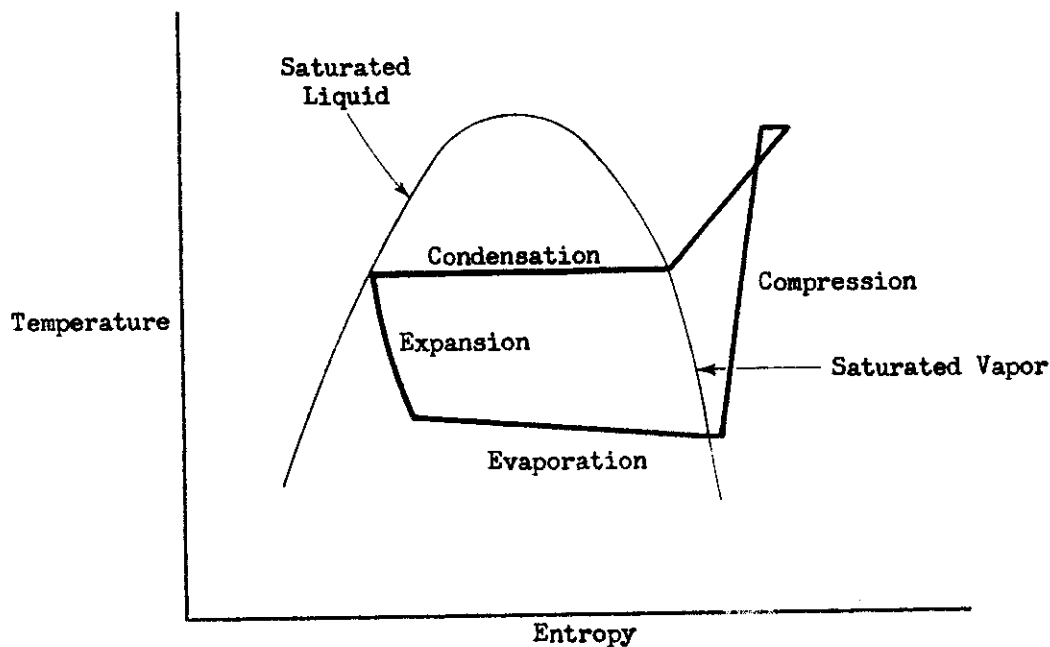


FIGURE 3: TEMPERATURE-ENTROPY AND PRESSURE-ENTHALPY DIAGRAMS FOR ACTUAL VAPOR CYCLES

Contrails

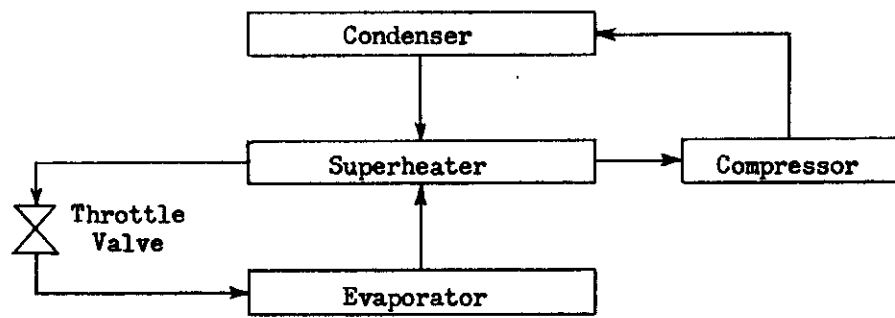


Figure 4 (a)

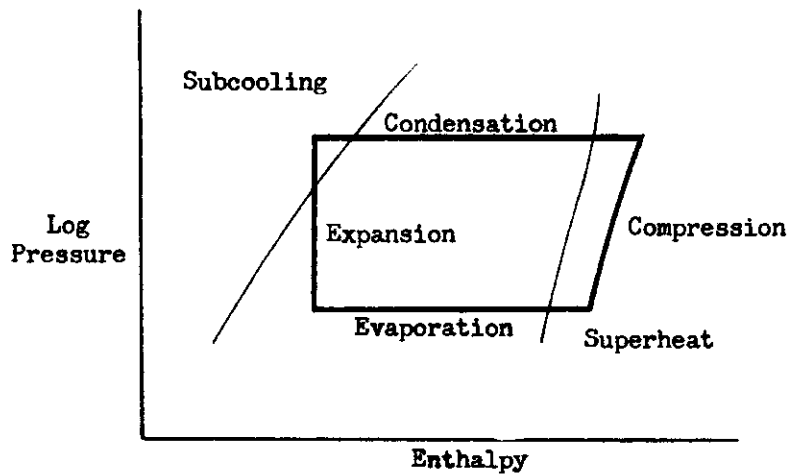
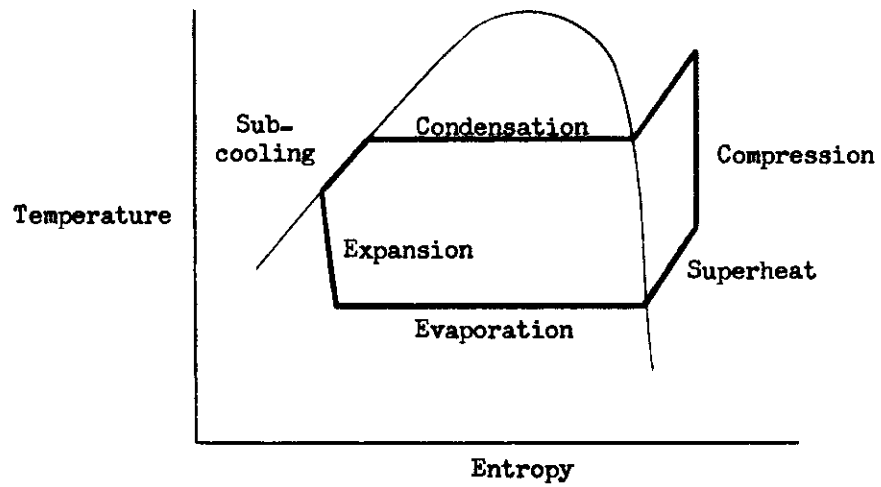


FIGURE 4: DIAGRAMS FOR VAPOR CYCLE WITH SUPERHEATER-SUBCOOLER

SECTION II

THERMODYNAMIC SELECTION OF REFRIGERANT

Several factors must be considered for the selection of an optimum refrigerant. For a vapor cycle operating in a conventional gravity environment, two sets of criteria are important. The first set depends upon the thermodynamic properties of the refrigerant which influence the quantitative behaviour of the vapor cycle. The second set of factors, such as corrosion and toxicity, is qualitative. For a vapor cycle operating in a zero-gravity environment, it is necessary to consider additional properties which may be of primary or moderate importance when body forces become negligible. However, this would entail postponement of the refrigerant selection until the most satisfactory method of vapor-liquid separation had been chosen. A preliminary examination revealed that it was unlikely that refrigerant selection would be measurable altered by the imposition of the zero-gravity condition. However, a detailed investigation of vapor-liquid separation techniques was initiated and is reported in Section III. The study reported in this section was concerned only with the thermodynamic selection of a refrigerant with the understanding that this selection might be influenced by the method of vapor-liquid separation.

An optimum refrigerant was to be selected for an evaporator temperature range of 40 to 55 degrees F, a condenser temperature range of 150 to 250 degrees F, and a cooling capacity of 400 to 4000 BTU/min. Over thirty refrigerants were selected on the basis of past experience for the initial screening process in order to eliminate those which were not of immediate value to the study. Table 1 lists the group of refrigerants with their critical values, and maximum and minimum table values. The following criteria are important for the thermodynamic selection of a refrigerant:

1. Freezing point
2. Boiling point
3. Critical temperature
4. Critical pressure
5. Evaporator pressure, P_E , at evaporator temperature, T_E
6. Condenser pressure, P_C , at condenser temperature, T_C
7. Specific volume of refrigerant at evaporator temperature
8. The coefficient of performance for the refrigerant
9. The evaporator cooling effect per unit volume of refrigerant entering the evaporator
10. The ratio of refrigerant vapor pressures in the condenser and evaporator

Contrails

Properties 1 through 4 are usually used in the initial screening process to eliminate those refrigerants which have no applicability in the given range of evaporator and condenser temperatures. In addition to the thermodynamic properties above, there is a set of qualitative properties whose importance in the selection of a refrigerant varies with the particular application. These properties are toxicity, flammability, and corrosiveness. Toxicity is an important criterion for a space vehicle vapor cycle refrigerant.

A large number of refrigerants were eliminated initially due to parameters such as critical temperature, evaporator vapor pressure, toxicity, flammability, and condenser vapor pressure. The remaining refrigerants were Freon 11, Freon 21, Freon 113, Freon 114, and Carrene 1. The physical properties of these refrigerants are shown in Table 2. The thermodynamic data on Carrene 1 are insufficient to examine it for the entire range, but it is believed to offer no distinct advantages over the Freons. The initial comparison between the Freons was based on the coefficient of performance at the given evaporator and condenser temperatures, using a compressor efficiency of 60 per cent and an evaporator superheat of 20 degrees. The results of these calculations are shown in Figure 5. Freon 11 has the highest coefficient of performance at all the given evaporator and condenser temperatures, with Freon 21, Freon 113, and Freon 114 following it in that order. The coefficient of performance increases as the difference between the evaporator and condenser temperature decreases. The relatively low critical temperature of Freon 114 causes its COP to drop considerably at the higher condensation temperatures. The difference between the COP of Freon 11 and Freon 21 decreases with increasing condenser temperatures.

The refrigeration effect per unit compressor volume (Q/V_i) is an important criterion for the selection of a refrigerant. For reciprocating compressors, a high value of this parameter is desirable; for centrifugal compressors which are high displacement machines, a low value of (Q/V_i) is used to indicate a good refrigerant. Rotary compressors use an intermediate value for (Q/V_i). The parameter (Q/V_i) is influenced very strongly by the vapor pressure (P_E) of the refrigerant in the evaporator. Volatile refrigerants which have a high vapor pressure at any given evaporator temperature have a high (Q/V_i). In using (Q/V_i) as a parameter for refrigerant selection, other criteria must still be considered simultaneously. For example, the critical temperature which may be low for a refrigerant which has a high (Q/V_i) may eliminate a particular refrigerant. Another factor is the condenser pressure, which, if excessive, requires specially designed compressors and condensers to withstand high internal pressures and leakages. Figure 6 shows a plot of (Q/V_i) for Freon 11, Freon 21, Freon 113, and Freon 114 at the evaporator and condenser temperatures under consideration. Freon 11 and 113, which have relatively low values of (Q/V_i), are suitable for centrifugal compressors, while Freon 21 and 114 are suited to rotary compressors.

Figure 7 shows the ratio of condenser pressure to evaporator pressure, (P_C/P_E), at the condenser and evaporator temperatures respectively plotted as a function of evaporator temperature. Freon 11 and 113 have the highest pressure ratios between the required temperature limits. Unfortunately, low volatility, which causes low (Q/V_i) (a property desirable for centrifugal compressors), is a property which is mutually exclusive of low pressure ratios. Nevertheless, Freon 11 is used with centrifugal compressors in spite of its comparatively

high pressure ratios.

Some consideration should be given to the pressure drop per unit length of channel for a refrigerant. This may become particularly important in the case of a long suction line between evaporator and compressor. For a single-phase fluid in turbulent flow, the pressure drop per unit length is given by Reference 1:

$$\frac{\Delta P}{\Delta L} = \frac{K_1}{e} \left(\frac{W}{A} \right)^{1.8} = \frac{K_2}{e} \left(\frac{1}{Q_E A} \right)^{1.8} \quad (1)$$

Of the refrigerants being considered, Freon 21 has the smallest pressure drop, while Freon 113 has the highest. The single-phase pressure drop factor is not a significant criterion in the present refrigerant selection.

Pressure drop in evaporator flow which is two-phase in character is more difficult to calculate. However, effects of the pressure drop give some estimate of the tolerable limits with different refrigerants. A pressure drop of 1 psia in the evaporator will reduce the boiling point by about 13 degrees F for Freon 113, by about 7 degrees F for Freon 11, by 3.5 degrees F for Freon 21, and by 3 degrees F for Freon 114. Hence, in actual evaporator design, for each 1 psia pressure drop in the evaporator, a 40 degree F discharge saturation temperature at the evaporator exit would require an evaporator inlet temperature which is higher by the difference given above for each refrigerant. Hence, for a given evaporator condition, heat transfer design will result in either larger evaporator sizes or lower allowable pressure drops for refrigerants for which $(\Delta T/\Delta P)$ is large.

Table 3 summarizes some of the criteria that have been mentioned previously for an evaporator temperature of 40 degrees F and a condenser temperature of 250 degrees F. For each property, the refrigerants are listed in order of decreasing desirability. Freon 11 has the highest coefficient of performance, and is preferred over Freon 113 which has the lowest (Q/V_i) , and also has an intolerable (P_C/P_E) . Freon 11 is thus the optimum refrigerant if a centrifugal compressor can be used for the entire cooling capacity range. A discussion of this subject follows later.

The Freon refrigerants may normally be contained in aluminum, provided no water is present. In a vapor cycle such as the one currently under investigation, there is little possibility for water being present in the Freons. As long as the Freons are not subjected to temperatures above 750 degrees F they are quite nontoxic. At high temperatures, decomposition occurs, leading to the poisonous gases hydrogen fluoride, hydrogen chloride, and phosgene. The Freon refrigerants are also nonflammable.

It has been stated earlier that Freon 11 appears to be the optimum refrigerant for this application if a centrifugal compressor may be used over the entire range of temperature and cooling capacity conditions. The concept of specific speed is useful in determining the application of the various types of compressors to a given problem. The specific speed may be expressed as

Contrails

$$N_s = \frac{N \sqrt{V}}{(g H_{ad})^{0.75}} = \frac{N \sqrt{V}}{6270 (H_{ad})^{0.75}} \quad (2)$$

Table 4, reproduced from Reference 1, shows the range of optimum specific speeds for the different compressor types. The limits of specific speeds for a centrifugal compressor are shown to be 0.06 - 0.2. The specific speed is shown as a range which encompasses the specific speed at the best efficiency. Although operation outside the range 0.06 - 0.2 is possible, the limits do define the range of good operating efficiencies. Figure 8 shows the centrifugal compressor speeds necessary to obtain for Freon 11 a specific speed of 0.06 as a function of evaporator load for the four extremes of temperature conditions. The minimum compressor speed is that associated with the stage which has the largest rpm value, since for the pressure ratio considered here multi-stage units are essential. For equal adiabatic heads, the speed of the last stage is the largest; since all stages rotate with this speed, it would be possible to recalculate the resultant specific speeds and efficiencies for the individual stages.

Figure 8 indicates the extremely high speeds required of a centrifugal compressor at the lower capacities. It is believed that the highest compressor speed which has been attained so far (and this is for a unit which is under development for the DC-8 commercial aircraft) is about 89,500 rpm. Therefore, even if a centrifugal compressor speed of 80,000 rpm were currently attainable (30,000 rpm has been considered practical until recently), the lower limit of applicability of Freon 11 would have to be set at a capacity of 7.5 tons (1500 BTU/min). Freon 21 would require even higher speeds than Freon 11 if it were used with a centrifugal compressor. A calculation similar to the one above for Freon 11 has been performed for Freon 113. The results are shown in Figure 9. The compressor speeds are significantly lower than those for Freon 11. With Freon 113, the lower limit for capacity (at 80,000 rpm) is now extended to 2.5 tons (500 BTU/min). Since Freon 21 is the only remaining refrigerant, it would appear to be the only refrigerant to use in the lower range of capacity in conjunction with a rotary compressor.

In summary, Freon 11 is the optimum refrigerant for a system capacity of 1600 BTU/min and above, using a centrifugal compressor. However, compressor speeds up to 80,000 rpm are required at a capacity of 1500 BTU/min. Such a compressor for Freon 11 is not yet available. A centrifugal compressor using Freon 12 and operating at 89,500 rpm has been designed and tested by the Carrier Corporation. This unit has a burst speed of 150,000 rpm.

At the smaller capacities for the current problem, Freon 21 and a rotary compressor may be used. It is also possible to use Freon 113 and a centrifugal compressor at the lower capacities; however the low COP of this refrigerant and the excessive pressure drop in the evaporator do not justify its use.

Contrails

LIST OF SYMBOLS

A	sq ft	Area
COP		Coefficient of performance
H_{ad}	BTU/lb	Adiabatic head for compression
N_S		Specific speed
N	rpm	Shaft speed
P_C	psia	Refrigerant vapor pressure in condenser
P_E	psia	Refrigerant vapor pressure in evaporator
$\frac{\Delta P}{\Delta L}$	psia/ft	Pressure drop per unit length
Q_E	BTU/lb	Cooling effect in evaporator
Q/V_i	BTU/cu ft	Cooling effect per unit volume of refrigerant at compressor inlet
$\frac{\Delta T}{\Delta P}$	degF/psia	Temperature drop per unit pressure drop
W	lbs/min	Weight flow of refrigerant
V	cu ft/min	Volumetric flow rate

Contrails

REFERENCES

1. Mason, J. L., Burriss, W. L., and Connolly, T. J., Vapor Cycle Cooling for Aircraft, WADC Technical Report 53-338, October 1953
2. Mason, J. L., Whitnah, G. R., and Larson, E. M., Study of Vapor-Cycle Refrigerants for High Performance Aircraft, WADC Technical Report 56-93, February 1958
3. Robinson, W. and Zimmerman, R. H., Equipment Cooling Systems for Aircraft, WADC Technical Report 54-359, Parts 1, 2, and 3, September 1954
4. Larson, V. H., Equipment Cooling Systems for Aircraft, WADC Technical Report 56-353, January 1958
5. E. I. Du Pont de Nemours and Company, Bulletins on Freon Refrigerants

TABLE 1

REFRIGERANT PROPERTIES

Refrigerant	Freezing Point (degF @ 14.7 psia)	Critical Temp (degF)	Critical Press (psia)	Minimum Table Values		Maximum Table Values	
				Sat Liquid Temp (degF)	Sat Liquid Press (psia)	Sat Vapor Temp (degF)	Sat Vapor Press (psia)
Mercury		3002	51400	220.0	0.007	1390.0	1100
Water	32	705.4	3206	32.0	0.09	705.4	3206.2
Carbon Tet.	-9.4	541	661	unstable at high temperatures			
Ethyl Ether		522.1	380.8				
Trichlorethylene		520.0	728.0				
Dichlorethylene		470.0	795.0				
Methylene Chloride	-142	421.0	670.0	10.0	1.38	140.0	26.79
Methyl Formate	-147.5	418.0	607.0	0.0	1.50	140.0	38.41
Freon 113	-31	417.4	495.0	-30.0	0.30	200.0	54.66
Freon 11	-168	388.4	635.0	-40.0	0.74	388.4	635.0
Ethyl Chloride		369.0	764.0				
Ethylamine	-115	362.0	815.0	-58.0	0.35	113.0	41.49
Freon 21	-211	353.3	750.0	-40.0	1.36	160.0	100.6
Sulfur Dioxide	-98	314.8	1141.5	-40.0	3.14	140.0	158.6
Methylamine	-134	314.0	1082.0	-58.0	1.32	113.0	98.76
Butane	-211	306.0	550.1	-30.0	3.4	180.0	160.0
Freon 114	-137	294.3	474.0	-80.0	0.46	140.0	84.8
Methyl Chloride	-153	289.4	969.0	-80.0	1.95	170.0	283.9
Isobutane	-229	272.7	537.0	-20.0	7.50	180.0	210.0
Ammonia	-107.9	271.2	1651.0	-107.8	0.88	180.0	307.8
Freon 12	-247	232.7	582.1	-155.0	0.12	125.0	582.1
Carrene 7	-247	221.1	631.0	-40.0	10.84	232.7	263.5
Freon 22	-256	204.8	716.0	-155.0	0.20	160.0	448.0
Propane	-310	202.0	661.5	-75.0	6.37	140.0	305.0
Propylene	-301	196.5	667.2	-50.0	16.0	90.0	195.0
Nitrous Oxide	-152	96.5	1050.0	-127.0	14.7	96.5	1050.0
Ethane	-278	90.1	708.3	-148.0	7.62	90.1	708.3
Carbon Dioxide	-109	87.8	1071.0	-147.0	2.14	87.8	1071.0
Freon 13	-296	83.8	579.0	-200.0	0.43	83.8	579.0
Ethylene	-272	48.8	731.8	-176.8	6.75	48.8	731.8
Freon 14	-312	-49.9	542.4	-250.0	1.1	-49.9	542.4
Methane	-297	-115.8	673.0	-260.0	15.0	-115.8	673.0
Air	-221	547.0					

TABLE 2

PHYSICAL PROPERTIES OF SUITABLE REFRIGERANTS

	FREON 11	FREON 21	FREON 113	FREON 114	CARRENE 1
Chemical Formula	C Cl ₃ F	C H Cl ₂ F	C Cl ₂ F - C Cl F ₂	C Cl F ₂ - C Cl F ₂	C H ₂ Cl ₂
Molecular Weight	137.38	102.93	187.39	170.93	84.93
Boiling Point - degF	74.78	48.06	117.63	38.39	105.2
Freezing Point - degF	-168	-211	-31	-137	-142
Critical Temperature - degF	388.4	353.3	417.4	294.3	480
Critical Pressure - psia	635	750	495	474	670
Critical Volume - cu ft/lb	0.0289	0.0307	0.0278	0.0275	
Specific Heat of Liquid (86 degF) BTU/lb-degF	0.209	0.256	0.218	0.238	
Specific Heat of Vapor (1 atm, 86 degF) BTU/lb-degF	0.135	0.140	0.161	0.160	
Specific Heat Ratio (1 atm, 86 degF)	1.136	1.175	1.080	1.088	
Density of Liquid (86 degF) lbs/cu ft	91.38	84.52	96.96	89.91	
Density of Vapor (saturated at boiling pt) lbs/cu ft	0.365	0.285	0.461	0.488	
Heat of Vaporization (at boiling pt) BTU/lb	78.31	104.15	63.12	59.00	
Thermal Conductivity of Liquid (86 degF) BTU/hr-degF-ft	0.0609	0.0697	0.0521	0.0447	
Thermal Conductivity of Vapor (1 atm) BTU/hr-degF-ft	0.00484	0.00569	0.00450	0.00646	
Viscosity of Liquid - centipoise	0.405	0.330	0.619	0.356	
Viscosity of Vapor (1 atm) centipoise	0.0111	0.0116	0.0104	0.0117	
Surface Tension (77 degF) dynes/cm	19	19	19	13	
Flammability	None	None	None	None	None
Toxicity*	5A	less than group 4 more than group 5	less than group 4 more than group 5	None	4A

* Underwriter's Laboratories: Group 1 - very toxic
 Group 6 - no evident toxicity
 Group 4A - between 4 and 5
 Group 5A - less toxic than 4, but more toxic than 6

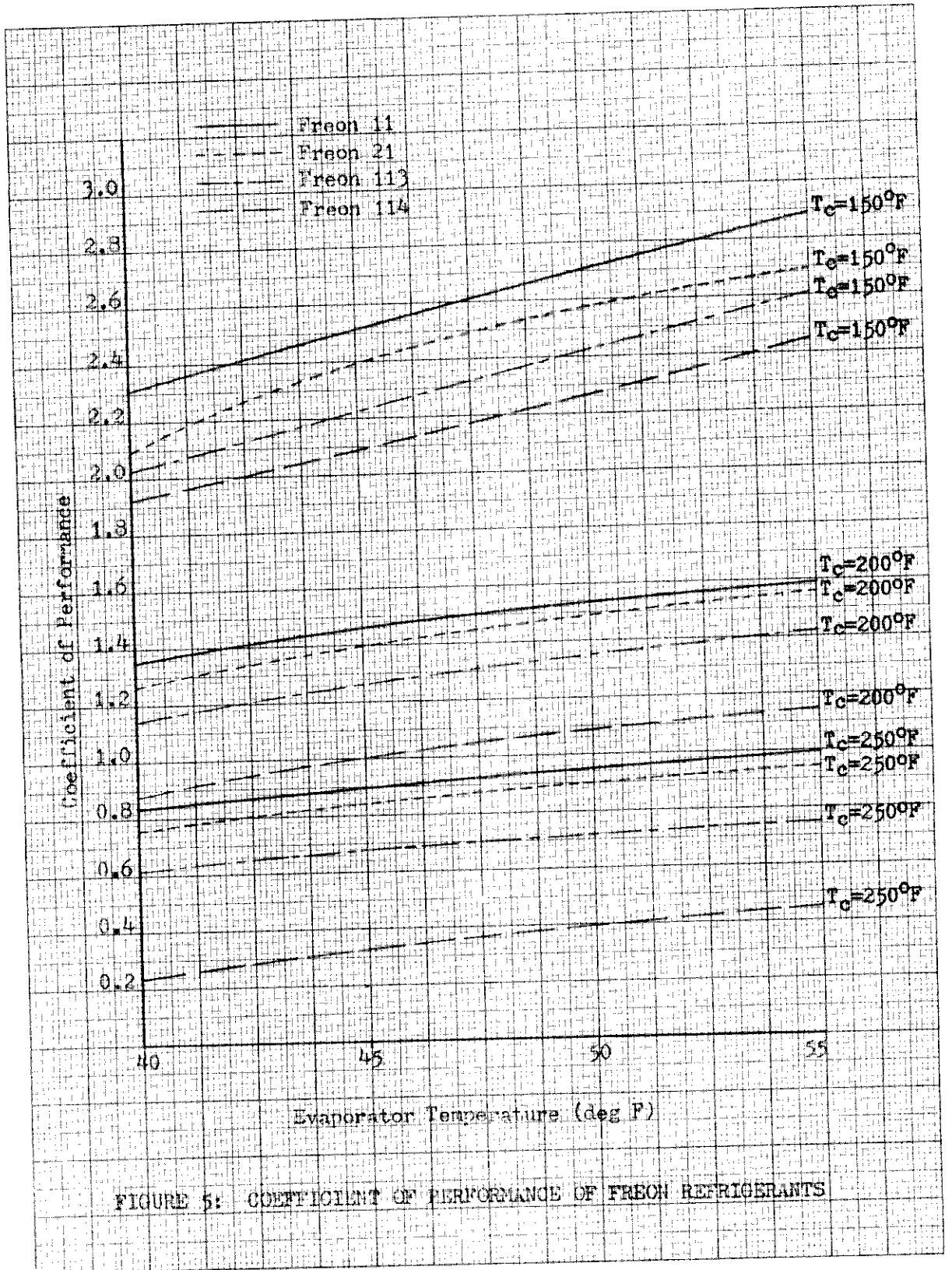
TABLE 3
SUMMARY OF PROPERTIES OF SELECTED REFRIGERANTS

Evaporator Temperature = 40 deg F
Condenser Temperature = 250 deg F

Coefficient of Performance COP		Q/V_i	P_C/P_E		P_C	Evaporator $\Delta T/\Delta P$			
F-11	0.85	F-113	2.06	F-114	20.4	F-113	102	F-114	3
F-21	0.77	F-114	4.15	F-21	23.2	F-11	182	F-21	3.5
F-113	0.63	F-11	6.7	F-11	26	F-21	295	F-11	6
F-114	0.28	F-21	11.1	F-113	38.5	F-114	310	F-113	13

TABLE 4
RANGE OF OPTIMUM SPECIFIC SPEEDS

Type of Compressor	Maximum N_S	Minimum N_S
Axial	1.0	0.3
Mixed Flow	0.3	0.2
Centrifugal	0.2	0.06
Rotary	0.005	0.002
Reciprocating	0.005	0.0001



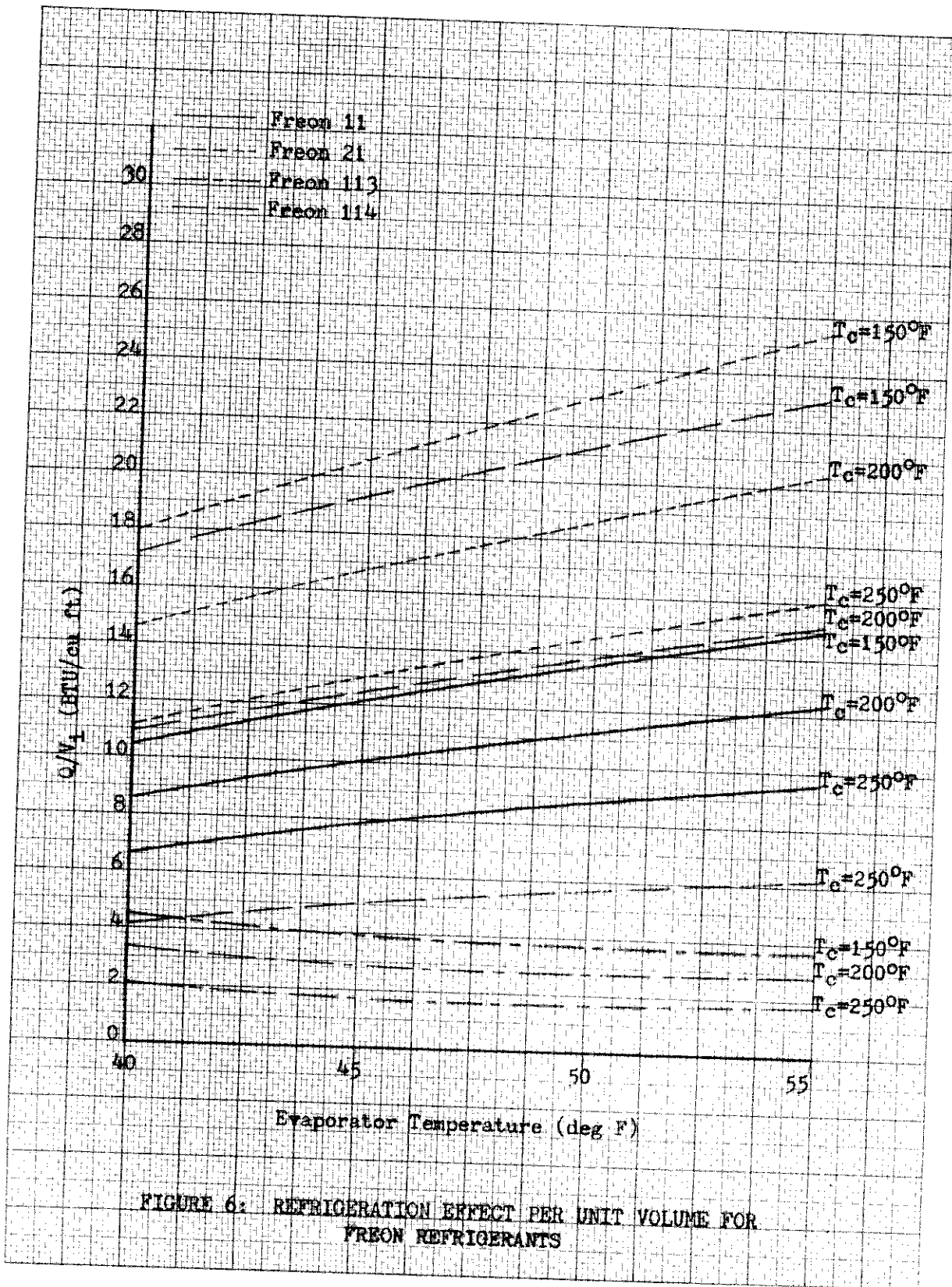


FIGURE 6: REFRIGERATION EFFECT PER UNIT VOLUME FOR FREON REFRIGERANTS

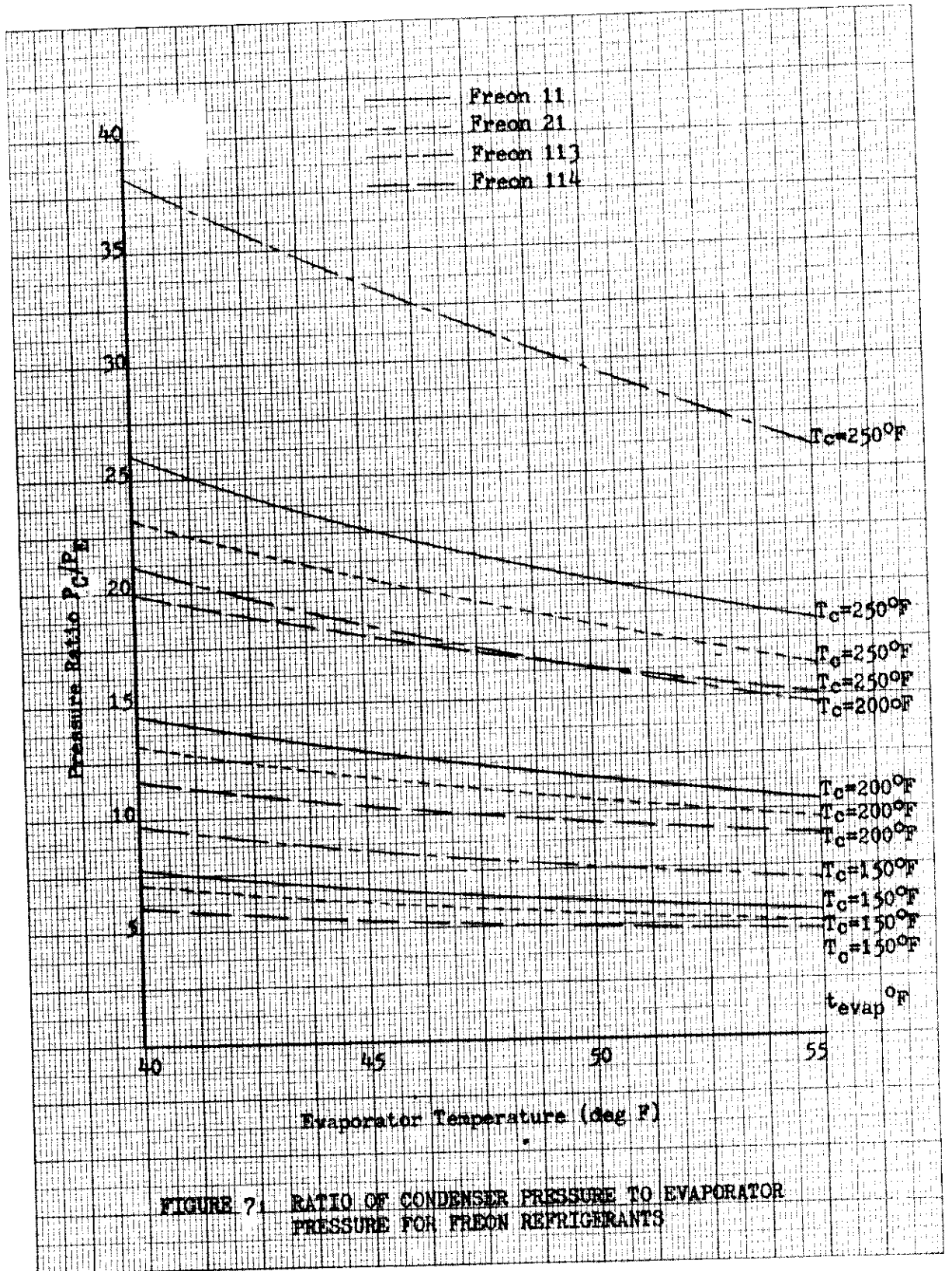


FIGURE 7. RATIO OF CONDENSER PRESSURE TO EVAPORATOR PRESSURE FOR FREON REFRIGERANTS

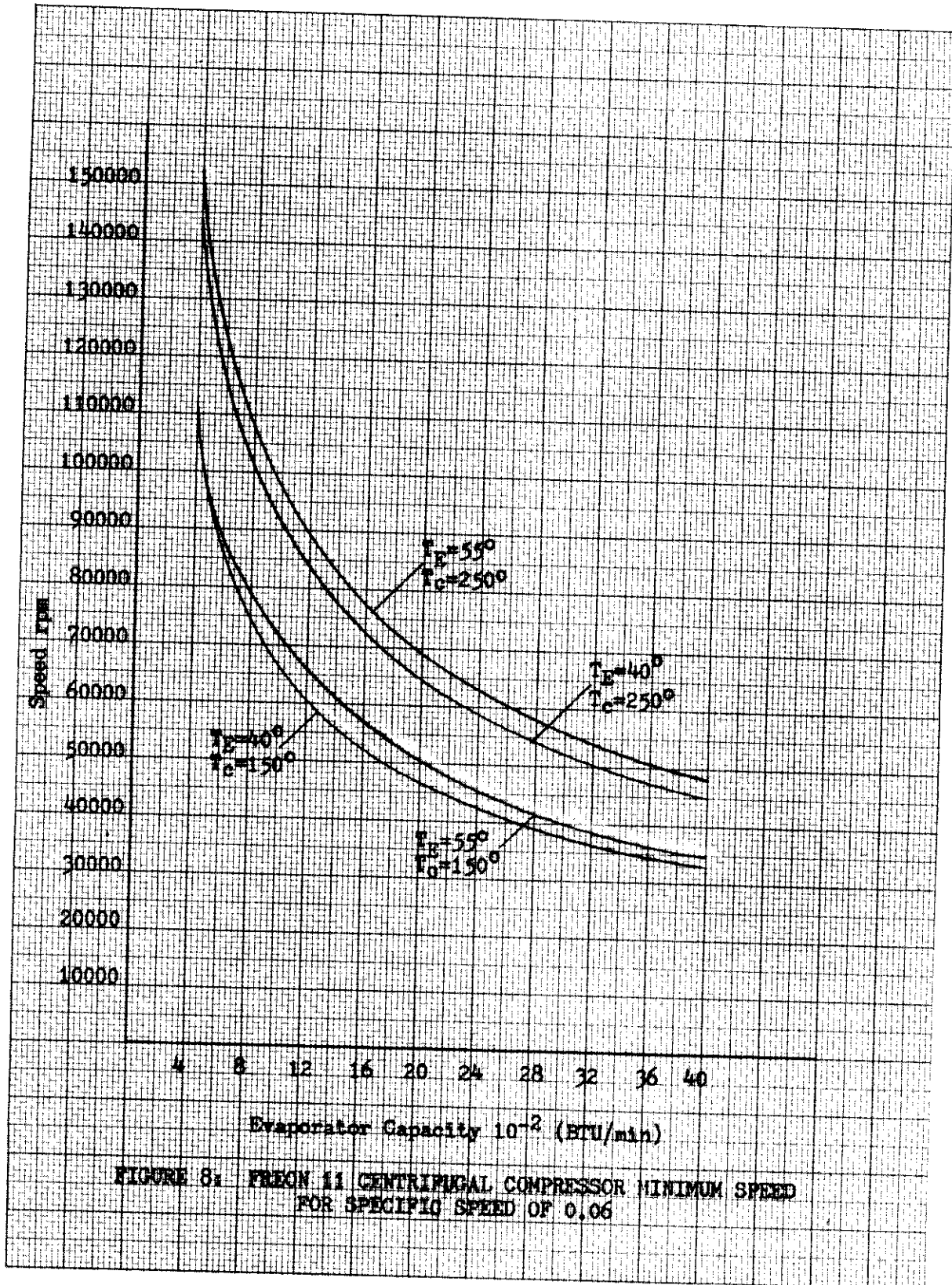


FIGURE 8: FREON 11 CENTRIFUGAL COMPRESSOR MINIMUM SPEED FOR SPECIFIC SPEED OF 0.06

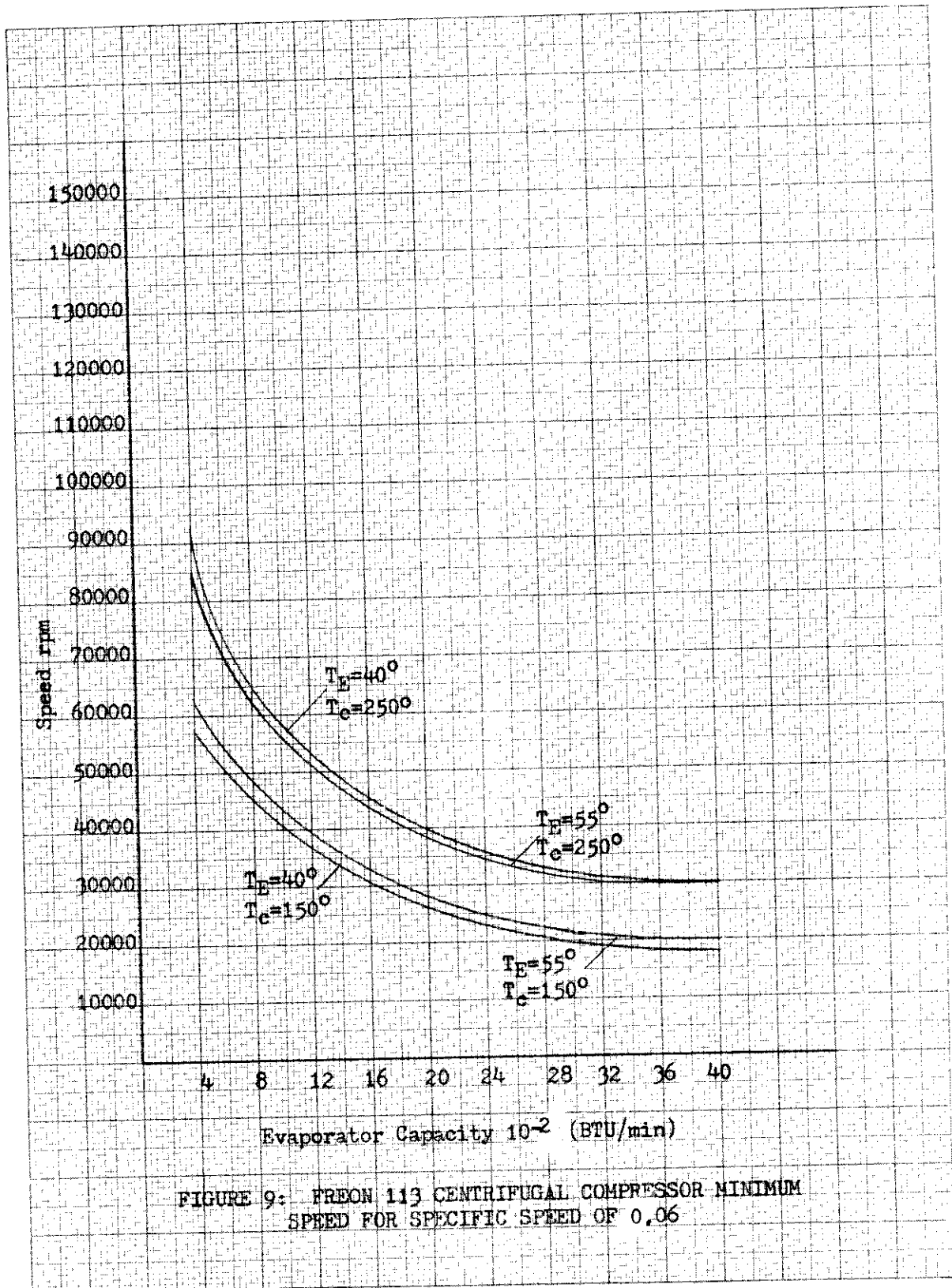


FIGURE 9: FREON 113 CENTRIFUGAL COMPRESSOR MINIMUM SPEED FOR SPECIFIC SPEED OF 0.06

SECTION III

VAPOR-LIQUID SEPARATION STUDY

In a vapor-liquid separation problem within a gravity field, the conditions of equilibrium, in the simplest case, take into account the forces of gravity and hydrostatic pressure acting on a fluid particle. For a fluid at rest in a gravity field, the weight per unit volume may be denoted by $\gamma = \rho g$; the gravitational acceleration is a vector of constant magnitude, and acts downward. For a fluid mixture of vapor and liquid, liquid and liquid, or vapor and vapor, separation or stratification may occur in a gravity field if the weight densities of the constituents of the mixture are different. In a zero-gravity field, however, potential differences due to the effect of gravity on density, on hydrostatic pressure, and on buoyancy are absent, and a bubble or a vapor pocket in a liquid medium will not migrate unless some force is imposed on it. The object of the vapor-liquid separation study was to examine the fundamental properties of fluids to determine what forces and fields other than those due to gravity could be utilized for separation.

Although it was immediately obvious that several fluid properties which are different in the vapor and liquid states are available for the separation problem, it was felt that it would be more valuable initially to examine all fluid properties to determine their applicability to the problem. The first step was to list all properties of fluids (not specific refrigerants) regardless of their applicability to the vapor-liquid separation problem. These properties included both physical, chemical, and other properties which may be used to define the state of a fluid. The properties were defined, and the differences in these properties for the vapor and liquid states were noted. Properties which had no such differences were eliminated, as were properties where the magnitude of the basic research effort to develop a feasible separation method was beyond the scope of this program. The remaining properties were then studied in detail to determine concepts and methods based on these properties.

A large number of properties were studied. These were:

PHYSICAL PROPERTIES

- Pressure
- Temperature
- Internal Energy
- Enthalpy
- Entropy
- Specific Heat
- Thermal Conductivity
- Thermal Diffusivity
- Critical Temperature
- Critical Pressure
- Freezing Point
- Boiling Point
- Latent Heats
- Coefficient of Thermal Expansion

Contrails

Compressibility
Absorptivity
Transmissivity
Reflectivity
Emissivity
Coefficient of Diffusion
Density
Viscosity

SURFACE PROPERTIES

Surface Tension
Capillary Constant
Spreading Coefficient
Contact Angle
Surface Adsorptivity

OPTICAL PROPERTIES

Optical Activity
Verdet Constant
Coefficient of Dispersion
Electrical Birefringence
Magnetic Birefringence

ACOUSTIC PROPERTIES

Acoustic Density

ELECTRICAL AND MAGNETIC PROPERTIES

Electrical Conductivity
Dielectric Constant
Magnetic Permeability
Magnetic Susceptibility

An initial study immediately eliminated a majority of the properties, leaving the following to be studied further:

Density
Viscosity
Surface Tension
Diffusion Coefficients
Magnetic Susceptibility

In any vapor-liquid separation problem, density difference between the two phases is the simple property by which the separation is effected, provided some potential field is exerted on the system. When the gravity field is absent or when its effects have been cancelled out by other forces, the potential field must be supplied by some artificial means. One method of supplying such a field is to rotate the equipment in which the separation is to be performed. However, in space vehicle systems where reliability is a primary criterion by

Contrails

which systems are compared, rotating machinery, particularly machinery for which there is no great backlog of operating experience, may not represent the most acceptable solution. Fluid transfer from a stationary component to a rotating unit and then to another stationary or rotating unit always presents a sealing problem. A more feasible solution is to generate the potential field within the fluid itself without actual rotation or movement of the equipment which handles the field.

The first method has been applied to the rotating condenser, while the second has been applied to the vortex evaporator and the spiral condenser.

The viscosity of a vapor is usually much smaller than that of the corresponding liquid phase; the difference between the two, however, has not been utilized in conventional separation methods where the density difference is always available even when the two phases are stationary. Although the viscosity difference itself is not utilized in this study, the straight-pipe condensation study does use the absolute viscosity of the vapor to form a continuous liquid condensate film.

When a fluid system is acted upon by a normal gravity field, the tendency in calculation and experimental work is to neglect those forces which, compared to that due to the gravity field, are relatively small. One such group of forces is that of cohesion and adhesion which results in the mutual attraction and repulsion between different or like molecules of the fluids and their containers. Many of the phenomena associated with the surfaces of fluids may be described by the proportionality constant which relates the work needed to create a fresh surface in the fluid to the amount of fresh surface created. The proportionality constant is called the surface tension, and may be expressed by

$$dW = \sigma dA$$

For a system to be in stable equilibrium, its potential energy must be at a minimum. Under this condition, a liquid which is not acted upon by any direct force on its surface (e.g., a free liquid droplet) will tend to assume an equilibrium state where its surface area is a minimum. Since, for any given volume, a sphere has minimum surface area, a free liquid droplet assumes this shape. When gravitational forces are absent, therefore, one would assume that the relative magnitude of surface forces may no longer be neglected. That this is true is amply demonstrated by the fact that in a zero-gravity environment a fluid such as water (whose adhesive forces are greater than its cohesive forces) will tend to wet the entire surface area of the container, while one such as mercury (where the cohesive-adhesive force relationship is reversed) will tend to form a sphere in the container. The magnitude of some representative surface tension forces is shown in Table 5. Since surface tension and its effects are not dependent on gravity, it is obvious that these forces may be utilized in a zero-gravity environment.

Another property of liquid surfaces which may be utilized in vapor-liquid separation is that of the pressure differential across curved liquid surfaces. The pressure on the concave side of a curved liquid side is greater than that on the convex side. The pressure P_i on the concave side of a spherical surface, in relation to the pressure P_o on the convex side may be expressed

Contrails

as

$$P_i = P_o + \frac{2\sigma}{R} \quad (3)$$

For a cylindrical surface, the relation is

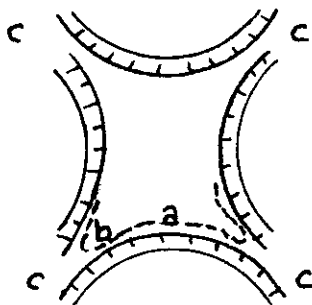
$$P_i = P_o + \frac{\sigma}{R} \quad (4)$$

so that the pressure differential is only half of that across a spherical surface having the same radius. For any arbitrary curved surface, the relation between the pressures on the concave and convex side is

$$P_i - P_o = \sigma \left(\frac{1}{R_1} + \frac{1}{R_2} \right) \quad (5)$$

where R_1 and R_2 are the principal radii of curvature.

Several ideas were evolved where the surface forces may be used for the separation of liquid and vapor. One such scheme for condensation is shown below.



A drop of vapor condensing at point (a) will migrate towards point (b), since the pressure on the concave side of the liquid film at (a) and (b) will be greater than that on the convex side. This pressure differential should cause migration of the condensate from (a) to (b) where it would collect and be drawn off at (c) into another pipe surrounding the actual condenser surface. Another surface effect which may be used is the capillary effect. In boiling or evaporation under zero gravity, the liquid may be fed by a series of straight capillary tubes or by some fibrous wick material (which simulates a collection of capillary tubes of varying lengths and diameters) onto the heat transfer area and the vapor led away by some suitable means. The capillary feed is independent of gravity, and is therefore operable in the zero-gravity condition. Wick materials may also be used for condensate collection in the condenser, but the removal of the liquid from the wick is more difficult.

Some thought was given to diffusion processes as a means of separation. However, molecular diffusion processes are inherently slow, and therefore do not seem applicable to the current problem.

Contrails

Separation of a vapor from a liquid, or vice versa, by electric or magnetic means holds some attraction for any zero-gravity power or refrigeration cycle, if the weight of the accessory equipment necessary to generate the required field is not prohibitive. In order to conveniently apply an electromagnetic force to a fluid which is to be transported, the fluid must be capable of conducting electricity or possess a sufficient magnetic moment. A particle possessing some magnetic moment may be attracted by a magnetic field, depending on the magnetic susceptibility of the substance. However, for most organic substances, including the refrigerant, the susceptibilities are so small that extremely large fields would be required to transport such fluids. It is obvious that for most of the common refrigerants which are nonconducting and possess very small magnetic susceptibilities, electromagnetic separation is not feasible. Another possibility which was investigated was the addition of agents to the refrigerants which would increase the magnetic susceptibilities of the solutions. For example, small quantities of metals such as sodium, potassium, and cesium may be dissolved in a refrigerant such as ammonia. With current applied to the solution, larger forces may be generated.

Electric fields may also be used for fluid transport when the fluids are conductive. Here again, the common refrigerant would have to be rendered conductive by the addition of metallic agents. Unfortunately, in many of these cases and those cited above, the solutions are not stable for indefinite periods; the solution of sodium in ammonia, when contained in a sealed system, is reported to be stable for about eight weeks.

It is believed that electromagnetic separation processes are not feasible for the zero-gravity vapor-liquid separation. When solutions are boiled or condensed, fractionation occurs whereby the vapor generated does not have the same composition as the solution, unless the solution is an azeotrope. In addition, even though one has a conducting fluid, the interactions of an electromagnetic field with a two-phase mixture are difficult to ascertain without a detailed experimental investigation. In this connection, some thought was given to the conduct of a pool boiling experiment in a conducting fluid, where electromagnetic forces equal and opposite to the gravity forces would be applied to simulate the zero-gravity effect. There are several obstacles to such a scheme. For example, since the current tends to flow mainly at the surface, it is not clear what the force distribution will be, particularly during the agitation due to boiling. The distribution of the current in the liquid-bubble mixture and the induced effect of the electrons on bubble formation are other phenomena which are not clearly understood.

In summary, density, viscosity, and surface tension appear to be the most promising properties available for immediate solutions to the vapor-liquid separation problem in zero gravity. Methods using the natural or induced electromagnetic properties of substances, or those based on the behaviour of two-phase fluids under acoustic disturbances are not believed to be feasible in the light of current knowledge.

Contrails

REFERENCES

ELECTRICAL PROPERTIES OF "FREON" REFRIGERANTS

1. Pollock, H. D. and Cooper, F. S., "Dielectric Strength," Phys. Rev., vol. 56, 1939, pp. 170-175
2. Charleton and Cooper, General Electric Review, September 1937, pp. 438-442
3. Fuoss, R. M., "Dielectric Constant," J.A.C.S., vol. 60, 1938, pp. 1633-1637
4. Thornton, N. V., Burg, A. B., and Schlesinger, H. I., "Decomposition by Electric Discharge," J.A.C.S., vol. 55, 1933, p. 3177
5. Baker, R. F. and Tate, J. T., Phys. Rev., vol. 53, 1938, p. 683
6. Bonch-Bruevich, A. M., Glikina, M. V., and Hokhberg, B. J., Exptl. Theoret. Phys. (U.S.S.R.), vol. 10, 1940, p.171
7. Skilling, H. H. and Brenner, W. C., "Electrical Strength of Nitrogen and 'Freon' Under Pressure," Electrical Communications, vol. 20, No. 4, pp. 287-294, reprinted from A.I.E.E. Transactions, vol. 61, 1942, April Section
8. Trump, J. G., Safford, F. J., and Cloud, R. W., "D-C Breakdown Strength of Air and 'Freon' in a Uniform Field at High Pressures," Electrical Engineering, vol. 60, March 1941, pp. 132-135
9. Charleton, E. E. and Cooper, F. S., Dielectric Strength of Insulating Fluids, General Electric Research Laboratory, No. 945, January 1939 and No. 865, September 1917
10. Berberich, L. J., et al, Part I - Electrical Breakdown of Perfluorocarbon Vapors and Their Mixtures with Nitrogen, A.I.E.E., Transactions Paper No. 55-493
11. Beacham, E. A. and Divers, R. T., "Dielectric Properties of Refrigerants," Refrigeration Engineering, July 1955
12. Foord, T. R., "Some Experiments on Positive Point-to-Plane Corona and Spark Breakdown of Compressed Gases," The Proceedings of the Institution of Electrical Engineers, vol. 100, Part II, No. 78, December 1953

TABLE 5
SURFACE TENSION OF LIQUIDS (AGAINST AIR)

Liquid	σ (dynes/cm)
Benzene	28.9
Carbon Tetrachloride	26.8
Ethyl Alcohol	22.3
Mercury	465
Water	72.8
Freon 11	19
Freon 12	9
Freon 13B1	4
Freon 21	19
Freon 22	9
Freon 112	23
Freon 113	19
Freon 114	13

Contrails

SECTION IV

VAPOR-LIQUID SEPARATOR STUDY

In any equipment where mass and heat transfer processes occur between two phases, there is always a possibility of one phase entraining another in the exit passages of the equipment. This possibility is even greater in the operation of equipment handling two-phase fluids in the zero-gravity case. Specifically, in a vapor cycle, vapor leaving the evaporator may entrain liquid droplets which could damage the compressor; and liquid leaving the condenser may contain vapor pockets, a condition which would cause vapor lock in the throttle valve. Either situation is intolerable for the reliable operation of a vapor cycle, particularly in a space vehicle. Although there have been instances reported in the literature of compressors handling wet vapors, this is not a desirable operating condition. Throttle valves are designed for an entirely liquid stream at the entrance to the valve.

There are several general approaches to ensure that only vapor enters the compressor and only liquid enters the throttle valve:

1. A superheat section may be provided in the evaporator.
2. A subcooling section may be provided in the condenser.
3. A separate superheater-subcooler is included in the vapor cycle.
4. Vapor-liquid separators are employed after both the evaporator and the condenser.

The subject of this discussion is the use of vapor-liquid separators in a zero-gravity vapor cycle. The study does not consider detailed designs of such separators, since the emphasis has been placed on solving the vapor-liquid separation problem directly in the particular equipment where the problem occurs, e.g., the vortex evaporator. This section considers the problems of including separators in the vapor cycle system, and enumerates the types of separators which may be used.

In considering the application of any vapor-liquid separator for zero-gravity operation, the quantity of the undesired phase and its distribution in the main fluid stream must be known. In the case of the evaporator, the fraction of liquid in the exit vapor stream, the size of the liquid droplets, and their distribution in the vapor stream are variables about which very little may be determined until some zero-gravity experiments are performed. Assuming a constant fraction of liquid in the evaporator exit stream still presents the problem of recycling the separated liquid back into the system. If the separated liquid is not recycled directly into the main refrigerant stream, but to a refrigerant storage system, a sufficient quantity of refrigerant must then be added to the main refrigerant stream to make up the deficiency. In any event, this creates a control problem in the case of both the evaporator and condenser. In a realistic situation where the fraction of the undesired phase might vary, the control problem would be even more acute. In the case of the evaporator, an additional pump is required to circulate separated liquid refrigerant back into the

evaporator, and this creates an additional weight penalty on the system.

Problems similar to those outlined above occur in the case of the separator following the condenser. Assuming that any entrained bubbles may be successfully separated, the vapor may be recycled to several points in the system. These are: to the condenser entrance (pumping power is required), to an intermediate compressor stage, or to the evaporator exit. If separators must be included in the system, one possible configuration is shown in Figure 10. In this system, separators are employed after both the evaporator and the condenser. An intermediate heat exchanger is included where the main liquid stream from the condenser is used to evaporate the liquid droplets which have been separated from the vapor stream leaving the evaporator. The vapor separated from the condenser liquid may be mixed with the vapor stream leaving the heat exchanger to ensure that no liquid enters the compressor. Many different possibilities in this configuration may be realized depending upon the fractions of vapor and liquid separated and the pressure and temperature levels involved. However, it appears that the vapor-liquid separation problem is best solved in the respective heat exchangers involved; such a solution leads to a more reliable and lighter system than one which is complicated by the addition of separators.

TYPES OF SEPARATORS

There are many types of separators available for removing an entrained fluid phase from another phase. These will be discussed below briefly. All methods of separation are not equally applicable to both the separation of liquid droplets from vapor streams and vapor bubbles or pockets from liquid streams. In those cases where the same method might be applicable to both the separation problems, the design conditions would be quite different, depending on whether the main stream is vapor or liquid.

Centrifugal Separators

In this type of separator a centrifugal force field is used to separate the denser liquid from the vapor. However, in the gravity-dependent unit, the denser liquid collects on the wall and is drawn off by the force of gravity as in an ordinary cyclone. In a zero-gravity situation, however, the liquid on the walls of the collector will not be removed by gravity. In such a case, a sponge, wick, or mesh material is required to trap the liquid drops. The collected liquid must then be removed by capillary action, pressure differential or mechanical expression of the wick material. Centrifugal separators have the advantage of having no moving parts, and are usually effective for a wide range of particle diameters. One type of separator for a vapor stream with entrained liquid droplets is shown in Figure 11. A similar type is reportedly manufactured by the Stewart-Warner Corporation using a wick material known as Liquid Lock.

Electrostatic Separators

Electrostatic separators may be used in a zero-gravity situation, since these separators do not depend on gravity for effective operation. The liquid droplets are charged negatively and attracted to a positive electrode where they may be collected. However, gravity does play a part in the normal drainage of the collected liquid; some other force field must be provided in the zero-gravity

Contrails

case. Electrostatic units also have no moving parts, but are usually more suitable for liquid droplets less than 20 microns in diameter. These separators may also require a heavy power supply, a factor not in favor of their application to space vehicles. On the other hand, electrostatic separators require little pressure drop.

Acoustic Devices

Acoustic devices are not strictly separators, but are used to agglomerate very small particles into larger drops which may then be collected more effectively. Such devices also need accessory equipment for wave generation. They are effective on particle diameters below 20 microns, but require additional collection devices. Acoustic devices usually have high efficiencies and low pressure drops.

Impingement Separators

There are a variety of devices in this category ranging from simple baffles to porous metal tubes and wick materials. Most baffle-type arrangements are effective only for particle diameters above 15 to 20 microns. Wire cloth or metallic fiber meshes are usually effective for entrained liquid particles with diameters from 10 to 15 microns. Porous metal tubes are effective for particle diameters of 5 microns. Pressure drops for mesh materials are usually lower than those for porous metal tubes. For most impingement-type separation in normal operation, liquid removal is by gravity; in the gravity-absent case, liquid removal from a wick material must be accomplished by some other means, such as capillarity or squeezing.

There are no separators currently available which are directly applicable to the zero-gravity problem without some development effort. As indicated above, the application of separators to a zero-gravity vapor cycle raises a number of recycling and control problems, and may detract from the over-all reliability of the cycle. For the purpose of this study, it was concluded that the emphasis should be placed on solving the vapor-liquid separation directly in the heat transfer equipment involved; that is, to design the heat transfer equipment to ensure a single-phase fluid at the exit of the unit.

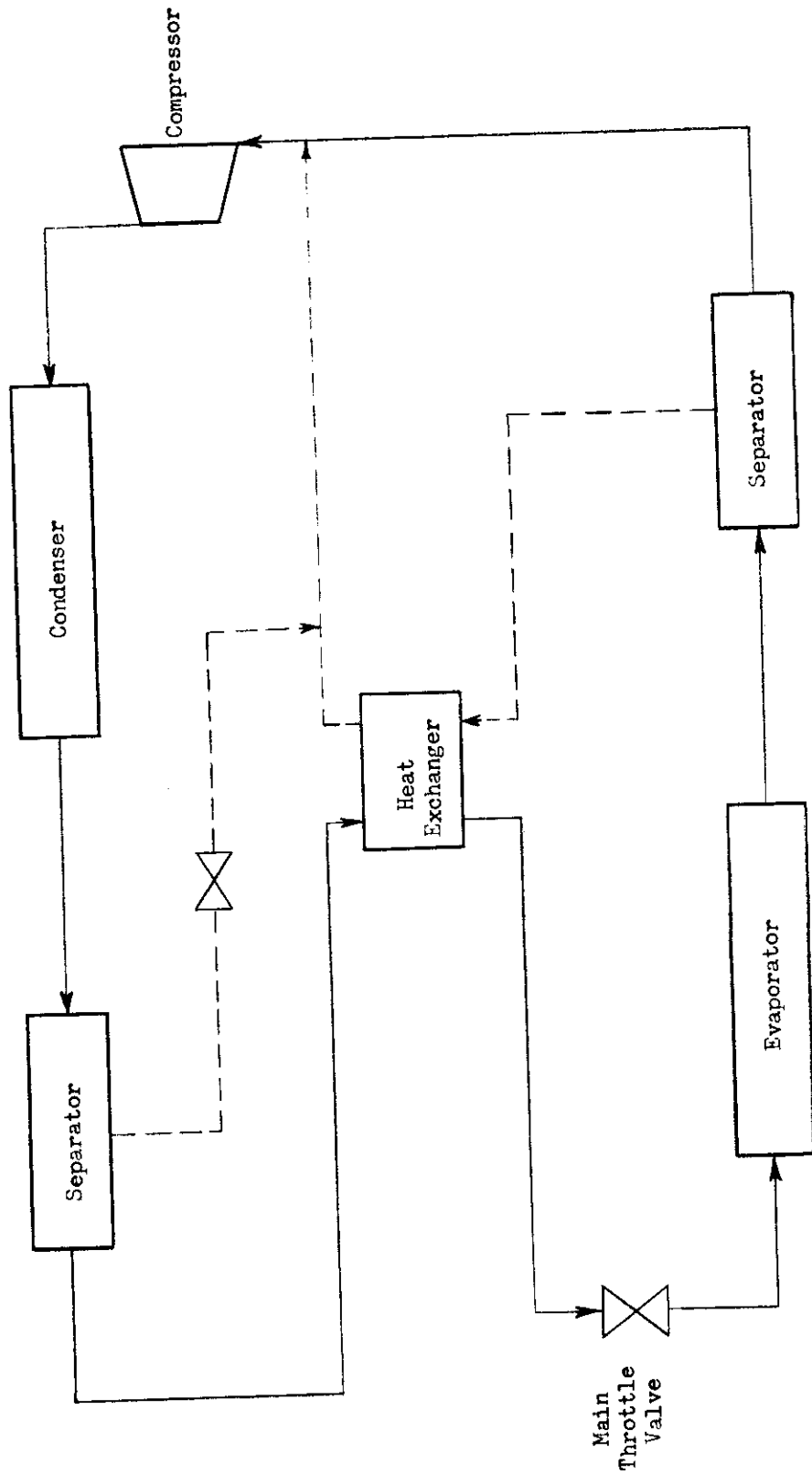


FIGURE 10: SCHEMATIC OF VAPOR CYCLE WITH SEPARATORS

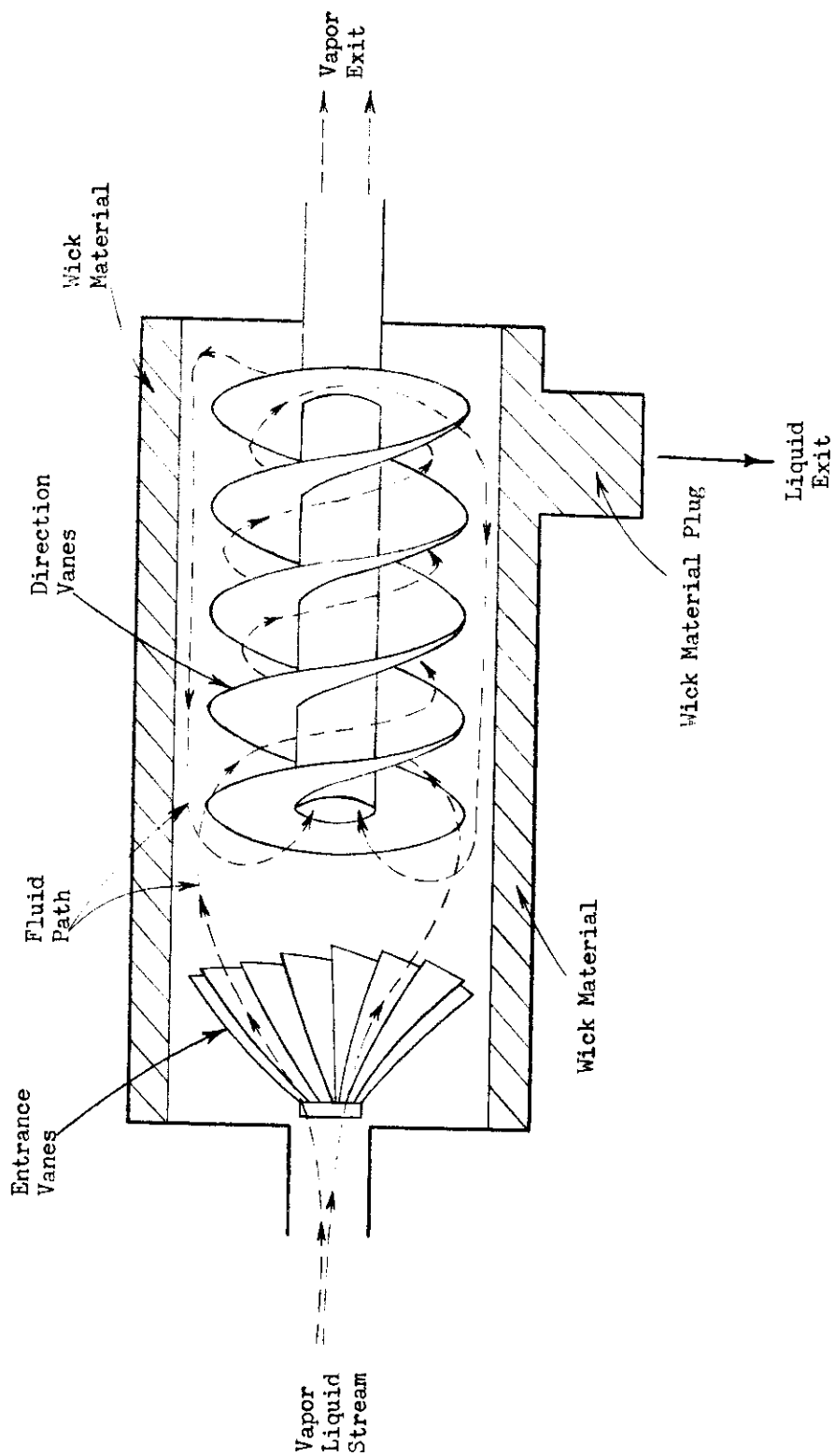


FIGURE 11: VAPOR-LIQUID SEPARATOR

Contrails

SECTION V

VORTEX EVAPORATOR STUDY

Prior to the consideration of any evaporator design, a detailed review of the current status of boiling theory and experiment was undertaken. This was necessary to understand the underlying effects of various fluid parameters on boiling, and the changes that would occur when the entire boiling mechanism would take place in the absence of gravity. A summary of the review is presented here, and the many references investigated are listed at the end of this section.

REVIEW OF BOILING THEORY AND EXPERIMENT

Regimes of Boiling

Although the details of the mechanisms in the individual regimes in boiling are not fully understood, experimental investigation shows clearly that as the rate of heat transfer increases, the boiling process passes through several regimes (Figure 12). These regimes are discussed below.

Convective Heating - The fluid is heated without the formation of bubbles. The heat is transferred from the hot surface to the fluid by convection. Free and forced convection under varied conditions have been studied by many investigators (36, 99, 137, 166). In this regime, q/A is proportional to ΔT .

Local Boiling - When the hot surface temperature is increased to a few degrees above the saturation temperature of the liquid, some bubbles are formed. These bubbles collapse as they grow because the temperature of the bulk of the fluid is still below the saturation temperature. The bubble growth and collapse cause an agitation in the boundary layer, and thus give higher rates of heat transfer than convective heating.

Bulk Boiling - When the bulk temperature of the fluid rises to the saturation temperature, the bubbles leave the heating surface without collapsing. The local and bulk boiling are both classed as nucleate boiling because vapor is formed at definite positions on the heating surface once a certain amount of superheat is reached. In nucleate boiling, $q/A \propto (\Delta T_{\text{sat}})^s$, where $s = 2.5$ to 4 .

Partial Film Boiling - As the temperature difference between the heated surface and the bulk liquid temperature increases, bubbles are formed at more points on the surface, covering a greater area of the surface with vapor. Since the vapor has a lower heat conduction coefficient, the curve of q versus ΔT shows a maximum and then falls as more vapor covers the surface. The point of maximum q is known as the burnout point, since an increase in q above this value results in transition to the next portion of the curve, with a large increase in surface temperature.

Contrails

Film Boiling - If the heating surface can withstand high temperatures, it will reach a point where the predominant method of heat transfer shifts from conduction to radiation, and the rate of heat transfer to the liquid begins to rise again with an increase in ΔT .

Since the heat transfer mechanism changes from one regime to the other, different methods of analysis and correlation are required for the different regimes.

Nucleate Boiling

Nucleate boiling is the process by which boiling takes place by the formation of bubbles at certain distinct points on the surface; it involves both dynamic and thermal processes. Some investigators have found experimentally that the latent heat transport by the bubble accounts for less than two percent of the high transfer rates observed in boiling. The most important mechanism of heat transfer is the agitation caused by the growth and collapse or escape of the bubble. A study of the formation and growth mechanism of bubbles leads to a better understanding of the nucleate boiling process. This process may be separated into the formation of the bubbles and the growth and motion of these bubbles, first as they grow on the hot surface, then after they break away from the hot surface and rise through the liquid.

The Formation of Bubbles - Bubbles are assumed to originate from "nuclei" whose nature is not clearly known. Nucleation can take place

1. In pure liquid and on smooth clean surfaces.
2. In liquids having suspended material.
3. On surfaces having small cavities.

In pure liquid and smooth, clean surfaces, nucleation is attributed to thermodynamic instability or to a statistical density fluctuation. Both approaches agree that in order for nucleation to occur, a certain amount of superheat in the liquid is needed. Surface tension opposes the growth of the bubbles and is of tremendous magnitude for small bubbles.

Assuming the bubble to be spherical,

$$P_V - P_L = \frac{2\sigma}{r} \quad (6)$$

Hence, for very small radii, one needs a large amount of superheat to resist the surface tension.

One important problem faced by different investigators is that of explaining how stable bubbles are formed.

Without going into detail, it can be stated briefly that from the kinetic theory some molecules have greater energies than the average energy distribution in the fluid. If two of these activated molecules collide and adhere, a nucleus is formed. The interface equilibrium condition for

Contrails

a pure vapor bubble surrounded by liquid may be written as

$$P_V - P_L = \sigma \left(\frac{1}{r_1} + \frac{1}{r_2} \right) \quad (7)$$

which results from a consideration of the forces on curved surfaces. For a spherical bubble or meniscus, this reduces to

$$P_V - P_L = \frac{2\sigma}{r} \quad (8)$$

The requirement $P_V > P_L$ is necessary for bubble growth, and T_L must be greater than T_V for evaporation. Using the perfect gas law and the Clausius-Clapeyron equation, we have

$$\frac{d P_V}{d T_V} \approx \frac{h_{fg}}{T_V} P_V \approx \frac{h_{fg} P_V}{R_V T_V^2} \quad (9)$$

On integrating Equation (9) and combining with Equation (7),

$$T_V - T_S = \frac{R_V T_S T_V}{h_{fg}} \left(1 + \frac{2\sigma}{P_L r} \right) \quad (10)$$

At high pressures, where $T_V - T_S$ is small,

$$T_V - T_S \approx 2 \frac{R_V T_S^2 \sigma}{h_{fg} P_L r} \quad (11)$$

which represents the superheat condition for a bubble of radius r . Nuclei of radii smaller than r should collapse, while those of radii greater than r should become bubbles and grow. Gravity appears to play no role in nucleation. The analysis above has considered only a pure liquid. For nucleation due to gas molecules entrapped in a heated liquid, we may write,

$$P_V - P_L = \frac{2\sigma}{R} - P_g \quad (12)$$

For a spherical nucleus containing w_g pounds of gas,

$$P_g = \frac{w_g R T_V}{\frac{4}{3} \pi r^3} \quad (13)$$

Then from Equations (12) and (13),

Contrails

$$\sigma_{\text{effective}} = \sigma - \frac{3 w_g R T_V}{8 \pi r^2} \quad (14)$$

and less superheat is required in this case. For a heated surface in water, where boiling begins at about 30 degrees F above saturation, Equation (11) predicts an equilibrium bubble radius of 10^{-4} inch. A cavity formation rate of this size has been predicted (137) to be only one per cubic inch per hour from which the conclusion may be drawn that free vapor nuclei, represented by Equation (11), are not as important as nucleation cavities or as gas nucleation, represented by Equation (14).

Although theories of nucleation show the significant factors influencing the formation of bubbles in pure and clean systems, they fail to explain the phenomena of boiling in actual practical systems. The former predict a required superheat of water around 90 degrees F, while boiling is actually observed with just a few degrees of superheat. It might be then worth studying boiling as nucleation that starts at the small cavities in the solid surface which entraps gas or vapor. If on the surface conical cavities exist having a liquid vapor surface convex downward, then the vapor pressure is less than the liquid pressure and the bubble might never collapse completely. It is enough to have one such bubble to start nucleation.

The Growth of Bubbles - The bubble growth and collapse mechanism in degassed subcooled liquids has been explained in detail by Ellion (63). A short description of this mechanism will be given here, and special points and factors which might lead to a better understanding of boiling under zero gravity will be emphasized.

After the bubble is formed on the heated surface, it begins to grow, pushing the superheated liquid film away from the wall. Heat is removed from the displaced film by conduction and convection to the bulk of the liquid and into the bubble. The bubble keeps growing, pushing the nearby liquid away until its top enters the subcooled liquid region. Condensation begins to take place at the top and evaporation continues at the lower part of the bubble. As the bubble grows, a bigger portion of its surface enters the subcooled liquid region, and thus the condensation rate increases until it surpasses the evaporation rate, after which the bubble begins to collapse. If the liquid has no subcooled region, the bubble continues to grow and detaches from the hot surface. Griffith (82) attributes the departure of the bubble from the heated surface to the inertia of the nearby liquid. This process of detachment of bubbles may take place even if the liquid is slightly subcooled because the condensation rate is slow and inertia forces can detach the bubble before it collapses.

The factors which affect bubble growth and collapse are:

Liquid Temperature - The growth rate of a bubble is governed by the Bernoulli relation

$$\frac{P_V - P_L}{\rho} = \frac{3}{2} \dot{r} + r \ddot{r} \quad (15)$$

Contrails

where P_V = pressure of vapor

P_L = pressure of liquid

r = radius of bubble

From this relation it can be seen that for the same liquid temperature the bubble growth rate is controlled by the degree of the superheat of the liquid film, and is independent of the bulk liquid temperature. Conversely, the collapse rate increases with a decrease in liquid bulk temperature. Although the growth rate remains constant for a lower liquid temperature, the life of the bubble is shorter and hence the radius will be smaller.

Wall Temperature - An increase in wall temperature causes more nuclei to be formed, causing a greater agitation of the hot liquid film. The greater turbulence gives rise to higher heat flux, but also to an increase in cooling rate, which results in an increase in the collapse rate and smaller bubble radii.

Effect of Pressure - Ellion (63) has found that the evaporation rate, and hence the bubble growth rate, decreased at higher pressures, resulting in smaller radii. He also found that the collapse rate is lower at higher pressures.

Surface Tension - For low surface tension liquids the bubble growth rate is slow and the bubbles have a tendency to remain stagnant on the heating element.

Effects of Acceleration on Boiling Heat Transfer

Several correlations in the literature show the effect of the gravitational field in boiling heat transfer. Rohsenow's (156) and Chang's (36) correlations are given in a following section. In Chang's correlation, if the term

$$Pr C_1 \left(\frac{q/A}{\sigma \alpha} \frac{\rho}{\rho_v} \frac{1}{\phi} \right)^n > (1 - Pr) \quad (16)$$

by some order of magnitude, then we may write

$$q/A = K g^{1/3 - 2n} (\Delta T)^{4/3 - 2n} \quad (17)$$

A number of expressions are reported in the literature for the critical heat flux which include the gravitational term. An expression in McAdams (137) which is due to Addoms shows

$$\left(q/A \right)_{crit.} = c \alpha \rho_v \left(g \alpha_c \right)^{1/3} \left(\frac{P_L - P_V}{P_V} \right)^n \quad (18)$$

Contrails

Using dimensional analysis to derive similarity criteria for the critical flux, Borishanskii (27) obtained the expression,

$$(q/A)_{\text{crit}} = K_2 \times (\rho_v)^{1/2} [\sigma g (\rho_L - \rho_v)]^{1/4} \quad (19)$$

Zuber (191) analyzed the critical condition from the standpoint of hydrodynamic stability, and obtained a completely analytical result,

$$(q/A)_{\text{crit}} = \frac{\pi}{24} \times (\rho_v)^{1/2} [\sigma g (\rho_L - \rho_v)]^{1/4} \left[\frac{\rho_L - \rho_v}{\rho_L} \right]^{1/2} \quad (20)$$

Griffith's correlation for both pool boiling and forced convection shows that the critical heat flux is proportional to the gravitational field raised to the 1/3 power; i.e.,

$$(q/A)_{\text{crit}} \propto g^{1/3} \quad (21)$$

The critical heat flux in boiling is shown to be proportional to the gravitational field raised to an exponent which varies between 1/3 and 1/4.

Methods of Correlating Data

Assuming that the heat flows from the hot element to the fluid and then to the vapor bubble, and that the controlling resistance to the heat transfer is the stagnant film around the vapor bubble, several correlations are available for predicting heat transfer coefficients.

Rohsenow Correlation - The assumptions in this correlation are:

1. Fritz (73) empirical equation for bubble diameter at detachment

$$D_b = C_d \left(\frac{2 g_0 \sigma}{g (\rho_L - \rho_v)} \right)^{1/2} \quad (22)$$

2. The bubble is a sphere when it detaches from the hot surface.
3. Frequency of formation depends only on size of bubble at break-off.

The correlation obtained is:

$$\frac{c_{pL} \Delta T_{\text{SAT}}}{h_{fg}} = C_{sf} \left[\frac{q/A}{\mu_L h_{fg}} \sqrt{\frac{g \sigma}{g (\rho_L - \rho_v)}} \right]^{0.33} \left[\frac{c_{pL} \mu_L}{k_L} \right]^{1.7} \quad (23)$$

Contrails

where C_{sf} is a constant depending on heating surface shape, material and fluid.

Forster and Zuber Correlation - By starting from the Rayleigh equation for the rate of growth of a bubble and neglecting the inertia term, and assuming that $R \frac{dR}{dt}$ is independent of time, Forster and Zuber (67) obtained

$$h = \frac{0.0012 (\Delta T)^{0.24} (P_v - P_l)^{0.75} k_L^{0.79} c_L^{0.45} \rho_L^{0.49}}{\sigma^{0.9} h_{fg}^{0.24} \mu_L^{0.29} \rho_L^{0.24}} \quad (24)$$

While Rohsenow assumes the movement of the bubble at the instant of break-off as the important criterion, Forster and Zuber assume the growth of the bubble as the governing criterion. Hence, Rohsenow's analysis fits large bubble formation, while Forster and Zuber's applies more to small ones.

Chang Correlation - Chang approached the problem as an extension of wave analysis of natural convection, and arrived at

$$h_b = 0.146 k \left[1 + Pr \left\{ C_1 \left(\frac{q/A \mu/\rho}{\sigma h_{fg}} \frac{\rho}{\rho_v} \frac{1}{\phi^2} \right)^n - 1 \right\} \right]^{3/2} \left[\frac{Pr \rho^2 \beta \Delta T_{SAT}}{\mu^2} \right]^{1/3} \quad (25)$$

Rohsenow suggests that two separate factors may be superposed to account for heat transfer in forced convection with boiling; that due to convection, and that due to bubble motion.

$$(q/A)_{total} = (q/A)_{forced\ convection} + (q/A)_{pool\ boiling}$$

The second factor has been considered elsewhere in this paper. The first term may easily be calculated from the appropriate convection formulas.

BOILING IN A ZERO-GRAVITY FIELD

The preceding discussion has shown that nucleation in heated liquids, the initiation of bubble formation, and subsequent growth of bubbles do not depend on gravity. The detachment of a bubble from a heated surface has been attributed mainly to the inertia of the surrounding liquid. It has been observed that bubbles will detach themselves from the lower surface of a heating element immersed in a liquid and will move a small distance downward against the force of gravity. It is expected, therefore, that in zero-gravity boiling, bubbles will form and detach themselves from the heated surface, but may not migrate away from the surface unless a small body force is present. If a true zero-gravity situation exists and no residual body forces are present, the large number of bubbles which form as heating continues may eventually blanket the heating surface with a vapor film reducing the heat transfer mechanism to film boiling. In the complete absence of gravity, one would expect the onset of film boiling soon after boiling has begun. If burnout is not a limitation, heat transfer will continue by conduction through the insulating vapor film so

that coefficients of heat transfer would be several orders of magnitude lower than those of nucleate boiling. Forced convection would have some effect on vapor removal by entrainment of some bubbles in the bulk flowing liquid, but this would not be of much benefit unless the heat surface were baffled sufficiently to cause agitation. However, Zuber (192) has reported that agitation by superficial means has little effect on the boiling heat transfer coefficient; but this is probably true only where the self-agitation of the boiling process exceeds considerably that which is produced by artificial means.

Siegel and Usiskin (181) at the National Aeronautics and Space Administration have made a photographic study of boiling during free fall conditions of approximately eight feet. A ribbon heater immersed in a beaker of water was used to produce heat fluxes which would vary from moderate nucleate boiling to burnout under gravity conditions. Their results indicate that gravity plays a dominant role in nucleate pool boiling. During free fall, the vapor remained adjacent to the heating surface, and bubbles were not pushed away from the surface during formation. This appears to contradict the importance of liquid inertia as a mechanism for detaching a bubble from the liquid surface. Since the zero-gravity condition was an extremely short one, some of the processes may have been passing through a transient stage. A small amount of friction was then added to the initial system raising g to a value of about 0.09. Under these conditions, it is reported that nucleate boiling appeared to continue through the free fall condition. This might indicate that even a small gravity field or artificial body force is sufficient to maintain nucleate boiling.

Merte and Clark (143) have made a study of pool boiling in an accelerating system where the acceleration is applied normal to the heating surface. The acceleration was varied from that due to gravity ($1-g$) to a value twenty-one times that of gravity. At fluxes up to 50,000 BTU/hr-sq ft, it was found that acceleration changed the q/A versus ΔT curves considerably; that is, a small degree of subcooling had a strong influence on the acceleration fluxes. At higher fluxes, there appeared to be no significant changes due to acceleration.

Gambill and Greene (74, 75) have induced artificial body forces in boiling by inserting twisted tapes inside the tubes of the boiling apparatus. This method forms the basis for the design of the vortex evaporator which is given later. Gambill's results indicate that at the same pumping power, peak heat fluxes are increased two-fold in tubes with tapes over those in bare tubes. Increased heat fluxes are also obtained as the number of twists per diameter length is increased.

DESIGN OF A ZERO-GRAVITY VORTEX EVAPORATOR

In using density differences for boiling under zero gravity, two choices are available to the designer. The first is to rotate the boiling apparatus or, in this case, the evaporator as Merte and Clark (143) have done for their pool boiling experiment; the other is to provide the artificial gravity force by inducing such motion in the fluid without rotating the equipment. The latter method is obviously the preferred one from the standpoint of simplicity, reliability, and the lack of any accessory equipment to provide rotation. Prior to the discussion of the design of the vortex evaporator, a general discussion of heat transfer in vortex flow will be presented.

Heat Transfer and Boiling in Vortex Flow

Gambill, Greene, and others (74, 75) have been studying heat transfer and burnout in tubes with internally twisted tapes since 1958 at the Oak Ridge National Laboratory of the Atomic Energy Commission. The stimulus for this work has been, at least partially, the applicability of vortex-tube fuel elements to nuclear reactor cores where burnout may be a problem. The work of Gambill, et al., has been performed with water. Other investigators have conducted similar experiments with boiling Freon, boiling mercury, and heating Santowax liquid, and this work will be mentioned later.

Gambill's experiments were performed with water flowing through copper and aluminum tubes; the twisted tapes were of 0.015-inch thick Inconel for all cases. The most reliable method of fitting the twisted tapes to the copper tubes was to first draw the tubing on a mandrel to an inside diameter which was slightly larger than the diameter of the tape. The tape was then inserted in the tube, and the latter drawn further until the tube inside diameter was from 0.002 inch to 0.003 inch less than the tape diameter. For tape insertion into aluminum tubes, three draws were made with an annealing of 550 degrees C between the second and third draws. With this method, a slight penetration of the tube wall by the tape was effected. The twist ratio y was defined as the number of diameters along the twisted length of the tape required for each 180-degree twist.

The inside diameters of the copper tubes varied from 0.136 inch to 0.249 inch, while the inside diameter of the aluminum tube was 0.249 inch. The internal diameter/twist ratio for the tapes varied from 2.3 to 12.0. Heat fluxes were varied from 0.8×10^6 to 8.0×10^6 BTU/hr-sq ft in the nonboiling tests, while those for local boiling varied from 2.3×10^6 to 9.3×10^6 BTU/hr-sq ft. Axial Reynolds numbers were varied from 5000 to 427,000.

In an earlier investigation (74), Gambill and Greene reported that the ratio of vortex-flow burnout heat fluxes to burnout heat fluxes was about two for water flowing in similar tubes at equal pumping powers. In the recent work (75), this conclusion has been confirmed. At a constant pumping power, the value of the ratio of burnout heat flux with vortex flow to that with straight flow ranged from 1.6 to 2.4 with 2.0 as an average.

For the forced convection, nonboiling experiments, the mean vortex-flow heat transfer coefficients, h_{vm} , were compared to equivalent mean axial-flow heat transfer coefficients, h_{am} , at equal bulk coolant temperature and weight flow rate. Two correlations, each with an average deviation of 10.1 per cent, were reported:

$$\frac{h_{vm}}{h_{am}} = 2.18 y^{-0.090} \quad (26)$$

and

$$\frac{h_{vm}}{h_{am}} = 1.65 \left(\frac{10^2 (3 f_f)^{\frac{1}{2}} \Delta t_f^{\frac{1}{2}}}{y} \right)^{0.084} \quad (27)$$

Correlations

These equations may be combined with the Colburn equation,

$$St = \frac{0.023 [1 + (D_i/L_h)^{0.7}]}{Pr^{2/3} Re^{0.2}} \quad (28)$$

to give the following correlation for average twisted-tape vortex-flow heat transfer coefficients:

$$\left(\frac{h_{vm}}{c_p G_a} \right) \left(\frac{y^{0.09}}{2.18} \right) = \frac{0.023 [1 + (D_i/L_h)^{0.7}]}{(Pr)_b^{2/3} (Re)_b^{0.2}} \quad (29)$$

The local-boiling regime was not investigated extensively. The few measurements were correlated with an average deviation of about 15 per cent by

$$\Delta t_{sat} = \frac{y^{0.81} (Q/A)^{1.35}}{0.34} \quad (30)$$

and

$$Q/A = 0.45 \frac{(\Delta t_{sat})^{0.74}}{y^{0.6}} \quad (31)$$

The burnout heat flux is dealt with extensively in Reference 75 and will not be discussed here.

Based on the standard friction factor definition for axial flow

$$f_a = \frac{D_i}{L_a} \frac{2 g_o}{v_a^2} \frac{144}{\rho_b} \Delta P \quad (32)$$

the axial friction factor for isothermal, nonboiling flow is expressed in Gambill's work as

$$f_a = 0.00089 y^{-0.6} D_i^{-1.2} \left(\frac{\mu_i}{\mu_b} \right)^{0.18} \quad (33)$$

and the pressure drop for single-phase flow through a tube with twisted tape is given as

$$\Delta P = 0.00089 \frac{v_a^2}{2 g_o} \frac{L_a}{D_i} \frac{\rho_b}{144} D_i^{-1.2} y^{-0.6} \left(\frac{\mu_i}{\mu_b} \right)^{0.18} \quad (34)$$

Contrails

Some significant results in the boiling of Freon 114 have been reported from the Oak Ridge Gaseous Diffusion Plant (personal communication, Reference 75). The tests were performed with Freon 114 in natural circulation through vertical, unpolished copper tubes with an ID of 3/4 inch and a length of 3 feet. For straight flow through the tubes, the values of peak heat flux and heat transfer coefficient obtained were 41,000 BTU/hr-sq ft and 2300 BTU/hr-sq ft-degF, respectively. The tubes were then fitted with aluminum tapes 0.040 inch thick with a diameter/twist ratio of 2.35 and 4.00. The peak heat flux increased to 67,000 BTU/hr-sq ft and the corresponding maximum heat transfer coefficient was 3500 BTU/hr-sq ft. For a temperature difference, ΔT_p , of 20 degrees F, the weight ratio of liquid to vapor at the tube exit decreased from 2.5 to 0.25, demonstrating the increased fraction of vaporization per pass in the vortex tube case.

Vortex Evaporator Design

The basis of design of the vortex evaporator is to induce an artificial "gravity" force in the fluid by rotating the fluid. The magnitude of this force may be expressed by $g = \omega^2 r$, where ω is the angular velocity and r is the radius of rotation which is assumed to be the inner radius of the tube. The function of the twisted tapes is to provide the force which continually moves the denser liquid to the tube wall where boiling takes place and to displace the vapor which would normally insulate the heat transfer surface from the liquid.

In the calculations for the volumes of evaporator cores used in this section, an estimate of the improvement in heat transfer due to the twisted tapes, which is more conservative than that due Gambill's work, is used. In any event, Gambill's experiments were performed with water, and similar experiments on the effect of twisted tapes on boiling of Freon refrigerants in tubes are necessary before any conclusive designs of zero-gravity vortex evaporators can be made. Since y represents the number of diameters per 180-degree twist, large values of y indicate relatively few twists. The acceleration due to rotation, $\omega^2 R$, is a function of y^2 . The tangential velocity at the inside tube wall, v_{tw} , may be written,

$$v_{tw} = \frac{\pi D_i (\text{rpm})}{(12) (60)} \quad (35)$$

At the tube wall, an acceleration, a_t , due to rotational motion may be written,

$$a_t = \frac{v_{tw}^2}{R_i} \quad (36)$$

If g' defines the number of "artificial gravity" units which may be induced by twisted tapes,

$$g' = \frac{a_t}{g} = \frac{v_{tw}^2}{g R} \quad (37)$$

Contrails

Since

$$\text{rpm} = 360 \frac{v_a}{y D_i} \quad (38)$$

we obtain

$$g' = \frac{1.845}{D_i} \left(\frac{v_a}{y} \right)^2 \quad (39)$$

Equation (39) shows immediately the large number of artificial gravity units that may be induced in small-diameter tubes with reasonable axial velocities.

From Gambill's results we have:

$$q/A \sim (\omega^2 r)^{0.6} \sim \omega^{1.2} \sim v_a^{1.2} \quad (40)$$

Since the calculation of the heat transfer coefficients in a vortex evaporator depends on the velocity of the fluid in the tubes, some value of axial velocity had to be chosen in order to calculate the rotational velocities. In an evaporator, the liquid refrigerant enters at a relatively low velocity, while the refrigerant vapor leaves at a much higher velocity. Using different functions for the variation of velocity in a tube from entrance to exit, one may calculate an average velocity which forms the basis for calculation of the artificial gravity term, $\omega^2 r$, and subsequently the heat transfer coefficient. In order to simplify the analysis, an average velocity equivalent to one-third the exit velocity is assumed here. The heat transfer coefficient for the twisted-tape may now be expressed by a modified Rohsenow correlation. This correlation gives reasonably accurate heat transfer coefficients and is convenient to use in this case, and the artificial gravity force may be introduced easily into the equation.

$$\frac{c_p \Delta T}{h_{fg}} = C_{SF} \left[\frac{q/A}{\mu_f h_{fg}} \sqrt{\frac{g_o \sigma}{g \left[1 + \left(\frac{\omega^2 r}{g} \right)^{0.6} \right] (\rho_L - \rho_V)}} \right]^{1/3} [\text{Pr}]^{1.7} \quad (41)$$

and hence

$$h = \frac{1}{C_{SF}} \frac{c_p}{h_{fg}^{2/3}} \left(\frac{1}{\sqrt{\frac{g_o \sigma}{g (\rho_L - \rho_V)} \left[1 + \left(\frac{\omega^2 r}{g} \right)^{0.6} \right]}} \right)^{1/3} \quad (42)$$

Contrails

The results of the design calculations are presented in Figures 13 to 21. Figures 22 to 24 compare the weights of plain-tube, plate-fin, and vortex-tube evaporators using Freon 11 at 40 and 55 degrees F evaporator temperatures and air-side pressure drops from 0.1 psia to 0.5 psia. The design characteristics of the plate-fin and vortex evaporators are shown in Tables 6 and 7. In addition, it is assumed that the temperature of the air leaving the evaporator is 60 degrees F; two temperature differences for the air entering and leaving the evaporator were used--25 degrees and 100 degrees. The volumes for the bare tube-fin evaporators are presented, not as any solution to the zero-gravity problem, but merely for comparison with the vortex-tube evaporators. Figure 1 also shows vortex evaporators for diameter/twist ratios of 10 and 3.5. For the value of $y = 3.5$, two values of average velocity have been used. One is simply one-third of the exit velocity; the other is obtained by

$$\begin{aligned}\bar{v} &= \frac{1}{v_{\text{exit}}} \int_0^{v_{\text{exit}}} v^{1/1.2} dv \\ &= \frac{6}{11} v_{\text{exit}}^{5/6}\end{aligned}\quad (43)$$

In all succeeding diagrams, the vortex-tube evaporator design is based on $y = 3.5$ with an average velocity equal to one-third of the exit velocity.

Details of the calculation procedures are shown in Appendix 1. As Figures 13 to 21 indicate, in all cases, the vortex-tube evaporator has a volume smaller than that of the corresponding plate-fin for the same heat load. Figures 22 to 24 show the estimated weights of the evaporators for the conditions given on each diagram. Although the vortex-tube evaporator has a volume advantage over the plate-fin, it is nevertheless heavier than the plate-fin. It is difficult to assess the exact magnitudes of the differences in volume and weight until some experimental work is performed on the boiling of Freon refrigerants in tubes with twisted tapes. The modified Rohsenow correlation used for the vortex evaporator design gives more conservative results than those obtained by using only Gambill's relation for the dependence of the heat transfer coefficient on the diameter to twist ratio, y . However, the increase in heat transfer due to the vortex generation is still sufficient to give a smaller volume for the vortex evaporator than for the plate-fin unit. For example, for a given change in y , Gambill's relation gives approximately twice the change in evaporator core volume compared to the change due to the modified Rohsenow correlation.

Gambill has presented some values for the change in friction factors for flow in vortex tubes versus flow in bare tubes. For the isothermal non-boiling case, friction factors in tubes with twisted tapes are increased by a factor of two or three over those in bare tubes, depending on tube diameter and the degree of tape twist. For local-boiling conditions, the ratio f_{LB}/f_a is presented as a function of $(\Delta t_{\text{sat}}/\Delta t_{\text{sub}})(1/P)$. The average value of this ratio is about 0.8 - 0.90, and it rises above unity only for values of $(\Delta t_{\text{sat}}/\Delta t_{\text{sub}})(1/P)$ which exceed 0.02. An estimate of the pressure drop in a vortex evaporator (excluding entrance and exit pressure drops) was made using

Contrails

the Lockhart-Martinelli method for two-phase flow and estimating the single-phase pressure drop from Figure 20 in Gambill (75). Table 8 shows the pressure drops on the Freon side for several cases of the vortex tube evaporators, and compares them with the corresponding pressure drops in plate-fin evaporators. Table 8 also includes a column showing Freon-side pressure drops in the plate-fin evaporators where the Freon-side flow length is equivalent to that in the vortex-tube case. The plate-fin evaporators were not optimized in any way for pressure drop, but were designed for minimum volume and weight. The hydraulic diameter for the plate-fin unit was smaller by a factor of about 2.5 than the hydraulic diameter of the vortex-tube evaporator.

Contrails

LIST OF SYMBOLS

A	sq ft	Heat transfer area
A_{face}	sq ft	Heat exchanger face area
A_{free}	sq ft	Heat exchanger free flow area
a	ft/sec ²	Acceleration
C	BTU/min-degF	Capacity rate equal to $w c_p$
C_{SF}		Constant in Rohsenow correlation
c_p	BTU/lb-degF	Specific heat
D_i	ft	Inner diameter
d	ft	Diameter
d_h	ft	Hydraulic diameter
f		Friction factor
f_{LB}/f_a		Ratio of local boiling to isothermal nonboiling friction factors
G	lbs/hr-sq ft	Mass flux
g	ft/sec ²	Gravitational acceleration
ϵ_c, ϵ_o	lbm-ft/lbf-sec ²	Dimensional constant
h	BTU/hr-sq ft-degF	Heat transfer coefficient
h_{fg}	BTU/lb	Latent heat of vaporization
ID	ft	Inner diameter
j		Colburn modulus - $(N_{\text{Re}}) (N_{\text{Pr}})^{2/3}$
K, K_H, K_P, K_R, K_C		Constants
k	BTU/hr-ft-degF	Thermal conductivity
L	ft	Flow length
L_h	ft	Heated length
NP		Number of flow passes
N_{Pe}		Peclet number ($c_p \rho v d_h/k$)
N_{Pr}, Pr		Prandtl number ($c_p \mu/k$)
N_{Re}, Re		Reynolds number ($\rho v d_h/\mu$)

Contrails

N_{St}, St		Stanton number ($h/G c_p$)
NTU		Number of heat transfer units
OD	ft	Outer diameter
ΔP	lbs/sq in	Pressure difference
Q	BTU/hr or BTU/min	Heat rate
r	ft	Radius
S_L	in	Tube spacing longitudinal to flow
S_T	in	Tube spacing transverse to flow
T	degF	Temperature
ΔT_{sat}	degF	= $T_w - T_{sat}$
ΔT_{sub}	degF	= $T_{sat} - T_b$
t		Fin thickness
U	BTU/hr-sq ft-degF	Over-all heat transfer coefficient
V	cu ft	Volume
v	ft/sec	Velocity of fluid
w	lbs/min	Mass flow rate
y		Twist ratio, number of diameters per 180-degree twist
α		Heat exchanger component volume ratio
β	(degF) ⁻¹	Volumetric coefficient of thermal expansion
ϵ		Exchanger heat transfer effectiveness
η_f		Fin effectiveness
η_o		Total surface effectiveness
μ	lbs/hr-ft	Viscosity
ρ	lbs/cu ft	Density
σ	lbs/ft	Surface tension
ω	1/sec	Angular velocity

Subscripts

a	refers to	axial
am		mean axial

Contrails

ave	average
b	bulk
c	cold side
d	derived
exit	exit value
f	film value
h	hot side
i	inner diameter or inner wall
in	entrance value
L	liquid
max	maximum
min	minimum
out	exit value
sat	saturation value
std	value at standard temperature and pressure
T	total
t	tangential
v	vapor
w	wall
1, 2	different heat exchanger sides

Contrails

REFERENCES

1. Addoms, J. H., Heat Transfer at High Rates to Water Boiling Outside of Cylinders, Doctorate in Science Thesis, Massachusetts Institute of Technology, 1948
2. Akin, G. A., Heat Transfer in Submerged Evaporators, Thesis, Massachusetts Institute of Technology, 1942
3. Akin, G. A. and McAdams, W. H., "Boiling Heat Transfer in Natural Convection Evaporators," Industrial & Engineering Chemistry, vol. 31, 1939, p. 487
4. Allred, J. C. and Blount, G. H., Experimental Studies of Taylor Instability, Univ. of Calif. Los Alamos Sc. Lab., Report LA-1600, 1954
5. Ashley, C. M., "Heat Transfer of Evaporating Freon-12," Refrigeration Engineering, vol. 43, 1942, p. 89
6. Averin, E. K., The Effect of the Material and the Mechanical Treatment of the Surface of the Heat Exchange in the Boiling of Water, A.E.R.E. Liberal Translation 562, 1954
7. Badger, W. L., Trans. A.I.Ch.E., vol. 13, Part II, 1920, p. 139
8. Bankoff, S. G., "Ebullition from Solid Surfaces in the Absence of Pre-existing Gaseous Phases," Trans. ASME, vol. 79, 1957, p. 735
9. Bankoff, S. G., "The Prediction of Surface Temperatures at Incipient Boiling," Preprint 4, A.I.Ch.E.-ASME Heat Transfer Conference, Chicago, 1958
10. Bankoff, S. G., "The Entrapment of Gas in the Spreading of a Liquid Over a Rough Surface," A.I.Ch.E. Journal, vol. 4, 1958
11. Bankoff, S. G. and Mikesell, R. D., "Bubble Growth Rates in Highly Subcooled Nucleate Boiling," Preprint 2, A.I.Ch.E.-ASME Heat Transfer Conference, Chicago, 1958
12. Bankoff, S. G. and Mikesell, R. D., Growth of Bubbles in a Liquid of Initially Nonuniform Temperature, ASME Paper 58-A-105, ASME Annual Meeting, New York, 1958
13. Bankoff, S. G., Colahan, W. J., and Barts, D. R., Summary of Conference on Bubble Dynamics and Boiling Heat Transfer Held at the Jet Propulsion Laboratory, June 15 and 16, 1956, Jet Propulsion Lab Memo No. 20-137, California Institute of Technology, 1956
14. Bashforth, F., and Adams, C., An Attempt to Test the Theories of Capillary Action, Cambridge University Press, 1883
15. Bellman, R. and Pennington, R. H., "Effects of Surface Tension on Taylor Instability," Quar. Appl. Math., vol. 12, 1954, p. 151

Contrails

16. Benjamin, M. W. and Miller, J. G., "The Flow of Saturated Water Through Throttling Orifices," Trans. ASME, vol. 63, 1941, p. 419
17. Bergelin, O. P., Gazley, Jr., Carl, Kegel, P. K., and Carpenter, F. G., Proceedings of Heat Transfer and Fluid Mechanics Institute, Berkeley, California, 1949, pp. 19-28
18. Bernath, L., Industrial & Engineering Chemistry, vol. 44, 1952, pp. 1310-1313
19. Bernath, L., "Prediction of Heat Transfer Burnout," Preprint 8, A.I.Ch.E. Heat Transfer Symposium National Meeting, Louisville, Kentucky, March 20-23, 1955
20. Birkhoff, G., Margulies, R. S., and Horning, W. A., "Spherical Bubble Growth," Phys. of Fluids, vol. 1, 1958, p. 201
21. Boarts, R. M., Badger, W. L., and Meisenburg, S. J., Trans. A.I.Ch.E., vol. 33, 1937, pp. 363-389
22. Boelter, L. M. K., Martinelli, R. C., and Jonassen, F., "Remarks on the Analogy Between Heat Transfer and Momentum Transfer," Trans. ASME, vol. 63, 1941, p. 447
23. Boelter, L. M. K., et al, Boiling Studies, Progress Report No. 1, Engineering Research Laboratory, University of California, August 1949
24. Bonilla, C. F. and Eisenberg, A. A., Industrial & Engineering Chemistry, vol. 40, 1948, pp. 1113-1122
25. Bonilla, C. F. and Perry, C. W., "Heat Transfer to Boiling Binary Liquid Mixtures," Trans. A.I.Ch.E., vol. 37, 1941, p. 685
26. Bonnet, W. E. and Guster, J. A., "Boiling Coefficients of Heat Transfer," Chemical Engineering Progress, vol. 47, 1951, p. 151
27. Borishanskii, V. M., "An Equation Generalizing Experimental Data on the Cessation of Bubble Boiling in a Large Volume of Liquid," Zhur. Tekh. Fiz., vol. 25, 1956, p. 252 [Soviet Physics - Technical Physics, vol. 1, No. 2, p. 438]
28. Boscov, J. L., Heat Transfer to Boiling Water Under Pressure, Thesis, Massachusetts Institute of Technology, 1947
29. Bosnjakovic, F., Techn. Mechanik u. Thermodynamik, vol. 1, 1930, p. 358
30. Bromley, L. A., Heat Transfer in Film Boiling from Horizontal Tube, Atomic Energy Commission MDDC-1628, BC-86, September 1947
31. Bromley, L.A., "Heat Transfer in Stable Film Boiling," Chemical Engineering Progress, vol. 46, 1950, p. 221
32. Brooks, C. H. and Badger, W. L., Trans. A.I.Ch.E., vol. 33, 1937, pp. 392-413

Contrails

33. Buchberg, H., Romie, F., Lipkin, R., and Greenfield, M., "Heat Transfer, Pressure Drop, and Burnout Studies with and without Surface Boiling for De-Aerated and Gassed Water at Elevated Pressures in a Forced Flow System," 1951 Heat Transfer and Fluid Mechanics Institute Preprints of Papers, Stanford University, 1951, p. 177
34. Carl, R. and Picornell, P., Local Boiling of Water in an Annulus, Masters Thesis, Massachusetts Institute of Technology, 1948
35. Carter, J. C., Effect of Film Boiling, Argonne National Laboratory 4766, February 7, 1952
36. Chang, Y. P., "A Theoretical Analysis of Heat Transfer in Natural Convection and in Boiling," Trans. ASME, vol. 79, 1957, p. 1501
37. Christiansen, R. M. and Hixson, A. N., "Breakup of a Liquid Jet in a Denser Liquid," Industrial & Engineering Chemistry, vol. 49, 1957, p. 1017
38. Cichelli, M. T. and Bonilla, C. F., "Heat Transfer to Liquids Boiling Under Pressure," Trans. A.I.Ch.E., vol. 41, 1954, p. 755
39. Cichelli, M. T. and Bonilla, C. F., "Heat Transfer Lecture," Atomic Energy Commission, Oak Ridge, Tennessee, NEPA-979, IER-13, vol. 2, pp. 150-186
40. Clark, H. B., Strenge, P. H., and Westwater, J. W., "Active Sites for Nucleate Boiling," Preprint 13, A.I.Ch.E.-ASME Heat Transfer Conference, Chicago, 1958
41. Clark, J. A. and Rohsenow, W. M., "Local Boiling Heat Transfer to Water at Low Reynolds Numbers and High Pressure," Trans. ASME, vol. 76, May 1954, pp. 553-562
42. Coffey, J. B., Thesis in Chemical Engineering, Massachusetts Institute of Technology, 1939
43. Cohen, P. and Vogel, K., The Effect of Dissolved Gases on the Bubble Point of H₂O, Westinghouse Atomic Power Division RM-7, February 20, 1950
44. Colburn, A. P., "A Method of Correlating Forced Convection Heat Transfer Data and a Comparison with Fluid Friction," Trans. A.I.Ch.E., vol. 29, 1933, p. 174
45. Colburn, A. P., Schoenborn, E. M., and Sutton, C. S., National Advisory Committee on Aeronautics, Technical Note 1498, 1948
46. Corty, C., and Foust, A. S., Preprint 1, Annual Meeting of the A.I.Ch.E., St. Louis, 1953
47. Corty, C. and Foust, A., "Surface Variables in Nucleate Boiling," Chemical Engineering Progress Symposium, Series 51, 1955, p. 1
48. Coulson, J. M. and Mehta, R. R., "Heat Transfer Coefficients Evaluated and Climbing Film Evaporator Test Described," Chemical Age, vol. 68, 1953, p. 421

Contrails

49. Cryder, D. S. and Finalborgo, A. C., Trans. A.I.Ch.E., vol. 33, 1937, pp. 346-361
50. Cryder, D. S. and Gilliland, E. R., "Heat Transmission from Metal Surfaces to Boiling Liquids," Refrigeration Engineer, vol. 25, 1933, p. 76
51. Cushnie, J. L. and Overturf, W. K., Heat Transfer Characteristics of a Forced Circulation Vertical Tube Evaporator, Thesis, Massachusetts Institute of Technology, 1940
52. Davidson, W. F., Hardie, P. H., Humphreys, C. G. R., Markson, A. R., and Ravese, T., "Studies of Heat Transmission Through Boiler Tubing at Pressure from 500-3000 Pounds," Trans. ASME, vol. 65, 1943, p. 553
53. Davies, R. M. and Taylor, G. I., The Mechanism of Large Bubbles Rising Through Extended Liquids and Through Liquids in Tubes, Proc. Roy. Soc., London, A-200, 1949, p. 375
54. Davis, E., "Heat Transfer and Pressure Drop in Annuli," Trans. ASME, vol. 65, 1943, pp. 755-758
55. DeBortoli, R. A., Green, S. J., Jacket, H. S., Roarty, J. P., Weiss, H., and Zerbe, J. E., Investigation of Burnout Heat Flux, Westinghouse Atomic Power Division
56. DeBortoli, R. A., Green, S. J., Letourneau, B. W., et al, Forced-Convection Heat Transfer Burnout Studies for Water in Rectangular Channels and Round Tubes at Pressures above 500 psia, Westinghouse Atomic Power Division 188, 1958
57. Dergarabedian, "The Rate of Growth of Vapor Bubbles in Superheated Water," Trans. ASME, vol. 75, 1953, pp. 537-545
58. Donald, M. B. and Haslam, F., "The Mechanism of the Transition from Nucleate to Film Boiling," Chemical Engineering Science, vol. 8, 1958, p. 287
59. Drew, T. B., "Boiling," Trans. A.I.Ch.E., vol. 33, 1937, p. 449
60. Durkan, F. P., Radiolytic-Gas Bubbles Improve Convective Heat Transfer in SUPO," Univ. of Calif. Los Alamos Sc. Lab., Nucleonics 13, No. 5, 1955, pp. 42-46
61. Dwyer, O. E., Horn, F. L., Schomer, R. T., Sheehan, T. V., and Weisman, J., Heat Transfer Rates for Crossflow of Water Through a Tube Bank at High Reynolds Number, Brookhaven National Laboratory-203, November 20, 1952
62. Dzhandzhgava, Sh. G., "Investigation of the Formation of Bubbles and of the Superheat," Dok. Ak. Nauk S. S. S. R., vol. 70, No. 3, 1950, p. 417
63. Ellion, M. E., Mechanism of Boiling Heat Transfer, Jet Propulsion Laboratory Memo No. 20-88, California Institute of Technology, March 1, 1954
64. Elrod, Jr., H. G., Turbulent Heat Transfer in Polygonal Flow Sections, NDA 10-7

Contrails

65. Faber, E. A. and Scoria, R. L., Trans. ASME, vol. 70, 1948, pp. 369-383
66. Forster, H. K., "On the Conduction of Heat into a Growing Vapor Bubble," Journal of Applied Physics, vol. 25, August 1954, pp. 1067-1068
67. Forster, H. K. and Zuber, N., "Growth of a Vapor Bubble in a Superheated Liquid," Journal of Applied Physics, vol. 25, April 1954, pp. 474-478
68. Forster, H. K. and Zuber, N., "Dynamics of Vapor Bubbles to Boiling Heat Transfer," A.I.Ch.E. Journal, vol. 1, December 1955, pp. 531-535
69. Forster, K. F. and Greif, "Heat Transfer to Boiling Liquid: Mechanism and Correlation," Trans. ASME, vol. 81, February 1959
70. Foust, A. S., Baker, E. M., and Badger, W. L., Trans. A.I.Ch.E., vol 35, 1939, pp. 45-71
71. Frenkel, J., Kinetic Theory of Liquids, Oxford University Press, 1946, p. 336
72. Fried, L., "Pressure Drop and Heat-Transfer for Two-Phase Two-Component Flow," CEP Symposium Series No. 9, vol. 5D
73. Fritz, W., Physik. Z., vol. 36, 1935, p. 379
74. Gambill, W. R. and Greene, N. D., "Boiling Burnout with Water in Vortex Flow," Chemical Engineering Progress, vol. 54, October 1958, pp. 68-76
75. Gambill, W. R., Bundy, R. D., and Wansbrough, R. W., "Heat Transfer, Burnout and Pressure Drop for Water in Swirl Flow Through Tubes with Internal Twisted Tapes," ORNL-2911
76. Garabedian, P. R., "On the Steady-State Bubbles Generated by Taylor Instability," Proc. Roy. Soc., London, A-241, 1957, p. 423
77. Gilmour, C. H., "Nucleate Boiling - A Correlation," Sec. Nat. Heat Transfer Conference, ASME, August 1958
78. Goldman, K. (Nuclear Development Associates, Inc.), "Heat Transfer to Supercritical Water and Other Fluids with Temperature Dependent Properties," Nuclear Engineering, Part I, Chemical Engineering Progress Symposium, Series No. 11, 1954, pp. 105-113
79. Green, S. J., Estimated Film Boiling Heat Transfer Coefficients at Burnout, Westinghouse Atomic Power Division, TH-132, September 1955
80. Green, S. J., Preliminary Investigation of the Effects of Vertically Downward Flow on Burnout Flux, Westinghouse Atomic Power Division, NDA, April 1956
81. Green, S. J. and Dibel, H. F., In-Pile Transfer Burnout Test at MTR, Westinghouse Atomic Power Division, LSR(IM)-1-2

Contrails

82. Griffith, P., Bubble Growth Rates in Boiling, Sc.D. Thesis, Massachusetts Institute of Technology, 1956 (Technical Report No. 8); Trans. ASME, vol. 80, 1958
83. Griffith, P., The Correlation of Nucleate Boiling Burnout Data, Massachusetts Institute of Technology Technical Report No. 9
84. Griffith, P. and Wallis, J. D., The Role of Surface Conditions in Nucleate Boiling, Massachusetts Institute of Technology, Technical Report No. 14, December 1958
85. Gunther, F. C., Photographic Study of Surface-Boiling Heat Transfer to Water with Forced Convection, Jet Propulsion Lab, MR6050, JJJ, California Institute of Technology, 1950
86. Gunther, F. C., "Boiling Heat Transfer to Water with Forced Convection," Trans. ASME, vol. 73, No. 2, February 1951
87. Gunther, F. C., Photographic Study of Surface-Boiling Heat Transfer to Water with Forced-Convection, Jet Propulsion Lab Progress Report No. 4-75, California Institute of Technology, June 28, 1956
88. Gunther, F. C. and Kreith, F., Proceedings of Heat Transfer and Fluid Mechanics Institute, 1949, pp. 113-126
89. Gunther, F. C. and Kreith, F., Photographic Study of Bubble Formation in Heat Transfer to Subcooled Liquids, Heat Transfer and Fluid Mechanics Institute, Berkeley, 1949, p. 113
90. Hage, H. J. and Brickwedde, F. G., Rate of Heat Transfer from a Horizontal, Heated Copper Tube in Boiling Liquid Hydrogen or Oxygen, National Bureau of Standards, A-366, November 1942
91. Harrison, W. B., Levine, Z., and Thomas, F. A., "Wetting Effects on Boiling Heat Transfer," Nuclear Science Abstracts, 1955
92. Harvey, E. N., Barnes, D. K., et al, Journal of American Chemical Society, vol. 67, 1945, pp. 156-157
93. Hayes, V. R. and Bartol, J. A., Heat Transfer to Water Flowing at Very High Velocities, Thesis, Massachusetts Institute of Technology, 1944
94. Haywood, R. W., Proceedings of the General Discussion on Heat Transfer, Institute of Mechanical Engineers, London and New York, ASME, 1951, pp. 63-65
95. Hunt, T. W., Jacket, H. S., and Roarty, J. D., An Investigation of Subcooled and Quality Burnout in Circular Channels, Westinghouse Atomic Power Division LSR(IM)-1, January 26, 1955
96. Insiger, T. H. and Bliss, H., "Transmission of Heat to Boiling Liquids," Trans. A.I.Ch.E., vol. 36, 1940, p. 491
97. Jacket, H. S., Roarty, J. D., and Sher, N. C., Boiling Pressure Drop in Rectangular Channels, Westinghouse Atomic Power Division TH-204, May 7, 1956

Contrails

98. Jakob, M., "Heat Transfer in Evaporation and Condensation," Mechanical Engineer, vol. 58, 1936, pp. 643-660
99. Jakob, M., Heat Transfer, Volume 1, J. Wiley & Sons Inc., New York, 1956
100. Jakob, M. and Fritz, W., Forsch Gebiete Ingenieur, vol. 2, 1931, pp. 434-447
101. Jakob, M. and Linke, W., Forsch Gebiete Ingenieur, vol. 4, 1933, pp. 75-78
102. Jens, W. H., "Boiling Heat Transfer: What Is Known About It," Mechanical Engineering Monthly, December 1954
103. Jens, W. H., and Leppert, G., Journal American Society Naval Engineers, vol. 67, 1955, p. 137
104. Jens, W. H. and Leppert, G., Journal American Society Naval Engineers, vol. 68, 1955, p. 437
105. Jens, W. H. and Lottes, P. A., Analysis of Heat Transfer Burnout, Argonne National Laboratory 4627, 1951
106. Johnson, H. A. and Abou-Sabe, A. H., "Heat Transfer and Pressure Drop for Turbulent Flow of Air-Water Mixtures in Horizontal Pipes," Trans. ASME, vol. 74, 1952, p. 977
107. Jordan, D. P. and Leppert, G., "Nucleate Boiling Characteristics of Organic Reactor Coolants," Nuclear Science and Engineering, vol. 5, No. 6, June 1959
108. Kaufman, S. J. and Isely, F. D., Preliminary Investigation of Heat Transferred to Water Flowing in an Electrically Heated Inconel Tube, National Advisory Committee for Aeronautics, RM-E 50G 31, September 1950
109. Kaulakis, A. F. and Sherman, L. M., Thesis in Chemical Engineering, Massachusetts Institute of Technology, 1938
110. Kazakova, E. A., Engineers Digest, vol. 12, 1951, pp. 81-85
111. King, W. J., "The Basic Laws and Data of Heat Transmission," Mechanical Engineer, vol. 54, August 1932, pp. 560-562
112. Kirschbaum, E., Krans, B., and Starck, D., VD1-Forschungheft 375, 1935
113. Knowles, J. W., Heat Transfer with Surface Boiling, Montreal Laboratories of the National Research Council, M Tec-187, February 16, 1946
114. Knowles, J. W., Canadian Journal of Research, vol. 26, 1948, pp. 268-270
115. Knudsen, J. G. and Katz, D. L., "Heat Transfer and Pressure Drop in Annuli," Chemical Engineering Progress, vol. 46, 1950, p. 490
116. Kreith, F. and Margolis, D., "Heat Transfer and Friction in Turbulent Vortex Flow," Appl. Sci. Res. Section A, vol. 8, 1959, pp. 457-473

Contrails

117. Kreith, F. and Summerfield, M., Investigation of Heat Transfer at High Heat Flux Densities: Literature Survey and Experimental Study in Annulus, Jet Propulsion Laboratory JPL-PR-4-65, California Institute of Technology, February 20, 1948
118. Kreith, F. and Summerfield, M., "Heat Transfer to Water at High Flux Densities with and without Surface Boiling," Trans. ASME, vol. 71, No. 7 October 1949
119. Kreith, F. and Summerfield, M., "Pressure Drop and Convective Heat Transfer with Surface Boiling at High Heat Flux; Data for Aniline and n-Butyl Alcohol," Trans. ASME, vol. 72, 1950, p. 869
120. Kreith, F. and Summerfield, M., Investigation of Heat Transfer at High Heat Flux Densities: Experimental Study with Water of Friction Drop and Forced Convection with and without Surface Boiling in Tubes, Jet Propulsion Laboratory JPL-PR-4-68, California Institute of Technology
121. Kruzhelein, G. N., Generalization of the Experimental Data on the Heat Transmission at the Boiling of Liquids Under the Conditions of Free Convection, Atomic Energy Commission Technical Report 2000, 1949
122. Kruzheilin, G. N., Generalization of Experimental Data of Heat Transfer to Boiling Liquids in Free Convection, Izv. Akad. Nauk S. S. S. R., No. 3, 1949, p. 701, Atomic Energy Commission Translation RT 2542
123. Kutateladze, S. S., Hydromechanical Model of the Critical Condition of Heat Transfer in Boiling Liquids for the Case of Free Convection, Zhur. Tekh. Fiz., vol. 20, 1950, pp. 1389-1392, Atomic Energy Commission Technical Report 1858
124. Kutateladze, S. S., A Hydrodynamic Theory of Changes in the Boiling Process Under Free Convection Conditions, Izv. Akad. Nauk S. S. S. R., Otd. Tekh. Nauk, No. 4, 1951, pp. 529-536, Atomic Energy Commission Technical Report 1441
125. Kutateladze, S. S., Heat Transfer in Boiling and Condensation, Mashgiz, Moscow, 1952
126. Kutateladze, S. S. and Schneiderman, L. L., "Experimental Study of the Influence of the Temperature of a Liquid on the Change of the Rate of Boiling," Problems of Heat Transfer During a Change of State, Moscow, 1953
127. Larson, R. T., "Factors Affecting Boiling in a Liquid," Industrial Engineering Chemistry, vol. 37, 1945, p. 1004
128. Levy, S., "Generalized Correlation of Boiling Heat Transfer," Trans. ASME, vol. 81, 1959, p. 37
129. Levy, S., Fuller, R. A., and Niemi, R. O., "Heat Transfer to Water in Thin Rectangular Channels," Trans. ASME, vol 81, May 1959, p. 129
130. Lottes, P. A., "Effects of Channel Geometry on the Power Density of a

Contrails

- Natural Circulation Boiling Channel at 300 psia," Argone National Laboratory Quarterly Report, January through March 1955
131. Lowdermilk, W. H. and Weiland, W. F., Some Measurements of Boiling Burnout, National Advisory Committee for Aeronautics, RM-E 54K10, November 23, 1954
 132. Lukomskii, S. M., "Heat Transfer at Boiling," Izv. Akad. Nauk S. S. S. R., No. 12, 1946, pp. 1753-1765
 133. Lukomskii, S. M. (Bevitt), An Investigation of the Maximum Heat Flux During the Boiling of Water in Vertical Tubes, IC-Trans-R-3
 134. Lyon, R. E., Foust, A. S., and Katz, D. L., A.I.Ch.E. Heat Transfer Symposium, St. Louis, Missouri, December 1953
 135. Martinelli, R. C. and Nelson, D. B., "Prediction of Pressure Drop During Forced Circulation Boiling of Water," Trans. ASME, August 1948
 136. Marx, J. W. and Davis, B. I., "Film Boiling Termination Mechanism," Journal of Applied Physics, vol. 23, 1952, p. 1354
 137. McAdams, W. H., Heat Transmission, Edition 3, Chapter 14, McGraw-Hill Book Company, Inc., New York, 1954
 138. McAdams, W. H., Addoms, J. N., and Kennel, W. E., "Heat Transfer Rates to Water with Surface Boiling," AECU 200
 139. McAdams, W. H., Addoms, J. N., Renaldo, P. M., and Day, R. S., Chemical Engineering Progress, vol. 44, 1948, pp. 639-646
 140. McAdams, W. H., Woods, W. K., and Byran, R. L., "Vaporization Inside Horizontal Tubes," Trans. ASME, vol. 63, 1941, p. 545
 141. McLean, E. H., Scherrer, V. E., and Faneuff, C. E., "Nucleate and Film Boiling Due to Repetitive Pulse Heating of Small Wires Immersed in Water," Preprints of Reactor Heat Transfer Conference, November 1956
 142. Mead, B. R., Romie, T. E., and Guibert, A. G., "Liquid Superheat and Boiling Heat Transfer," 1951 Heat Transfer and Fluid Mechanics Institute Preprints, Stanford University Press, 1951, p. 209
 143. Merte, Jr., H. and Clark, J. A., A Study of Pool Boiling in an Accelerating System, University of Michigan Research Institute Project No. 2646, November 1959
 144. Minden, G. S., Heat Transfer to Water Flowing in an Annulus, Thesis, Massachusetts Institute of Technology, 1947
 145. Morgan, A. I., Bromley, L. A., and Wilke, C. R., Industrial & Engineering Chemistry, vol. 41, 1949, pp. 2767-2769
 146. Motte, E. I., Film Boiling of Flowing Subcooled Liquid, Thesis, University of California Radiation Laboratory 2511, June 1954

Contrails

147. Mumm, J. F., "Heat Transfer to Boiling Water Forced Through an Electrically-Heated Tube," Reactor Heat Transfer Information Meeting, Brookhaven National Laboratory, BNL-2446, October 1954
148. Nukiyama, S. J., Society of Mechanical Engineers, Japan, vol. 37, 1934, pp. 367-374, 553-554
149. Peck, R. E. and Reddie, W. A., "Heat Transfer Coefficient for Vaporization Conditions on Horizontal Tubes," Industrial & Engineering Chemistry, vol. 43, 1951, p. 2926
150. Plesset, M. and Zwick, S. A., "A Non-Steady Diffusion Problem with Spherical Symmetry," Journal of Applied Physics, vol. 23, 1952, p. 95
151. Plesset, M. and Zwick, S. A., "The Growth of Vapor Bubbles in Superheated Liquids," Journal of Applied Physics, vol. 25, 1954, pp. 493-500
152. Plesset, M. and Zwick, S. A., "On the Dynamics of Vapor Bubbles in Liquids," Journal of Mathematics and Physics, vol. 33, 1955, p. 308
153. Rhodes, F. H. and Bridges, C. H., "Heat Transfer to Boiling Liquid," Trans. A.I.Ch.E., vol 35, 1939, p. 73
154. Roberts, H. A., A Review of Net Boiling Transfer and Pressure Drop from the Literature, A.E.R.E. ED/M 22, 1955
155. Robinson, D. B. and Katz, D. L., "Effect of Vapor Agitation on Boiling Coefficients," Chemical Engineering Progress, vol. 47, 1951, p. 317
156. Rohsenow, W. M., "A Method of Correlating Heat-Transfer Data for Surface Boiling Liquids," Trans. ASME, vol. 74, 1952, p. 969
157. Rohsenow, W. M., Boiling Burnout Newsletter No. 2, Brookhaven National Laboratory, January 5, 1955
158. Rohsenow, W. M. and Clark, J. A., "Heat Transfer and Pressure Drop Data for High Heat Flux Densities to Water at High Sub Critical Pressures," 1957 Heat Transfer and Fluid Mechanics Institute, Stanford University Press, p. 193
159. Rohsenow, W. M. and Clark, J. A., "Study of the Mechanism of Boiling Heat Transfer," Trans. ASME, July 1951, p. 609
160. Rosenthal, M. W., "Transient Boiling Investigation," Reactor Heat Transfer Progress, Nuclear Development Associates-26, April 27, 1956 .
161. Sabersky, R. H. and Gates, C. W., "On the Start of Nucleation in Boiling Heat Transfer," Jet Propulsion, vol. 25, February 1955, p. 67
162. Sabersky, R. H. and Mulligan, H. E., "On the Relationship Between Fluid Friction and Heat Transfer in Nucleate Boiling," Jet Propulsion, vol. 25, January 1955, p. 9

Contrails

163. Sarukhanian, G., Heat Transfer on Evaporation, Atomic Energy Commission Technical Report 2063, 1953
164. Sauer, E. T., Cooper, H. B. H., Akin, G. A., and McAdams, W. H., "Heat Transfer to Boiling Liquids," Mechanical Engineer, vol. 60, 1938, p. 669
165. Scherrer, V. E., McLean, E. A., and Faneuff, C. E., "Study of the Boiling Process," Boiling Burnout Progress, Naval Research Laboratory, February 23, 1956
166. Schmidt, E. H. W., "Heat Transmission by Natural Convection at High Centrifugal Acceleration in Water-Cooled Gas-Turbine Blades," Proceedings of the General Discussion on Heat Transfer, London, September 1951
167. Schwarz, K., Investigations of the Density Distribution, Water and Steam Velocities as Well as the Pressure Loss in Vertical and Horizontal Up-Flow Boiler Tubes, Atomic Energy Commission Technical Report 2314, 1954
168. Scorah, R. L., "Heat Transfer from Metal to Boiling Water," Heat Transfer Lectures Volume I, AECU-116, NEPA-804, December 1948
169. Sieder, E. N. and Tate, G. E., "Heat Transfer and Pressure Drop of Liquids in Tubes," Industrial & Engineering Chemistry, vol. 28, 1936, p. 1429
170. Siegel, R. and Usiskin, G., "A Photographic Study of Boiling in the Absence of Gravity," 1959 Aviation Conference, Los Angeles, ASME Paper 59-AV-37
171. Sterman, L. S., "Theory of Heat Transfer in Boiling Liquids," Zhur. Tekh. Fiz., vol. 23, 1953, p. 342
172. Sterman, L. S., "On the Theory of Heat Exchange on Boiling in Pipes," Heat Transfer (Boiling), A.E.R.E. Liberal Translation 579
173. Sterman, L. S., "Investigation of Heat Exchange by Boiling Liquids in Tubes," Zhur. Tekh. Fiz., vol. 24, 1954, p. 2046; A.E.R.E. Translation 565
174. Stroebe, et al, Industrial & Engineering Chemistry, vol. 31, 1939, pp. 200-206
175. Tagaki, S., "Theory of Formation of Bubbles," Journal of Applied Physics, vol. 24, December 1953, pp. 1453-1462
176. Taylor, G. I., "The Instability of Liquid Surfaces When Accelerated in a Direction Perpendicular to Their Plane," Proc. Roy. Soc., London, A-202, 1950, p. 81
177. Treschov, G. G., "Experimental Investigation of the Mechanism of Heat Transfer in Surface Boiling," Teploenergetika, vol. 3, No. 5, 1957, p. 44
178. Trilling, L., "The Collapse and Rebound of a Gas Bubble," Journal of Applied Physics, vol. 23, 1952, p. 14

Contrails

179. Trusela, R. A. and Clodfelter, R. G., "Heat Transfer Problems of Space Vehicle Power Systems," Preprint 154C, S.A.E. National Aeronautic Meeting, April 5-8, 1960
180. Untermeyer, S., "Boiling Reactors: Direct Steam Generation for Power," Nucleonics, vol. 12, No. 7, 1954, p. 43
181. Usiskin, C. M. and Siegel, R., An Experimental Study of Boiling in Reduced and Zero Gravity Fields, ASME Paper 60-HT-10
182. Wallis, C. and Griffith, P., Liquid and Gas Distribution in a Two-Phase Boiling Analogy, Massachusetts Institute of Technology Technical Report No. 13, December 1958
183. Weatherhead, R. J., Burnout with Net Steam Generation in Vertical, Round and Rectangular Channels at 2000 psia, Argonne National Laboratory, October 4, 1956
184. Westwater, J. W., "Boiling of Liquids," Advances in Chemical Engineering, Academic Press Inc., New York, 1956
185. Westwater, J. W. and Perkins, A. S., "Measurements of Bubbles Formed in Boiling Methanol," A.I.Ch.E. Journal, vol. 2, 1956, p. 471
186. Westwater, J. W. and Santagelo, J. G., "Photographic Study of Boiling," Industrial & Engineering Chemistry, vol. 47, August 1955, pp. 1065-1070
187. Wigner, E. P., Rate of Rise of Bubbles, Atomic Energy Commission Document-1983, April 7, 1944
188. Wisner, K. L., Jour. Phys. Chem., vol. 26, 1922, p. 301
189. Zuber, N., Thesis for Master of Science Degree, University of California, Los Angeles, 1954
190. Zuber, N., Stability of Boiling Heat Transfer, ASME Paper 57-HT-4
191. Zuber, N., On the Maximum Heat Flux in Pool Nucleate Boiling of Subcooled Liquids, Department of Engineering Memorandum, University of California, Los Angeles, 1957
192. Zuber, N., Hydrodynamic Aspects of Boiling Heat Transfer, Ph.D. Thesis, University of California, Los Angeles, June 1959
193. Zuber, N. and Tribus, M., Further Remarks on the Stability of Boiling Heat Transfer, Atomic Energy Commission Report AECU 3631, 1958
194. Zwick, S. A. and Plesset, M. S., Notes on the Dynamics of Small Vapor Bubbles in Liquids, ASTIA Document AD-40932, February 1954
195. Zysina-Molozhen, L. M., "Some Data on the Number of Centers of Vaporization in Boiling on Industrial Heating Surfaces," Problems of Heat Transfer During a Change of State, G.E.I., Moscow, 1953

TABLE 6

DESIGN CHARACTERISTICS OF PLATE-FIN EVAPORATORS

Freon Side

Type of fins	Straight
Fin height	0.1 in
No. of fins per inch	10
Fin thickness	0.005 in
Thickness of parting plate	0.014 in
Hydraulic diameter (d_h)	0.00792 ft
Material	Aluminum

Air Side

Type of fins	Herringbone
Fin height	0.45 in
No. of fins per inch	18
Fin thickness	0.005 in
Thickness of parting plate	0.014 in
Material	Aluminum

TABLE 7

DESIGN CHARACTERISTICS OF VORTEX EVAPORATORS

(Reference: Kays, W. M. and London, A. L., Compact Heat Exchangers, McGraw-Hill Book Company, New York, 1958, Figure 100)

Staggered Tubes - Rectangular (Crimped) Fins

$$\text{Tube ID} = 0.25 \text{ in}$$

$$\text{Tube OD} = 0.30 \text{ in}$$

$$S_T = S_L = 0.60 \text{ in}$$

Freon 11 Side

$$A_{\text{free}}/A_{\text{face}} = 0.1362$$

$$\text{Heat Transfer Area/Volume} = 26.18 \text{ sq ft/cu ft}$$

$$d_h = 0.02083 \text{ ft}$$

Air Side

$$\text{Fin thickness (t)} = 0.01 \text{ in}$$

$$\text{Fin height} = 0.15$$

$$\text{No. of fins per inch} = 6.8$$

$$A_{\text{free}}/A_{\text{face}} = 0.534$$

$$\text{Heat Transfer Area/Volume} = 179 \text{ sq ft/cu ft}$$

$$d_h = 0.1192 \text{ ft}$$

TABLE 8
FREON 11 SIDE PRESSURE DROP IN EVAPORATORS

Evaporator Temperature degF	Air-Side ΔT degF	Air-Side ΔP psi	Vortex-Tube		Freon-Side Pressure Drops		Plate-Fin Flow Length Equal to Vortex Tube
			psi	Freon Vapor Exit Velocity	psi	Freon Vapor Exit Velocity	
40	25	0.1	.153	50.0	0.718	61.6	0.36
		0.3	.142	50.0	0.488	55.9	0.29
		0.5	.138	50.0	0.426	54.0	0.25
40	100	0.1	.127	50.0	0.444	67.5	0.234
		0.3	.119	50.0	0.350	64.9	0.190
		0.5	.118	50.0	0.318	64.0	0.184
55	25	0.1	.580	50.0	0.182	13.9	0.164
		0.3	.504	50.0	0.207	12.4	0.178
		0.5	.464	50.0	0.173	11.9	0.159

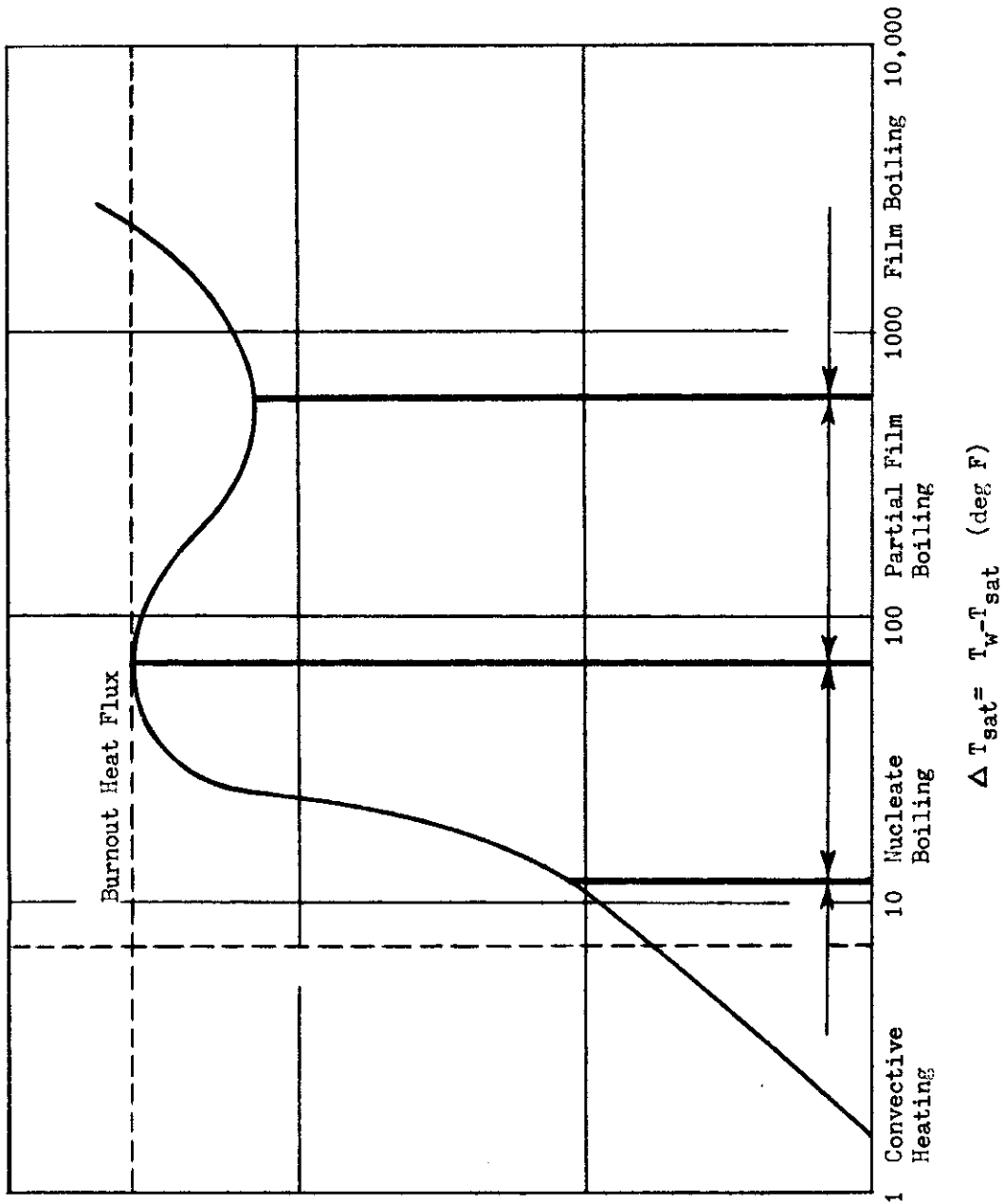


FIGURE 12: REGIMES OF BOILING

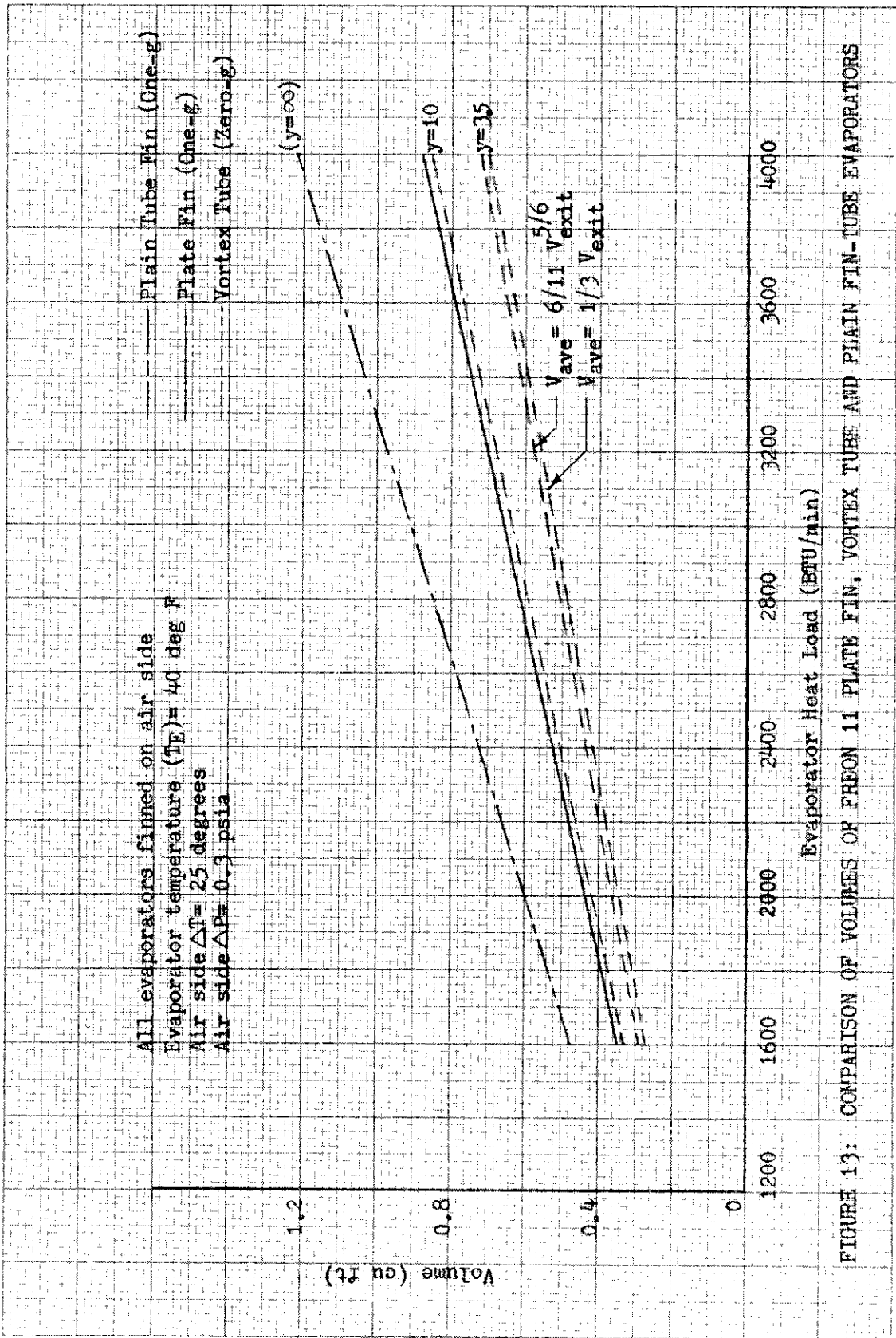


FIGURE 13: COMPARISON OF VOLUMES OF FREON 11 PLATE FIN, VORTEX TUBE AND PLAIN FIN-TUBE EVAPORATORS

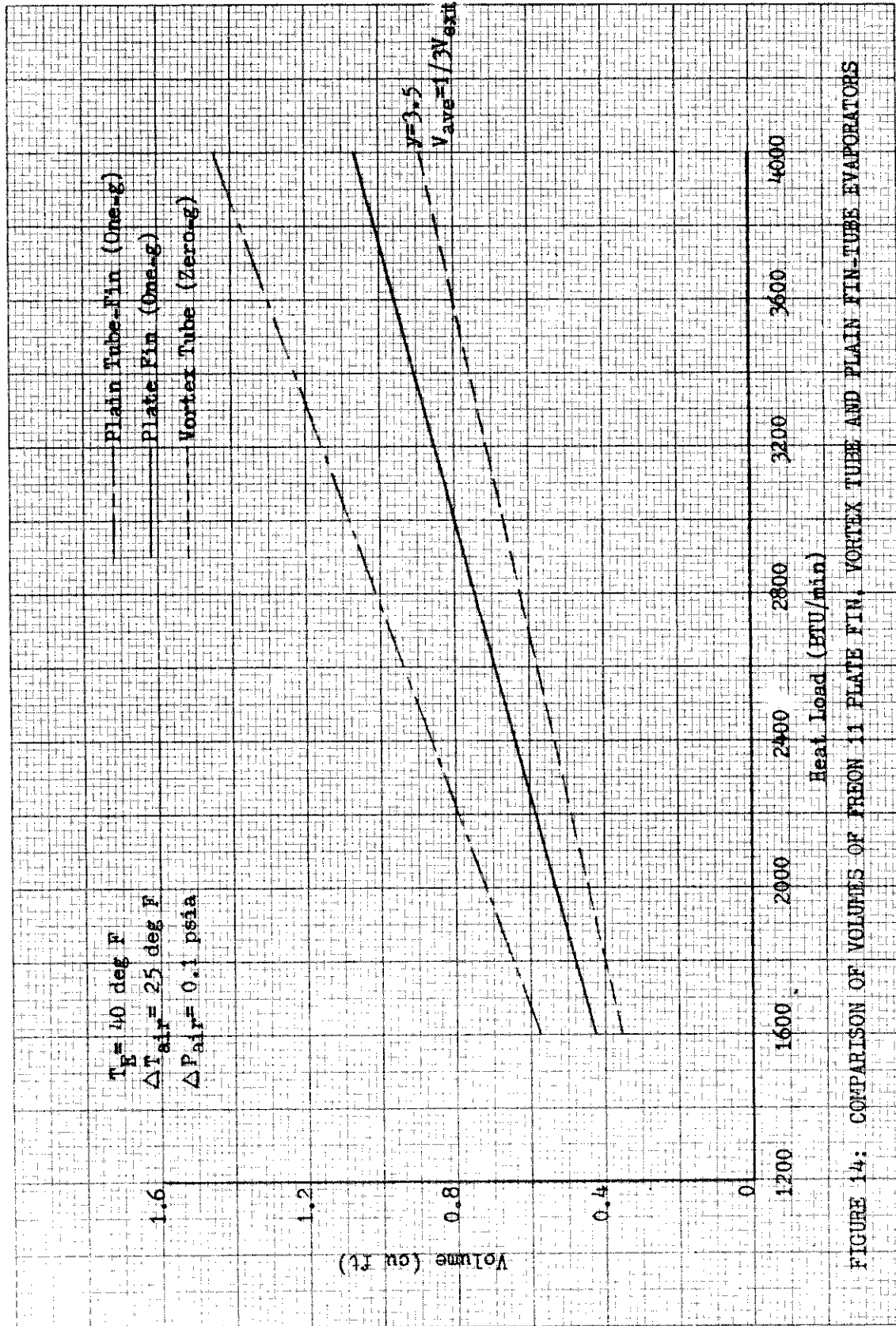


FIGURE 14: COMPARISON OF VOLUMES OF FREON 11 PLATE FIN, VORTEX TUBE AND PLAIN FIN-TUBE EVAPORATORS

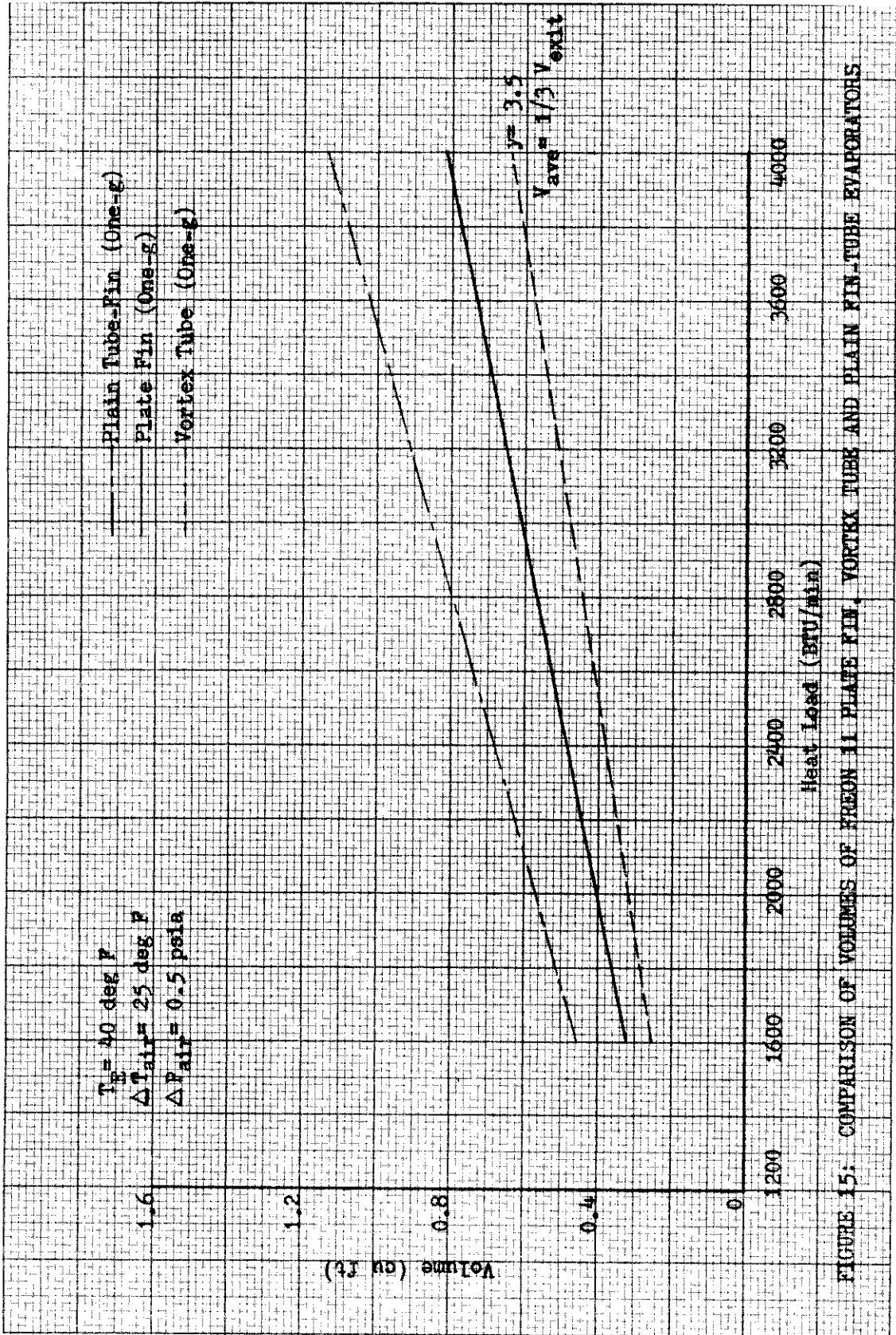


FIGURE 15: COMPARISON OF VOLUMES OF FREON 11 PLATE FIN, VORTEX TUBE AND PLAIN FIN-TUBE EVAPORATORS

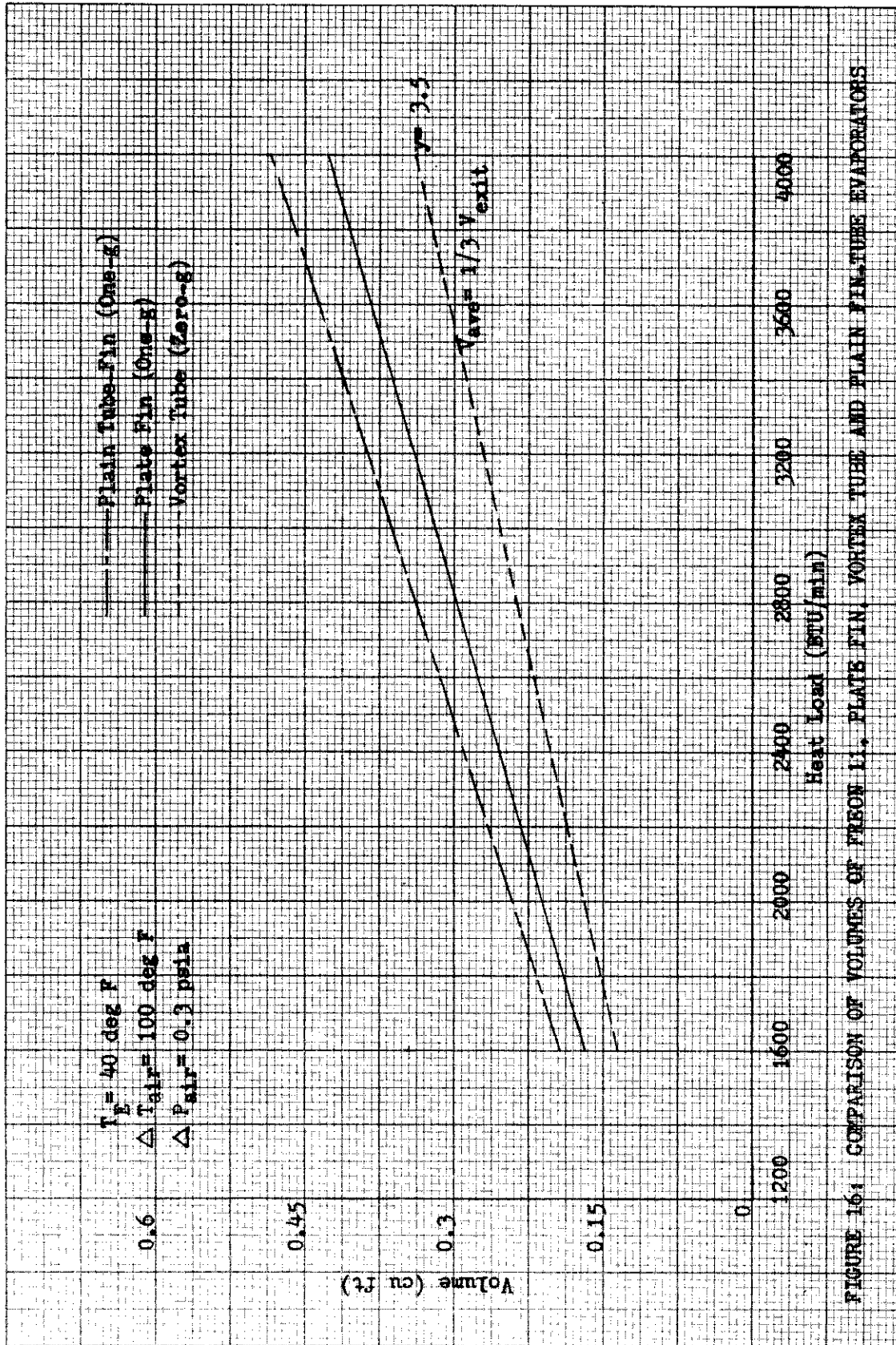


FIGURE 164. COMPARISON OF VOLUMES OF FREON L1, PLATE FIN, VORTEX TUBE AND PLAIN FIN-TUBE EVAPORATORS

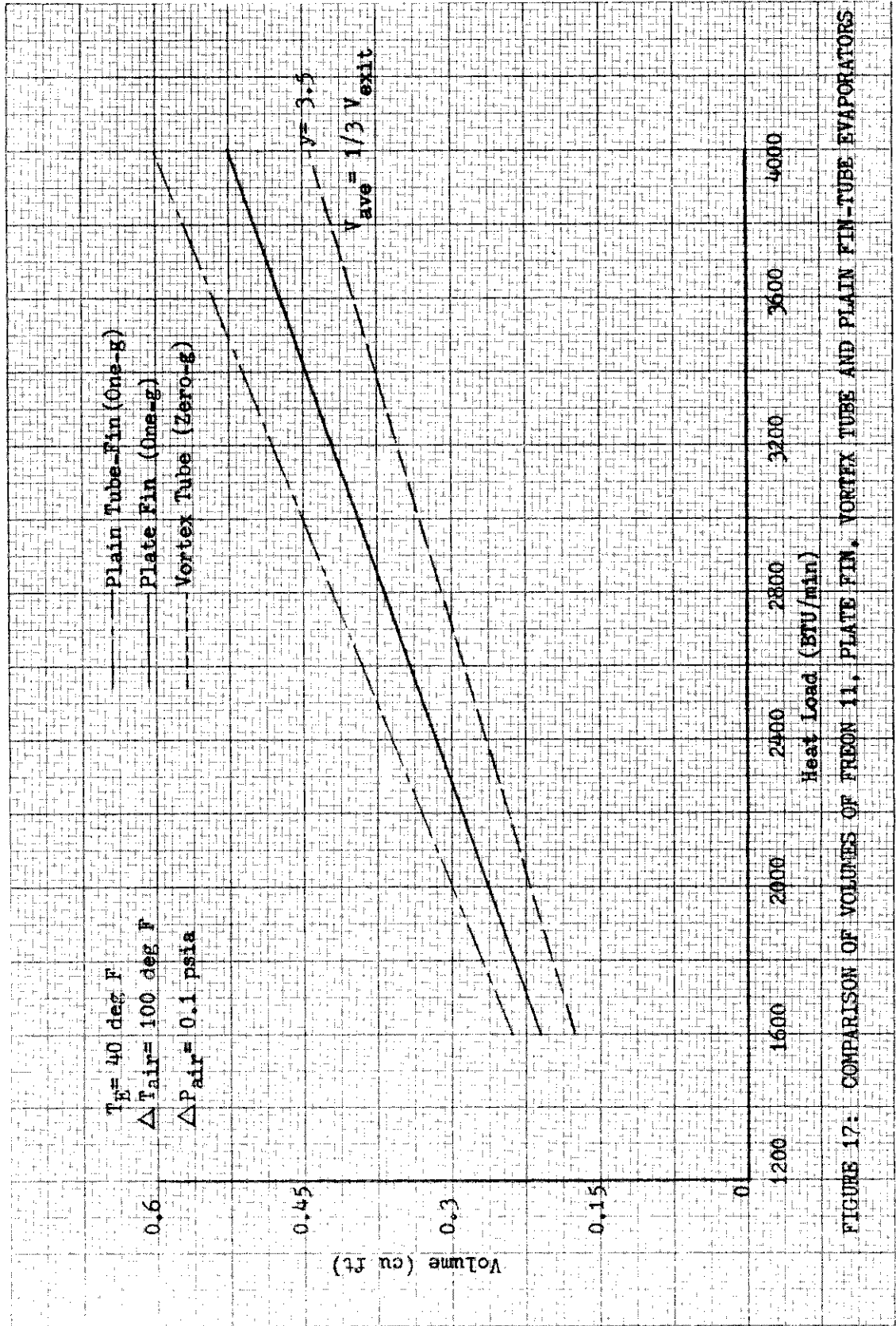


FIGURE 17: COMPARISON OF VOLUMES OF FREON 11, PLATE FIN, VORTEX TUBE AND PLAIN FIN-TUBE EVAPORATORS

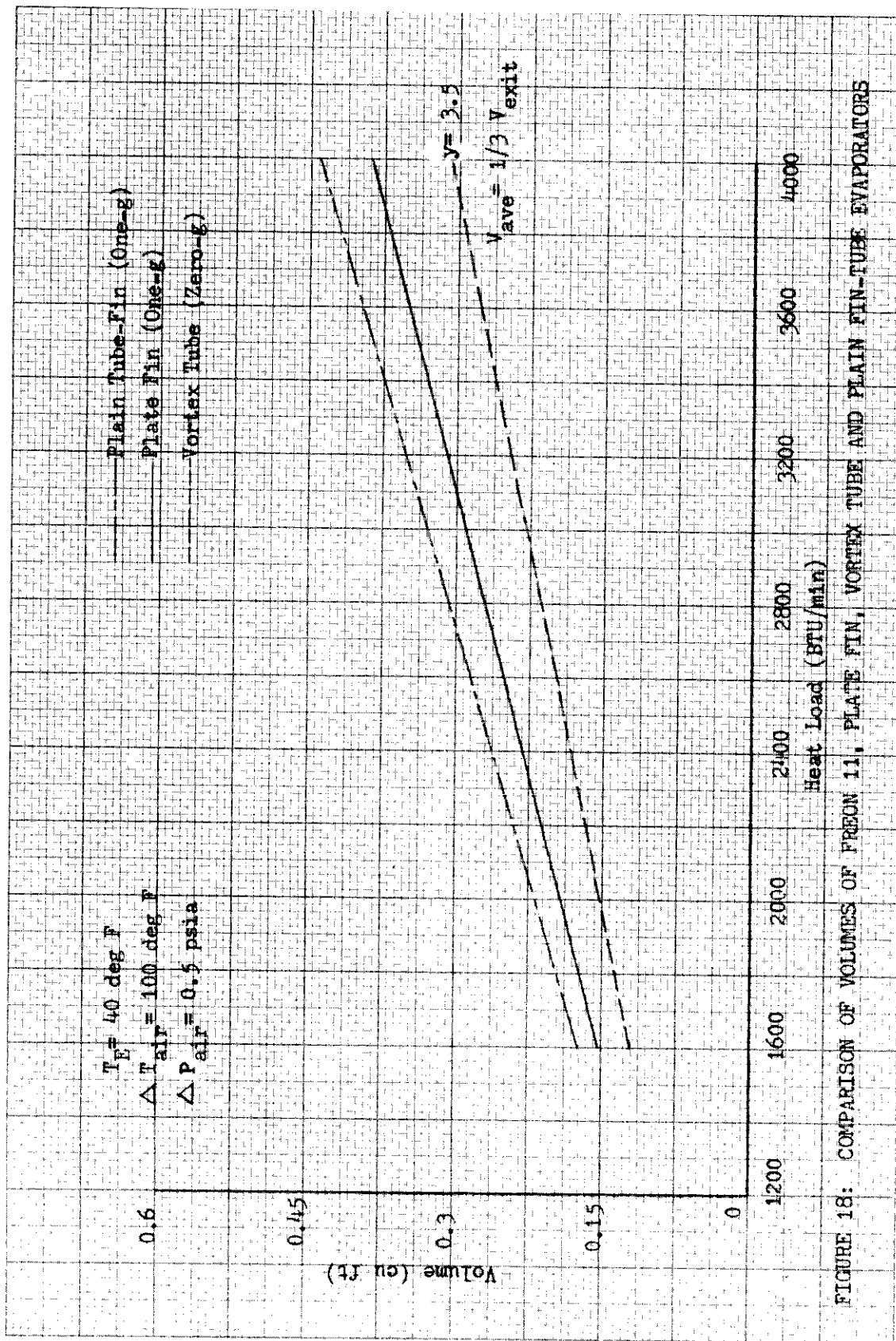


FIGURE 18: COMPARISON OF VOLUMES OF FREON 11, PLATE FIN, VORTEX TUBE AND PLAIN FIN-TUBE EVAPORATORS

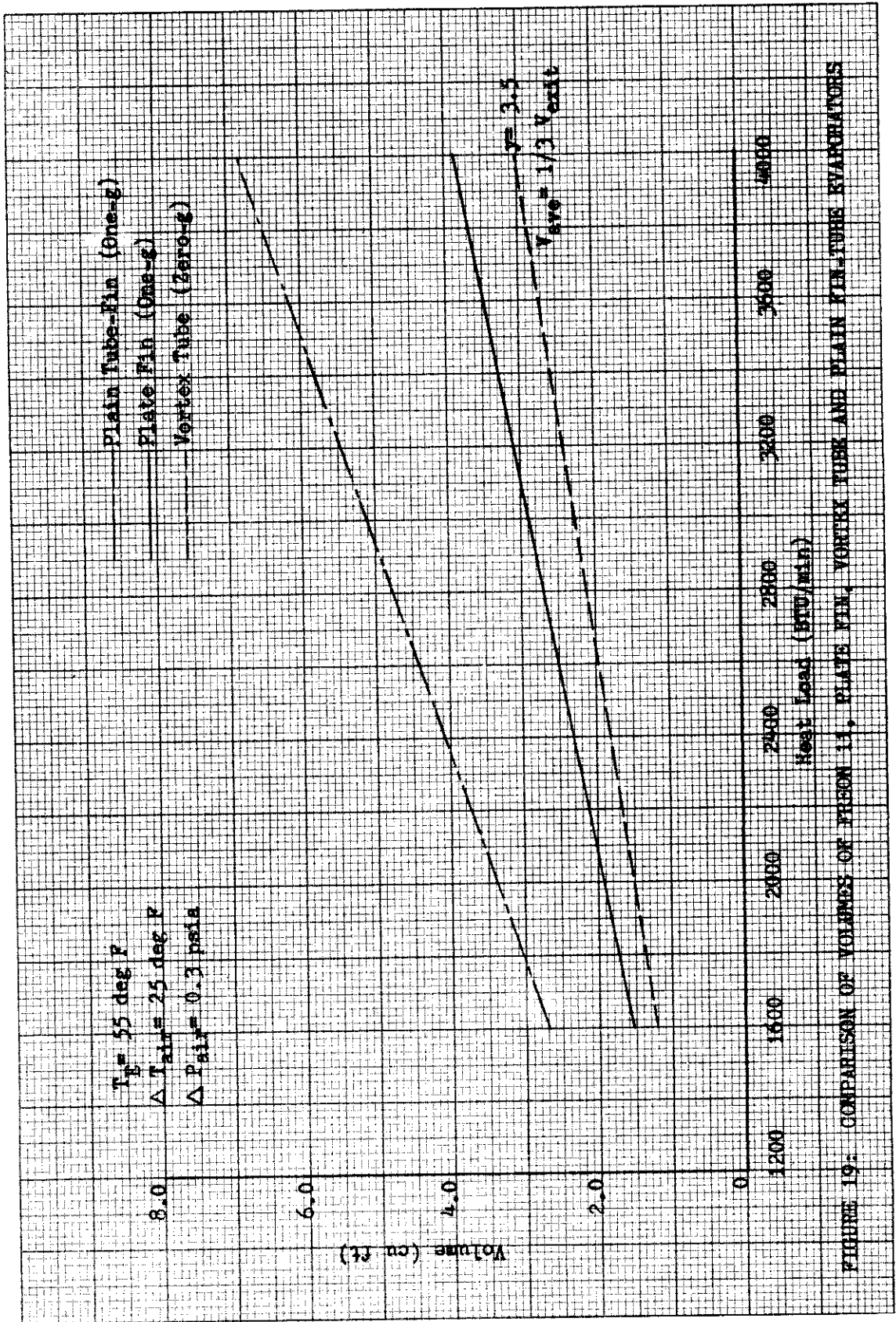


FIGURE 19. COMPARISON OF VOLUMES OF FIGURE 11, PLATE FIN, VORTEX TUBE AND PLAIN FIN-TUBE EXHAUSTORS

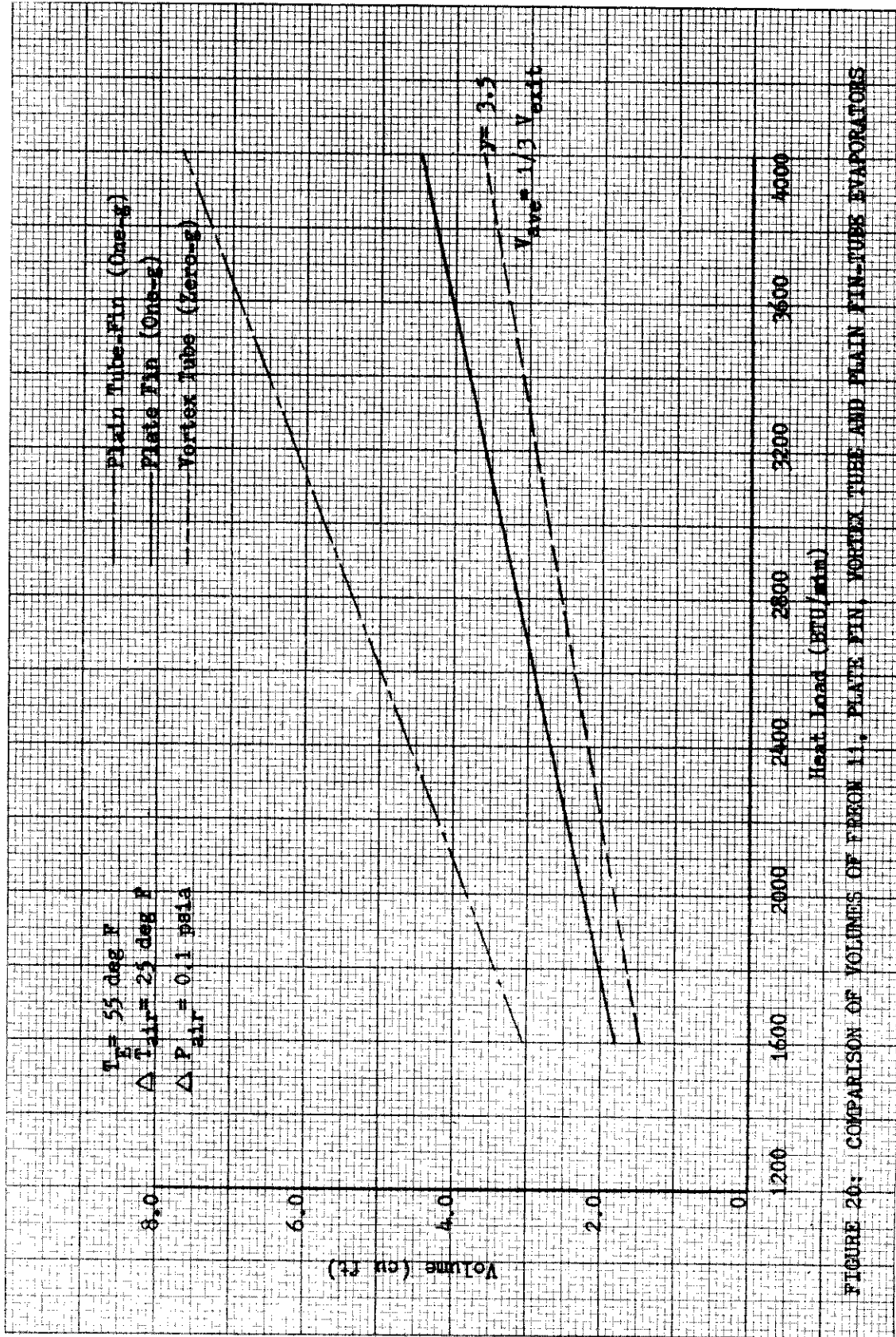


FIGURE 20: COMPARISON OF VOLUMES OF FERON 11, PLATE FIN, VORTEX TUBE AND PLAIN FIN-TUBE EVAPORATORS

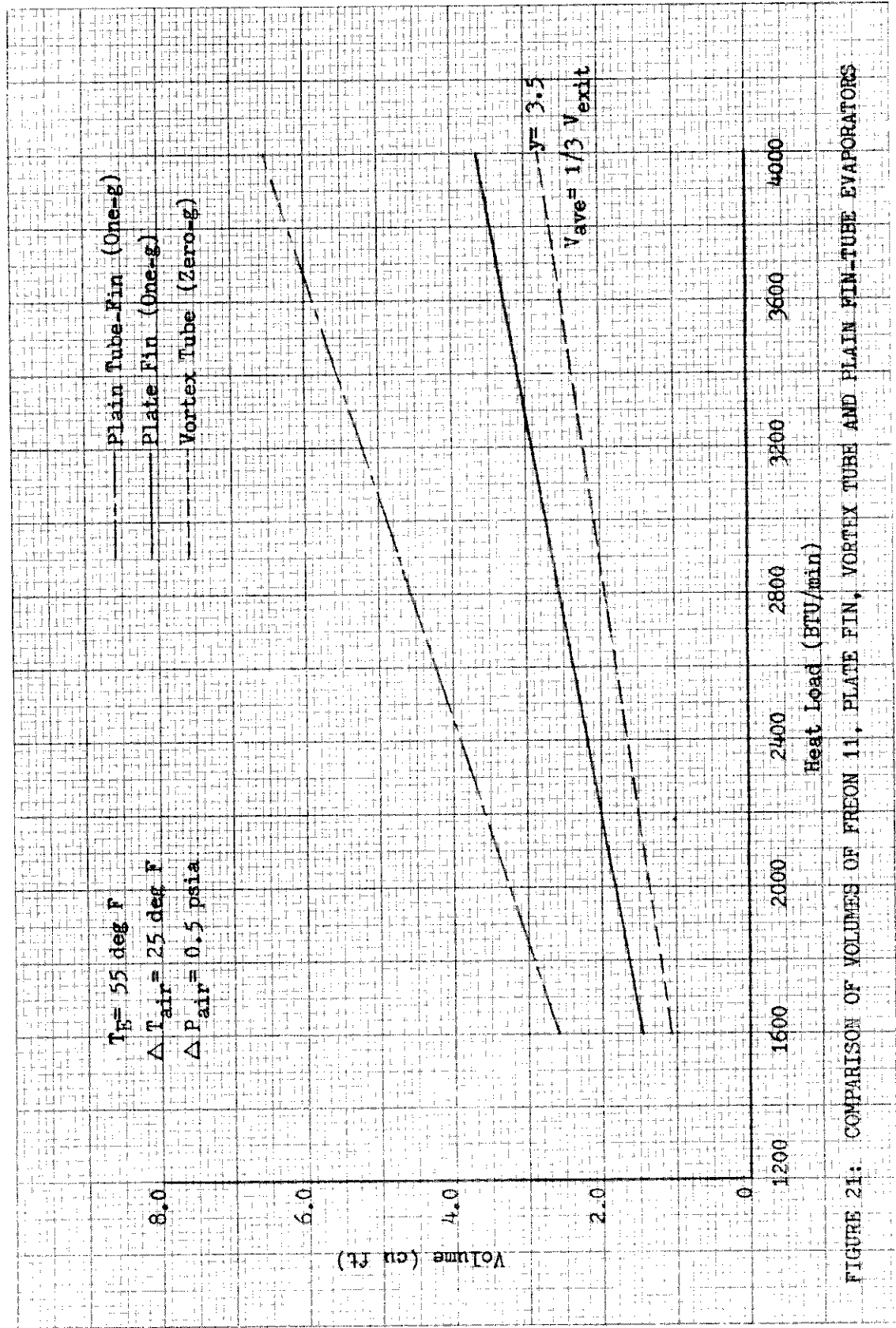


FIGURE 21: COMPARISON OF VOLUMES OF FREON 11, PLATE FIN, VORTEX TUBE AND PLAIN FIN-TUBE EVAPORATORS

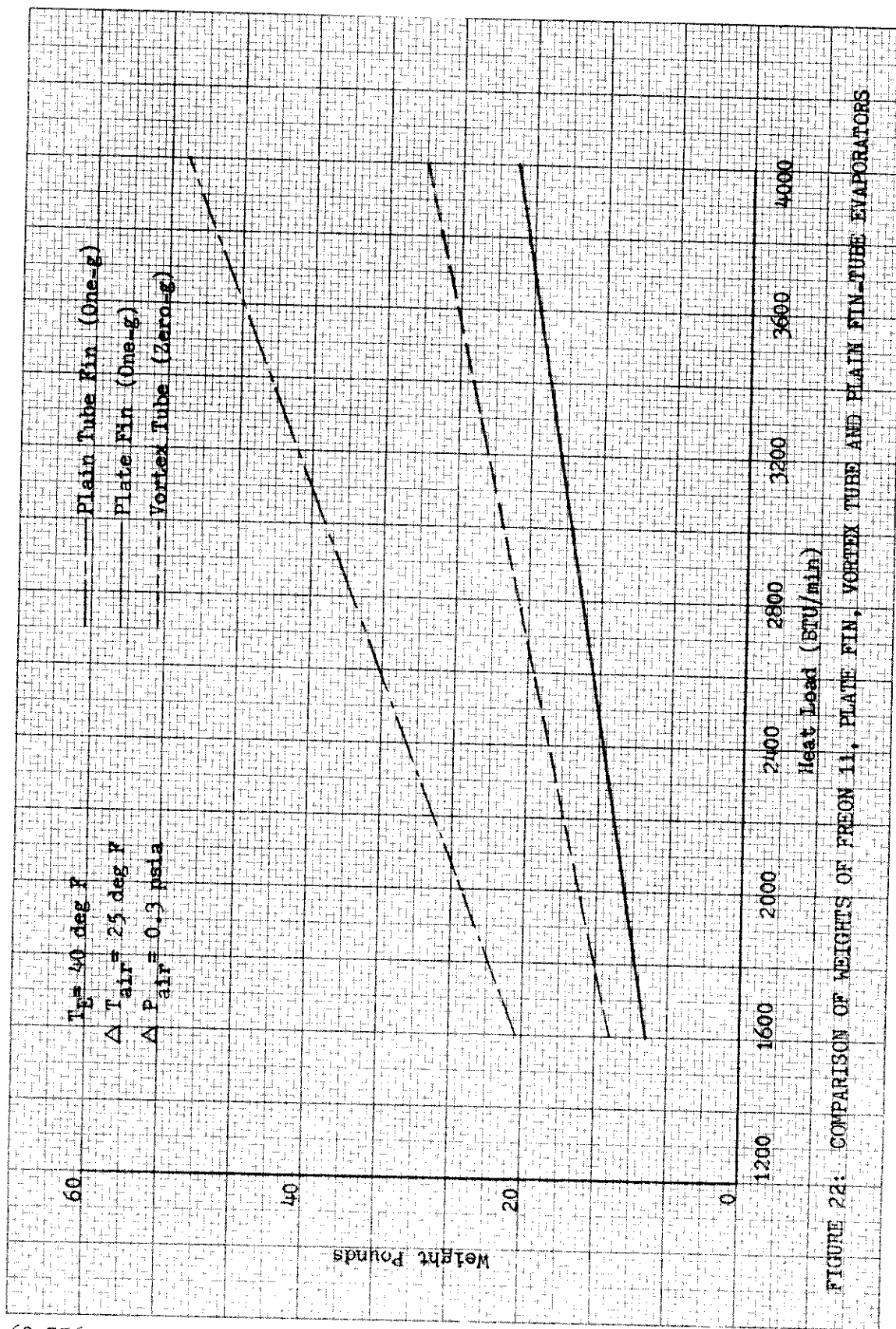


FIGURE 22: COMPARISON OF WEIGHTS OF FREON 11, PLATE FIN, VORTEX TUBE AND PLAIN FIN-TUBE EVAPORATORS

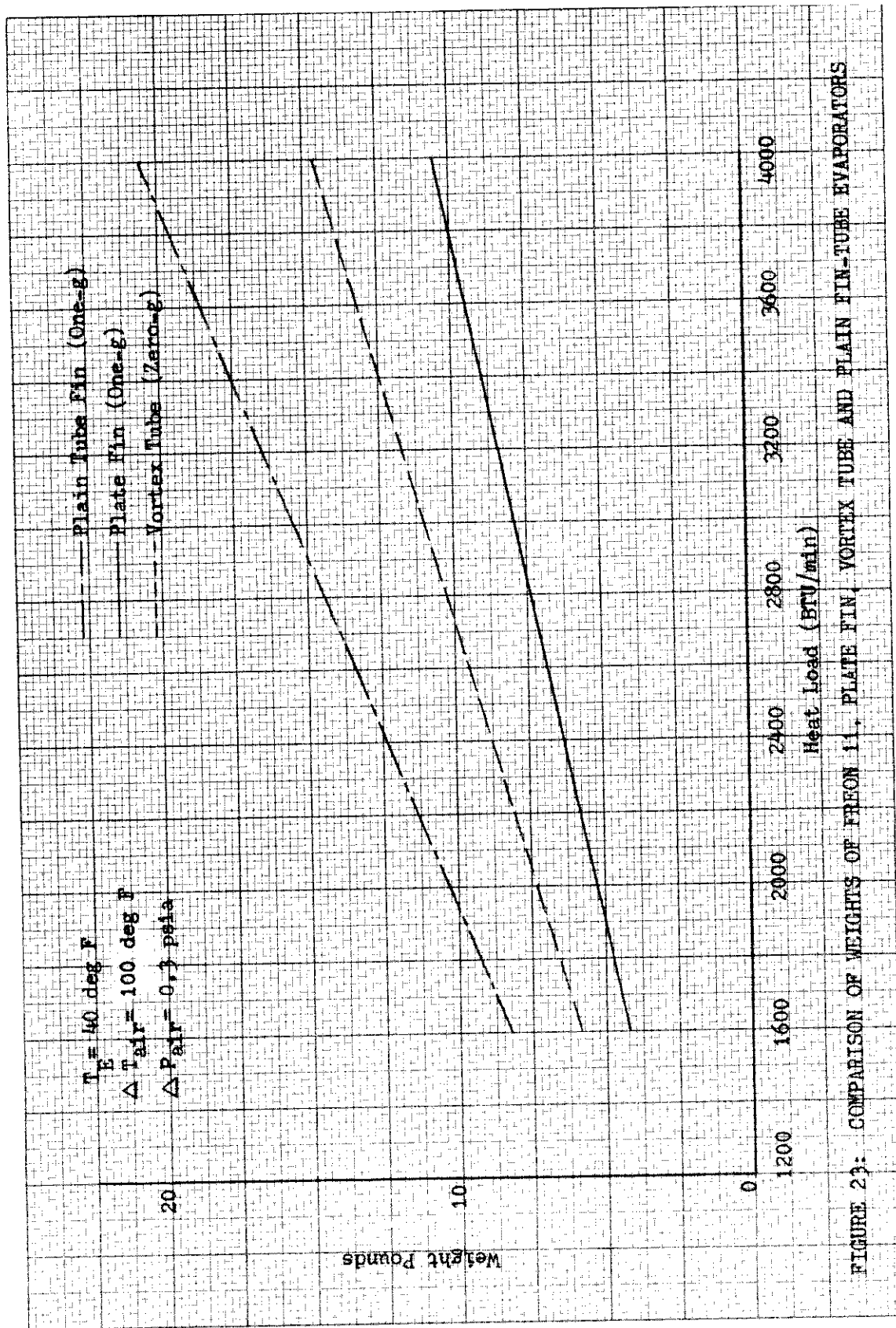


FIGURE 23: COMPARISON OF WEIGHTS OF FFEON 11, PLATE FIN, VORTEX TUBE AND PLAIN FIN-TUBE EVAPORATORS

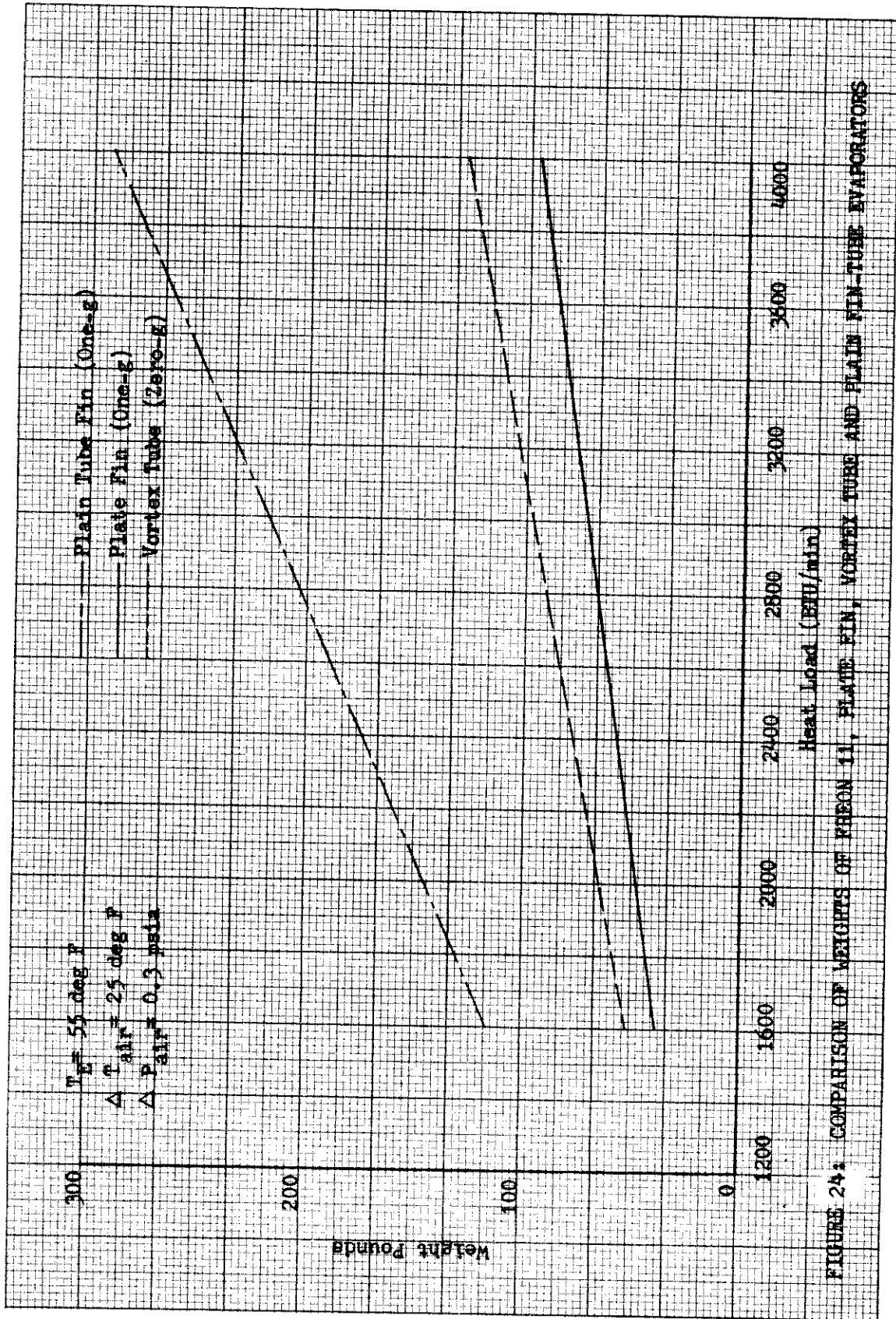


FIGURE 24: COMPARISON OF WEIGHTS OF KHEON 11, PLATE FIN, VORTEX TUBE AND PLAIN FIN-TUBE EVAPORATORS

Contrails

Contrails

SECTION VI

ROTATING CONDENSER STUDY

It has been indicated in a previous section that an obvious way to overcome the absence of the gravity force in any equipment which depends on this force for satisfactory operation is to provide an artificial force to compensate for the absent body forces. In this way, density differences between liquid and vapor may still be used for separation. In this study, the artificial force is supplied by rotating the equipment itself, in contrast to the spiral condenser where the body forces are induced in the fluid without actually rotating the condenser.

Although it was believed initially that the rotating condenser would not represent the best solution to the zero-gravity condensation problem, it was necessary to analyze and design such a condenser for several reasons. First, it provides a definitive solution to the zero-gravity vapor-liquid separation problem. Second, only a complete design would afford a basis for comparison with other units. Third, the design would provide some experience in the characteristics of rotating heat transfer machinery for zero-gravity operation.

The purpose of the study was to design a condenser for a vapor cycle in which the high-pressure vapor refrigerant from the compressor may be condensed entirely under zero-gravity conditions.

The design of a rotating condenser, in which the separation of liquid from its vapor is carried out based on density variation in the refrigerant, will be discussed below. The centrifugal field associated with the rotation drives the condensate outward along the disc, and the problem arising from the absence of gravity forces can be solved. The problem involves the determination of an optimum heat transfer coefficient corresponding to an optimum angular velocity for the condenser. The optimum condition is one corresponding to an optimum combination of power and weight; i.e., where the rotating condenser has the minimum penalty on the system. A method of designing such a condenser is presented. Numerical results will also be reported.

THEORETICAL BACKGROUND

A theory of rotating condensation has been analyzed by Sparrow and Gregg (1). Their study is based on a system in which a cooled disc rotates in uniform saturated vapor. The condensate moves outward along the disc under the effect of a centrifugal force field. Their investigation resulted in a description of the heat transfer characteristics of the system.

The condensate layer is assumed incompressible. The three velocity components, the pressure, and the temperature are given by the following five equations:

Continuity:

$$\frac{1}{r} \frac{\partial}{\partial r} (r V_r) + \frac{1}{r} \frac{\partial V_\phi}{\partial \phi} + \frac{\partial V_z}{\partial z} = 0 \quad (44)$$

Contrails

Energy:

$$\rho c_p \frac{D T}{D \tau} = k \nabla^2 T \quad (45)$$

Navier-Stokes:

$$\rho \left(\frac{D V_r}{D \tau} - \frac{V_\phi^2}{r} \right) = - \frac{\partial p}{\partial r} + \mu \left(\nabla^2 V_r - \frac{2}{r^2} \frac{\partial V_\phi}{\partial \phi} - \frac{V_r}{r^2} \right) \quad (46)$$

$$\rho \left(\frac{D V_\phi}{D \tau} + \frac{V_r V_\phi}{r} \right) = - \frac{1}{r} \frac{\partial p}{\partial \phi} + \mu \left(\nabla^2 V_\phi + \frac{2}{r^2} \frac{\partial V_r}{\partial \phi} - \frac{V_\phi}{r^2} \right) \quad (47)$$

$$\rho \frac{D V_z}{D \tau} = - \frac{\partial p}{\partial z} + \mu \nabla^2 V_z \quad (48)$$

Gravity forces and viscous dissipation terms are omitted and it is assumed that there is angular symmetry and that the shape of the radial and tangential velocity profiles do not change with different values of r . The assumption that the temperature is a function of z alone implies the existence of a condensate layer of uniform thickness over the disc.

The method consists of using von Karman's solution for the problem of a disc rotating in a uniform, single-phase medium (2). The following boundary conditions apply:

At the surface of the disc ($z = 0$):

$V_r = 0$	There is no motion relative to the disc
$V_z = 0$	
$V_\phi = r \omega$	
$T = T_w$	Fluid temperature is equal to wall temperature

At the liquid vapor interface ($z = \delta$):

$\tau_{zr} = 0$	Negligible shear stress between liquid and vapor
$\tau_{z\phi} = 0$	
$T = T_{sat}$	Liquid is at saturation temperature

As a result of this investigation, the heat transfer coefficient and the condensate layer thickness were found to be functions of the Prandtl number, a dimensionless parameter $c_p \Delta T / h_{fg}$, and other variables.

The heat transfer coefficient, the condensate layer thickness, the

velocity and temperature profiles, and the torque momentum required may then be calculated (1). The problem was solved numerically (on an IBM 653 electric computer) for Prandtl numbers in the range of 0.003 to 100, and for values of $c_p \Delta T / h_{fg}$ in the range of 0.0001 to 1. Numerical correlations were obtained which involve the assumptions that energy convection and acceleration terms are negligible. These results will be referred to later.

Experimental investigations on condensation on a horizontal rotating disc have also been reported (3). The experimental results deviate by about 25 per cent from the theoretical results, and this deviation is probably due to the fact that in the theoretical analysis the drag between vapor and liquid was not included initially.

Subsequently Sparrow and Gregg (6) have examined the effect of vapor drag on rotating condensation. The torque required is larger and the heat transfer coefficient is lower than that calculated initially.

DESIGN AND OPERATIONAL PROBLEMS

A step-by-step design method is presented in the Appendix using the results of the theoretical analysis. Certain problems in the design and development of a rotating condenser will be discussed first. One type of configuration is proposed (see Figure 25) and discussed in relation to design requirements.

The main requirements can be divided into five groups of functions which influence condenser performance. These requirements are:

Vapor Supply

1. The vapor should be properly fed to both sides of each disc.
2. The pressure drop of the vapor has to be equal between the compressor and each supply nozzle.

Condensation

1. There should be no interaction between discs.
2. Both sides of each disc should be fully utilized.

Liquid Removal

1. The liquid has to be collected and removed.
2. Vapor must be prevented from leaving the condenser with the liquid.
3. The pressure drop of the liquid must be equal between every "collector end" and the liquid main.

Coolant Supply and Removal

1. The coolant should be led into and discharged from a rotating shaft.

Contrails

2. Leakage of refrigerant must be prevented at the two shaft inlets.

General

1. Maximum reliability.
2. Small pressure drop on the refrigerant side.
3. Small pressure drop on the coolant side.
4. Small weight.

A configuration for the rotating condenser is shown in Figure 25. The design will be discussed with reference to the above requirements.

Vapor Supply

The high-pressure vapor refrigerant from the compressor (see the Flow Diagram in Figure 26) enters the main supply pipe. Four pipes, running parallel to the condenser shaft, join the vapor main, from which the vapor is radially supplied to the condenser as shown. (The number four is chosen arbitrarily; the purpose is to distribute the vapor uniformly around the shaft.) This type of solution is preferred over an axial type of vapor supply to satisfy the requirement that the vapor is to be supplied equally to both sides of the discs. The total pressure drop will also be smaller in this way. The requirement that the pressure at each vapor outlet be the same can easily be satisfied by proper piping design.

Condensation

The required condensation rate is maintained by continuous liquid removal from the condenser surfaces, which is effected by the centrifugal force obtained from the rotation of the disc. (It will be shown later that $h \sim \omega^{1/2}$ and $\delta \sim \omega^{-1/2}$. It follows that $h \sim 1/\delta$; i.e., the thinner the condensate layer, the better the heat transfer coefficient will be.)

It is desirable to keep the rpm at a constant level. A sudden change would cause ripples on the condensate surface, and this would result in a drag between the vapor and the film. It was indicated previously that this drag is one reason for the deviation between measured and theoretically predicted values for the heat transfer coefficient. By using the arrangement shown for the vapor supply, it is assured that both sides of each disc (the total calculated heat transfer area) will be utilized.

As far as interaction between discs is concerned, the minimum distance necessary to avoid interference is twice the boundary layer thickness over a disc. Obviously, the smaller this distance is, the smaller the weight of the condenser will be, and also, the smaller the pressure drop which will occur on the coolant side. Structural requirements will probably determine the spacing between the discs. There must be enough space between discs for the vapor supply nozzles. It is also important that these nozzles should be outside the boundary layers.

There are two possibilities; the boundary layer thickness can be smaller (or equal) or bigger than the thickness of the condensate layer.

Contrails

Sparrow and Gregg show the velocity distribution in Figures 8 and 9 (1). At low values of $\delta(\frac{\omega}{\nu})^{1/2}$ the tangential velocity of the liquid at the liquid vapor interface is nearly the same as that on the surface of the disc. At high values of $\delta(\frac{\omega}{\nu})^{1/2}$ the tangential velocity drops going outward in the condensate layer and at the value of $\delta(\frac{\omega}{\nu})^{1/2} = 5$ the tangential velocity is about three per cent of that at the disc surface. In the second case, the boundary layer has practically the same thickness as the condensate layer, in which case there is no problem. The vapor will be outside the boundary layer as will be the nozzles. (In this case, the assumption of zero shear stress between liquid and vapor is correct.) In the first case, however, the boundary layer thickness can be fairly large and there must be a shear force between the liquid and the vapor. The boundary conditions, $\tau_{z\phi} = \tau_{zr} = 0$, applied by Sparrow and Gregg (1), are not true. Nandapurkar (3) points out that the deviation between the theoretical and experimental results (up to 25 per cent) is due to the assumption that the vapor shear stress is negligible.

For the purpose of finding the minimum distance between the discs and the vapor supply nozzles, the thickness of the boundary layer can be found with good accuracy. As the tangential velocity of the liquid at the liquid vapor interface was found to be nearly equal to that on the disc surface, a new disc can be imagined, having the thickness of the disc plus the condensate layer, rotating in the vapor medium with the same angular velocity as the original disc did. The thickness of the boundary layer in the vapor can be calculated based on the method of Schlichting (4), who solved the problem for a rotating disc, using von Kármán's method of solution. Using the transformation function, a correlation for the tangential velocity distribution is:

$$V = r\omega G(\xi) \quad (49)$$

where V is the tangential velocity in the vapor. The numerical values of the function $G(\xi)$ are calculated as a function of $\xi = z\sqrt{\frac{\omega}{\nu}}$ by Cochran (5).

The vapor outside the boundary layer is practically at rest. If we take:

$$G(\xi) = V / r\omega = 0.02 \quad (50)$$

then Table 5.2 (4) gives the value by extrapolation for:

$$\xi = z\sqrt{\frac{\omega}{\nu}} = 4.6 \quad (51)$$

The thickness of the boundary layer in the vapor will then be:

$$\sigma = 4.6\sqrt{\frac{\nu}{\omega}} \quad (52)$$

where σ is the boundary layer thickness in the vapor, and the value $\sigma + \delta$ gives the minimum distance between the disc and the nozzle.

Two assumptions were made during the calculations of σ :

Contrails

1. The axial velocity of the vapor resulting from the condensation does not affect the thickness of the tangential boundary layer.
2. The velocity of the vapor without the rotation of the disc would be zero.

The second assumption suggests a somewhat larger distance between discs and nozzles than that calculated above.

Liquid Removal

The removal or separation of liquid from vapor is the greatest problem under zero-gravity conditions. In the case of the proposed design, the liquid, under the effect of centrifugal force, would go through a gap on both sides of each disc and would be collected in a narrow annular channel. The thickness of the gap could be either the thickness of the condensate layer under design conditions, or could be variable. In the first case, at higher rpm's, there is a chance that vapor will get into the liquid collector; however, large variations in the rpm should not be expected for several other reasons. In the latter case, when the gap is variable, its thickness can be controlled from the rpm of the shaft and can be adjusted in such a way that the opening would always be the thickness of the condensate layer, corresponding to the existing rpm.

During the design of the gap through which the condensate leaves, there is one important problem to be considered. The condensate layer rotates with the disc. When the condensate arrives at the gap, however, the other side of the liquid will be in touch with the stationary wall (see Figure 27). So there is also a boundary layer near the stagnant wall, and fluid separation and back flow might occur. Schlichting (4) shows this in his work. In his example, however, a large body of liquid with infinite diameter rotates near a stationary wall. In the present case, if the vapor between the discs is prevented from rotating with the discs, only the thin layer of liquid (plus the vapor in the boundary layer) will rotate. Therefore it is suggested that the nozzles should supply the vapor with an impulse against the direction of rotation of the discs. In addition, the larger the distance between discs and nozzles, the smaller the percentage of vapor which will tend to rotate with the discs.

Whether or not separation will occur depends greatly on the angle of the resultant velocity. In practice, separation will probably not occur if this angle is equal to or larger than 15 degrees. This angle can be calculated from:

$$\theta = \tan^{-1} \frac{V_r}{V_\phi} \quad (53)$$

where the velocity components can be found either from Figures 8 and 9 (1) or from Figure 5.10 (4). Creating a suction in the direction of flow also prevents back flow and separation.

It is important to design the gap properly because when back flow occurs, after a period of time, an oscillatory motion of the condensate will occur and the condenser will cease to operate properly. The two main sizes of the gap (a and b in Figure 27) are critical and have to be determined experimentally.

Contrails

The liquid will be collected in a narrow annular channel. There appears to be no danger of back flow once the liquid is in the collector; the continuous supply of liquid--assuming proper operation of the gaps--would prevent this. Surface tension also tends to keep the liquid in the channel.

The liquid is removed along the circumference of the channel as shown. The manifolds join the main liquid line. By proper piping design the requirement of equal pressure drop in all the branches may be satisfied easily.

Coolant Supply and Removal

The coolant supply for the condenser can be carried out in several ways. Three different solutions are briefly outlined below.

1. The coolant flows axially inside the rotating shaft. The discs are cooled by conduction only and they act as "rotating fins".
2. The coolant flows axially in the rotating shaft and the total amount of coolant flows radially inside the discs.
3. The coolant flows axially inside the shaft and a certain portion of the coolant, necessary to obtain the required cooling effect with given temperature difference, flows radially in each disc, while the major portion of the coolant flows axially through the shaft.

The second solution is shown in Figure 25, and the heat transfer calculations on the coolant side will be based on this type of arrangement.

There are three major problems in the design. The first is the calculation of the sizes of the channels in which the coolant flows (width of discs). Small pressure drop and light weight are the factors to be considered. The second is the supply and discharge of the coolant into and from the rotating shaft. This is essentially a sealing problem. One solution for this would be the application of rotary unions at the two ends of the shaft. Another type of solution is shown in Figure 26. The third is the prevention of the leakage of the refrigerant at the two entrances of the rotating shaft. This is a common sealing problem between a rotating shaft and its housing. Several types of solution exist.

The general requirements, maximum reliability, small pressure drops, and small total weight, are governing factors during the whole design procedure.

PRESSURE DROP CONSIDERATIONS

Refrigerant Side

The pressure drop in the condenser is important because the work necessary to overcome it has to be supplied by the compressor. In the conventional heat exchangers used in common practice, the condensation takes place at decreasing pressures because of the pressure drop occurring as the refrigerant passes through the condenser. In this case, however, (using the condenser shown in Figure 25) the pressure drop is not continuous. There is a

Contrails

pressure drop in the vapor line between the compressor and the supply nozzle. (This can be calculated from equations or charts applicable to vapor flow in pipes.) As an approximation, the vapor pressure in the annulus between the discs may be assumed to be constant.

There is friction between the moving condensate and the disc which is overcome by the momentum supplied by the rotation. Essentially, the total pressure of the liquid increases as it passes outward on the surface of the disc. The pressure at the circumference of the disc will be:

$$p = p_{\text{vapor}} + \frac{1}{2} \rho (v_r^2 + v_\phi^2) \quad (54)$$

The velocity components can be found from Figures 8 and 9 (Reference 1) and

$$\Delta p_{\text{disc}} = -\frac{1}{2} \rho (v_r^2 + v_\phi^2) \quad (55)$$

The minus sign shows that the pressure increases. (In order to get the correct amount of pressure increase, an efficiency also has to be taken into account for the pressure drop due to friction which is overcome by the momentum of the liquid.)

Finally, the pressure drop in the liquid collectors is not as important as at the parts of the condenser discussed above. The higher pressure drop in the condenser will result in a smaller pressure drop required through the throttling valve.

The pressure drop in the condenser depends mostly on the pressure drop in the vapor supply lines; a total pressure increase in the condenser is also possible. The application of a rotating condenser does not seem to result in any disadvantage in this respect, compared to a conventional condenser. It must be remembered, however, that the pressure gain is accomplished by power supplied through the rotating shaft of the condenser.

Coolant Side

The pressure drop on the coolant side is important because it determines the size and power requirement of the circulating pump. Computation procedures will be shown during the numerical calculations.

DYNAMIC AND STRESS PROBLEMS AFFECTING HEAT TRANSFER CALCULATIONS

It is not the subject of this work to discuss mechanical design procedures; however, in certain aspects they affect the heat transfer calculations.

The rotating hollow shaft of the condenser is also the passage of the coolant, so its design influences the condenser performance. The minimum diameter and wall thickness of the shaft will be determined by stress considerations, and also has to be checked against the critical rpm. Only if these requirements are satisfied can the final heat transfer calculations be carried out. Stress considerations will also define the wall thickness of the discs and the housing. These affect the dead weight of the condenser. As will be seen later, the selection of the optimum condenser is based on penalty calculations on which the

condenser dead weight has a strong effect.

PENALTY ON THE SYSTEM

It is expected that the rotating condenser will be located inside the space vehicle and that a secondary heat transfer fluid (such as Dowtherm A or NaK alloy) will be used to transfer heat from the condenser to a radiator where final heat dissipation to space occurs. Any conclusive consideration of penalty must include not only the fixed weight of the entire condenser-heat transfer loop-radiator assembly, but also the penalty effect of this assembly on the vehicle secondary power system (which supplies the power for rotation of the condenser), the secondary power system fuel, and ultimately to the vehicle take-off weight and the weight of the primary fuel necessary to boost the payload. The entire penalty consideration is also a function of the vehicle mission duration. For mission durations of any length, it is expected that solar and nuclear power sources will provide vehicle secondary power.

In this discussion, penalty considerations have been confined to the condenser assembly fixed weight and the power requirement, excluding the subcooler (if necessary) and the radiator. It is believed that the fixed weight calculation is sufficient to indicate the applicability of the rotating condenser. Assuming the arrangement shown in Figures 25, 26, 29, the fixed weight consists of the weights of the rotating discs and shaft, the housing and bearings, the motor, piping, coolant pump and motor, and the weight of the refrigerant and coolant. The power is that required to rotate the condenser shaft and that supplied to the coolant pump.

RESULTS AND DISCUSSION

Based on the calculation procedures described in Appendix 2, rotating condensers have been designed for several vapor cycle conditions. The program involved condenser design for vapor cycles in the capacity range between 400 BTU/min and 4000 BTU/min. The evaporation temperature varied between 40 degrees F and 55 degrees F, the condensation temperature varied between 150 degrees F and 250 degrees F. Freon 11 has been used as the refrigerant, and it was chosen originally primarily because of COP considerations. On the coolant side, several coolants were considered. Dowtherm A has been selected over liquid metals like NaK because of its bigger specific heat which resulted in smaller pump, motor, and power requirements. In addition, if NaK had been used, the discs might have to be made of steel instead of aluminum, which would increase the total penalty.

The condenser design consisted of the determination of a fixed weight for each application. (The actual optimum condenser can be found only if the duration of the flight and the characteristics of the vehicle power supply system are known.)

Several vapor cycles were examined in the capacity and temperature ranges defined by the problem. The calculations were carried out on an IEM 704 electric computer. The programming followed the steps of the calculation procedure presented in Appendix 2. There were two input parameters for each cycle, the angular velocity and the number of discs. Five values for the angular velocity (between 18,800 and 902,400 /hr), and twelve values for the number of discs (between 1 and 120) were chosen.

Contrails

The most important outputs are the condenser dead weight (including the weight of the necessary motors and pump) and the total power requirement (necessary to operate the condenser and its accessories). These are functions of many variables and can be represented as follows:

$$W_d = f(Q_o, T_o, T_c, N, \omega)$$

$$P = f(Q_o, T_o, T_c, N, \omega)$$

The results of the numerical calculations are presented in graphical form. An example for the calculation of one point, i.e., the calculation of one value for W_d for a specific cycle is given in Appendix 2.

Figures 30 - 32 show the variation of the condenser dead weight vs. the number of discs. Figures 33 - 35 show the variation of the required power vs. the number of discs. In both cases, the angular velocity, system capacity, evaporation and condensation temperatures are parameters.

It is necessary to emphasize here that since detailed stress calculations were not performed, the fixed weight of the condenser may be reduced considerably by diminishing the wall thicknesses of the shell, discs, and other components. In such a case, the fixed weight may be lowered by a factor of two or three. In the calculations, a shell and disc thickness of $3/64$ inch was used, while the wall thickness of the shaft is $1/8$ inch. In addition, the maximum angular velocity, ω , used is 902,400 per hour, which corresponds to a speed of 2400 rpm. The fixed weight of the condenser will be reduced by operating the condenser at a higher speed; however, this will also increase the power requirement. At low capacities the power requirement is small, but at an evaporator capacity of 4000 BTU/min, the power requirement is considerable.

The basic correlations derived by Sparrow and Gregg (1) are true for laminar flow only. They claim (referring to Schlichting's work) that the limit when transition starts is at about

$$Re = \frac{r_o^2 \omega}{\nu} = 3.5 \times 10^5 \quad (56)$$

In the present work, h has been calculated from an expression experimentally determined by Nandapurkar (5). His measured results corresponded to Reynolds numbers in the range of $5 - 48 \times 10^5$.

H. L. Dryden (7) examined transition in flow near a rotating disc. He, too, claims that the flow depends on the Reynolds number $r^2 \omega / \nu$. In his work he refers to Reynolds numbers obtained by others, at which transition occurs. These values are: Goldstein, 80,000 (8); Riabouchinsky, 230,000 (9); and Theodoresen and Regier, 310,000 (10), who conducted tests where a disc with a one-foot radius rotated with a speed of 525 rpm. Transition occurred at a radial distance of 9.6 inches, the flow being laminar at smaller radii and turbulent at larger radii.

In the present problem, Reynolds numbers corresponding to the optimum values of ω and N are much larger than the ones referred to above. The effect

Contrails

of turbulence is not clarified. Work on condensation over a rotating disc in turbulent flow is not yet available. It is estimated, however, that the heat transfer coefficient will increase somewhat, while the torque required to rotate the condenser may increase. The total effect can not be predicted easily.

Contrails

LIST OF SYMBOLS

A	ft	Heat transfer area
b	ft	Half disc thickness
c_p	BTU/lb-degF	Specific heat of refrigerant
c_{pc}	BTU/lb-degF	Specific heat of coolant
D	ft	Diameter
f		Friction factor
g_o	lbm ft/lbf hr ²	Constant
H	ft	Coolant side pressure drop
h	BTU/hr-sq ft-degF	Condensation heat transfer coefficient
h	BTU/lb	Enthalpy
h_c	BTU/hr-sq ft-degF	Coolant side heat transfer coefficient
h_{fg}	BTU/lb	Latent heat
K		Constant
k	BTU/hr-ft-degF	Conductivity of refrigerant
k_w	BTU/hr-ft-degF	Wall conductivity
L	ft	Length
M	lbf-ft	Torque
N		Number of discs
P	HP	Total power
P_1	HP	Rotating power
P_2	HP	Pumping power
Pr		Prandtl number
p	lbf/sq ft	Pressure
Δp	lbf/sq ft	Pressure difference
Q	BTU/min	Condenser load
Q_o	BTU/min	System capacity
q	BTU/lb	Condensation heat per pound
q_o	BTU/lb	Refrigerating effect per pound
Re		Reynolds number
r	ft	Radius

Contrails

r_o	ft	Disc radius
r_i	ft	Shaft inside radius
r_s	ft	Shaft outside radius
SFC	lbs/hr HP	Specific fuel consumption
s	ft	Wall thickness
T	hrs	Duration
T_w	degF	Wall temperature
T_{sat}	degF	Saturation temperature
T_c	degF	Condensation temperature
T_o	degF	Evaporation temperature
ΔT	degF	$T_{sat} - T_w$
ΔT_{LM}	degF	Log mean temperature difference
t_{ci}	degF	Coolant inlet temperature
t_{co}	degF	Coolant outlet temperature
U	BTU/hr-sq ft-degF	Over-all heat transfer coefficient
V_r	ft/sec	Radial velocity
V_z	ft/sec	Axial velocity
V_ϕ	ft/sec	Tangential velocity
v	cu ft/lb	Specific volume
W	lbs	Weight
W_c	lbs/min	Coolant flow rate
W_d	lbs	Dead Weight
\dot{W}_r	lbs/min	Refrigerant flow rate
Y		Dimensionless parameter
Z	ft	Disc spacing
δ	ft	Condensate layer thickness
ϵ		Heat exchanger effectiveness
η		Efficiency
θ		Velocity angle

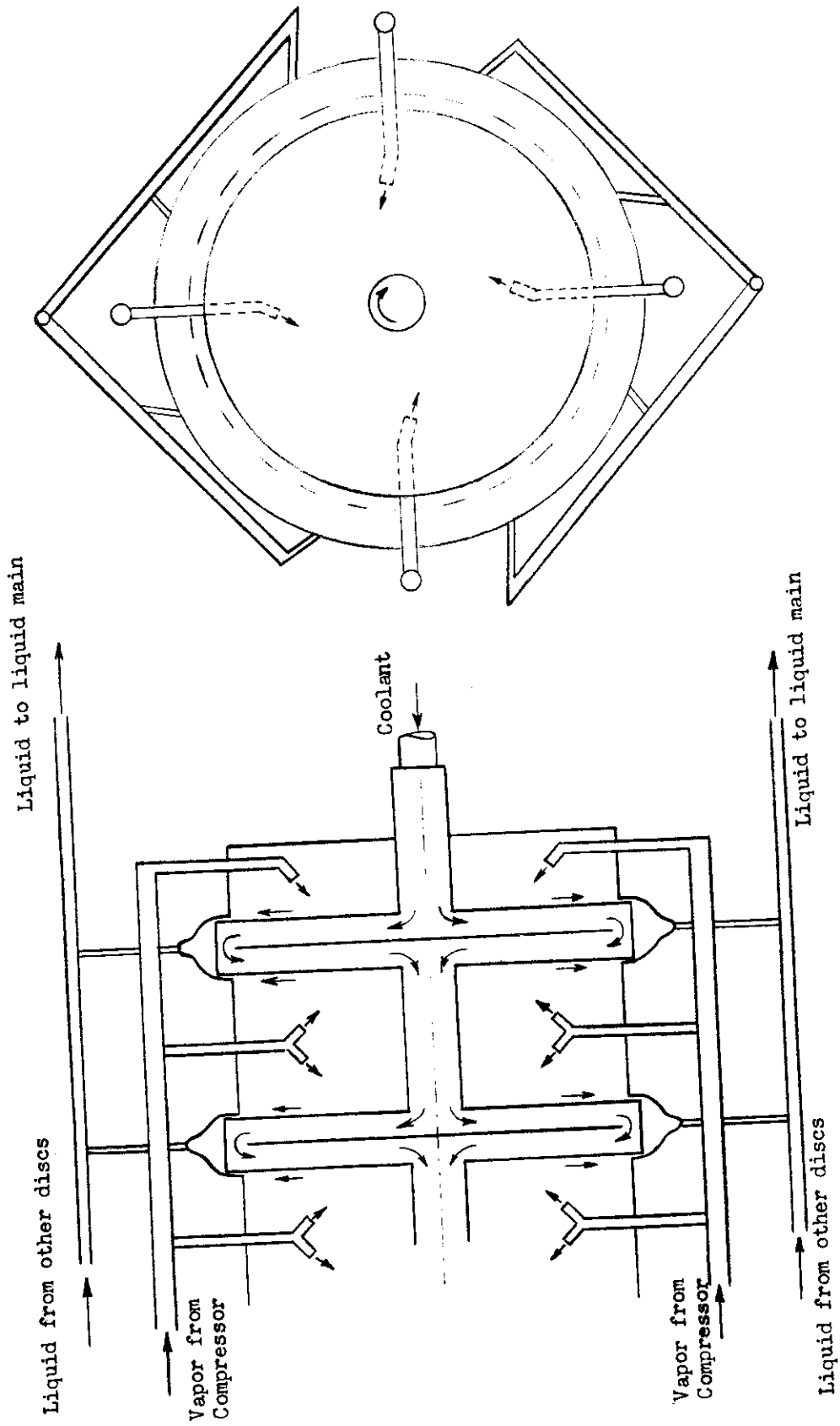
Contrails

μ	centipoise	Viscosity
ν	sq ft/hr	Kinematic viscosity
ρ	lbs/cu ft	Density
δ	ft	Boundary layer thickness
τ	lbs/sq ft	Shear stress
ω	radians/hr	Angular velocity
r, ϕ, z		Coordinate directions

Contrails

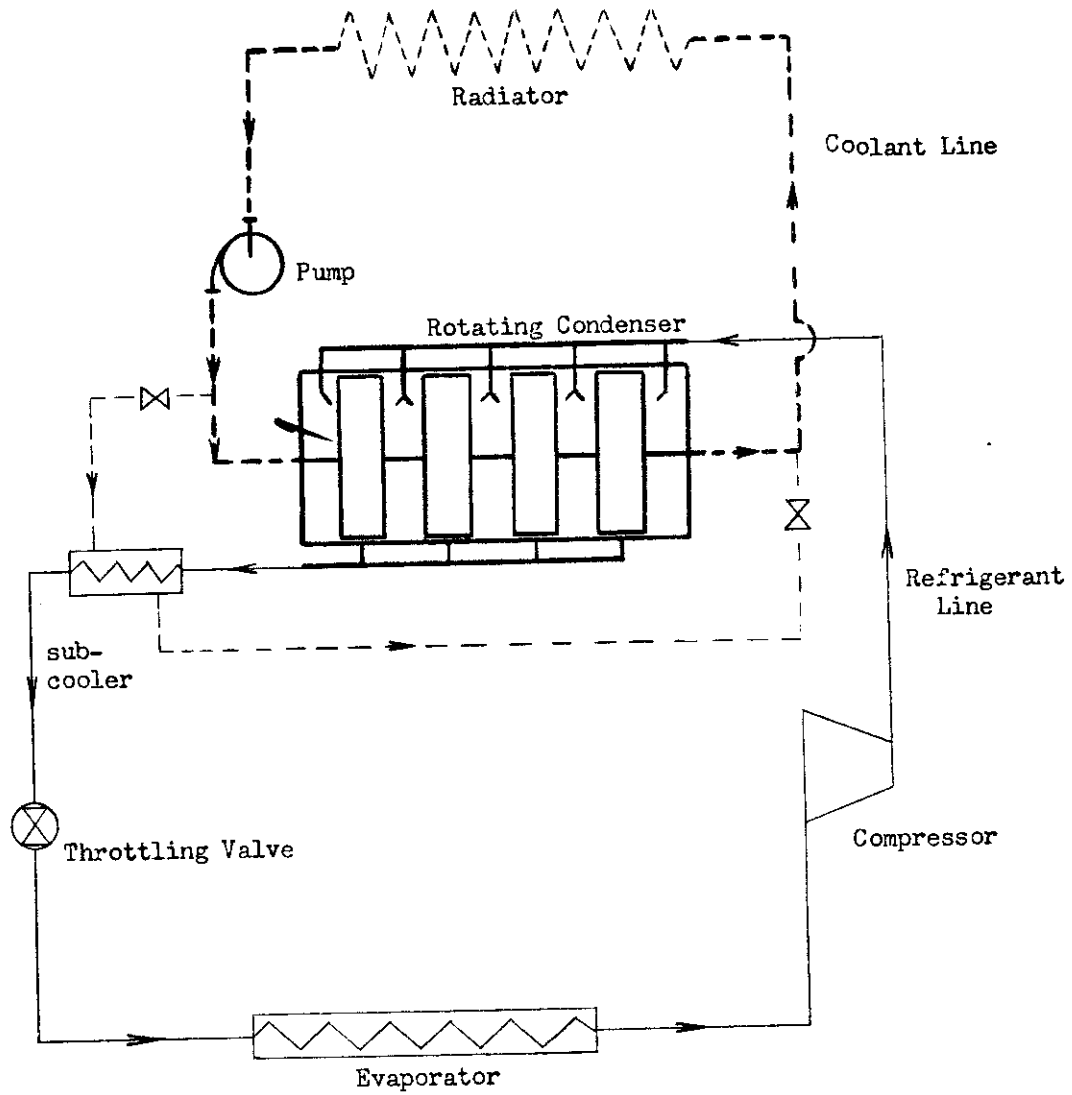
REFERENCES

1. Sparrow, E. M. and Gregg, J. L., "A Theory of Rotating Condensation," Trans. ASME, vol. 81, 1959, pp. 113-120
2. Von Karman, T., "Laminare und Turbulente Reibung," ZAMM, vol. 1, 1921, p. 233; NACA TM 1092, 1946
3. Nandapurkar, S. S., Condensation on Rotating Surface, Sc.D. Thesis, North Carolina State College, University Microfilm Inc., Ann Arbor, Michigan, 1958
4. Schlichting, H., Boundary Layer Theory, McGraw-Hill Book Company, Inc., New York, 1955, pp. 75-80
5. Cochran, W. G., "The Flow Due to a Rotating Disc," Proc. Camb. Phil. Soc., vol. 30, 1934, p. 365
6. Sparrow, E. M. and Gregg, J. L., "The Effect of Vapor Drag on Rotating Condensation," Trans. ASME, Series C, vol. 82, No. 1, 1960, pp. 71-72
7. Dryden, H. L., in Turbulent Flows and Heat Transfer, edited by C. C. Lin, Princeton University Press, 1959
8. Goldstein, S., Proc. Cambr. Phil. Soc., vol. 31, Part 2, 1935, p. 232
9. Riabouchinsky, D., Bull. de l'Institut Aerodyn. de Koutchino, Moscow, 1914
10. Theodorsen, T. and Regier, A., Experiments in Drag of Revolving Discs, Cylinders and Streamline Rods at High Speeds, NACA Report 793, 1944



Rotating Condenser

Figure 25



Flow Diagram

Figure 26

Contrails

Figure 27 - Rotating Condenser - Gap Design
 Figure 28 & 29 - Rotating Condenser Configuration

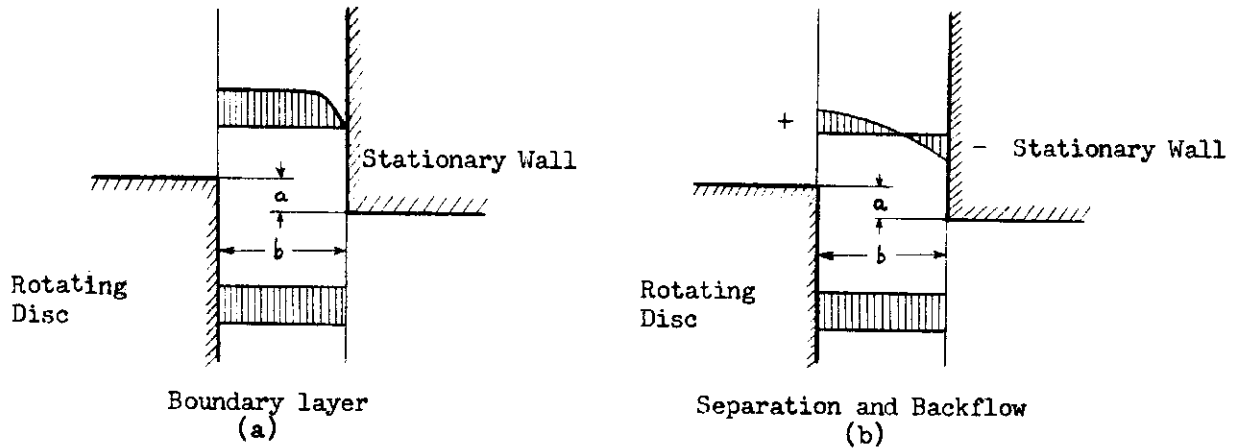


Figure 27

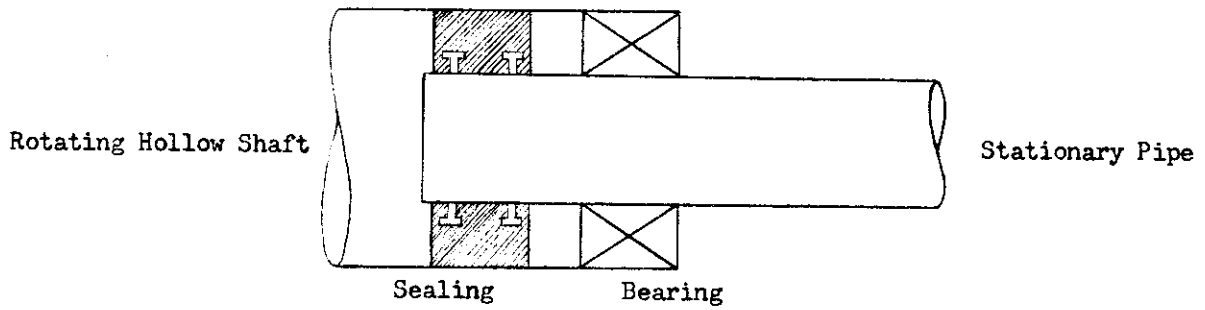


Figure 28

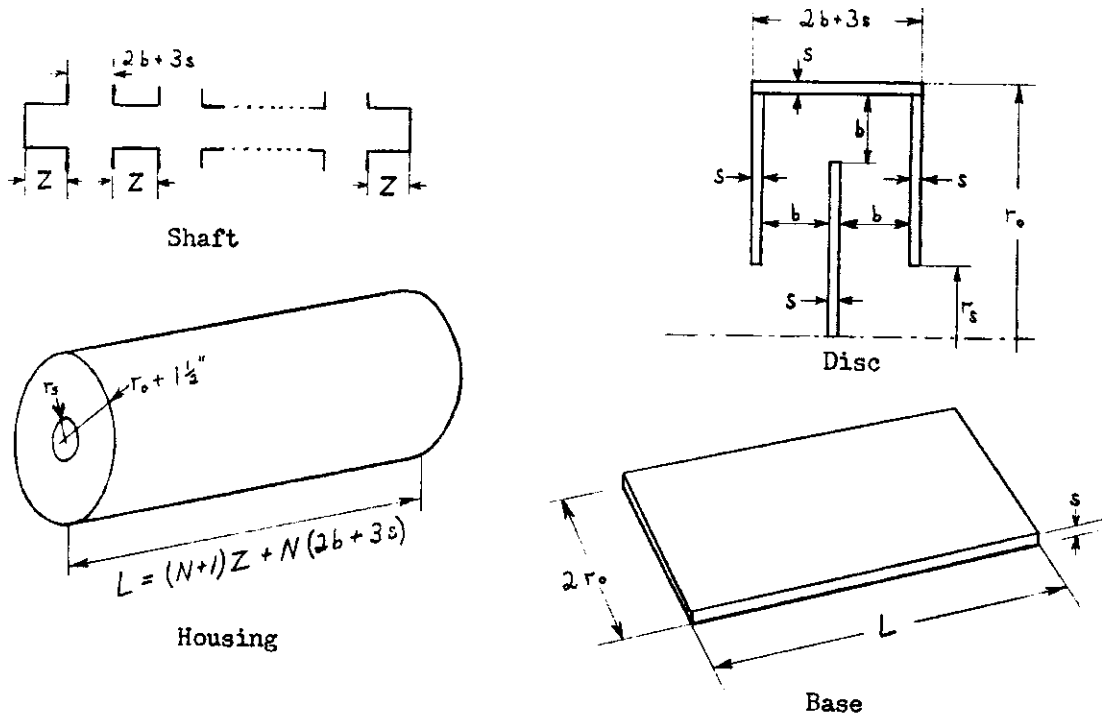
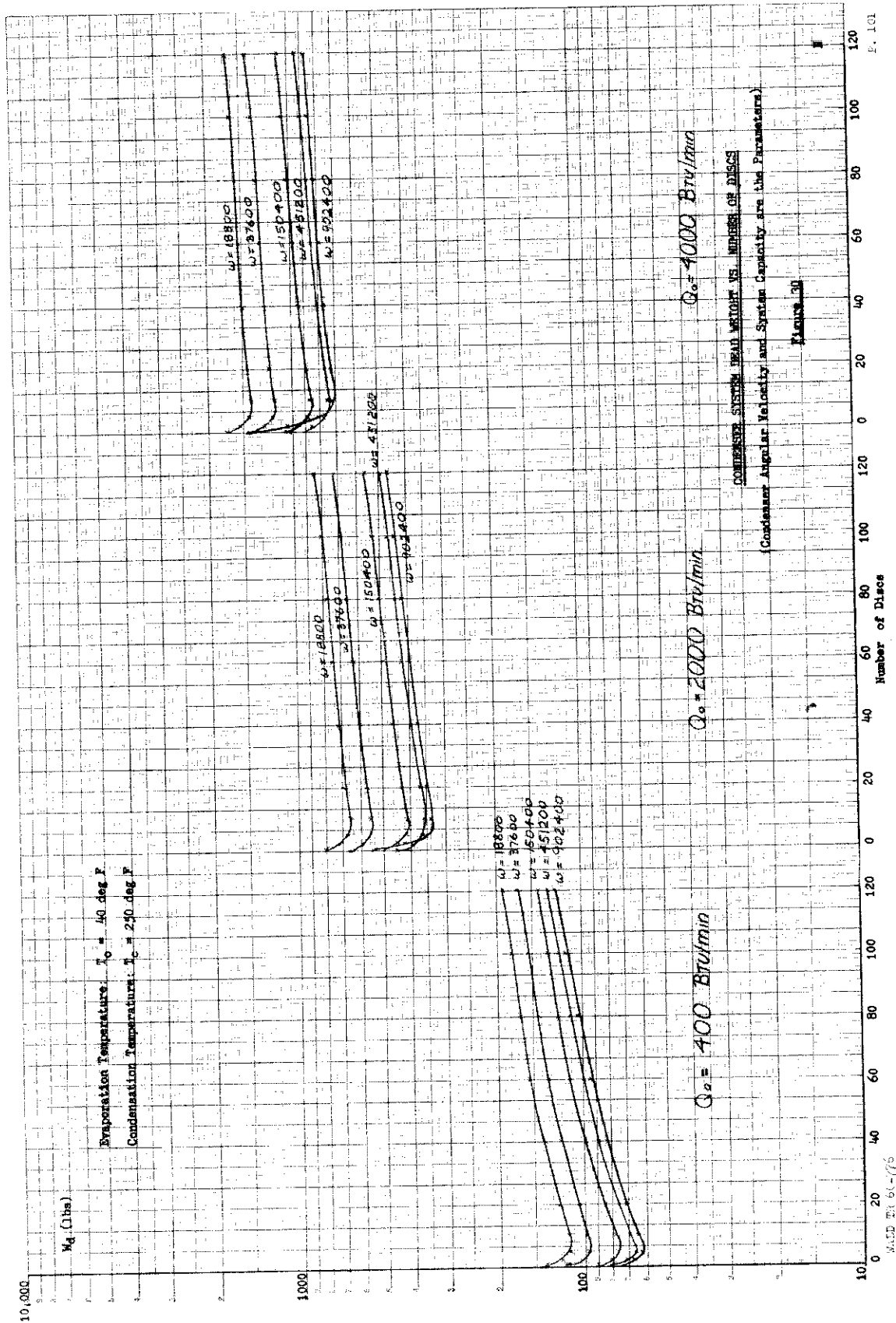
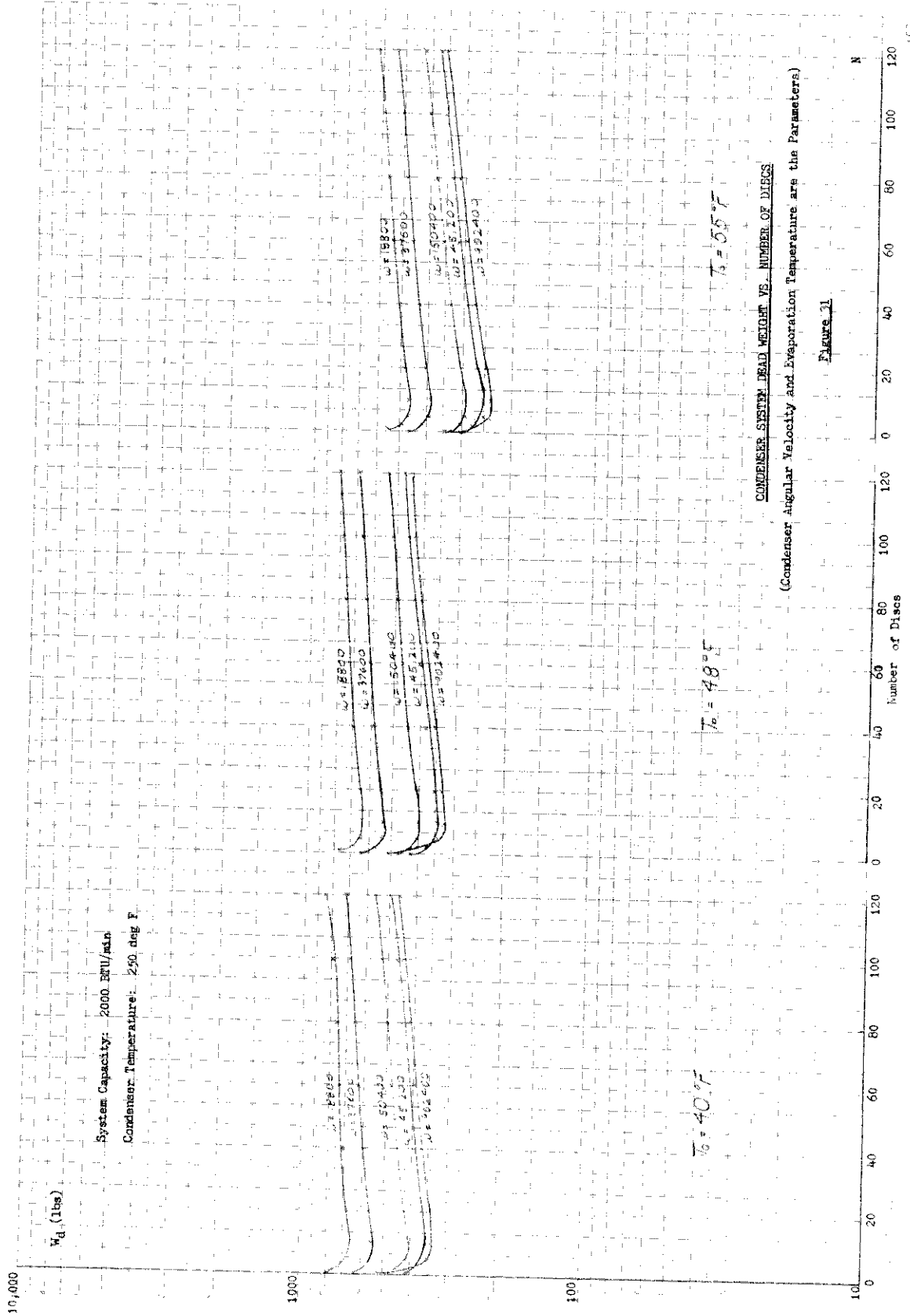
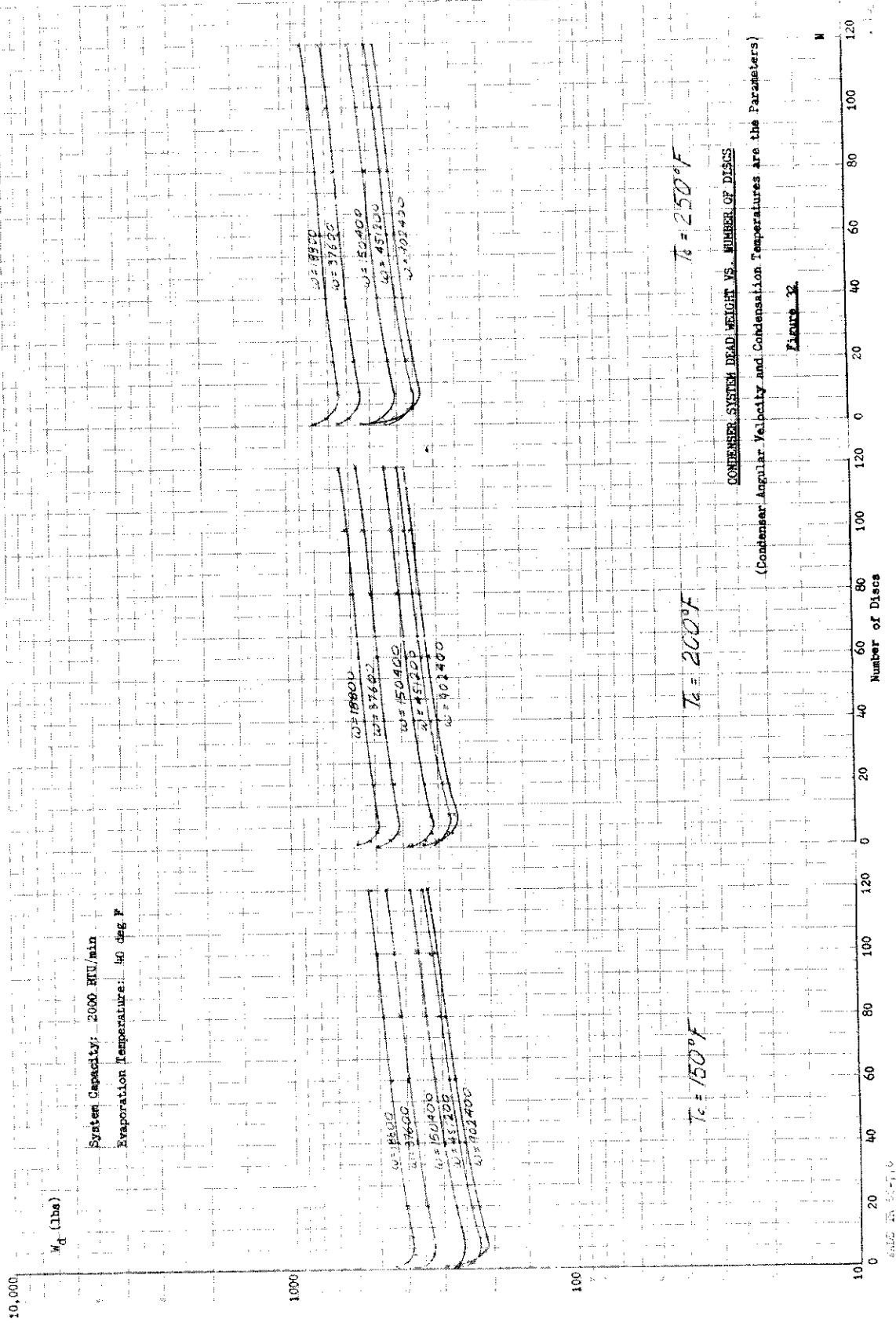


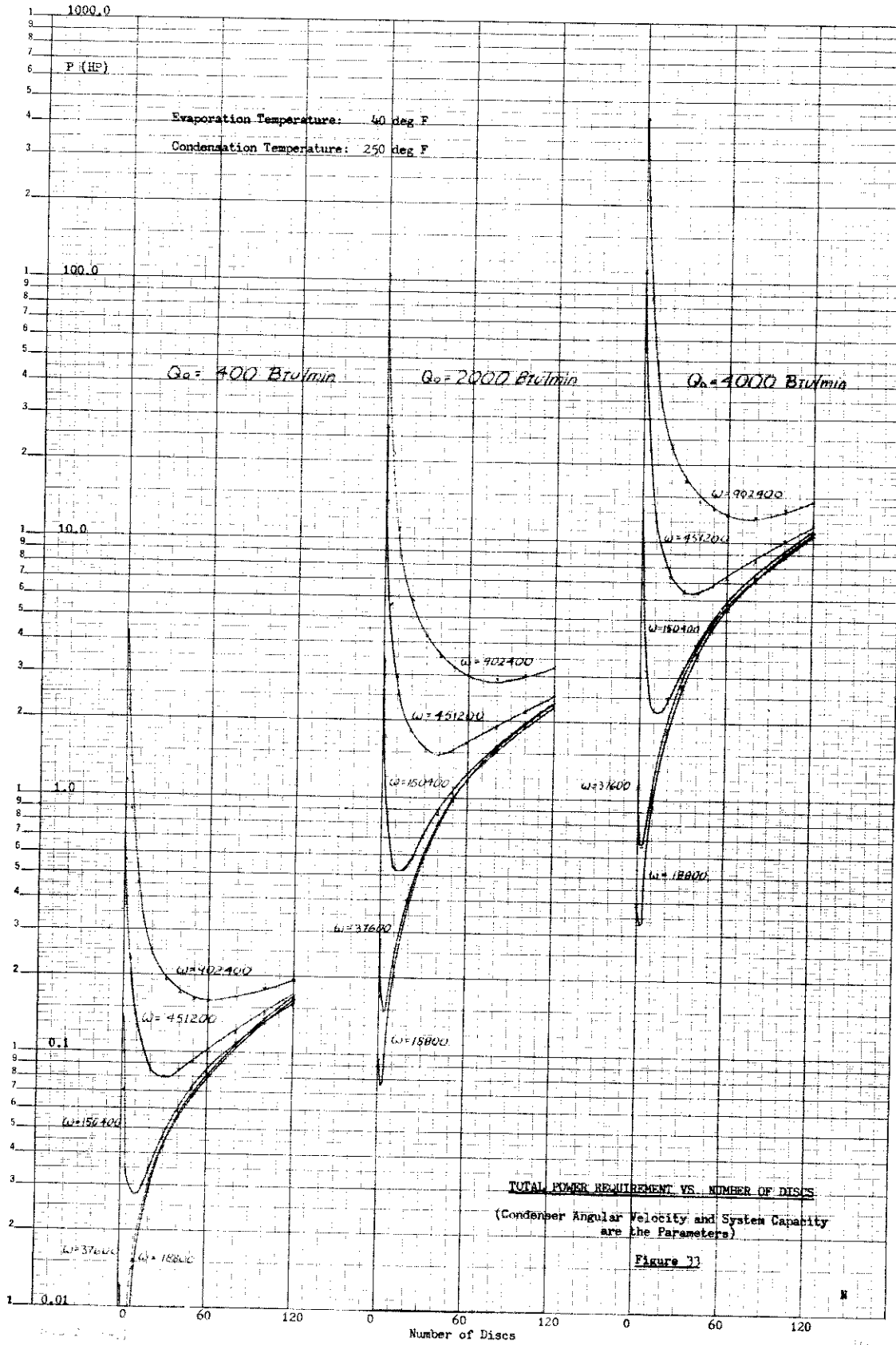
Figure 29



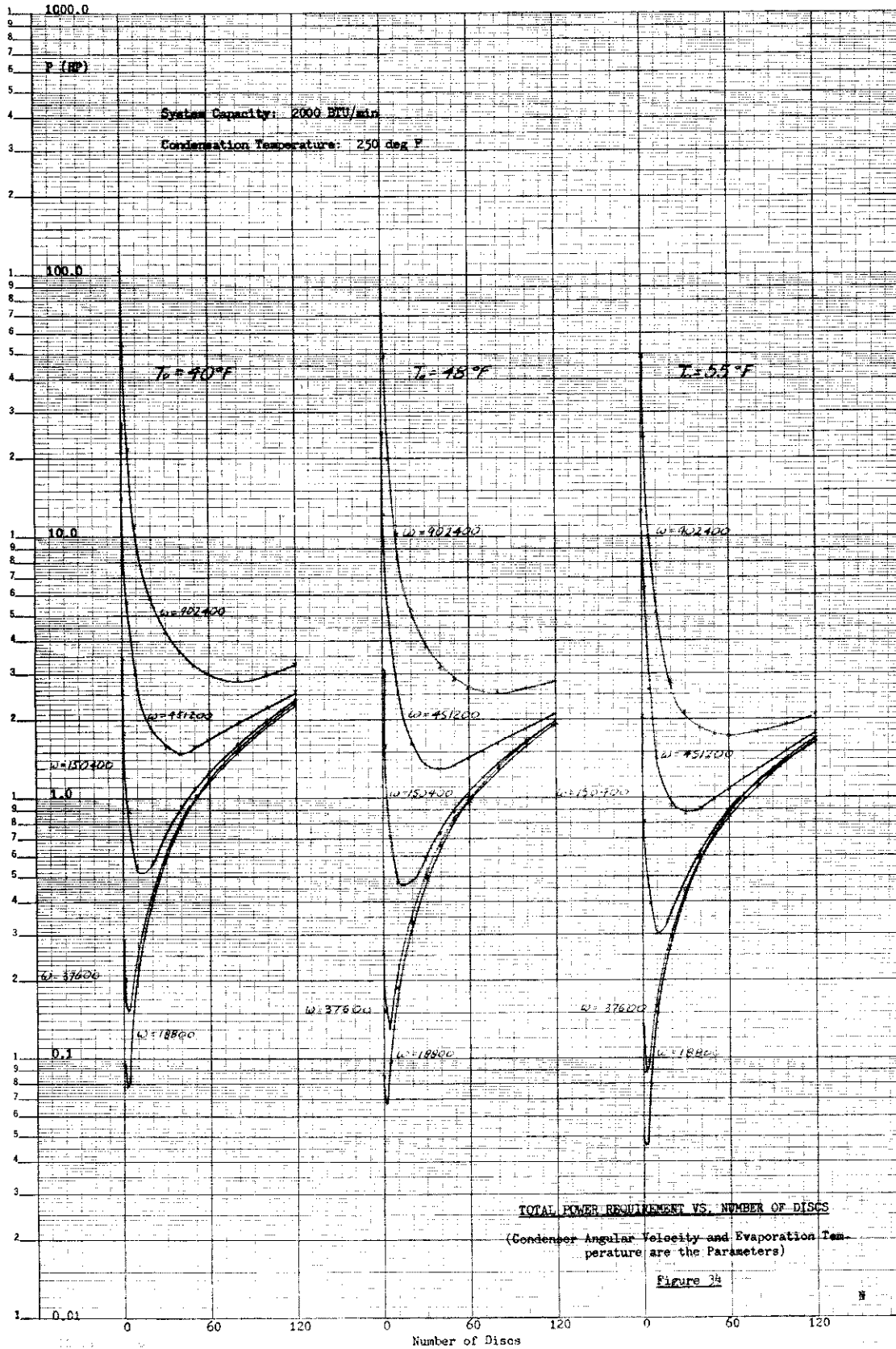




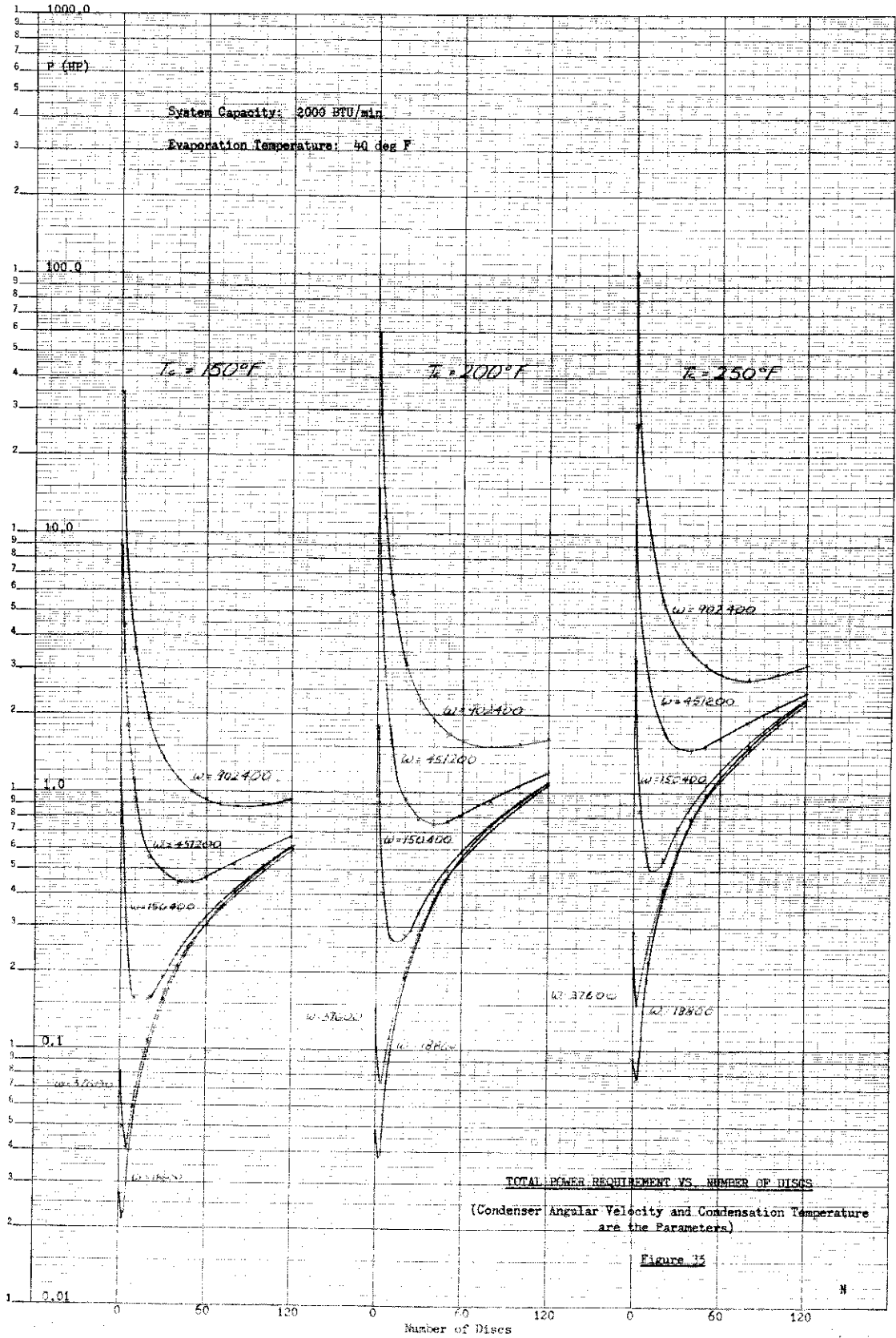
Contrails



Contrails



Contrails



SECTION VII

SPIRAL CONDENSER STUDY

There are two basic condenser configurations available to a space vehicle vapor cycle cooling system. Since the ultimate heat sink is the space environment itself, a radiator is a required component of any such system. The first of the two configurations places the condenser passages directly in the radiator; the vapor enters the radiator, condenses in the passages, and heat of condensation is transferred to the radiator wall which dissipates the heat to space. In this case, the condenser is placed outside the vehicle, and is connected to the compressor and the throttle valve within the vehicle by the necessary piping. The other configuration consists of installing the entire vapor cycle including the condenser within the space vehicle and connecting the condenser and radiator with a suitable heat transfer loop. In the second case, a pump is required to circulate the heat transfer fluid between the condenser and the radiator.

Several factors determine the choice between the two systems. In some cases, the condenser structure itself, as in the case of the rotating and spiral condenser, will not allow integration of radiator and condenser. If an integral radiator-condenser can be designed, there is no necessity for the piping, pump, and heat transport fluid which comprise the intermediate loop; and this is favorable from a penalty standpoint. Micrometeoritic penetration is a hazard with which the designer of the radiator-condenser must contend. If penetration of an integral radiator-condenser occurs, the refrigerant would probably be lost to space. In the case of the intermediate loop, the heat transfer fluid would be lost, but the vapor cycle system itself would remain intact. In any case, the system would be inoperable until the damage was repaired, and the supply of refrigerant or heat transfer fluid was replenished.

RADIATOR-CONDENSER SYSTEMS

Since the radiation process is not directly affected by gravity, actual radiator designs and configurations have not been considered in this study. However, a comparison of the radiation and condensation heat transfer process and the relative magnitude of the coefficients involved is of some value.

A heat transfer coefficient for the outer surface of the radiator may be defined as

$$h_R = \frac{q/A}{T_R - T_S} \quad (57)$$

where q/A is the heat flux (BTU/hr-sq ft-degF)

T_R is the radiator surface temperature (degR)

T_S is the sink temperature (degR)

For simplicity, the sink temperature is assumed to be 0 degrees R. The heat flux

Contrails

is given by the expression,

$$q/A = \sigma \epsilon T_R^4 \quad (58)$$

where σ is the Stefan-Boltzman constant equal to 1.71×10^{-9} BTU/hr-sq ft-(degR)⁴

ϵ is the emissivity of the radiator surface.

The radiation heat transfer coefficient may now be written as

$$h_R = \sigma \epsilon T_R^3 \quad (59)$$

Assuming heat transfer through a condensate film by conduction only, the minimum value of the condensing heat transfer coefficient may be written as (Appendix 5)

$$h_c = \frac{4 k}{d_h} \quad (60)$$

where h_c is the condensation heat transfer coefficient (BTU/hr-sq ft-degF)

d_h is the hydraulic diameter of the flow passage (ft)

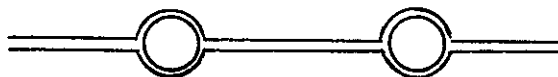
k is the thermal conductivity of the liquid phase (BTU/hr-ft-degF).

A minimum ratio for the condensing-side heat transfer coefficient to the radiating-side heat transfer coefficient is

$$\frac{h_c}{h_R} = \frac{4 k}{\sigma \epsilon d_h T_R^3} \quad (61)$$

The value of this ratio is shown in Table 9 for several fluids and temperatures. Its significance is that where the magnitude of the ratio is large, the over-all heat dissipation process is limited by the radiation process; this is even more valid when the actual condensation coefficients are larger than the minimum selected here. It is assumed in Table 9 that the emissivity, ϵ , was equal to 1.0, and that the radiator surface temperature was equal to the condensation saturation temperature, making the values of $(h_c/h_R)_{\min}$ even more conservative.

An estimate was also made of the length of tubing which must be installed in an integral radiator-condenser to condense the Freon refrigerant entirely. A radiator-condenser with the Freon condensing in tubes and the heat being dissipated by radiation from both the tubes and the connecting fins was chosen, as shown below.



Contrails

The tube ID was 0.44 inch, and the fin thickness was 0.03 inch. The condenser heat load was 4400 BTU/min, and the saturation temperature was 250 degrees F. For a conservative wall temperature (calculated) of 140 degrees F, it was found that 1170 feet of tubing would be required for complete condensation. This maximum length is calculated by assuming a minimum h_c equal to 4 k/dh. If it is assumed that h_c is infinite, that is, that the radiator wall is at a temperature equal to the Freon 11 saturation temperature (250 degrees F), a minimum length of 633 feet of tubing is still required. Although the calculations are extremely simplified, they do indicate the orders of magnitude involved.

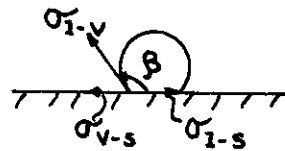
CONDENSATION UNDER ZERO GRAVITY

As a vapor comes into contact with a surface whose temperature is maintained below that of the saturation temperature of the vapor, condensation occurs. If the liquid wets the surface, as condensation occurs, the liquid spreads out on the surface, forming a continuous film which remains stationary in the absence of forces. In general, the film moves under the action of body forces (such as gravity), pressure forces, and contact forces exerted by the vapor at the liquid-vapor interface. If the liquid does not wet the surface, the condensate forms drops which grow during the condensation process and coalesce with other drops due to natural interference or to relative motions between the drops. Condensation may begin in the form of discrete drops which grow and coalesce so as to produce a continuous film.

The amount of information available on the heat transfer and fluid dynamics involved in drop-wise condensation is small compared to the understanding of the film-type condensation process. Whether a particular fluid-surface combination results in drop-wise or film-type condensation is a matter for experimental observation.

Consider a drop formed on a surface and denote the surface tension forces by σ ; σ_{l-v} between the liquid and vapor phases; σ_{l-s} between the liquid and solid phases; and σ_{v-s} between the vapor and solid. Equilibrium of the drop (the drop at rest neglecting gravity and pressure forces) requires that

$$\cos \beta = \frac{\sigma_{v-s} - \sigma_{l-s}}{\sigma_{l-v}}$$



Where the contact angle β is less than 90 degrees the drop will spread out on the surface to form a continuous film. From observation of a particular fluid-surface combination, either the contact angle may be measured, or the general tendency to form a film or discrete drops may be noted. The condensation of sulphur vapor on glass forms a continuous film. Water vapor forms a film on most clean surfaces unless surface active agents are added. It is a matter of common observation that liquid mercury generally forms drops on surfaces.

The heat transfer rates which have been observed in drop-wise condensation are many times greater than those which are obtained when a continuous

Contrails

film is formed. Although this fact is explained by the intimate contact between vapor and cooled surface which occurs in drop-wise condensation (as compared to the resistance to heat flow represented by a continuous film), no satisfactory theory for drop-wise condensation has been worked out.

When a condensing fluid forms a continuous film on the heat transfer surface, the mechanisms involved can be described. The interface between the liquid and vapor phases can be considered to be at the saturation temperature (see Reference 1 for a discussion of this point). The resistance to heat flow is mainly localized in the liquid film. This resistance, which controls the heat transfer rate, determines the condensation rate and thus the film build-up. In the absence of external forces on the liquid film, the interface between phases would propagate into the vapor phase (as in melting and freezing phenomena), and no steady-state solution would exist. When external forces acting on the liquid layer cause motion, then the liquid is moved along the surface and eventually collected by some means. The tendency of the interface to propagate into the vapor phase (by heat transfer) is balanced by the removal of the film and a steady-state condition is obtained.

Significant analytical contributions to our knowledge of film-type condensation have attributed the sole or major role in the film removal to gravity forces. In the rotating condenser, film removal is accomplished by rotating the cooling surface.

In systems where gravity (or any other constant body force) is absent, the removal of the film is effected by pressure forces and shearing stresses exerted by the moving vapor on the liquid-vapor interface. An analysis of such a condensation process is shown in Section VIII. In the spiral condenser, the film removal is accomplished by rotating the fluid with the condenser to separate the vapor and liquid and the stresses exerted on the liquid by the moving vapor. Since such systems have become of interest only recently, due to the feasibility of flight in space, it is not surprising that the literature of film condensation does not supply design information on gravity-free systems.

The liquid film flow at the heat transfer surface may be laminar, turbulent, or in the process of transition. The details of transition are not well known, but it is observed that a liquid film initially laminar will eventually become turbulent if allowed to grow sufficiently thick. The criterion used to determine whether a condensate film will be laminar or turbulent is a critical value of the film Reynolds number (utilizing the flow through the film and the equivalent diameter in its computation). Thus if the flow per unit width in a two-dimensional system or the flow per unit perimeter in a circular system is Γ , the Reynolds number of the film can be written in the form $4\Gamma/\mu$, where μ is the viscosity of the liquid film. When vapor shear stress is absent, the suggested criterion for transition to turbulence is $4\Gamma/\mu = 1800$ (2). When significant vapor shear stresses are acting on the film, the critical Reynolds number may be as low as 200 (3).

The computation of laminar film condensation logically follows from the application of well-known laws of heat conduction and laminar shear stress to simplified models of the real physical process. In most cases the assumptions which have been made in order to construct a simple, yet realistic, model of the physical process have been checked by experiment or by more detailed calculations in some instances.

Contrails

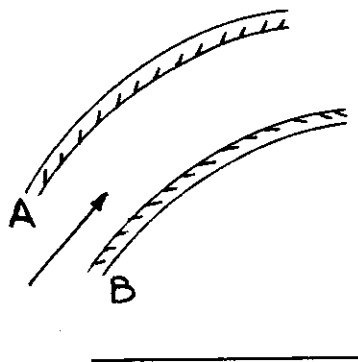
The analytical techniques for predicting the behavior of turbulent condensing films are semi-empirical. Due to lack of knowledge of the turbulent processes in sufficient detail, the computations depend on the assumption of certain analogies between momentum and heat transfer as well as the use of experimentally determined (or assumed) velocity profiles and skin-friction laws. The actual numerical computations are much more involved and the train of logic much less satisfying in the case of turbulent films as compared to laminar films. The reasonable agreement of these analyses with experiment as well as their ability to predict trends make them an important and useful addition to the state-of-the-art knowledge of film condensation.

DESIGN OF A SPIRAL CONDENSER

The use of a spiral condenser* for zero-gravity condensation is based somewhat on the same premises as the use of a vortex evaporator for zero-gravity evaporation. Since condensate removal in conventional units is usually accomplished by gravity forces, some other device must be employed when gravity is absent. One such device is to rotate the cooling surface (rotating condenser), and the other is to rotate the fluid without having to rotate the condenser itself. A vortex tube with twisted tape is not applicable to the condensation problem where it is desired to remove the liquid from the heat transfer surface and supply it with fresh vapor.

The spiral condenser itself is a simple device. It consists (see Figure 36) of two long metal strips which are wound concentric with each other to provide the spiral fluid passages. The ends may be sealed off by welding and headers may be provided to lead the fluids in and out of the unit. Studs may be used at regular intervals between the two strips to provide structural integrity. If fins are required, there should be no difficulty in providing these on either or both sides, although conventional units have not used fins up to the present time. Both fluids may be passed either in parallel or counterflow spirals, or one fluid may be in spiral flow while the other is in a direct crossflow through the exchanger.

Consider a curved passage such as that shown below, in which vapor is flowing in the passage which is cooled by fluid in two concentric curved passages on either side of the passage shown. Kreith (4) has shown that heat transfer on



*A spiral heat exchanger for conventional uses is currently manufactured by the American Heat Reclaiming Corporation, New York, New York.

a concave wall A is better than that on wall B. Hsuan Yeh (5) has shown that due to the high mixing of fluid in the vicinity of wall A, a high heat transfer rate is obtained. Lower-energy fluid in the boundary layer of wall A will tend to travel inwards, while higher-energy fluid tends to travel towards A, producing a good mixing effect of hot and cold condensate. In addition, the outer part of the condensate layer on wall B will tend, due to centrifugal action, to move away from wall B. The force on the liquid will be much higher than that on the vapor, due to the greater density of the liquid. Hence, two effects are taking place in the curved passage. The condensate layer on wall B will be kept small due to centrifugal action, thus ensuring good heat transfer. The condensate layer on wall A may grow thicker than that on wall B, but may have a temperature close to that of wall A, due to severe mixing in this region. For water-to-air heat exchangers, Kreith's data indicate that the heat transfer rates for concave and convex walls together have the same mean value as that for the flat plate case. For the design here, condensation heat transfer coefficients based on Reference 3, which takes into account the effect of high vapor velocities on condensation, have been used.

In general, plate-fin heat exchangers are not used when one of the fluids is a liquid metal. The heat transport fluid used here is sodium-potassium alloy with a 22 per cent sodium and a 78 per cent potassium composition. It has a low melting point (12 degrees F) and a high conductivity. Its viscosity is low, and since the fluid conducts electricity an electromagnetic pump may be used in the loop, if desired. Two sizes of tube-fin condensers have been designed, the main difference being the inside diameter of the tubes. The design characteristics for these condensers are shown in Tables 10 and 11. The volumes of the tube-fin condensers are shown in Figures 37 and 38. As expected, the volumes of the small-diameter tube condensers are considerably smaller than those of the larger-diameter tube units. However, the smaller-diameter tubes have been used for NaK heat transfer only recently, and the possibility of fouling in small tubes is greater.

Figure 36 shows the diagram of a spiral condenser. Figure 38 also shows the volumes of the spiral counterflow condensers for two cases. The volumes of the small-diameter tube-fin condensers are considerably smaller than those of the spiral condensers. The spiral condenser volumes are more comparable with those of the larger tube-fin units. If the fouling characteristic in small-diameter tubes is neglected, the volumes of the spiral condenser should be compared with those of the small-diameter tube-fin units. Although the NaK-side core pressure drop in the small tube-fin condensers is about fifty times that in the larger tube-fin units, the absolute magnitude is still negligible, about 0.009 psi.

Figure 39 shows the variation in volume and pressure drop for two variations of the counterflow spiral condenser. From Reference 3, the Freon 11 heat transfer coefficient may be written

$$h_{F-11} = 0.065 \left(\frac{c_{p1} \rho_1}{2 \mu_1 \rho_v} k_1 f \right)^{\frac{1}{2}} G_{mv} \quad (62)$$

which shows the heat transfer coefficient to be linearly proportional to the mass

Contrails

flux. If the mass flux is kept constant, the total volume of the condenser varies linearly with the heat load. In Figure 39, the flow area is varied (to keep G constant) by varying the spiral condenser length while keeping the plate spacing constant. In this case, the Freon-side and NaK-side pressure drops are constant with the heat load. The second variation shown in Figure 39 is that where the flow area is kept constant, so that the mass flux is proportional to the heat load. In this case, the volume does not change appreciably with the heat load. The change in the heat load is counterbalanced somewhat by the change in the heat transfer coefficient. A calculation procedure for a spiral counterflow condenser is shown in Appendix 3. Pressure drop information is also included.

The changes in core volume and pressure drop obtained by changing the plate spacing on the NaK side of a spiral counterflow condenser are shown in Table 12 and Figure 40. The condenser length is kept constant and is equal to one foot. As expected, NaK-side pressure drops and, consequently, the NaK pumping power are high at low values of plate spacing. One method of reducing the NaK-side pressure drop is to pass the NaK through the condenser in a crossflow relation to the spiral Freon 11 passage. Such a calculation is shown in Appendix 3. The volume of the crossflow condenser is larger than that of the comparable counterflow unit, assuming the same plate spacing for the NaK and Freon sides. However, since the NaK now has a much larger free flow area, the pressure drop on the NaK side is negligible. Because of this, a smaller plate spacing may be chosen on the NaK side, which reduces the total crossflow condenser volume compared to the counterflow case. The NaK-side pressure drop may still be kept negligible. There may still be some advantage for the counterflow unit from the standpoint of manifolds and header systems. Also, in zero-gravity operation, a nonwetting liquid such as NaK will not maintain good mechanical contact with the heat transfer surface, and the passages must be kept filled with the fluid. This represents some advantage for the counterflow condenser where the NaK is also in a spiral passage and hence experiences a centrifugal force which increases contact with at least one section of the spiral wall.

In the discussion above, the volumes given are the core volumes of the heat exchangers and do not include the shells or the header system. The pressure drops referred to are the core values and do not include entrance and exit losses or any values for ducts. It is believed necessary to construct and test a spiral condenser system to obtain sufficient heat transfer information for condensation in curved passages, before a complete design for a specific mission can be made. In any event, the spiral condenser volumes are considerably larger than those of the comparable tube-fin units. The Freon 11 side volume of a spiral condenser may be reduced by using fins. However, spiral condensers with fins have not yet been constructed, and some experimentation and development is necessary before reliable designs can be made.

Contrails

LIST OF SYMBOLS

A	sq ft	Heat transfer area
A_{face}	sq ft	Heat exchanger face area
A_{free}	sq ft	Heat exchanger free area
c_p	BTU/lb-degF	Specific heat
D	ft	Diameter
d_h	ft	Hydraulic diameter
f		Fanning friction factor
G	lbs/hr-sq ft	Mass flux
G_m	lbs/hr-sq ft	Totally condensed mean mass flux
G_{mv}	lbs/hr-sq ft	Mean vapor mass flux
g	ft/sec ²	Gravitational acceleration
h	BTU/hr-sq ft-degF	Heat transfer coefficient
Δh	BTU/lb	Enthalpy difference
h'_{fg}	BTU/lb	Latent heat of vaporization plus superheat enthalpy
k	BTU/hr-ft-degF	Thermal conductivity
L	ft	Flow length
N_{Pr}		Prandtl number
N_{Re}		Reynolds number
P	lbs/sq in	Pressure
ΔP	lbs/sq in	Pressure difference
Q, q	BTU/hr	Heat rate
s	ft	Linear condenser length
T	degF	Temperature
ΔT_{sat}		$= T_{wall} - T_{sat}$
t	in	Distance between plates (width of passage)
U	BTU/hr-sq ft-degF	Over-all heat transfer coefficient
V	cu ft	Volume
v	ft/sec	Velocity
w	lbs/min	Mass flow rate
X		Lockhart and Martinelli correlation factor

Contrails

β
 ϵ
 ϵ
 T
 μ
 ρ
 σ
 ϕ

lbs/hr-ft Liquid-surface contact angle
 lbs/hr-ft Exchanger heat transfer effectiveness
 lbs/cu ft Emissivity
 lbs/ft Mass flow per unit width or perimeter
 Viscosity
 Density
 Surface tension
 Square root of ratio of two-phase to
 vapor pressure drops

Subscripts

Al	refers to	Aluminum
ave		Average
C		Condenser; condensate
c		Cold side
F-11		Freon 11
h		Hot side
l		Liquid
lm		Logarithmic mean
max		Maximum
mix		Two-phase
NaK		NaK or Sodium Potassium
R		Radiator surface
S		(Heat) sink
sat		Saturated
T		Total
tt		Turbulent-turbulent flow
V		Vapor
wall		Wall
1, 2		Entrance, exit

Contrails

REFERENCES

1. Jakob, M., Heat Transfer, Volume I, John Wiley and Sons Inc., New York, 1949, p. 660
2. McAdams, W. H., Heat Transmission, McGraw-Hill Book Company, Inc., New York, 1954, p. 334
3. Carpenter, E. F. and Colburn, A. P., "The Effect of Vapor Velocity on Condensation Inside Tubes," Proceedings of the General Discussion on Heat Transfer, London, July 1951
4. Kreith, F. "The Influence of Curvature on Heat Transfer to Incompressible Fluids," Trans. ASME, vol. 77, 1955, pp. 1247-1256
5. Yeh, Hsuan, "Boundary Layer along Annular Walls in Spiraling Flow," Trans. ASME, vol. 80, May 1958

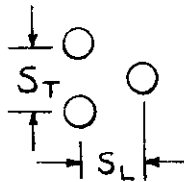
TABLE 9
MINIMUM RATIOS FOR CONDENSING-SIDE TO RADIATING-SIDE
HEAT TRANSFER COEFFICIENTS FOR INTEGRAL RADIATOR-CONDENSERS

Fluid	Saturation Temperature degF	Condensation Tube Diameter in	$(h_c/h_R)_{\min}$
Freon 11	320	0.5	3.6
Freon 11	320	2.0	0.9
Freon 11	250	0.5	1.57
Freon 11	150	2.0	3.25
Mercury	400	0.5	640
Mercury	400	0.5	160
Sodium	800	0.5	1120
Sodium	1250	0.5	396
Sulphur	400	2.0	2.0
Sulphur	1100	2.0	0.5

TABLE 10

DESIGN CHARACTERISTICS OF SMALL TUBE-FIN CONDENSERS

Staggered tubes, NaK inside tubes
Tube outside diameter = 0.1875 in
Tube inside diameter = 0.1375 in
Tube wall thickness = 0.025 in



$$S_T = S_L = 0.375 \text{ in}$$

Freon 11 Side

Fin height = 0.09375 in
Fin thickness = 0.01 in
Number of fins per inch = 10 (Rectangular fins, crimped at base)
 $A_{\text{free}}/A_{\text{face}} = 0.450$
Heat transfer Area/Volume = 487 sq ft/cu ft
Hydraulic diameter = 0.003696 ft

NaK Side

$A_{\text{free}}/A_{\text{face}} = 0.106$
Heat transfer Area/Volume = 37.0 sq ft/cu ft
Hydraulic diameter = 0.01146

TABLE 11

DESIGN CHARACTERISTICS OF LARGE TUBE-FIN CONDENSERS

(Reference: Kays, W. M. and London, A. L., Compact Heat Exchangers, McGraw-Hill Book Company, New York, 1958)

Staggered tubes, NaK inside tubes

Surface CF - 8.7 - 5/8 J

Tube outside diameter = 0.645 in

Tube inside diameter = 0.55 in

Tube wall thickness = 0.010 in

Freon 11 Side

Staggered circular finned tubes

$A_{\text{free}}/A_{\text{face}} = 0.628$

Heat transfer Area/Volume = 65.7 sq ft/cu ft

Number of fins per inch = 8.7

Hydraulic diameter = 0.0383 ft

NaK Side

$A_{\text{free}}/A_{\text{face}} = 0.0955$

Heat transfer Area/Volume = 8.31 sq ft/cu ft

Hydraulic diameter = 0.0471 ft

TABLE 12

TOTAL VOLUME AND NaK PRESSURE DROP FOR COUNTERFLOW SPIRAL CONDENSERS

Evaporator heat load = 4000 BTU/min
 Condenser length(s) = 1.0 ft
 Width of Freon 11 passage = 0.25 in

Evaporator Temperature degF	Condenser Temperature degF	NaK Hydraulic Diameter in	NaK-Side Pressure Drop psi	Condenser Total Volume cu ft
40	250	0.50	39.1	3.56
		0.75	12.3	4.42
		1.0	5.13	5.30
		1.5	1.592	7.20
		2.0	0.702	9.25
		2.5	0.370	11.35
		3.0	0.226	13.87
40	150	0.50	9.86	2.00
		0.75	4.04	2.46
		1.0	1.32	3.055
		1.50	0.418	4.23
		2.00	0.186	5.50
55	250	1.50	1.492	6.625
55	150	1.0	1.20	2.77

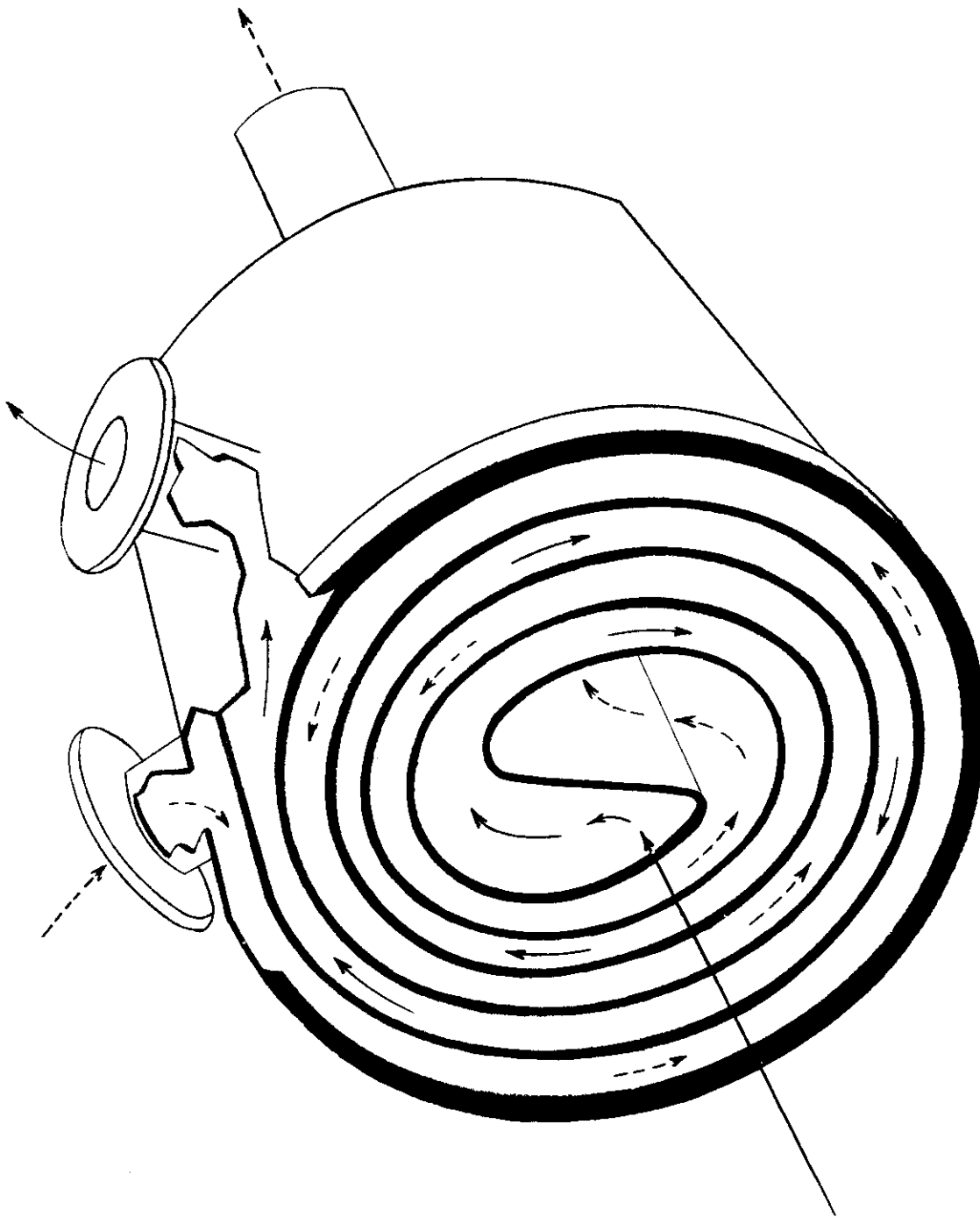


FIGURE 36: DIAGRAM OF A SPIRAL CONDENSER (FLUIDS IN COUNTERFLOW)

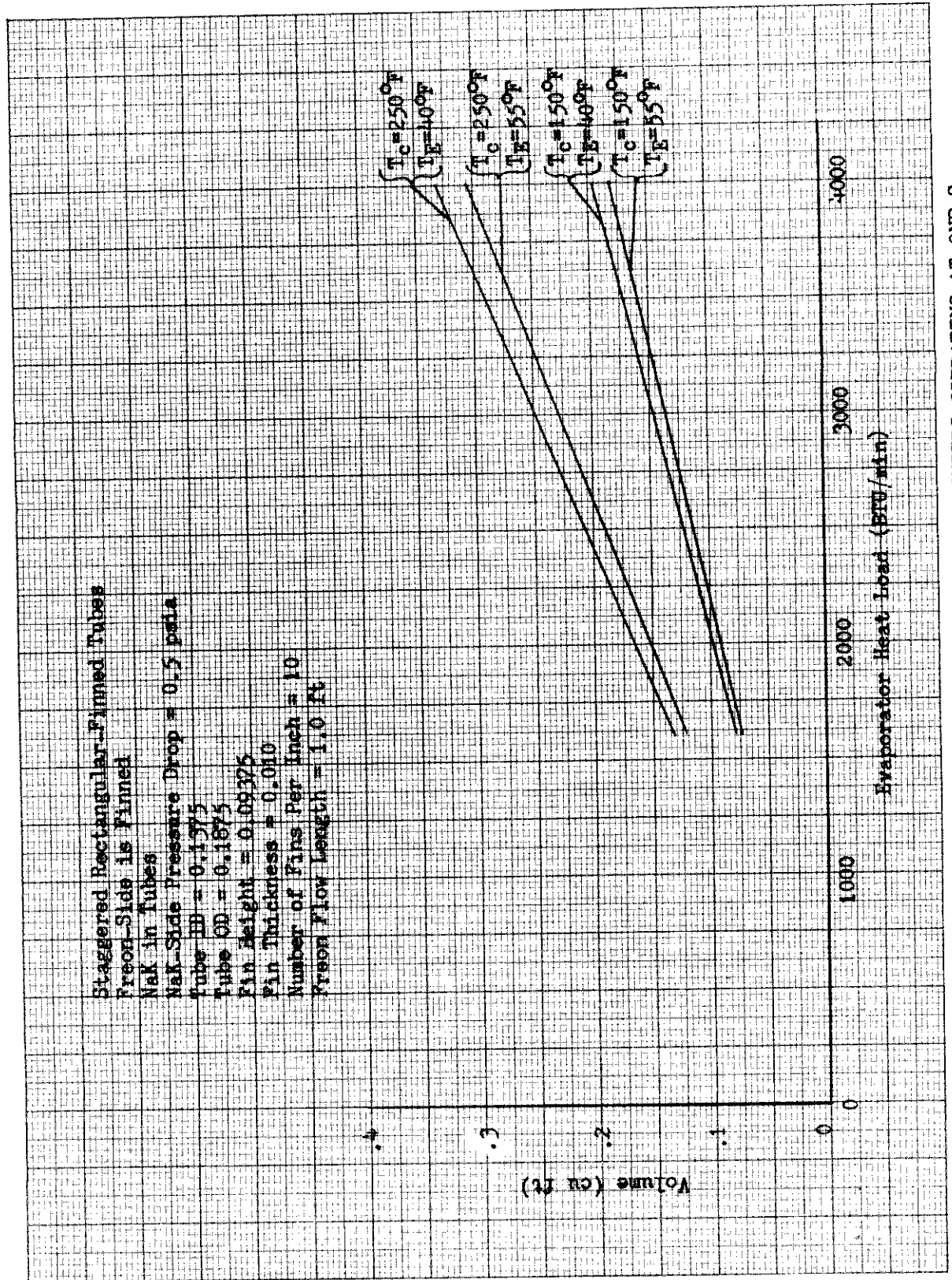


FIGURE 37: VOLUMES OF SMALL FREON 11 TUBE-FIN CONDENSERS OPERATING AT ONE-G

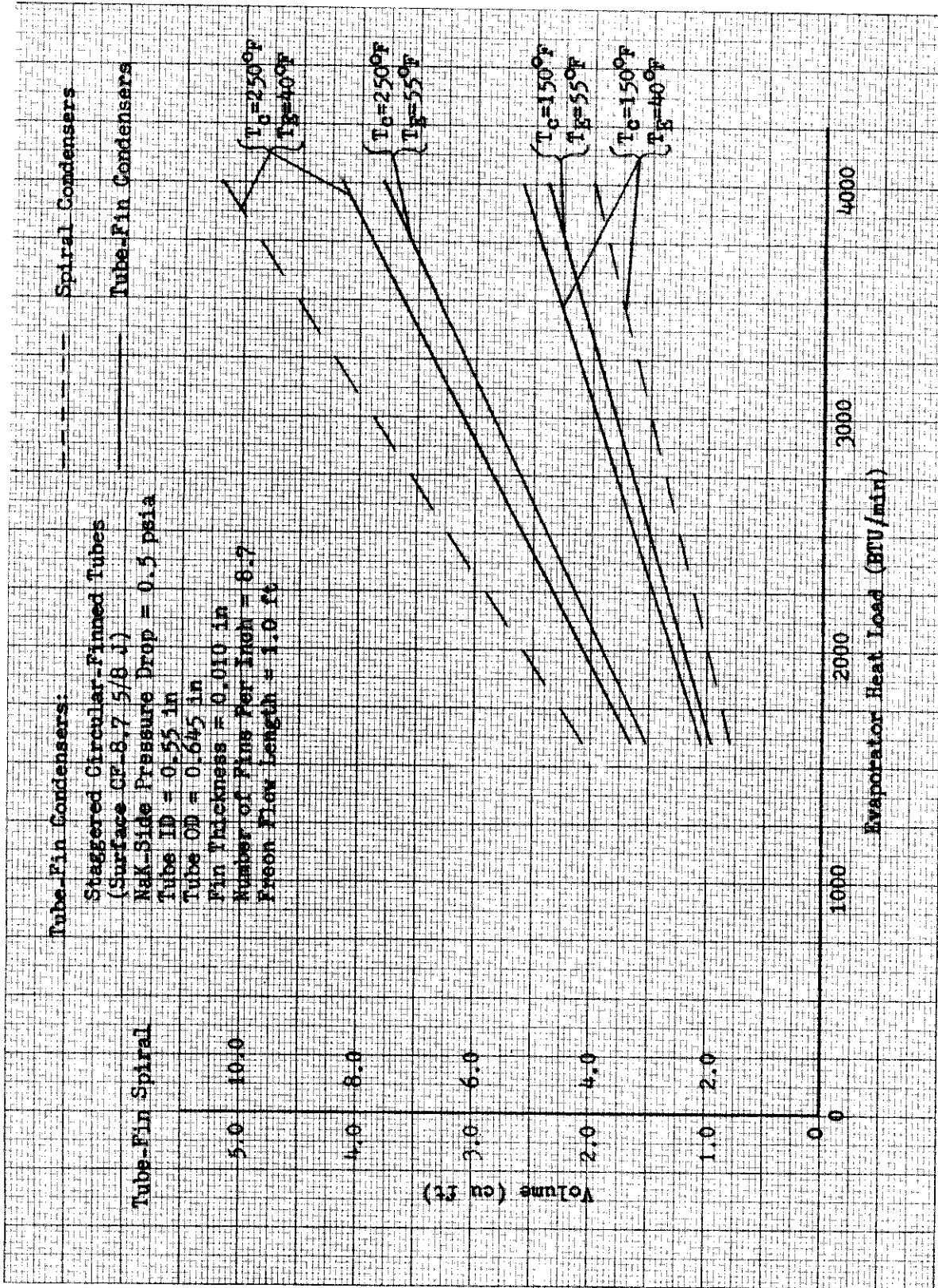


FIGURE 38: COMPARISON OF VOLUMES OF FREON 11 SPIRAL CONDENSER (ZERO-G) WITH LARGE TUBE-FIN CONDENSERS (ONE-G)

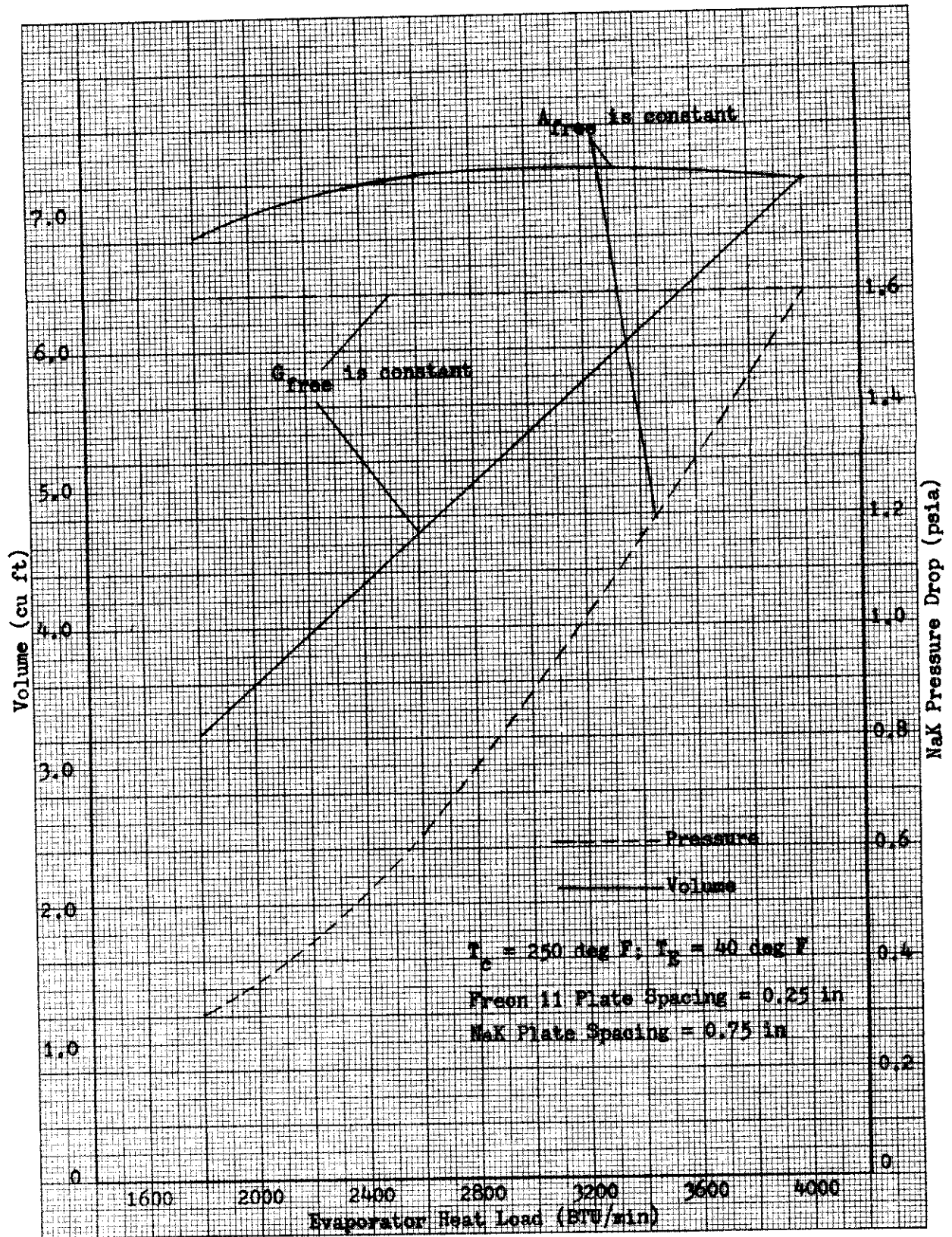


FIGURE 39: VOLUME AND PRESSURE DROP FOR FREON 11 SPIRAL CONDENSER

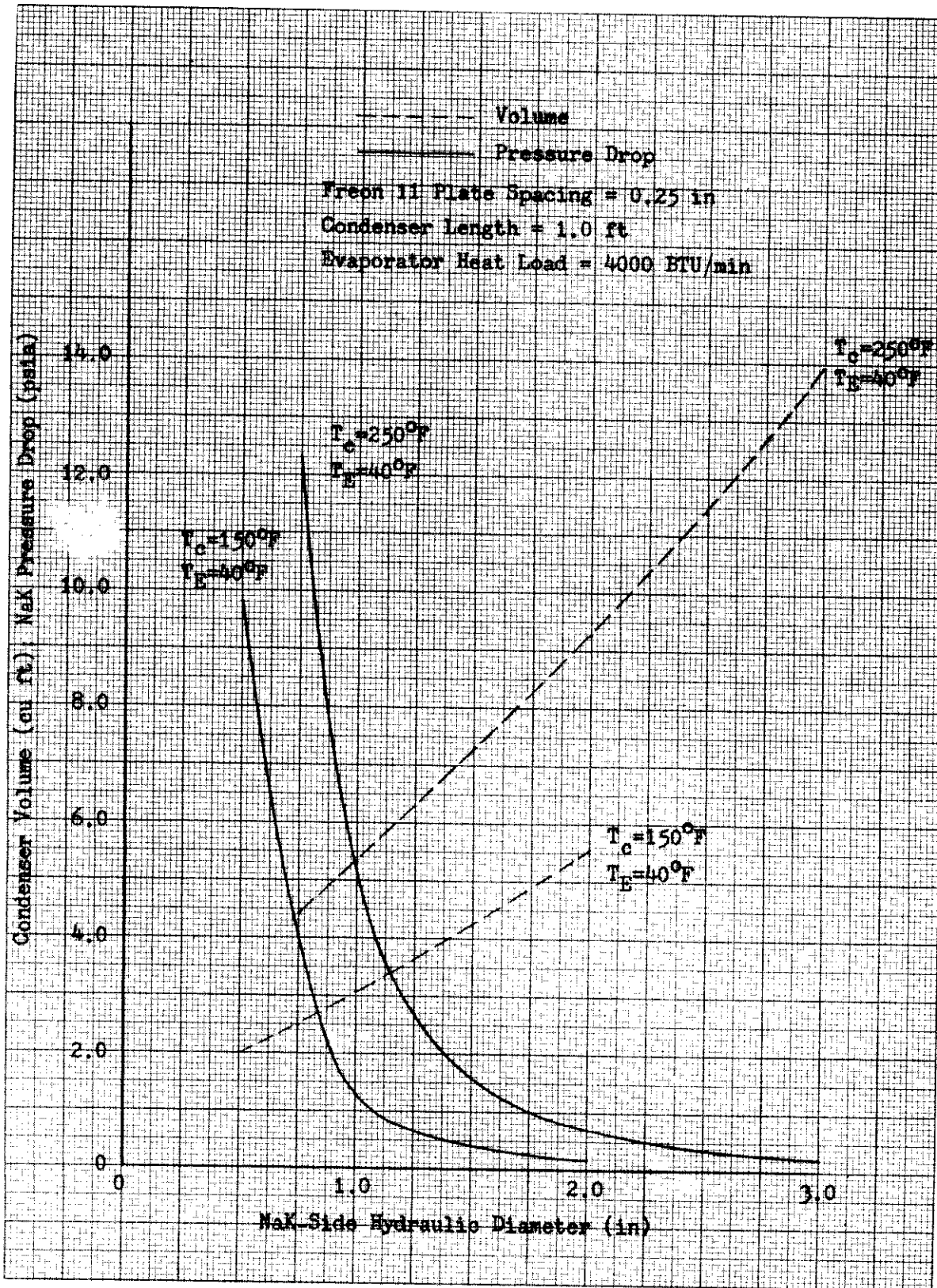


FIGURE 40: VARIATION OF FREON 11 SPIRAL CONDENSER VOLUME
AND PRESSURE WITH NaK-SIDE HYDRAULIC DIAMETER

Contrails

TOTAL VOLUME AND NaK PRESSURE DROP FOR COUNTERFLOW SPIRAL CONDENSERS

Evaporator heat load = 4000 BTU/min
Condenser length(s) = 1.0 ft
Width of Freon 11 passage = 0.25 in

Evaporator Temperature degF	Condenser Temperature degF	NaK Hydraulic Diameter in	NaK-Side Pressure Drop psi	Condenser Total Volume cu ft
40	250	0.50	19.55	1.78
		0.75	6.15	2.21
		1.0	2.57	2.66
		1.5	0.79	3.62
		2.0	0.35	4.64
		2.5	0.18	5.69
		3.0	0.11	6.96
40	150	0.50	4.90	1.00
		0.75	2.02	1.24
		1.0	0.66	1.54
		1.50	0.21	2.13
		2.00	0.09	2.77
55	250	1.50	0.75	3.32
55	150	1.0	0.60	1.39

Contrails

SECTION VIII

FILM CONDENSATION UNDER ZERO GRAVITY

In normal practice, the gravity forces acting on the liquid film formed in a condensation process are effective in separating the liquid and vapor phases and collecting the condensate. The gravity-free condenser may be rotated so that a similar effect is produced. The case wherein no body force is acting seems not to have been considered in detail.

An analysis for the growth of a laminar condensing film moved by a constant vapor shear stress in the absence of body forces can be made quite simply along the lines of the original Nusselt approach.

Under the action of a constant vapor shear stress, and without the action of gravity, the velocity distribution in the film will be linear.

The velocity distribution is given by:

$$u = \frac{\tau_v y}{\mu} \quad (63)$$

The average film velocity is

$$\bar{u} = \frac{\tau_v \delta}{2\mu} \quad (64)$$

and the condensate flow is

$$\Gamma = \frac{\rho \tau_v \delta^2}{2\mu} \quad (65)$$

Equating local heat flow rate to the local condensation rate, and once again assuming a linear temperature distribution, the film thickness is found to be

$$\delta = \left(\frac{3k\Delta T\mu x}{\rho\tau_v h_{fg}} \right)^{1/3} \quad (66)$$

The local heat transfer coefficient is

$$h = k \left(\frac{3k\Delta T\mu x}{\rho\tau_v h_{fg}} \right)^{-1/3} \quad (67)$$

Contrails

and the mean coefficient over a plate of length L is

$$h_m = 1.04 k \left(\frac{\rho \tau_v h_{fg}}{k \Delta T \mu L} \right)^{1/3} \quad (68)$$

The above results for the average heat transfer coefficient can be put in the form of dimensionless ratios:

$$\frac{h_m L}{k} = 1.04 \left(\frac{c_p \Delta T}{h_{fg}} \right)^{-1/3} \left(\frac{c_p \mu}{k} \right)^{1/3} \left(\frac{\rho \tau_v L^2}{\mu^2} \right)^{1/3} \quad (69)$$

The first dimensionless ratio is the familiar Nusselt number, $h_m L/k$, a heat transfer parameter. The term $(c_p \Delta T/h_{fg})$, which occurs in condensation problems, is the ratio of the subcooling heat effect to the latent heat effect. The dimensionless group $(c_p \mu/k)$, entirely made up of properties of the liquid, is the Prandtl number. The remaining dimensionless ratio can be shown to be a Reynolds number based on plate length. The Reynolds number based on film thickness is

$$\frac{4 \Gamma}{\mu} = \frac{4}{\mu} \left(\frac{\rho \tau_v \delta^2}{2 \mu} \right) = \frac{2 \rho \tau_v \delta^2}{\mu^2} \quad (70)$$

The above analysis predicts the heat transfer and flow properties of a laminar condensing film in the absence of gravity where the sole effect on the motion of the liquid film is the action of a constant shear stress at the liquid-vapor interface. The assumptions made are those common to most condensation analyses.

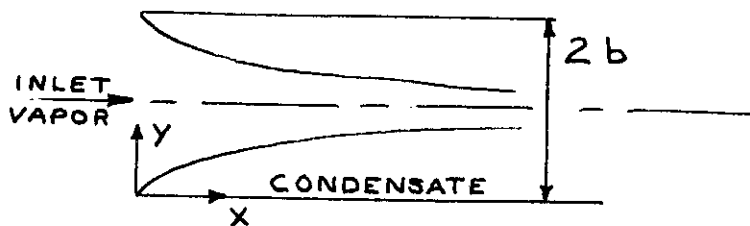
For applications where condensation occurs inside tubes and channels, the above analysis must be generalized to include the effects of varying vapor shear stress along the film length (due to variations in vapor and film properties along the tube) and for the effect of pressure gradient.

In order to learn some of the characteristics of the condensation process within a duct when body forces are absent, a two-dimensional problem is considered here. The analysis for a round tube will be similar but more complicated algebraically.

Consider a two-dimensional duct formed by two parallel plates spaced the distance $2b$ apart. Each plate is maintained at the temperature T_w , which is below the saturation temperature of the vapor. In order to simplify the analysis, it will be assumed that the vapor enters the duct in the saturated state and that pressure changes which take place along the duct are sufficiently small so that the vapor density and temperature remain constant.

A liquid film will form on each wall, and the liquid film will move along the wall under the action of shearing stresses exerted on the liquid film

by the vapor at the liquid-vapor interface and by the pressure gradient along the duct. Of particular interest from the following analysis is the length of duct required to condense all of the inlet vapor.



VELOCITY DISTRIBUTION IN THE CONDENSATE LAYER

The assumption is made that inertia effects are negligible in the condensate flow and therefore the condensate layer is in force equilibrium. This assumption is common to approximate analysis of the condensation process and has been shown to be a good assumption so long as the Prandtl number of the condensate is sufficiently small.

The details of the derivation may be found in Appendix 4. The velocity distribution within the condensate layer is given by

$$u = \frac{\tau_v}{\mu} y - \frac{1}{\mu} \frac{dP}{dx} y \left(\delta - \frac{y}{2} \right) \quad (71)$$

The average velocity within the condensate layer may be obtained by integration:

$$u_{ave} = \frac{\tau_v \delta}{2\mu} - \frac{1}{3\mu} \left(\frac{dP}{dx} \right) \delta^2 \quad (72)$$

The condensate flow rate per unit depth of duct, Γ , is

$$\Gamma = \rho \delta u_{ave} = \frac{\rho \delta^2}{\mu} \left(\frac{\tau_v}{2} - \frac{\delta}{3} \frac{dP}{dx} \right) \quad (73)$$

The velocity distribution is dependent on the pressure gradient and on the shear stress exerted at the liquid-vapor interface. With gas flow in the positive x-direction, along the tube, the shear stress τ_v will be positive; that is, the shear stress will aid the flow of condensate. When the pressure falls in the direction of flow, the condensate velocity is augmented by pressure forces. An adverse pressure gradient of sufficiently great magnitude would produce negative velocities within the condensate layer, that is, back flow. A simple analysis of the condensate layer cannot be expected to be valid in the case of back flow. A plot of the velocity distribution within the condensate layer for various values of the dimensionless ratio of pressure gradient to shear stress is shown in Figure 41. The condition on the pressure gradient so that back flow will not occur is

Contrails

$$\left(\frac{dp}{dx}\right)_{\max} = \frac{\tau_v}{\delta} \quad (74)$$

The above analysis is only appropriate for laminar condensate flow. The film Reynolds number is given by

$$\frac{4\Gamma}{\mu} = \frac{4\rho\delta^2}{\mu^2} \left(\frac{\tau_v}{2} - \frac{\delta}{3} \left(\frac{dp}{dx} \right) \right) \quad (75)$$

For cases where the condensate flows without pressure gradient or vapor shear stress (gravity flow), the criterion for the transition to turbulence within the condensate layer has been $4\Gamma/\mu = 1800$. With vapor shear stress the value of the film Reynolds number at the onset of turbulence has been estimated to be as low as 200. A criterion for transition to turbulence which has been suggested by Carpenter (4) and later used by Rohsenow (2) assumes that transition will occur when the wall shear stress takes on a definite value independent of the applied vapor shear stress. These estimates have been used to determine the transition point when vapor shear stress acts in addition to gravity within the condensate film. Since the pressure gradient within the duct has the same effect on the velocity distribution as the gravity force, it seems reasonable to use the same criterion for the onset of turbulence. Thus the condensate layer will be assumed to remain laminar until the wall shear stress reaches the critical value given by

$$\frac{D_e}{\nu} \sqrt{\frac{\tau_o}{\rho}} = 150 \quad (76)$$

Note that the equivalent diameter is used in the critical shear stress relation and therefore the criterion for the onset of turbulence will also depend on the condensate layer thickness. The above expression may be written,

$$\frac{\delta}{\nu} \sqrt{\frac{\tau_o}{\rho}} = \frac{150}{4} = 37.5 \quad (77)$$

The wall shear stress is given by

$$\tau_o = \tau_v + \left(-\frac{dp}{dx} \right) \delta \quad (78)$$

THE ENERGY EQUATION APPLIED TO THE CONDENSATE LAYER

The heat transfer rate at the wall of the duct is set equal to the net enthalpy flux through a control surface surrounding the condensate layer, neglecting the effect of liquid subcooling. The wall heat transfer rate is evaluated by assuming the temperature distribution across the condensate layer to be linear. The details of this derivation may be found in Appendix 4. The

Contrails

result is

$$\frac{k(T_{\text{sat}} - T_w)}{\delta h_{fg}} = \frac{dT}{dx} \quad (79)$$

CONTINUITY RELATION

The principle of conservation of mass is applied to the flow inside the duct. The mass rate of flow entering the duct is $2 \rho_g U_o b$. The mass rate of flow of gas and condensate at an arbitrary section of the duct is

$$2 \rho_g U(b - \delta) + 2 \Gamma$$

The continuity relation is

$$2 \rho_g U_o b = 2 \rho_g U(b - \delta) + 2 \Gamma \quad (80)$$

MOMENTUM RELATION FOR THE GAS FLOW

The momentum theorem of steady flow is applied to a control surface surrounding an element of the gas flow. The pressure is assumed uniform across the gas flow and the gas is treated in bulk; that is, the gas is characterized by a single velocity U . In this analysis, the momentum transfer across the liquid-vapor interface is assumed to be negligible. The details of the derivation may be found in Appendix 4. The result is

$$(b - \delta) \frac{dP}{dx} = U^2 \rho_g \frac{d\delta}{dx} - \tau_v - 2 U \rho_g (b - \delta) \frac{dU}{dx} \quad (81)$$

SHEAR STRESS RELATION

Since the gas flow is treated in bulk, that is, the gas flow is characterized by a single value of velocity U at any section of the duct, some experimental law must be used to relate the vapor shear stress to this bulk velocity.

Bergelin, Kegel, Carpenter, and Gazley (4) have correlated the vapor shear stress acting on a condensate film in terms of the gas flow Reynolds number and a parameter of the condensate film, as shown in Figure 42. This parameter, $\Gamma \sigma_w / \rho \sigma$, is the volume rate of flow of condensate per unit depth multiplied by the ratio of the surface tension of water to the surface tension of the condensate. For the numerical results obtained here, the lowermost curve, corresponding to a zero value of this parameter, was used. It was found convenient to fit a power law to this curve, the power law being valid for Reynolds numbers between 2×10^4 and 10^6 . This power law is

$$\frac{\tau_v}{\frac{1}{2} \rho_g U^2} = \frac{0.0911}{(Re)^{0.252}} \quad (82)$$

Contrails

where the gas flow Reynolds number, Re , is given by

$$Re = \frac{4\rho_g U(b-\delta)}{\mu_g} = \frac{4U(b-\delta)}{\nu_g} \quad (83)$$

SUMMARY OF EQUATIONS

Condensate Flow (along one wall)

$$\Gamma = \frac{\rho \delta^2}{\mu} \left(\frac{\tau_v}{2} - \frac{\delta}{3} \left(\frac{dp}{dx} \right) \right) \quad (84)$$

Energy Equation

$$\frac{d\Gamma}{dx} = \frac{k(T_{sat} - T_w)}{\delta h_{fg}} \quad (85)$$

Momentum Equation for Gas Flow

$$(b-\delta) \frac{dp}{dx} = \rho_g U^2 \frac{d\delta}{dx} - \tau_v - 2U\rho_g(b-\delta) \frac{dU}{dx} \quad (86)$$

Continuity

$$\rho_g U_0 b = \rho_g U(b-\delta) + \Gamma \quad (87)$$

Shear Stress Relation

$$\tau_v = \frac{1}{2} \rho_g U^2 \left\{ \frac{0.0911}{\left(\frac{4U(b-\delta)}{\nu_g} \right)^{0.252}} \right\} \quad (88)$$

These five equations may be used to determine the variation along the duct of the five unknown variables, Γ , δ , τ_v , p , and U .

DIMENSIONLESS FORMULATION

Before proceeding with the numerical solution of the preceding equations, it is useful to formulate the problem in terms of dimensionless variables. The local gas velocity is normalized with respect to the inlet velocity, the condensate flow rate with respect to the inlet gas flow, and the condensate layer thickness and the distance downstream from the inlet by the channel half-spacing. The pressure and shear stress are normalized with respect to the gas dynamic head at duct entrance. Using the bar above a variable to indicate that it is dimensionless, there follows:

Contrails

$$\bar{U} = U/U_0$$

$$\bar{T} = T/\rho_c U_0 b$$

$$\bar{\delta} = \delta/b$$

$$\bar{x} = x/b$$

$$\bar{\gamma}_v = \gamma_v/\frac{1}{2}\rho_c U_0^2$$

$$\bar{P} = P/\frac{1}{2}\rho_c U_0^2$$

In terms of these dimensionless variables, the governing equations may be written in the following form:

Condensate Flow

$$\bar{T} = \frac{\rho U_0 b \bar{\delta}^2}{\mu} \left(\frac{\bar{\gamma}_v}{4} - \frac{\bar{\delta}}{6} \left(\frac{d\bar{P}}{d\bar{x}} \right) \right) = \left(\frac{U_0 b}{\gamma_c} \right) \left(\frac{\gamma_c}{\nu} \right) \bar{\delta}^2 \left(\frac{\bar{\gamma}_v}{4} - \frac{\bar{\delta}}{6} \left(\frac{d\bar{P}}{d\bar{x}} \right) \right) \quad (89)$$

Energy Equation

$$\frac{d\bar{T}}{d\bar{x}} = \frac{k(T_{sat} - T_w)}{\rho_c U_0 b h_{fg} \bar{\delta}} = \frac{k(T_{sat} - T_w)}{h_{fg} \mu_c} \left(\frac{\gamma_c}{U_0 b} \right) \frac{1}{\bar{\delta}} \quad (90)$$

Momentum Relation for Gas Flow

$$(1 - \bar{\delta}) \frac{d\bar{P}}{d\bar{x}} = 2 \bar{U}^2 \frac{d\bar{\delta}}{d\bar{x}} - \bar{\gamma}_v - 4 \bar{U} (1 - \bar{\delta}) \frac{d\bar{U}}{d\bar{x}} \quad (91)$$

Continuity

$$1 = \bar{U} (1 - \bar{\delta}) + \bar{T} \quad (92)$$

Contrails

Shear Stress Relation

$$\bar{\tau}_v = \frac{0.0911 \bar{U}^2}{\left\{ \left(\frac{4U_o b}{\nu_c} \right) \bar{U} (1 - \bar{\delta}) \right\}^{0.252}} \quad (93)$$

Note that the numerical solution of the above dimensionless equations requires the specification of the initial values of the dependent variables; i e.,

$$\begin{aligned} \bar{x} &= 0 & \bar{T} &= 0 \\ \bar{\delta} &= 0 & \bar{P} &= \bar{P}_o \\ & & \bar{U} &= 1 \end{aligned}$$

In addition, the solution will depend on the values of the following dimensionless parameters:

$$A = \frac{4K(T_{sat} - T_w)}{h_{fg} \mu_g C} = \frac{4K(T_{sat} - T_w)}{h_{fg} \mu C} \left(\frac{\mu}{\mu_g} \right) \quad (94)$$

$$B = \frac{C}{4} \left(\frac{\nu_c}{\nu} \right) = \frac{U_o b}{\nu} \quad (95)$$

$$C = \frac{4U_o b}{\nu_c} \quad (96)$$

The dimensionless number C is the Reynolds number of the gas flow at the tube entrance. B is the gas flow Reynolds number multiplied by the ratio of the kinematic viscosities of gas to liquid (or a liquid flow Reynolds number). A is a condensation number ($k[T_{sat} - T_w]/h_{fg} \mu$) divided by the gas flow Reynolds number and multiplied by the ratio of viscosities of the liquid to gas.

The solution may be written in functional form,

$$\{\bar{P}, \bar{T}, \bar{U}, \bar{\delta}\} = f \left\{ x_o, P_o, \frac{4U_o b}{\nu_c}, \left(\frac{\mu}{\mu_g} \right) \left(\frac{\nu_c}{\nu} \right), \frac{K(T_{sat} - T_w)}{h_{fg} \mu} \right\} \quad (97)$$

For a given fluid (with known properties), a solution may be obtained when the duct half-spacing b is specified, the inlet gas velocity U_o , the inlet pressure level P_o , and the saturation to wall temperature difference ($T_{sat} - T_w$) are known.

Contrails

METHOD OF SOLUTION

Using the definitions (94), (95), and (96) in equations (89), (90), (91), (92), and (93), the system of equations to be solved is

$$\bar{\Gamma} = B\bar{\delta}^2 \left(\frac{\bar{\tau}_v}{4} - \frac{\bar{\delta}}{6} \left(\frac{d\bar{P}}{d\bar{x}} \right) \right) \quad (98)$$

$$\frac{d\bar{\Gamma}}{d\bar{x}} = \frac{A}{\bar{\delta}} \quad (99)$$

$$(1 - \bar{\delta}) \frac{d\bar{P}}{d\bar{x}} = 2 \bar{U}^2 \frac{d\bar{\delta}}{d\bar{x}} - \bar{\tau}_v - 4 \bar{U} (1 - \bar{\delta}) \frac{d\bar{U}}{d\bar{x}} \quad (100)$$

$$1 = \bar{U} (1 - \bar{\delta}) + \bar{\Gamma} \quad (101)$$

$$\bar{\tau}_v = \frac{0.0911 \bar{U}^2}{(C \bar{U} (1 - \bar{\delta}))^{0.252}} \quad (102)$$

The initial condition on the condensate layer thickness is $\bar{\delta} = 0$ at $x = 0$. From (99) above, it may be seen that initially the rate of growth of the condensate layer is infinite, and consequently numerical procedures are not appropriate. Since the condensate flow rate will depend mainly on the shear stress $\bar{\tau}_v$ when $\bar{\delta}$ is small, an analytical solution may be used to calculate $\bar{\delta}$ and $\bar{\Gamma}$ for small values of $\bar{\delta}$, then a numerical scheme adopted for larger values of $\bar{\delta}$.

The starting solution is obtained from equations (98) and (99), assuming $\frac{\bar{\delta}}{6} \frac{d\bar{P}}{d\bar{x}}$ is negligible compared to $\bar{\tau}_v/4$, and that $\bar{\tau}_v$ remains constant at its initial value, which from equation (102) is

$$(\bar{\tau}_v)_{x=0} = \frac{0.0911}{(C)^{0.252}} \quad (103)$$

From (98)

$$\frac{d\bar{\Gamma}}{d\bar{x}} = \left(\frac{B(\bar{\tau}_v)_{x=0}}{4} \right) 2 \bar{\delta} \left(\frac{d\bar{\delta}}{d\bar{x}} \right) \quad (104)$$

Contrails

From (99)

$$\frac{d\bar{\Gamma}}{d\bar{x}} = \frac{A}{\bar{\delta}} \quad (105)$$

Therefore

$$\bar{\delta}^2 \frac{d\bar{\delta}}{d\bar{x}} = \frac{2A}{B(\bar{\tau}_v)_{x=0}} = \left(\frac{2}{0.0911}\right) \frac{A}{B} (C)^{0.252} \quad (106)$$

and

$$\frac{\bar{\delta}^3}{3} = \left(\frac{2}{0.0911}\right) \frac{A}{B} (C)^{0.252} \bar{x} \quad (107)$$

since $\bar{\delta} = 0$ when $\bar{x} = 0$.

$$\bar{\delta}^3 = 65.8 \frac{A\bar{x}(C)^{0.252}}{B}; \quad \bar{\delta} = 4.03 \left(\frac{A\bar{x}}{B}\right)^{1/3} C^{0.084} \quad (108)$$

The dimensionless condensate flow rate per unit depth of channel is

$$\bar{\Gamma} = 0.371 A^{2/3} B^{1/3} C^{-0.084} \quad (109)$$

Once the starting values of $\bar{\delta}$ and $\bar{\Gamma}$ have been obtained from the above analytical solution, the solution is continued numerically. Given the values of $\bar{\delta}$ and $\bar{\Gamma}$ at the point $x = x_0$, a value of $\bar{\delta}$ at the point $x = x_1$ is estimated. The value of $\bar{\Gamma}$ at $x = x_1$ is calculated from a finite-difference approximation to equation (99).

$$\frac{\bar{\Gamma}_1 - \bar{\Gamma}_0}{\bar{x}_1 - \bar{x}_0} = \frac{2A}{\bar{\delta}_0 + \bar{\delta}_1} \quad (110)$$

With $\bar{\Gamma}_1$ and $\bar{\delta}_1$ known, the value of U_1 is calculated from equation (101) and the value of $\bar{\tau}_{v_1}$ from equation (102). An approximate value of $\frac{d\bar{\delta}}{d\bar{x}}$ may be obtained from the finite-difference formula

$$\frac{d\bar{\delta}}{d\bar{x}} = \frac{\bar{\delta}_1 - \bar{\delta}_0}{\bar{x}_1 - \bar{x}_0}$$

The value of $\frac{d\bar{U}}{d\bar{x}}$ may be obtained from equation (101) by differentiation. Enough information is now available to calculate $\frac{d\bar{P}}{d\bar{x}}$ from equation (100).

The calculated and estimated values of $\bar{\tau}_v$, $\bar{\delta}$, and $\frac{d\bar{P}}{d\bar{x}}$ are

Contrails

substituted into equation (98) and a value of \bar{P} at $x = x_1$ is found. If the value of \bar{P} , resulting from this cycle of computations, does not agree with the value found from equation (110), then the process is repeated with an improved guess for $\bar{\delta}$ until sufficiently good agreement is obtained. This process is continued until the solution is obtained up to complete condensation.

At each step in the numerical procedure, a check should be made that the wall shear stress is below the value assumed as the criterion for transition to turbulence; that is,

$$\frac{\tau_0}{\rho} \leq 1405 \left(\frac{\nu}{\delta} \right)^2$$

or in dimensionless form

$$\bar{\tau}_0 = \frac{\tau_0}{\frac{1}{2} \rho_0 U_0^2} \leq \frac{2810}{(B \bar{\delta})^2} \left(\frac{\rho}{\rho_0} \right) \quad (111)$$

In order to illustrate the use of the preceding analysis, a numerical solution has been obtained for the following values of the dimensionless parameter, A, B, and C.

$$A = (1.62) (10^{-5})$$

$$B = (4.76) (10^4)$$

$$C = (1.57) (10^5)$$

These values apply for a low-velocity (about 5 ft/sec) Freon vapor entering a two-dimensional duct with a spacing of about $\frac{1}{2}$ inch. The saturation to wall temperature difference is about 35 degrees F.

A numerical solution has been obtained up to $\bar{x} = 800$. These numerical results are tabulated in Appendix 4, and the variations of some important physical quantities are shown in Figure 43. At a distance from the duct inlet of 800 half-spacings, only 26 per cent of the inlet vapor has condensed.

The application of the criterion previously discussed would indicate transition occurs far downstream since the film Reynolds number at this point is in excess of 2000. If a film Reynolds number of 1000 is critical, then transition should occur at $\bar{x} = 300$. More study of this point is required to fix the transition criterion; however, these results point out the practical importance of a turbulent film condensation solution. The rate of condensation may be expected to be more rapid for turbulent than for laminar film condensation. An extension of this work would result in a better understanding of condensation in pipes in a zero-gravity environment. It is premature to predict any new equipment concepts from such a study.

Contrails

LIST OF SYMBOLS

A		Dimensionless parameter - $\frac{4 k [T_{\text{sat}} - T_w]}{h_{fg} \mu c} \left(\frac{\mu}{\mu_g} \right)$
B		Dimensionless parameter - $\frac{c}{4} \left(\frac{\nu_g}{\nu} \right)$
C		Dimensionless parameter - gas flow Reynolds number at the tube inlet - $\frac{4 U_o b}{\nu_g}$
D_e	in	Equivalent diameter of the duct
T	degF	Temperature
T_{sat}	deg F	Saturation temperature
T_w	degF	Wall temperature
U	ft/sec	Bulk velocity of the gas
b	in	Half-spacing between the plates
h_{fg}	BTU/lb	Latent heat of vaporization
k	BTU/hr-ft-degF	Thermal conductivity of the condensate
p	lbs/sq in	Pressure
u	ft/sec	Velocity within the condensate layer
Γ	lbs/hr-ft	Condensate flow rate per unit depth
δ	in	Thickness of the condensate layer
μ	lbs/hr-ft	Viscosity of the condensate
μ_g	lbs/hr-ft	Viscosity of the vapor
ν	sq ft/hr	Kinematic viscosity of the condensate
ν_g	sq ft/hr	Kinematic viscosity of the vapor
ρ	lbs/cu ft	Density of the condensate
ρ_g	lbs/cu ft	Density of the vapor
σ	lbs/ft	Surface tension at the condensate-vapor interface
τ	lbs/sq ft	Shear stress
τ_o	lbs/sq ft	Shear stress at the duct wall
τ_v	lbs/sq ft	Shear stress at the condensate-vapor interface
ϕ		Denotes a dimensionless function of the gas Reynolds number

Contrails

REFERENCES

1. Sparrow, E. M. and Gregg, J. L., "A Boundary-Layer Treatment of Laminar-Film Condensation," Trans. ASME, Journal of Heat Transfer, February 1959, p. 13
2. Rohsenow, W. M., Webber, J. H., and Ling, A. T., "The Effect of Vapor Velocity on Laminar and Turbulent Film Condensation," Trans. ASME, 1956, p. 1637
3. Lehtinen, J. A., Film Condensation in a Vertical Tube Subject to Varying Vapor Velocity, Sc.D. Thesis, Department of Mechanical Engineering, Massachusetts Institute of Technology, May 1957
4. Bergelin, O. P., Kegel, P. K., Carpenter, F. G., and Gazley, C., Co-Current Gas-Liquid Flow in Vertical Tubes, Fluid Mechanics and Heat Transfer Institute, Berkeley, California, 1949

Contrails

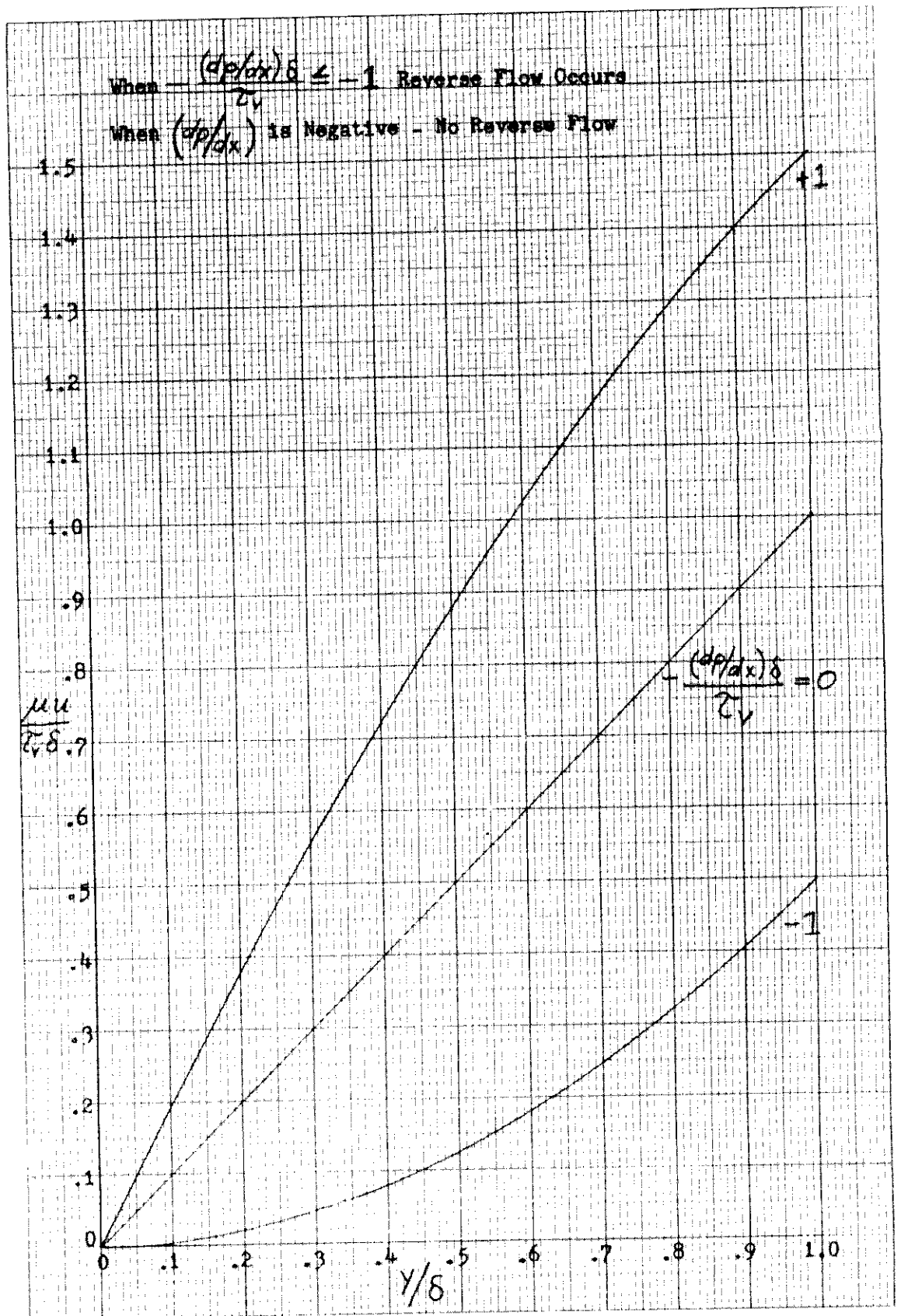


FIGURE 41: CONDENSATE VELOCITY DISTRIBUTION

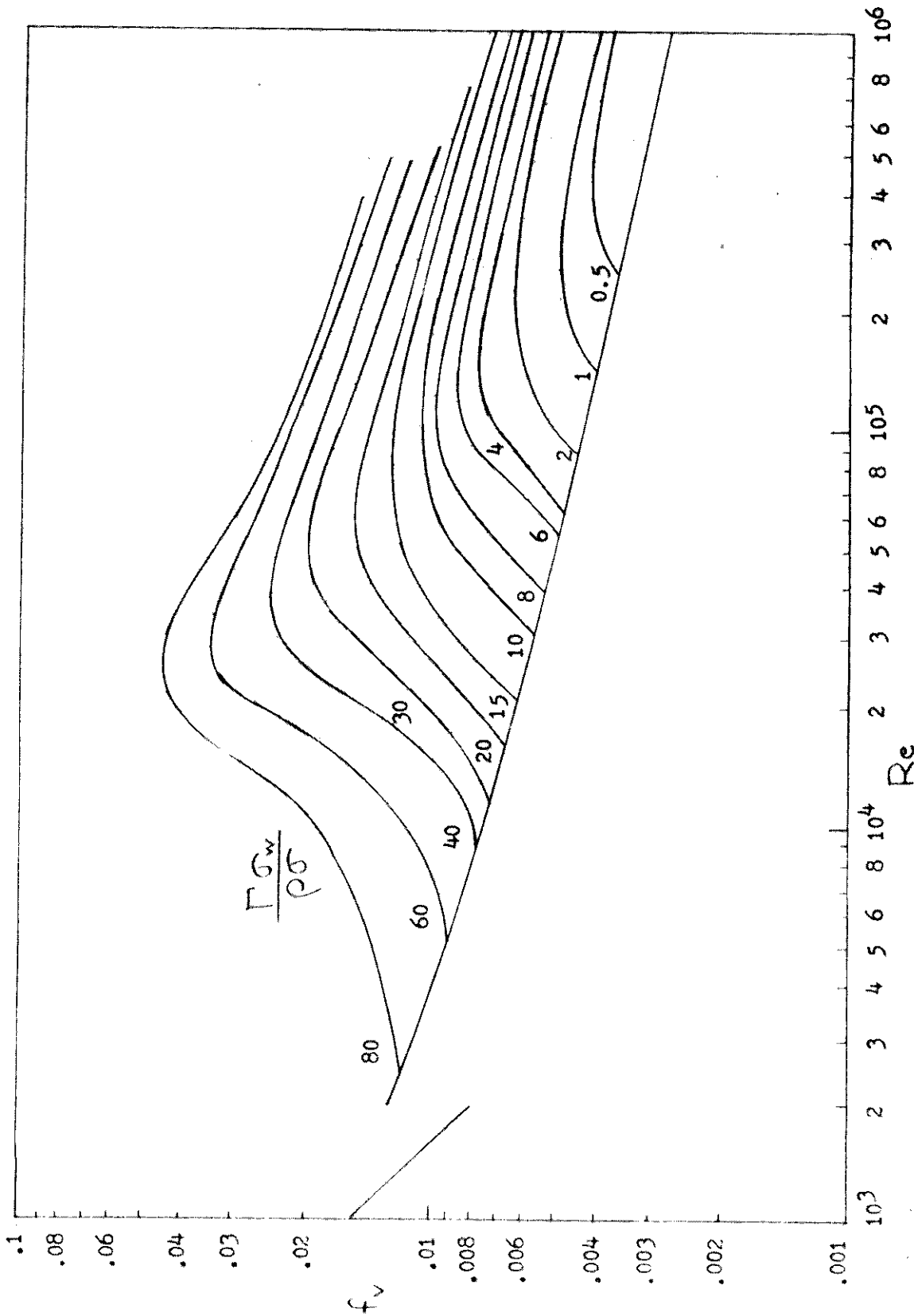


FIGURE 42: WETTED-WALL TUBE FRICTION FACTOR DATA
OF BERGELIN, KECEL, CARPENTER, AND GAZLEY

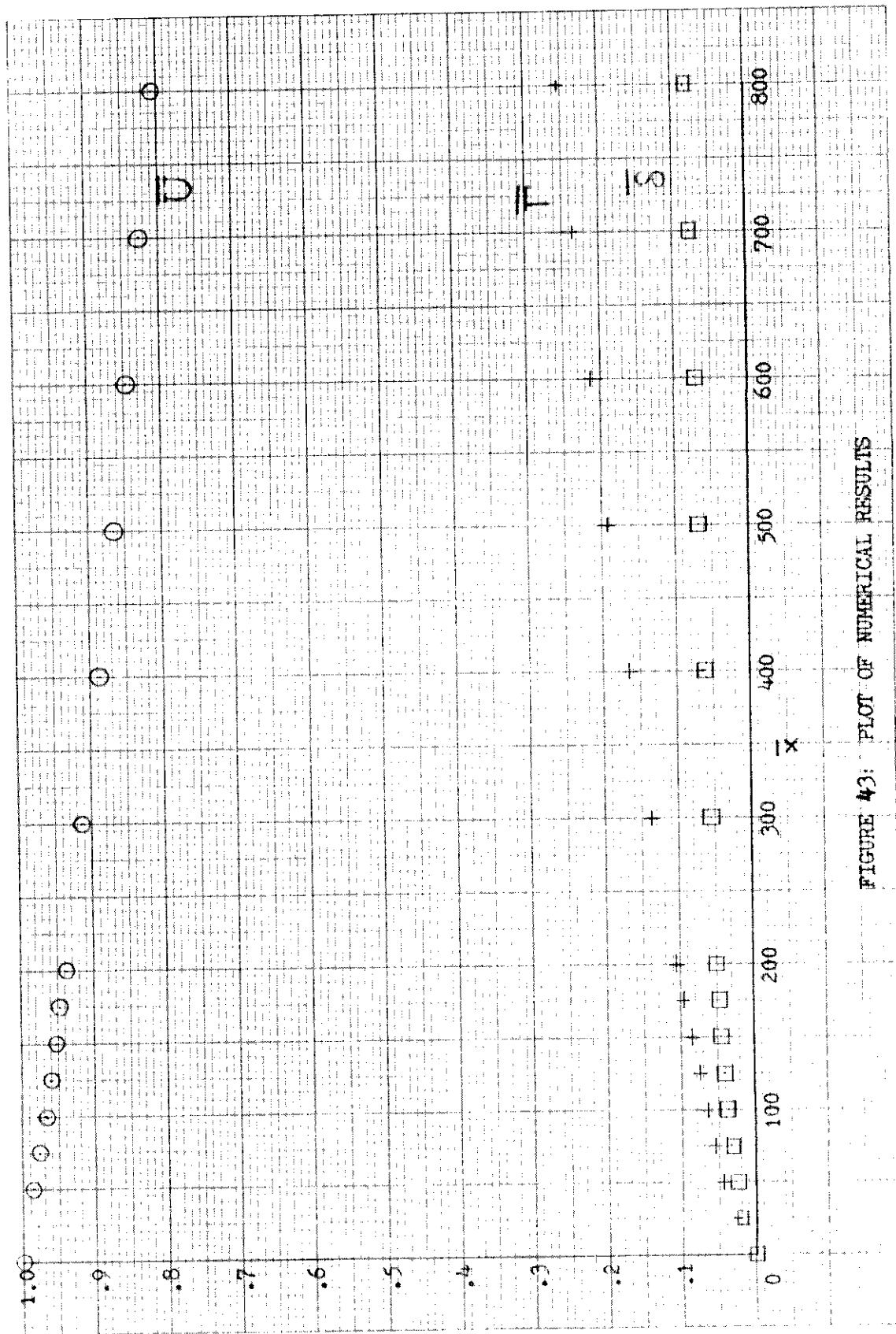


FIGURE 43: PLOT OF NUMERICAL RESULTS

SECTION IX

EXPANDER STUDY

In a conventional vapor cycle, liquid refrigerant from the condenser is expanded at constant enthalpy through a constant-pressure or constant-enthalpy expansion valve and then fed to the evaporator. The expansion, which occurs from the high condenser pressure to the relatively low evaporator pressure (allowing for losses) is irreversible and produces no work. For such an ideal vapor cycle shown in Figure 44, the coefficient of performance is given as

$$\text{COP} = \frac{h_3 - h_1}{h_4 - h_3} \quad (112)$$

The replacement of the constant enthalpy expansion process by one which is isentropic has two beneficial effects on the performance of the vapor cycle: first, the enthalpy of the refrigerant entering the evaporator is decreased, thereby increasing the total refrigeration effect available in the evaporator, and consequently decreasing the refrigerant flow rate; second, the work output of the isentropic expansion may be used to diminish the net work input to the vapor cycle. The isentropic process and increased refrigeration effect are shown in Figure 44 as 1 - 1' - 2. The coefficient of performance may now be expressed as

$$\text{COP} = \frac{h_3 - h_{1'}}{(h_4 - h_3) - (h_1 - h_{1'})} = \frac{(h_3 - h_1) + (h_1 - h_{1'})}{(h_4 - h_3) - (h_1 - h_{1'})} \quad (113)$$

However, since the increase in the evaporator capacity is

$$\Delta h = (h_1 - h_{1'})$$

we may write

$$\text{COP} = \frac{(h_3 - h_1) + \Delta h}{(h_4 - h_3) - \Delta h} \quad (114)$$

Expanders have not been used in vapor cycles for several reasons. Figure 45 shows the coefficient of performance of a Carnot cycle, a vapor cycle using isenthalpic expansion, and a vapor cycle using isentropic expansion. The refrigerant is Freon 11, and an evaporator temperature of 50 degrees F was used. The compressor efficiency was taken as 60 per cent, and the efficiency of the expansion process was taken as 100 per cent (ideal). At small "lifts", that is, when the temperature difference between the condenser and evaporator is small, e.g., 100 degrees, the gain in the coefficient of performance is slight, so that the development of an expansion machine can not be justified. For example, at a condenser-evaporator temperature difference of 100 degrees (Figure 45), the increase in coefficient of performance obtained by replacing an isenthalpic expansion by an isentropic one is only about

Contrails

18 per cent. However, at a temperature difference between condenser and evaporator of 200 degrees F, the increase obtained is 50 per cent, and the development of an expander appears much more attractive.

The effort in this study was directed toward an analysis of the performance gains to be achieved by the addition of an expansion engine to a vapor cycle operating at the temperature limits given in this study. Three other variations were included. The first consisted of a cycle where the benefits of the expander appeared only as an increase in the evaporator cooling capacity and the work output of the expander is not utilized to diminish the net work input into the system. The second consisted of the basic system (vapor cycle with throttle valve) with a superheater-subcooler added to superheat the refrigerant vapor from the evaporator by subcooling the liquid refrigerant from the condenser. The purpose of adding the superheater was to provide comparison with an accomplished method of increasing the coefficient of performance. The last variation was one where both an expansion engine and a superheater were included in the system. The systems investigated were:

1. Basic system with throttle valve and no expansion machine or superheater.
2. System with expander, where the expansion work is not utilized.
3. System with expander, where the expansion work is utilized.
4. System with superheater-subcooler, no expander.
5. System with superheater and subcooler, where expansion work is not utilized.
6. System with superheater and subcooler, where expansion work is utilized.

The systems were analyzed for Freon 11 and for a capacity of 1000 BTU/min. The results of the initial study, which was performed for an evaporator temperature of 40 degrees F and a condenser temperature of 150 degrees F, are shown in Table 13. The compressor efficiency was assumed to be 60 per cent, and a 65-per cent efficiency was assumed for the expansion machine.

Table 13 indicates that for a 110-degree difference between evaporator and condenser, an expander provides no distinct advantage. The coefficient of performance increases by only about 9 per cent, and the decrease in compressor size is only about 3 per cent. Such a small increase in performance at these temperatures does not justify either the development of an expansion machine or the weight penalty involved when the throttle valve is replaced with such a machine. Another factor that must be taken into account, in the light of the very small gain in performance that is obtained, is the addition of another rotating component to the system and the effect of this addition on the overall reliability of the system. About 35 per cent of the COP increase shown in Table 13 is due to the increase in the refrigeration effect obtained in the evaporator, while the remainder of the reduction is due to the expansion work supplied. This indicates immediately that very little gain in performance is possible unless the expansion work is utilized.

Contrails

For the small temperature difference between evaporator and condenser (110 degrees), a superheater-subcooler provides greater benefit to the vapor cycle than does an expansion machine. Although the increase in coefficient of performance is small, superheating prevents liquid intake into the compressor and ensures that only liquid enters the throttle valve. Although the evaporator refrigeration effect increases, this is offset by the higher compression work due to superheat.

For the cycle under consideration here, there appears to be no advantage to using an expansion machine instead of a throttle valve between evaporator and condenser temperature limits of 40 degrees F and 150 degrees F, respectively.

The second group of systems investigated was similar to that above, except for a difference in condenser and evaporator temperatures of 210 degrees (condenser temperature 250 degrees F, evaporator temperature 40 degrees F). The assumptions were the same as those used previously; the calculations were performed for a range of efficiencies for the expansion machine, and several values of effectiveness for the superheater-subcooler. The results of the studies where the expansion machine or superheater is added separately to the basic cycle are shown in Figure 46. For an expander efficiency of 65 per cent, a vapor cycle with an expansion machine (with work utilization) gives a 33 per cent increase in the coefficient of performance over a basic vapor cycle with a throttle valve. An expander with 80 per cent efficiency gives a COP increase of 42 per cent. There appears to be no advantage to using an expander instead of a superheater unless the expansion work is utilized to decrease the net work input to the compressor. A superheater-subcooler will increase the COP by 23 per cent over the basic cycle with throttle valve. Tables 14 and 15 give some actual calculated values.

Figure 47 shows the effect on cycle COP of including both an expansion machine and a superheater-subcooler to the cycle. When both an expander and a superheater are used in the system, and the expansion work is utilized, the system is penalized at all values of effectiveness other than zero. In other words, the maximum coefficient of performance obtained with an expander where the work is utilized may be increased no further by the addition of a superheater-subcooler. In fact, as Figure 47 shows, the COP decreases with increasing superheater effectiveness. As the superheater-subcooler effectiveness increases, the expander operates increasingly in the subcooled liquid region, while the vapor enters the compressor at higher degrees of superheat. The increase in amount of useful work obtained as one proceeds further into the subcooled liquid region is not sufficient to balance the increase in work input to the compressor due to vapor superheat, and the net effect is one of decrease in COP. These relative effects are a function of the particular refrigerant used, and may not be of the same magnitude in all cases.

Although the expansion machine is not concerned directly with the zero-gravity problem, its development is justified by the increase in performance obtained for space vehicle vapor cycles which will operate with large temperature differences between the condenser and evaporator. Very little information is available in the literature on turbines to handle two-phase fluids with such high liquid content, although efficiencies of 75 to 80 per cent have been obtained from small turbines with single-phase fluids. A small effort was expended to determine turbine characteristics for a particular case. In a vapor

Contrails

cycle with a condenser temperature of 250 degrees F and an evaporator temperature of 40 degrees F, it is proposed to replace the throttle valve by a turbine with a 60-per cent adiabatic efficiency. This substitution results in a theoretical increase in the COP of 30 per cent and reduces the refrigerant flow rate by about 15 per cent, thereby reducing the size of all other components in the system. For an evaporator heat load of 4000 BTU/min, the turbine diameter was 2.5 inches and the speed was approximately 45,000 rpm. The refrigerant enters the turbine nozzles in the saturated liquid state and leaves the nozzles as a mixture with a liquid fraction of about 50 per cent by weight. A turbine with an efficiency of 60 per cent is more realistic than one with an efficiency of 100 per cent; however, the former may still be somewhat high.

Contrails

TABLE 13
SUMMARY OF NUMERICAL RESULTS

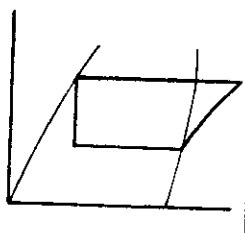
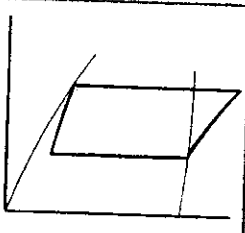
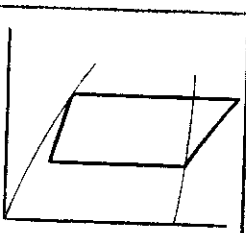
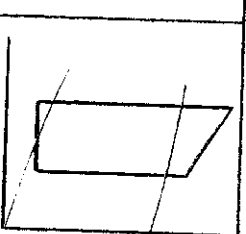
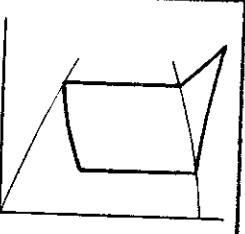
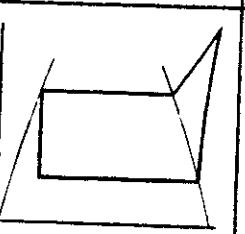
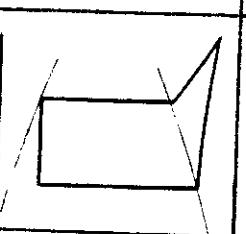
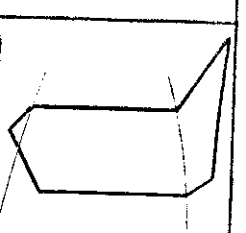
SYSTEM	Basic System	System with Expander	System with Expander (Expansion Work Is Not Utilized)	System with Suction-Liquid Heat Exchanger
Pressure Enthalpy Diagram				
Temperature Entropy Diagram				
Refrigeration Effect BTU/lb	58.09	59.54	59.54	63.35
Compression Work W BTU/lb	26.49	26.49	26.49	28.08
Condensation Head BTU/lb	84.58	84.58	84.58	91.43
Refrigerant Flow Rate w_r lbs/min	17.25	16.75	16.75	15.78
Compressor Volume V_i cu ft/min	93.96	91.14	91.14	93.33
Coefficient of Performance COP	2.19	2.38	2.25	2.25

TABLE 14

VAPOR CYCLE SYSTEM WITH EXPANSION MACHINE
INCREASE IN COP WITH VARYING EXPANDER EFFICIENCIES

Evaporator Temperature = 40 deg F

Condenser Temperature = 250 deg F

Expander Efficiency η_T	Refrigerant Flow Rate (lbs/min)	Compressor Volumetric Flow Rate (cu ft/min)	COP Work Not Utilized	COP Work Utilized
No Expander	29.05	158.1	0.777	---
10	28.35	154.3	0.797	0.812
20	27.7	150.8	0.815	0.847
30	27.05	147.3	0.835	0.885
40	26.45	144.0	0.854	0.925
50	25.85	140.8	0.873	0.964
60	25.3	137.8	0.892	1.008
70	24.8	135.0	0.911	1.052
80	24.25	132.0	0.931	1.100
90	23.78	129.4	0.950	1.148
100	23.34	127.0	0.969	1.200

TABLE 15

VAPOR CYCLE WITH THROTTLE VALVE AND SUPERHEATER
INCREASE OF COP WITH VARYING SUPERHEATER EFFECTIVENESS

$$T_E = 40 \text{ deg F}$$

$$T_C = 250 \text{ deg F}$$

Superheater Effectiveness ϵ	Refrigerant Flow Rate (lbs/min)	Compressor Volumetric Flow Rate (cu ft/min)	COP
No Superheater	29.05	158.1	0.777
0.109	26.75	153.2	0.818
0.216	24.75	148.5	0.843
0.322	23.05	144.0	0.869
0.426	21.55	140.1	0.894
0.526	20.2	136.0	0.921
0.606	19.32	133.9	0.937
0.726	18.05	130.2	0.965
0.856	16.83	126.7	0.986
1.00	15.68	123.3	0.998

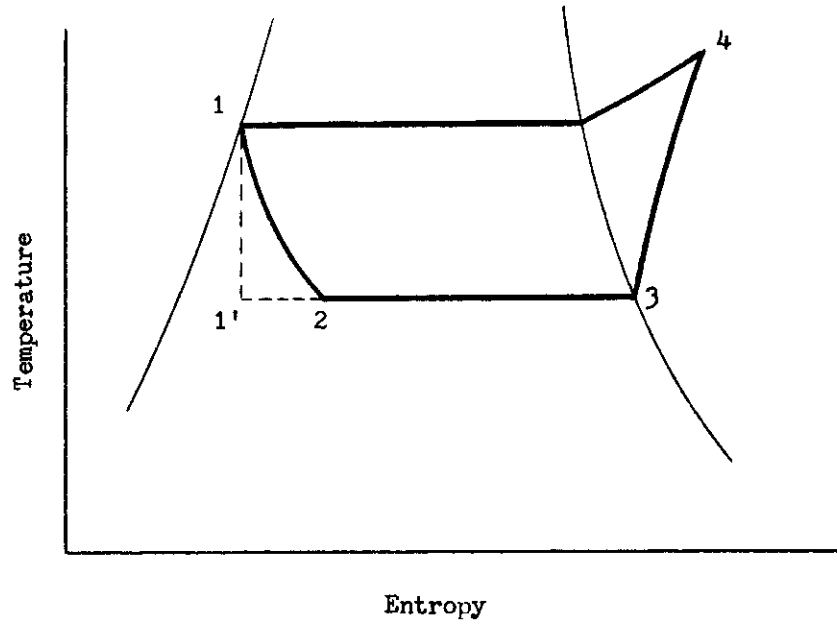


FIGURE 44: CONSTANT-ENTHALPY EXPANSION VERSUS
CONSTANT-ENTROPY EXPANSION IN A VAPOR CYCLE

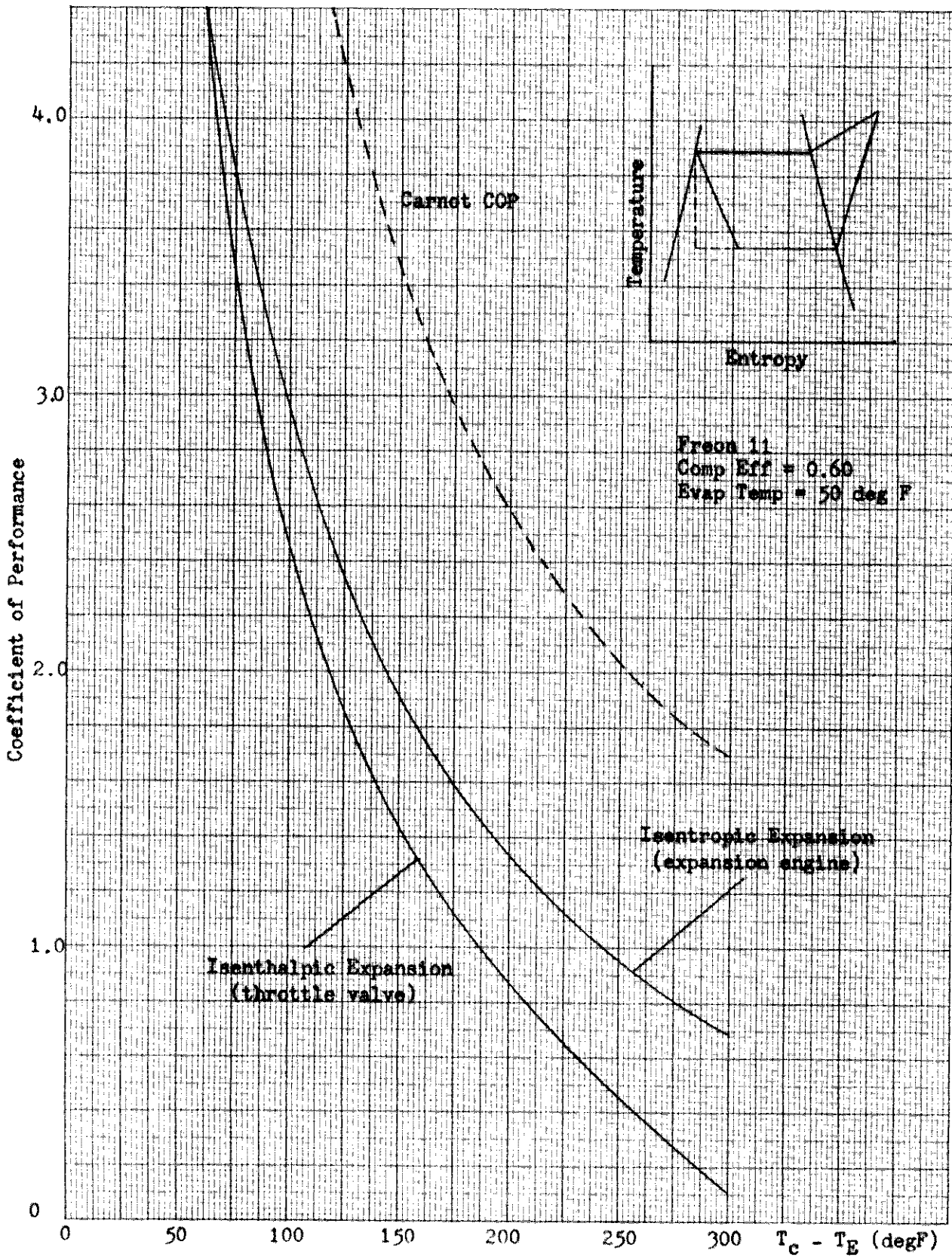
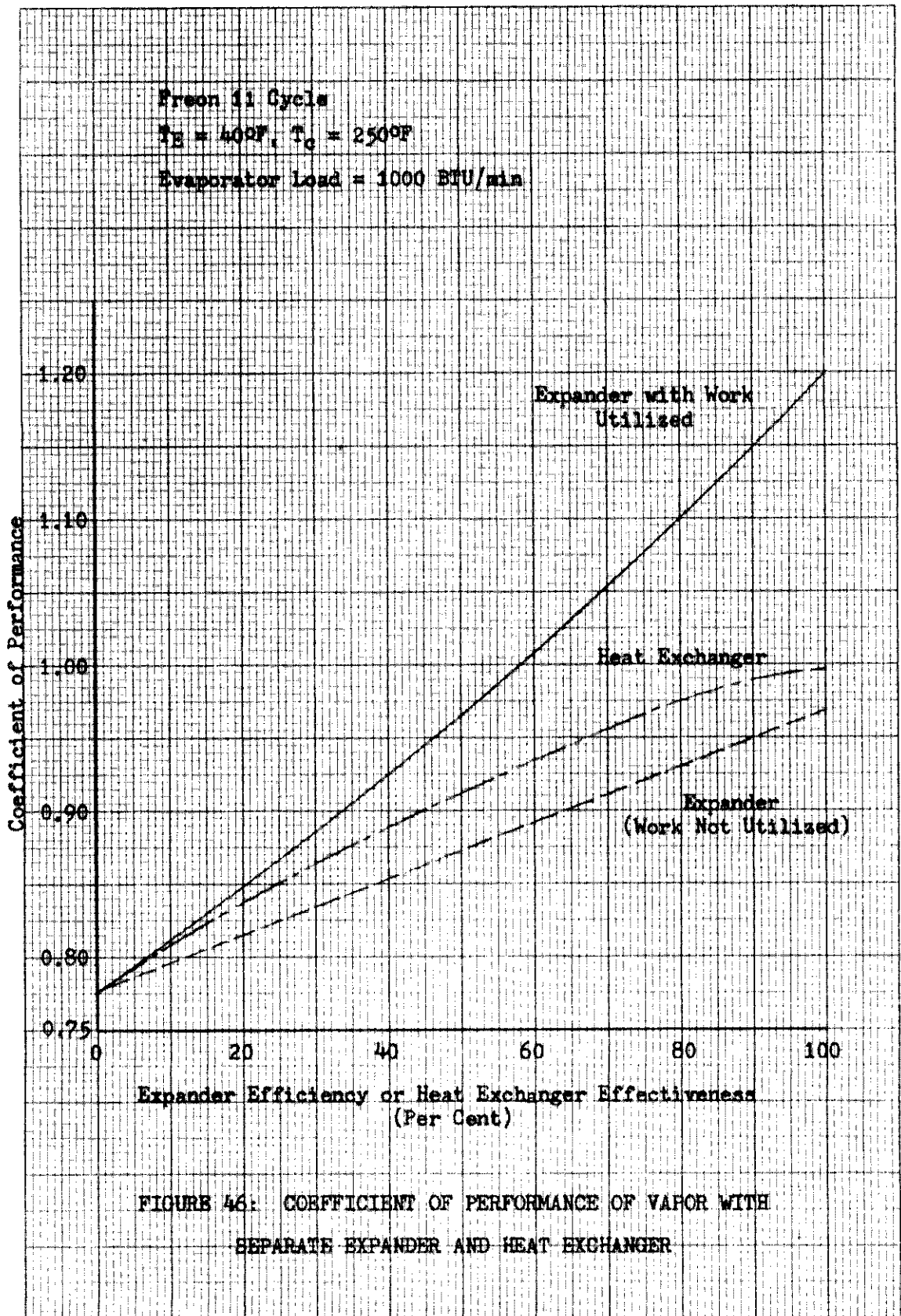
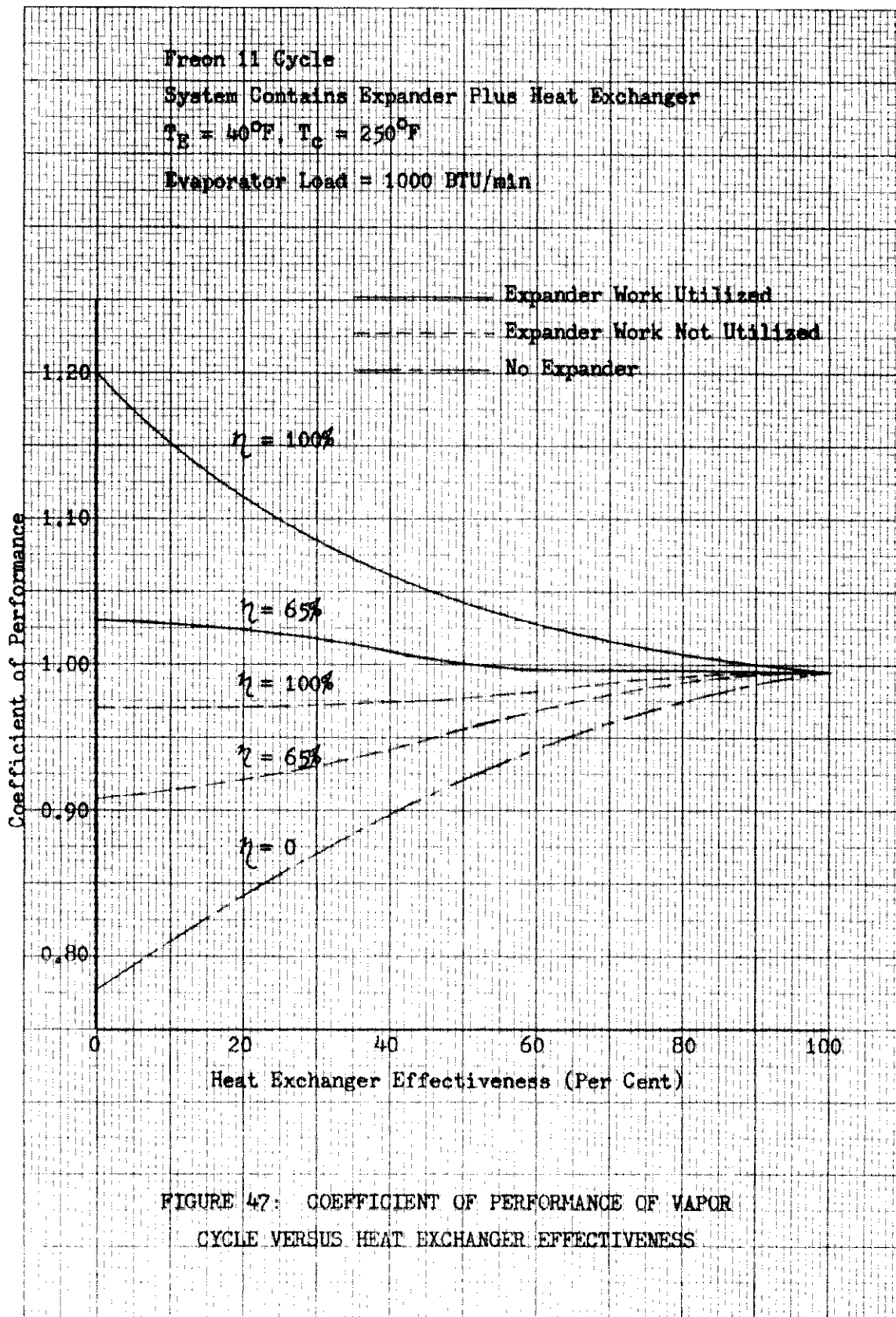


FIGURE 45: EFFECT OF REPLACING THE ISENTHALPIC PROCESS BY AN ISENTROPIC PROCESS IN A VAPOR CYCLE





Contrails

Contrails

SECTION X

WICK MATERIALS STUDY

One method of solving the vapor-liquid separation problem in a zero-gravity environment is to utilize surface forces which are not dependent on the gravitational field for their existence. The adhesive attraction that liquids exhibit for solid surfaces constitutes such a force. The actual configuration of a heat exchanger using surface forces for vapor-liquid separation is still open to question. One method is to fill the liquid side of the heat exchanger (evaporator) with groups of fine capillary tubes through which liquid is fed by capillary action to the heat transfer surface. Only that amount of liquid required for the specified heat transfer rate by boiling is fed to the surface. No excess liquid is present at the heat transfer surface, so that the possibility of liquid entrainment in the vapor is kept to a minimum. In the case of the evaporator, vapor exit passages must be designed carefully in order to prevent any free liquid leaving the evaporator. Fibrous wick-type materials may be used for the same purpose as straight capillary tubes. These materials may be considered as composed of randomly oriented capillary tubes of varying diameters and lengths. Application of wick materials to condensation is somewhat more difficult than the corresponding application to evaporation. One method would be to install a plug of wick material filled with liquid condensate; fresh condensate would enter the plug on the condenser side and would be removed continuously at the opposite end of the plug. The liquid-filled plug would provide an effective vapor barrier and could be designed to condense any vapor not already condensed on the main condenser surface.

There is practically no information in the literature about the specific problem here. There is information on flow through porous media, and in some cases heat transfer through such media, but the results cannot be extrapolated easily to provide any useful data for the current problem. Surface phenomena are not always explained easily, and results of experiments in surface tension and capillarity are very often nonreproducible. Cyclic hydration and dehydration of a material give different values for measurements of capillary and flow phenomena at the same points in each cycle; hysteresis is not uncommon in surface-active materials.

Before designing any heat exchanger using wick materials for liquid feed or liquid removal, it is necessary to understand the underlying fluid mechanics and heat transfer phenomena which govern transfer processes in these materials. A basic approach was necessary in order to draw general conclusions about the behavior of wick materials for liquid storage and liquid transfer processes, so that the optimum material could be selected for a given space vehicle application. Since, for the evaporator and condenser applications, the heat transfer processes would not occur directly within the wick material, the initial emphasis in the study was placed on fluid mechanics processes in the selected materials; these fluid mechanics processes would control the heat transfer processes and would be the limiting factor in any heat exchanger.

SELECTION OF MATERIALS

There are several criteria which must be satisfied for the selection

Contrails

of wick materials for this application:

1. The storage capacity of the material for the refrigerant (weight of refrigerant per unit weight or volume of material) should be high.
2. The capillary rise against gravity of the liquid in the material should be high.
3. The rate of rise of the liquid to the height in (2) should be high.
4. The material should have a low density.
5. The material should retain dimensional stability when immersed in the liquid. It should not react chemically with the liquid.
6. The material should be easily wetted by liquids; this requires that the contact angle between the surface of the material and the liquid be less than 90 degrees.
7. Within the given operating range, the material characteristics and surface behavior should be independent of temperature.

Twenty-five materials were selected and these were tested initially to eliminate those materials which were unsuitable for the present application. Although water is not a selected refrigerant in this study, it was considered to be an adequate fluid for all the tests on wick materials in this study. However, before any final design of a wick evaporator may be made, the selected group of materials must be tested with the Freon refrigerants. In general, the primary application was considered to be for the evaporator, although the optimum material for the evaporator would be equally applicable to the condenser, providing that temperature dependence did not alter the performance of the material. The following variables were measured for all materials. The measured values are shown in Table 16.

1. Density of the dry specimen.
2. The maximum height to which water rose in the dry specimen against gravity, and the time to reach this height.
3. Rate of rise of water in the dry specimen against gravity
4. Density of the wet specimen.
5. Ratio of wet to dry volume, wet to dry weight, and wet to dry density of the material specimens.
6. Maximum water absorption per unit weight of material.
7. Maximum water absorption per unit volume of material.

In addition to the tests listed above, specimens were checked for deterioration after they had been wetted and then dried. The rate of evaporation of water

Contrails

under atmospheric conditions from wet specimens both with and without a water supply from the bottom of the specimen was also measured. The continuous water supply to the specimen was arranged by keeping $\frac{1}{4}$ inch of the length of the specimen at the bottom immersed in water. If a specimen dries out in the atmosphere, even when a continuous supply of water by capillarity is ensured, the material will probably not be adequate for use in a heat exchanger. The rate of rise of water in the specimens is shown in Figure 48. Figure 49 shows the weight decrease of specimens as a function of time when evaporation takes place with a liquid supply at the bottom of the specimen, while Figure 50 shows the results for evaporation from wet specimens without any water supply. On the basis of the tests described above, the six materials listed below were selected for further experimentation:

1. Silica Vitreous Fiber Batt
2. Silica Vitreous Fiber Bulk
3. Cellulose Sponge
4. Wicking Felt No. 7544*
5. Wicking Felt No. 7545
6. Wicking Felt No. 7546

The results of further tests on these six materials are reported in Table 17, which also includes the results of the previous tests on these materials reported in Table 16.

The silica fiber batt** has the highest water absorption per unit weight and the lowest water absorption per unit volume of the six materials. The vertical rise of water in dry batt is quite rapid, but uneven, and the maximum height of rise is 1.5 inches. Measuring the rise of water in wet batt is somewhat more difficult. This was done by coloring the water slightly with potassium permanganate. The effect of adding potassium permanganate to water, if any, would be to lower the surface tension. It is interesting to note, however, that the rise of water in the wet specimen was to a level of 5 inches. This result is not unusual in the light of the characteristics of surface phenomena. A dry material presents a completely different surface to a liquid than a material which has already been wetted.

The silica bulk material has a water absorption equal to about 25 per cent that of the silica batt, and a water absorption per unit volume which is approximately 45 per cent higher than that of the batt. The capillary rise of water in the bulk material is to a height of approximately 6.5 inches, and the rate is greater than that for the silica batt. In some bulk specimens, the

*All felts used in this study were provided by the American Felt Company, Glenville, Connecticut.

**The standard product is composed of SiO_2 (about 96 per cent) with the remainder consisting of the oxides of iron, aluminum, titanium, calcium, boron, and other metals. The material is composed essentially of vitreous fibers and is available in a series of forms for use in high temperature applications.

Contrails

maximum height of rise was even greater than 6.5 inches.

Both types of silica fiber appear to have no dimensional stability and need internal support when wet. The batt material collapses under the weight of the absorbed water, with a substantial decrease in the thickness of the material. Measurements on the bulk material were made by packing a glass tube of large diameter with the material. Although both forms of silica appear to be stiffer and more brittle after the wet specimens have been dried, no appreciable deterioration of the material was observed.

The cellulose sponge has a high water absorption per unit weight and a low water absorption per unit volume which is comparable to the silica batt. The highest capillary water rise for this material was 7 inches, which was the height of the largest sample obtained. It is probable that the maximum capillary rise for a larger sample would be higher. The dimensional stability and rigidity of the sponge are superior when compared to the silica specimens. Wetting the material and drying it several times cause only minor changes in the physical structure.

The three felts selected for further testing were three of the wicking felts manufactured by the American Felt Company, Glenville, Connecticut, Nos. 7544, 7545, and 7546. The grade 7544 is manufactured in both an untreated and treated (acid-neutralized) version; the latter exhibits superior behavior for this application. The three materials are quite similar in their behavior. The values for water absorption per unit weight are of the same order of magnitude for each felt, and are approximately equal to the values for the silica bulk fiber, but less than those for the batt or the sponge. The values for water absorption per unit volume for the felts are approximately 20 per cent higher than those for the silica bulk fiber and the cellulose sponge, and about twice as high as that for the silica batt. Felt No. 7544 (treated) showed the highest capillary rise for the three felts--5.75 inches, which was also limited by the height of the available sample.

An interesting phenomenon was observed during the testing of Felt No. 7545. An initial determination of capillary rise showed a very low height for water. The material was then dried and the test for capillary rise was repeated. In the subsequent test, the water rose to a higher level in a shorter time. The tests were repeated until the maximum rise remained the same for consecutive tests and the time required to reach this maximum level remained the same. Felt No. 7544 was then tested in a similar manner. As indicated previously, water rose to the maximum height in the first test. In subsequent tests, the water still rose to the maximum height. However, the time of rise was less for the second test than for the preceding one. For the fifth test, the time to reach the maximum height was still less than that for the first test, although the time was increasing. Felt No. 7546 was not available initially and hence a smaller number of tests have been reported for this material.

All three felts have excellent dimensional stability and rigidity. They can be cut to fit any shape and may be manufactured in several forms. The three felts have higher densities than most of the other materials investigated. Immersion in water or water flow through the material did not alter their shape or appearance. When ordinary tap water is used for the experiments, the felts, which are ordinarily ivory-white in color, tend to show some brown discoloration

after several days of testing. This discoloration is probably due to bacterial degradation of the wool fibers, and is not noticed when distilled water is used. The transient behaviour described above indicates that wick materials may undergo considerable fiber rearrangement before some steady-state performance characteristics are obtained. It is obvious that for a space vehicle mission of any duration, it is important to have detailed information about both the transition and the steady-state behavior of these materials. A thorough understanding of capillarity in wick materials is not only necessary for the application of these materials to heat exchangers operating under zero gravity, but may also provide information which may be used to design and manufacture optimum materials for this application.

An additional material which may be applied to this problem is a substance called "Liquid Lock". Measurements on this material, which is based on silica fiber, have been made by the Stewart-Warner Corporation. The information reported is not extensive, but it is claimed (1) that the material has a water absorption of 15.45 pounds water per pound of dry batt material and 1.16 pounds of water per pound of material in staple weave form. The capillary rise of water in the material is rapid, reaching a height of 5 inches in about 2 minutes. No samples of this material were available.

CAPILLARY PHENOMENA IN WICK MATERIALS

A simple method of simulating capillary phenomena in wick materials is to study capillarity in tubes of small diameter. A well-known fact is that when a length of small diameter tubing, open at both ends, is placed vertically with one end immersed in a liquid contained in a reservoir, the level of liquid in the tubing will either rise above or sink below the level of liquid in the reservoir. It is not proposed to discuss capillarity in detail here. Such discussions may be found in the literature (2, 3, 4). The relative magnitude of the forces of cohesion and adhesion between the liquid in question and the solid surface with which it is in contact, determines the curvature of the surface and whether the liquid rises or sinks below the level in the reservoir. A pressure difference exists across the curved liquid surface in the tubing and is given by $2\sigma/R$, where σ represents the surface tension of the liquid and R the radius of curvature of the surface. For equilibrium to be established,

$$\frac{2\sigma}{R} = \rho g h \quad (115)$$

where h is the capillary rise. For a spherical meniscus

$$R = \frac{r}{\cos \theta}$$

where r is the radius of the tube and θ is the angle of contact between the liquid and the solid surface. By substitution,

$$h = \frac{2\sigma \cos \theta}{\rho g r} \quad (116)$$

The liquid rise in wick materials is similar to that in a capillary tube, but

is a far more complicated case. As mentioned previously, a wick material may be considered to be composed of a group of randomly oriented capillaries. The time that a liquid takes to reach an equilibrium height in a wick material is, however, greater than that for the same liquid in a straight tube. In the former case, the liquid has to travel through a large number of small passages oriented in all directions. The height to which the liquid rises is a function of the surface tension of the liquid, the contact angle between the liquid and the solid surface, the radius of the passage, the liquid density, and the gravitational acceleration. The surface tension of most liquids may be found in the literature; the contact angle may be determined by using surface tension measurements made by two methods, one of which is dependent upon, and the other is independent of, the angle of contact. Two examples of such methods are the capillary rise and bubble pressure methods of determining surface tension. The radius of the passage must be determined either independently of other variables, or, if all other variables are known, may be determined from a surface tension experiment.

One explanation for the variation in the maximum height of rise of water in the felt materials is that wool felt materials tend to swell internally when soaked in water. Hence soaking a material would tend to reduce the radius of the flow passage and would improve capillary action. If the fibers were not completely elastic, they would not return to their original formation on drying, so that the original capillary rise could not be reproduced. The smaller radius of a flow passage would account for the increasing capillary rise in each succeeding experiment. When a wick material is dry, the contact angle between the solid surface and the liquid would have a characteristic value. However, once the material is completely wet, the contact angle is theoretically zero, since it may be assumed that a thin film of the liquid coats the entire surface. The smaller contact angle may then account for the fact that the liquid rises to a higher level in a material already wetted by the liquid than in a dry material.

In the expression for capillary rise, the gravitational acceleration appears in the denominator. Theoretically, in the zero-gravity environment, one would expect an infinite capillary rise in an infinite capillary tube. In a finite tube, however, the liquid would rise only to the end of the tube, and perhaps slightly beyond. Once the liquid rises outside the tube, the direction of the surface forces changes, and the liquid would start to flow back. It is conceivable that an oscillatory motion with decreasing amplitude would be established at the end of the tube.

FLOW IN CAPILLARY TUBES

In order to gain a fuller understanding of the flow of liquids through wick materials, it was decided to first study the flow of liquids through capillary tubes. Liquids may travel through tubes or materials by capillary action only or by forced flow due to an imposed pressure. The flow of a liquid through a capillary tube is given by the Poiseuille equation,

$$Q = \frac{\pi R^4}{8 \mu L} (P_1 - P_2) = K_1 \frac{\Delta P}{L} = K_2 \frac{\Delta H}{L} \quad (117)$$

Contrails

where Q is the volumetric flow rate, R is the inside diameter of the tube, P_1 and P_2 are the pressures at the ends of the tube, μ is the viscosity of the liquid, and L is the length of the tube.

The test apparatus for capillary flow is shown in Figure 51. A glass capillary tube 6 inches long and having a nominal inside diameter of 0.5 mm was used in a horizontal position initially. The glass tube was connected through a 0.25-inch plastic tube to a constant head water tank, and the discharge rate was measured for a given difference in head between the constant water level in the tank and that of the water in the capillary tube. With the tube in the horizontal position, a head of 10 mm of water had to be established before discharge from the tube occurred. With the tube in the vertical position, no such lag in the initiation of flow was obtained. The effect of gravity and any deviation of the tube from the horizontal may account for the observed lag. The values for flow obtained in the vertical and horizontal positions with varying pressure heads, and the calculated values from Poiseuille's equation have been plotted in Figure 52. The experimental values for flow are much higher than the calculated values. Unfortunately, the tolerance limits for the glass capillary tubes which were available were quite poor; for the tube used, the diameter of the bore was $0.5 \text{ mm} \pm 0.25 \text{ mm}$. Since the radius appears to the fourth power in Poiseuille's equation, the variation in bore diameter is sufficient to explain the deviation between the observed and calculated values for flow. The values shown in Figure 52 were reproduced several times within the accuracy of the measuring technique.

Following the tests with the positive pressure heads, the constant-head water tank was lowered until the level of water in the tank was below that in the capillary tube. These experiments were also carried out with the tube in both the vertical and the horizontal positions. Starting with the levels equal, no flow from the tube to the tank occurred until a (negative) head of -40 mm water was reached. There was some difference again in the flow with the tube in the horizontal and vertical positions. In the vertical position, no flow or movement of water is observed until a head of -40 mm of water is reached. In the horizontal position, when a head of -25 mm is reached, the meniscus begins to retreat in the tube, but stops after moving a short distance. At -40 mm, the water flows out from the tube in the tank, as in the vertical case. The flow lag for the horizontal case may be due, again, to the effect of gravity on the meniscus, and any deviation of the tube angle from the horizontal position. It is interesting to note that the head of -40 mm of water is the level to which water will rise by capillary action in a tube with an inside diameter equal to 0.5 mm.

The pressure difference across a curved liquid surface has been shown to be equal to $2\sigma/R$, and in a capillary tube of radius r , this pressure is

$$P = \frac{2\sigma \cos \theta}{r} \quad (118)$$

This pressure difference may be considered as a force per unit area which pulls liquid up a capillary tube until the force is balanced by the weight of liquid below the curved surface. For equilibrium, as before,

$$\frac{2\sigma \cos \theta}{r} = \rho g h$$

This "pulling" force may be considered to be the force which holds the liquid in the tube under negative pressure heads. Flow begins when the absolute value of the negative pressure head exceeds this pulling force.

Figure 53 shows the change in meniscus shape due to gravity, the flow versus pressure head schematic, and the variations in meniscus radius for horizontal tubes. For vertical tubes, no flow lag occurs at positive heads and gravity has no effect on the meniscus shape.

FLOW IN WICK MATERIALS

Since wick materials may be simulated by groups of capillaries, flows through the passages of wick materials are effected by the same forces as those which effect flows in capillary tubes. Hence, flow and pressure head may be correlated in wick materials just as in capillary tubes. The constants appearing in the equations

$$Q = K_1 \frac{\Delta P}{L} \quad ; \quad Q = K_2 \frac{\Delta H}{L} \quad (119)$$

are a function of the wick material and the liquid. Theoretically, the values of the constants may be determined by measuring the flow rates of liquids through wick materials for varying pressure heads. Then, if the Q versus ΔH curve is a straight line,

$$K_2 = L \tan \alpha \quad (120)$$

where $\tan \alpha$ is the slope of the line and L is the length of the wick specimen. The apparatus constructed to perform such an experiment is shown in Figure 54. Instead of a capillary tube, a glass tube with an inside diameter of 0.25 inches or greater was packed with a measured length of the specimen of wick material to be tested.

Preliminary tests indicated that the flow rate of water through a wick material under a constant pressure head decreases with time. This disturbing fact (if true for all combinations of wick materials and liquids) is of primary importance in the performance of wick materials, where mission duration is of any magnitude. A correlation based on an equation such as $Q = K_2 \Delta H/L$ is no longer possible, unless some steady-state behavior is obtained. It was the objective of the rest of the experimental program to classify this behavior, and to determine the point at which steady-state operation may be obtained.

Some of the initial results of the tests were quite contradictory. The flow rate decreases with time in a semiexponential manner. The same effect was observed when the specimen was soaked for a long period prior to the tests. If the specimens were kept in the tube for about 12 hours, without any pressure head, but still soaked in water, the flow rate for an identical pressure head after the twelve-hour period was observed to be higher than that corresponding to the previous value at the same pressure head. This flow would then proceed to decrease with time. In the case of the sponge, a higher pressure head resulted in a lower flow rate, which is a completely contradictory effect. It is possible, however, that this effect was caused by channeling in the wick material

Contrails

which may be due to nonuniform packing of the material in the glass tube. Different samples of the same material gave varying values of flow rates with time. Care was taken to use samples in which the fibers were oriented to the flow pattern in the same way, so that the last effect indicates the nonhomogeneity of the material in a given direction. This factor is important for the manufacture of any material for this application.

In order to improve the data, a second series of tests was planned in which flow through the wick material was continued on a 24-hour basis. Each specimen was measured, weighed, and packed carefully into the tube to prevent any channeling of water through a free passage. Distilled water was used in the apparatus as shown in Figure 54. The sample specimen was used and the flow rate through the material was measured for pressure heads of 200 mm (approximately 8 inches), 400 mm (approximately 16 inches), and 600 mm (approximately 23.5 inches) of water. The initial pressure was 200 mm of water, and the flow rate through the material was measured several times during a period of 48 hours. At the end of this period, the pressure head was raised to 400 mm of water, without interrupting flow. The flow rate measurements were continued as before, and then repeated for a pressure head of 600 mm of water.

Table 18 shows the physical data for the wick material specimens, and Figures 55 to 60 show the decrease of flow rate with time. Even with a duration of 48 hours, flow rates do not level off completely at a steady-state value, although a plot on rectangular co-ordinates does show the approach to steady-state operation. At the beginning of a 48-hour period, the flow rate increases proportionately to the increase in the pressure head; however, at the end of this period, the flow rate drops below that of the corresponding rate for the previous run. This is not a contradictory effect as shown in the schematic in Figure 61. If two identical samples of a given material were used, the specimen subjected to the higher pressure would give a proportionately higher flow rate at any given time. For example, in these experiments, the flow rate at a 400 mm pressure after 48 hours at this pressure should be compared with the flow rate that would have been obtained had the experiment with the 200 mm pressure been continued for 96 hours. In some cases, the final flow rate is quite small, and such materials would be unsatisfactory for the application here. The experiment with Felt No. 7546 was continued beyond 144 hours; although the flow rate does not continue to decrease as rapidly as before, completely constant flow rates were never attained. It is interesting to note that for the first 100 minutes of operation the initial flow rate is fairly constant.

Several explanations may be offered (5) for the drastic decreases in flow rate which were observed, some of which were large enough to cause the final rates to be a small fraction of the initial flow rate. The experiments above consumed a considerable amount of time, and it was not possible to test the hypotheses offered below. It is proposed, however, to continue these experiments beyond the scope of this program.

It is a characteristic of wool fibers to swell when they are immersed in water for more than a few minutes. Wicking felts such as those used in the tests are made by compression of individual fibers or fiber bundles to form a solid mat. When such felts are soaked in water for some time, individual fibers swell and decrease the free flow area in the material, thus decreasing the flow rate. In addition to the swelling of individual fibers, bundles of fibers

swell internally, increasing the effect on the flow rate. The internal swelling of the fibers does not result in any measurable increase in the dimensions of the specimen. The swelling effect has also been noticed when wool felts are used for filtration of particles in solutions. In some cases, the swelling is sufficient to completely block any flow of liquid through the material. Another effect about which very little is known, and about which nothing is reported in the literature, is the effect of surface-active materials on small amounts of dissolved gases in liquids flowing through these materials. Dissolved gases are apparently released from these liquids during flow through the material, and entrapped in the tiny pores of the material. These minute bubbles form a "gas lock" which has been reported to prevent flow completely (5) even when the thickness of the specimen was only 1/8 inch. Unfortunately, this effect would be particularly noticeable with water which usually contains some dissolved oxygen. One way to check this hypothesis is to use a liquid which does not tend to dissolve any atmospheric gases or to desorb the water either by vigorous boiling or other means.

It is evident that effects such as those reported above are of primary importance in the consideration of any wick material for space vehicle heat exchanger use. The little data that have been published on this subject have been measured over short periods of time during which some of the above effects do not appear. In the applications that are being considered here, where there is an interplay between surface phenomena, fluid mechanics, and two-phase heat transfer, it is necessary to use carefully controlled experiments when only one or two variables are investigated at any time.

HEAT TRANSFER IN WICK MATERIALS

No actual heat transfer tests were performed since the major effort was expended in studying the fluid mechanics behavior of wick materials. The following discussion assumes that the flow rate through the wick material is not time-dependent and that the material does not change its characteristics with time.

It was shown previously that if the flow rate through the wick material varies as the pressure head and inversely as the length (Figure 52), then

$$Q = K_1 \frac{\Delta P}{L} = K_2 \frac{\Delta H}{L}$$

where Q is expressed in lbs/min-sq ft. If the liquid is fed at one surface of the wick material and evaporated at the other, and liquid flow is due to capillary action only, the maximum flow rate obtainable is

$$Q_{\max} = K_2 \frac{H}{L} \quad (121)$$

where H is the height to which the liquid rises in the same material under usual gravity conditions. The only resistance to flow is friction in the material, and as long as frictional resistance does not overcome capillary action, flow will continue. The maximum heat transfer rate obtainable is limited by the maximum flow rate, so that

Contrails

$$(q/A)_{\max} = K_2 \frac{H}{L} h_{fg} \quad (\text{BTU}/\text{min-sq ft}) \quad (122)$$

where h_{fg} is the latent heat of evaporation at the liquid temperature and pressure, and assuming that the liquid is at its saturation temperature for the given pressure. If more liquid is evaporated than may be supplied by capillarity, the wick will begin to dry out and the exit temperature on the air side will rise, which is intolerable. Since K_2 , H , and h_{fg} are fixed for any given combination of wick material and liquid, the only method available to increase the maximum flow rate and hence the heat transfer rate is to reduce the thickness of the material.

The wick material in the evaporator serves several purposes. It provides the necessary liquid feed to the heat transfer surface to maintain the desired heat transfer rate without providing any excess of liquid which may be entrained by the vapor and drawn into the compressor. The wick material acts as a storage for the liquid refrigerant; the amount of storage capacity available depends on the thickness of the wick material. In cases where liquid feed by capillarity is insufficient to support the required heat transfer rate, a pressure head may be imposed on the material to obtain the necessary flow.

Fisher (6) gives some information for an air-water evaporator filled on the water side with the wick material known as Liquid Lock. Heat fluxes up to 40,000 BTU/hr-sq ft were obtained. However, the correlations are not general enough, so that extension to the current work is not possible. Allingham and McEntire (7) have reported the results of some experiments on boiling coefficients in a wick evaporator, using a "Libby-Owens-Ford Microglass unbonded 'B' fiber" filled with water on one side, and oil on the other. A schematic of their apparatus is reproduced in Figure 62. A correlation, similar to that of Gilmour (8) was attempted for boiling from a wick-covered surface. The following correlation is given in their paper:

$$\left(\frac{h}{c_p G'} \right) \left(\frac{c_p M}{k} \right)^{0.6} \left(\frac{\rho_L \sigma}{P^2} \right)^{0.21} = 0.072 \left(\frac{D_e G'}{\mu} \right)^{-0.77} \quad (123)$$

where $G' = \frac{q}{A \epsilon h_{fg}}$, and $\epsilon = \text{porosity factor} = 1 - \frac{\rho_{\text{wick}}}{\rho_{\text{fiber}}}$ and

- q/A is the heat flux in BTU/hr-sq ft
- h is the heat transfer coefficient in BTU/hr-sq ft-degF
- c_p is the liquid specific heat in BTU/lb-degF
- k is the liquid thermal conductivity in BTU/hr-ft-degF
- P is the absolute pressure in lbf/sq ft
- D_e is a dimension parameter

Contrails

- μ is the liquid viscosity in lbf/hr-ft
- ρ is the liquid density in lbm/cu ft
- σ is the liquid surface tension in lbf/ft

The applicability of the above correlation to the zero-gravity case is open to serious question. With any wick material above the heat transfer surface, there is the possibility of liquid feed to the surface by gravity. A more serious objection is to the dimensionality of the term $(\rho_L \sigma / \rho^2)$ in the above correlation. As given in Reference 7, the term is dimensionless only if it is multiplied by the factor g/g_0 . Since the tests in Reference 7 were not carried out at conditions different from $g = g_0$, the validity of the method for calculating the exponent of the term $(\rho_L \sigma / \rho^2)$ and indirectly that of some of the other constants is doubtful for the zero-gravity condition. In the few heat transfer measurements in wick materials found in the literature, the time duration of the experiments is small, so that any variation in wick material behavior with time would pass unnoticed.

There is little doubt that wick materials are applicable to the problem of zero-gravity evaporators, and probably to that of zero-gravity condensers. However, it is necessary to investigate the behavior of these materials under as many as possible of the same conditions as they will encounter in space vehicle zero-gravity operation. A fundamental approach from the standpoint of the fluid mechanics behavior of wick materials is necessary, not only because it limits the maximum heat transfer rate, but also since it affects actual heat exchanger configuration and design. Actual heat transfer measurements are necessary, but only after the fluid mechanics behavior of the specific material is understood fully. When this has been done, it should be possible to select the optimum wick material for a particular mission application without resorting to a completely empirical approach.

Contrails

REFERENCES

1. Study of Liquid Feed Control to Wick Type Boilers (unpublished), South Wind Division of Stewart-Warner Corporation, Indianapolis, Indiana, 1958
2. Sears, F. W., Mechanics, Addison-Wesley Press, Inc., Cambridge, Massachusetts, 1944
3. Prandtl, L., Essentials of Fluid Dynamics, Hafner Publishing Company, New York
4. Prandtl, L. and Tietjens, O. G., Fundamentals of Hydro- and Aeromechanics, McGraw-Hill Book Company, Inc., New York, 1934
5. Davis, Norman, American Felt Company, Glenville, Connecticut, Personal Communication
6. Fisher, J. T., Simplified Method of Liquid Lock Boiling Water to Air Heat Exchanger Calculation, Stewart-Warner Corporation, South Wind Division, Indianapolis, Indiana, 1958
7. Allingham, W. D. and McEntire, J. A., Determination of Boiling Film Coefficient for a Heated Horizontal Tube in Water-Saturated Wick Material, ASME Paper 60-HT-11, August 1960
8. Gilmour, C. H., "Nucleate Boiling - A Correlation," Chemical Engineering Progress, vol. 54, No. 10, October 1958, pp. 77-79
9. Merte, Jr., H. and Clark, J. A., Pool Boiling in an Accelerating System, ASME Paper 60-HT-22, August 1960
10. Usiskin, C. M. and Siegel, R., An Experimental Study of Boiling in Reduced and Zero Gravitational Fields, ASME Paper 60-HT-10, August 1960

TABLE 16
PHYSICAL PROPERTIES AND ABSORPTION CHARACTERISTICS OF WICK MATERIALS

Sample Number & Material	Dry Condition			Soaked Condition			Volume Weight Density Ratio			Maximum				
	Width in.	Height in.	Thick-ness in.	Volume cu.in.	Weight lbs.	Density lbs./cu.ft.	Thick-ness in.	Height in.	Time min.	Volume cu.in.	Weight lbs.	Density lbs./cu.ft.	Rise in.	Maximum Density lbs./cu.ft.
1. Silica Batt	4.0	5.0	1.0	20.0	0.0287	2.47	1.5	3	3	12.5	0.406	70.0	0.625	14.17
2. Silica Bulk	Diameter 1.875 in. Length 10 in.	1.875	10	27.64	0.207	12.9	6.5	8	8	27.64	0.857	53.5	1.00	4.14
3. Cellulose	3.188	5.0	0.75	11.95	0.0221	3.18	5.0	3195	3.375	5.25	0.240	26.8	1.30	10.90
4. Synthetic (Herd)	2.75	4.563	1.313	16.47	0.0287	3.00	0.875	20	2.75	4.563	1.313	16.47	1.00	8.69
5. Vinyl Sponge	2.938	5.0	0.875	12.85	0.0132	1.78	0.375	1010	2.938	5.0	0.875	12.85	1.00	18.42
6. Vinyl Sponge No. 1	2.688	4.25	1.094	12.50	0.0116	1.60	0	-	2.688	4.25	1.094	12.50	1.00	13.20
7. Natural Sponge No. 2	4.5	6.75	1.25	37.99	0.0264	1.20	0.5	15	5.0	7.25	1.375	49.8	1.311	18.33
8. Fiberglass	1.5	5.875	1.0	8.81	0.0298	5.82	0	-	1.5	5.875	1.0	8.81	1.00	3.30
9. Sample No. 1	1.5	5.875	1.125	9.91	0.0066	1.15	0	-	1.5	5.875	1.125	9.91	1.00	15.33
10. Sample No. 2	1.625	6.5	1.25	13.20	0.0242	3.17	0	-	1.375	7.25	1.125	11.21	0.849	4.54
11. Wall Insulation	4.438	6.0	1.0	26.63	0.0149	0.964	0	-	3.75	6.0	1.125	25.31	0.950	6.22
12. Mineral Wool	3.25	6.125	1.25	24.88	0.0198	1.375	0	-	3.0	6.125	1.25	22.96	0.922	7.55
13. Am. Felt Co. 3074	3.0	6.0	0.563	10.12	0.0485	8.27	0.5	1220	3.0	6.0	0.563	10.12	1.00	6.99
14. Am. Felt Co. 3267	3.063	5.25	0.5	8.04	0.0132	2.83	0.25	360	3.063	5.25	0.375	6.04	0.751	10.5
15. Am. Felt Co. 7544 (untreated)	3.25	6.063	0.813	16.0	0.174	18.7	3.0	5150	3.25	6.063	0.813	16.0	1.00	3.53
16. Am. Felt Co. 7544	3.0	6.0	0.75	13.5	0.174	22.3	5.75	460	3.0	6.0	0.875	15.75	1.168	3.22
17. Am. Felt Co. 7545	2.875	6.25	0.813	14.60	0.137	16.1	2.625	19940	2.875	6.188	0.813	14.47	0.990	3.92
18. Am. Felt Co. 7546	Diameter 0.28 in. Length 11.63 in.	0.28	11.63	0.717	0.0084	20.2	4.375	6600	Diameter 0.28 in. Length 11.94 in.	0.737	0.038	72.3	1.03	3.68
19. Am. Felt Co. 8537	3.125	6.0	0.875	16.40	0.108	11.4	0.5	1220	3.375	6.0	0.875	17.71	1.081	5.10
20. Am. Felt Co. 51018	3.0	6.0	0.75	13.5	0.0882	11.3	1.0	1220	3.0	6.0	0.75	13.5	1.00	4.70
21. Am. Felt Co. 51021	3.0	6.0	0.75	13.5	0.0948	12.1	0.25	1220	3.0	6.0	0.75	13.5	1.00	5.74
22. Am. Felt Co. 7545-B-1787	2.875	6.0	0.663	1.075	0.0121	19.5	0.5	1425	2.875	6.0	0.663	1.075	1.00	4.46
23. Am. Felt Co. 8430-B-12383	3.0	6.063	0.663	1.136	0.0077	11.7	0	-	3.0	6.063	0.663	1.136	1.00	6.86
24. Am. Felt Co. 51002-B-1954	2.875	6.0	0.663	1.079	0.0121	19.4	0	-	2.875	6.0	0.663	1.079	1.00	3.82
25. Am. Felt Co. 51018-B-2373	3.0	6.0	0.663	1.125	0.0088	13.5	0	-	3.0	6.0	0.663	1.125	1.00	4.13

TABLE 17

PHYSICAL PROPERTIES AND ABSORPTION CHARACTERISTICS OF WICK MATERIALS

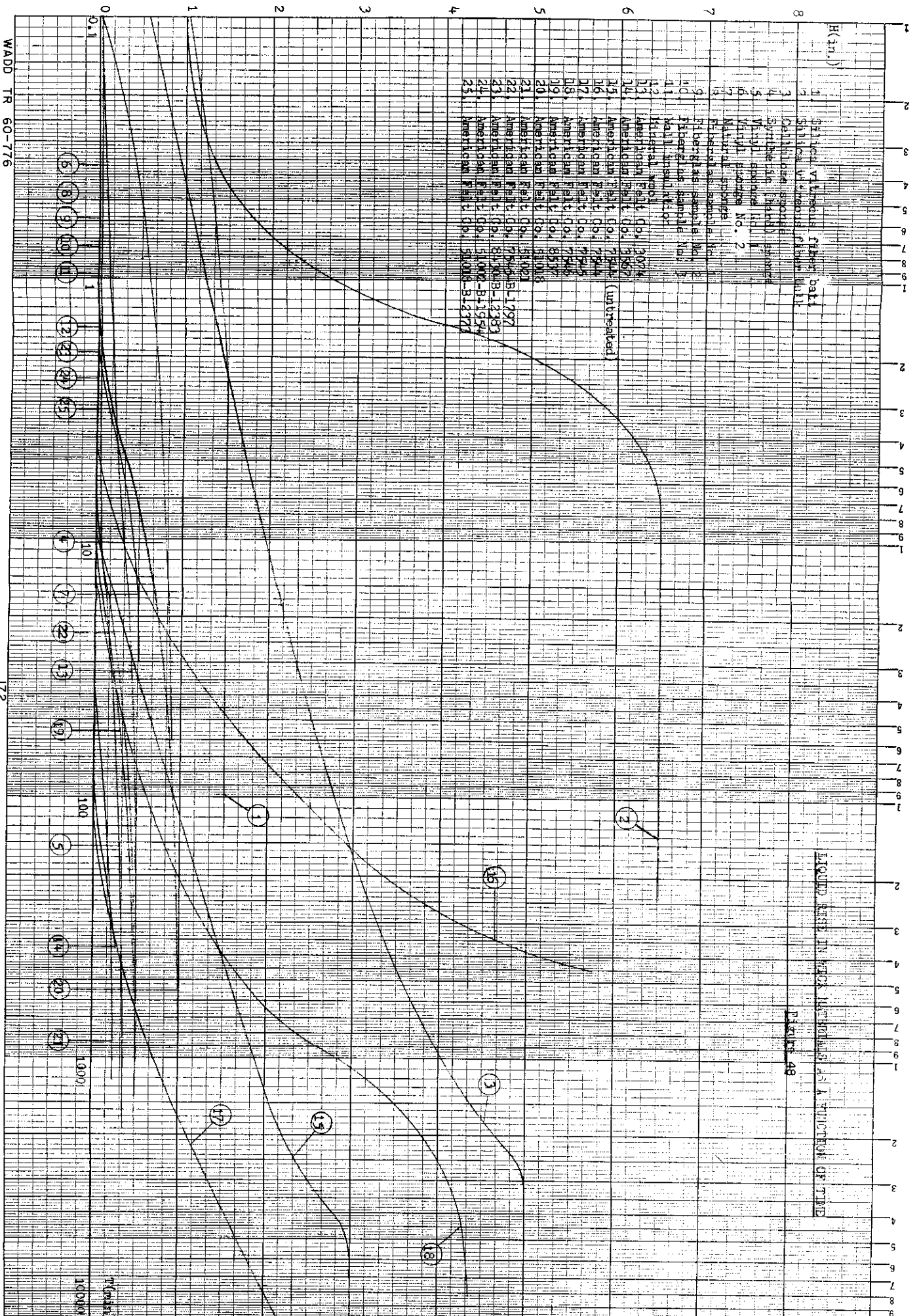
Sample Number & Material	Dry Condition				Soaked Condition				Volume Weight Ratio V_w/V_d	Density Ratio P_w/P_d	Maximum Water Absorption							
	Width	Height	Thick-ness	Density	Width	Height	Thick-ness	Density										
	in.	in.	in.	lbs./cu.ft.	in.	in.	in.	lbs./cu.ft.	lbs./cu.ft.	lbs./lb.	cu.ft.							
16/1 American	3.0	6.0	0.75	22.3	5.75	460	3.0	6.0	0.875	15.75	0.560	61.5	1.17	3.22	2.75	2.22	49.4	
16/2	2.938	6.0	0.813	21.1	5.75	150	2.938	6.0	0.813	14.3	0.560	67.5	1.00	3.22	3.22	2.22	46.5	
16/3	2.938	6.0	0.813	20.7	5.75	180	2.938	6.0	0.813	14.3	0.561	67.7	1.00	3.27	3.27	2.27	47.0	
16/4	2.938	6.0	0.813	20.7	5.75	240	2.938	6.0	0.813	14.3	0.560	67.5	1.00	3.23	3.23	2.23	46.8	
36/1 Felt	2.938	6.0	0.75	22.5	5.75	460	2.938	6.0	0.813	14.3	0.569	68.7	1.08	3.31	3.06	2.31	51.8	
36/2	2.875	6.0	0.813	21.2	5.75	293	2.938	6.0	0.813	14.3	0.553	66.6	1.02	3.22	3.15	2.22	47.0	
36/3	2.875	6.0	0.813	21.2	5.75	310	2.875	6.0	0.813	14.01	0.554	68.4	1.00	3.23	3.23	2.23	47.2	
36/4	2.875	6.0	0.813	21.2	5.75	420	2.875	6.0	0.813	14.01	0.550	67.7	1.00	3.20	3.20	2.20	46.7	
36/5 Company	2.875	6.0	0.813	20.7	5.75	450	2.875	6.0	0.813	14.01	0.546	67.2	1.00	3.24	3.24	2.24	46.5	
37/1	3.063	6.0	0.75	21.8	5.75	308	3.0	6.0	0.813	14.63	0.567	67.0	1.00	3.20	3.20	2.20	46.1	
37/2	3.0	6.0	0.813	20.9	5.75	490	3.063	6.0	0.813	14.8	0.568	66.5	1.02	3.19	3.12	2.19	45.6	
37/3	2.938	6.063	0.813	21.2	5.75	335	3.0	6.063	0.813	14.8	0.568	66.5	1.02	3.19	3.12	2.19	45.6	
37/4 No. 7544	3.0	6.0	0.813	20.7	5.75	340	3.0	6.0	0.813	14.63	0.568	67.1	1.00	3.25	3.25	2.25	46.5	
38/1 American	3.0	6.063	0.75	17.8	1.375	2680	3.0	6.063	0.813	14.78	0.487	57.0	1.08	3.45	3.19	2.45	43.8	
38/2	3.0	6.063	0.813	16.6	3.25	2410	3.0	6.125	0.813	14.95	0.505	58.3	1.01	3.63	3.59	2.63	42.8	
38/3	2.938	6.063	0.813	16.3	3.75	45	2.938	6.125	0.813	14.62	0.503	59.3	1.01	3.68	3.64	2.68	43.7	
39/1 Felt	3.125	6.0	0.75	16.8	0.625	1220	3.063	6.125	0.813	15.28	0.525	59.3	1.09	3.84	3.53	2.84	47.7	
39/2	3.0	6.125	0.813	16.5	4.0	280	3.0	6.188	0.813	15.1	0.518	59.3	1.01	3.62	3.58	2.62	43.4	
39/3	3.0	6.063	0.813	16.8	4.0	80	3.0	6.063	0.813	14.8	0.523	61.0	1.00	3.62	3.62	2.62	44.2	
39/4 Company	3.0	6.063	0.813	16.8	4.0	145	3.0	6.063	0.813	14.8	0.523	61.0	1.00	3.62	3.62	2.62	44.2	
17/1	2.875	6.25	0.813	16.1	2.625	19940	2.875	6.188	0.813	14.5	0.535	63.9	0.99	3.92	3.96	2.92	47.2	
17/2	2.913	6.125	0.813	16.6	3.5	430	2.813	6.125	0.813	14.01	0.481	59.2	1.00	3.58	3.58	2.58	42.7	
17/3 No. 7545	2.813	6.125	0.813	16.9	5.25	1440	2.813	6.125	0.813	14.01	0.477	58.8	1.00	3.49	3.49	2.49	42.0	
WADD TR 60-776																		

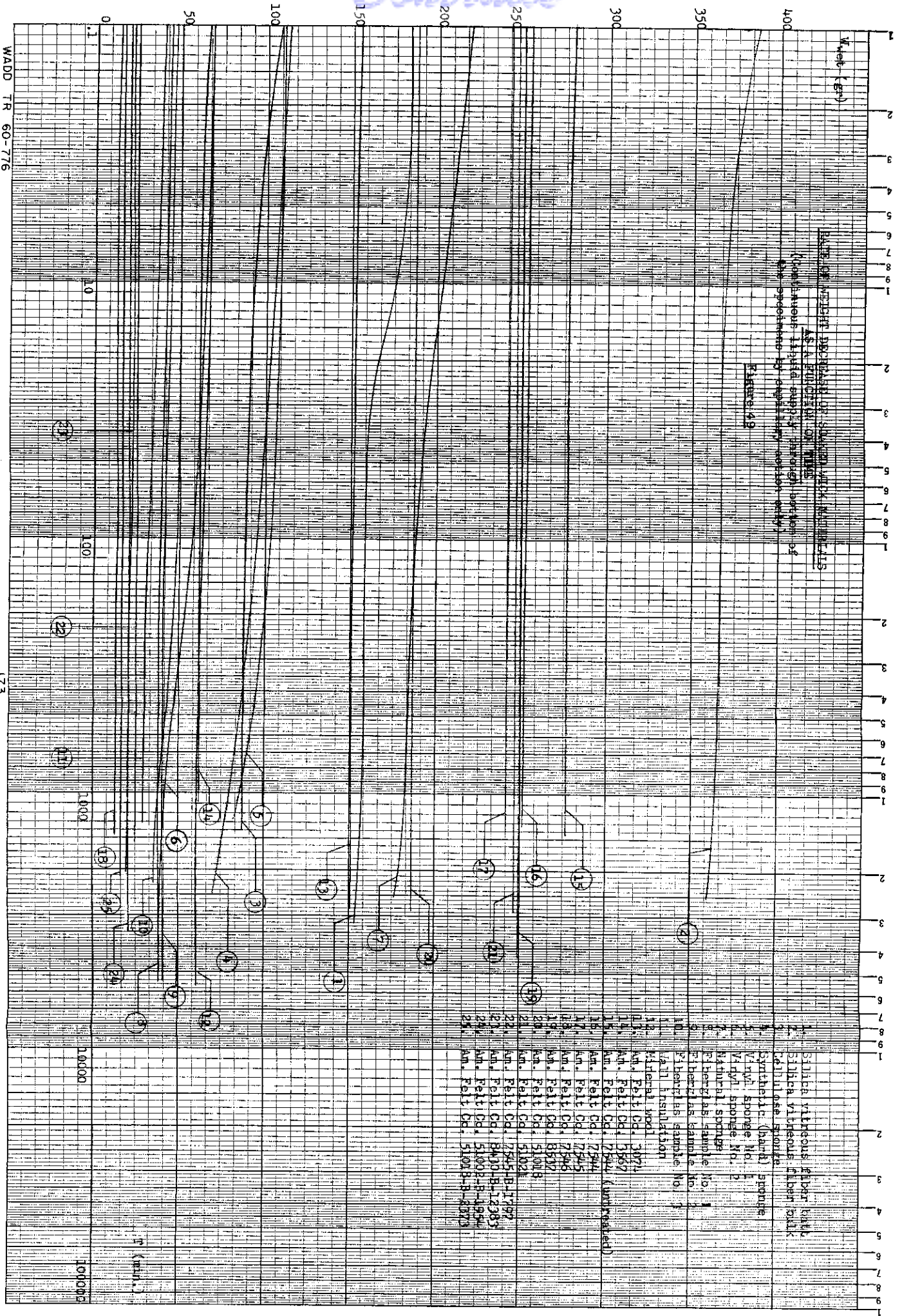
TABLE 17
PHYSICAL PROPERTIES AND ABSORPTION CHARACTERISTICS OF WICK MATERIALS (Continued)

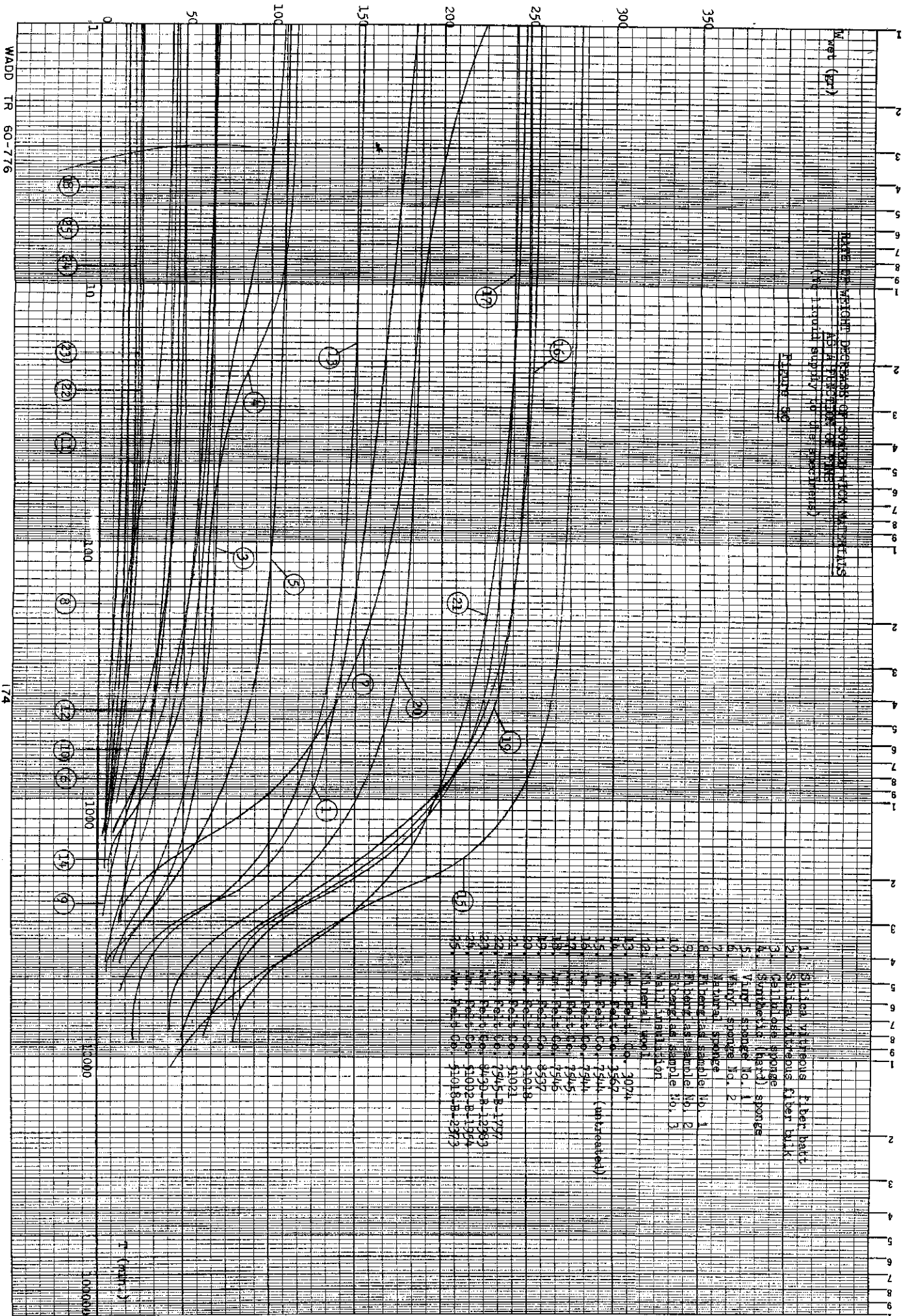
Sample Number & Material	Dry Condition			Maximum Rise			Soaked Condition			Volume Weight Density			Volume Weight Density Ratio			Maximum Water Absorption			
	Width in.	Height in.	Thick-ness in.	in.	min.	Time in.	in.	Thick-ness in.	Volume cu.in.	Weight lbs.	Density lbs./cu.ft.	V _w /V _d	W _w /W _d	P _w /P _d	lbs./lb.	cu.ft./cu.ft.			
26. Silica Batt	4.0	5.0	1.0	20.0	0.0287	2.47	1.5	35	4.125	5.25	0.625	13.5	0.337	43.2	0.675	11.78	17.4	10.77	26.6
27. Silica Batt	2.875	5.125	1.0	14.73	0.0215	2.52	5.0	4.320	2.875	5.25	0.375	5.66	0.267	81.2	0.384	12.41	32.3	11.41	28.6
28. Silica Batt	4.0	5.0	1.0	20.0	0.0287	2.47	1.375	3	4.0	5.0	0.625	12.5	0.388	66.9	0.625	13.54	21.7	12.54	31.1
1. Silica Batt	4.0	5.0	1.0	20.0	0.0287	2.47	1.5	3	4.0	5.0	0.625	12.5	0.406	70.0	0.625	14.17	22.6	13.17	32.6
29. Silica Batt	4.0	5.0	1.0	20.0	0.0287	2.47	1.5	2	4.0	5.0	0.625	12.5	0.390	67.4	0.625	13.62	21.8	12.62	31.2
30. Silica Bulk	Diameter 1.875 in. Length 9 in.			24.8	0.205	14.2	6.25	31	Diameter 1.875 in. Length 9 in.	24.8	0.793	55.1	1.00	3.87	3.87	4.14	4.14	3.14	40.9
2. Silica Bulk	Diameter 1.875 in. Length 10 in.			27.64	0.207	12.9	6.5	8	Diameter 1.875 in. Length 10 in.	27.64	0.857	53.5	1.00	4.18	4.18	4.18	4.18	3.18	36.6
31. Silica Bulk	Diameter 1.875 in. Length 10 in.			27.64	0.185	11.6	7.5	42	Diameter 1.875 in. Length 10 in.	27.64	0.773	48.3	1.00	4.18	4.18	4.18	4.18	3.18	36.6
32. Cellulose Sponge	1.613	5.0	0.75	5.98	0.0121	3.54	3.5	60	1.75	5.25	0.875	8.04	0.122	26.3	1.35	10.10	7.51	9.09	31.9
33. Cellulose Sponge	3.188	5.0	0.75	11.95	0.0242	3.50	4.5	2580	3.313	5.188	0.875	15.03	0.206	23.7	1.26	8.50	6.76	7.49	26.2
34. Cellulose Sponge	3.25	5.0	1.50	24.38	0.0507	3.59	5.0	1338	3.50	5.25	1.75	32.15	0.617	33.1	1.32	12.18	9.23	11.18	40.02
3. Cellulose Sponge	3.188	5.0	0.75	11.95	0.0221	3.18	5.0	2195	3.375	5.25	0.875	15.5	0.240	26.8	1.30	10.90	8.40	9.90	31.5
35. Cellulose Sponge	4.438	7.25	2.063	66.4	0.130	2.79	7.0	2665	4.625	7.375	2.313	78.9	1.340	24.3	1.19	10.31	8.68	9.31	26.0
18. Am. Felt Co. No. 7546	Diameter 0.28 in. Length 11.33 in.			0.717	0.0084	20.2	4.375	6600	Diameter 0.28 in. Length 11.94 in.	0.737	0.038	72.3	1.03	3.68	3.58	2.68	2.68	2.68	53.4

TABLE 18
PHYSICAL DATA FOR CAPILLARY FLOW WICK MATERIAL SPECIMENS

	Silica Batt	Silica Bulk	Cellulose Sponge	Am. Felt Co. No. 7544	Am. Felt Co. No. 7545	Am. Felt Co. No. 7546
Dry Weight (lbs)	0.992×10^{-3}	1.76×10^{-3}	0.925×10^{-3}	3.72×10^{-3}	3.17×10^{-3}	3.15×10^{-3}
Length (in)	4	4	4	4	4	4
Diameter of Sample (in)	0.228	0.228	0.228	0.305	0.295	0.28
Diameter of Tube (in)	0.228	0.228	0.228	0.338	0.338	0.303
Dry Density (lbs/cu ft)	10.11	18.0	9.39	22.03	19.99	21.76
Soaking Period (days)	1	1	1	3	3	3







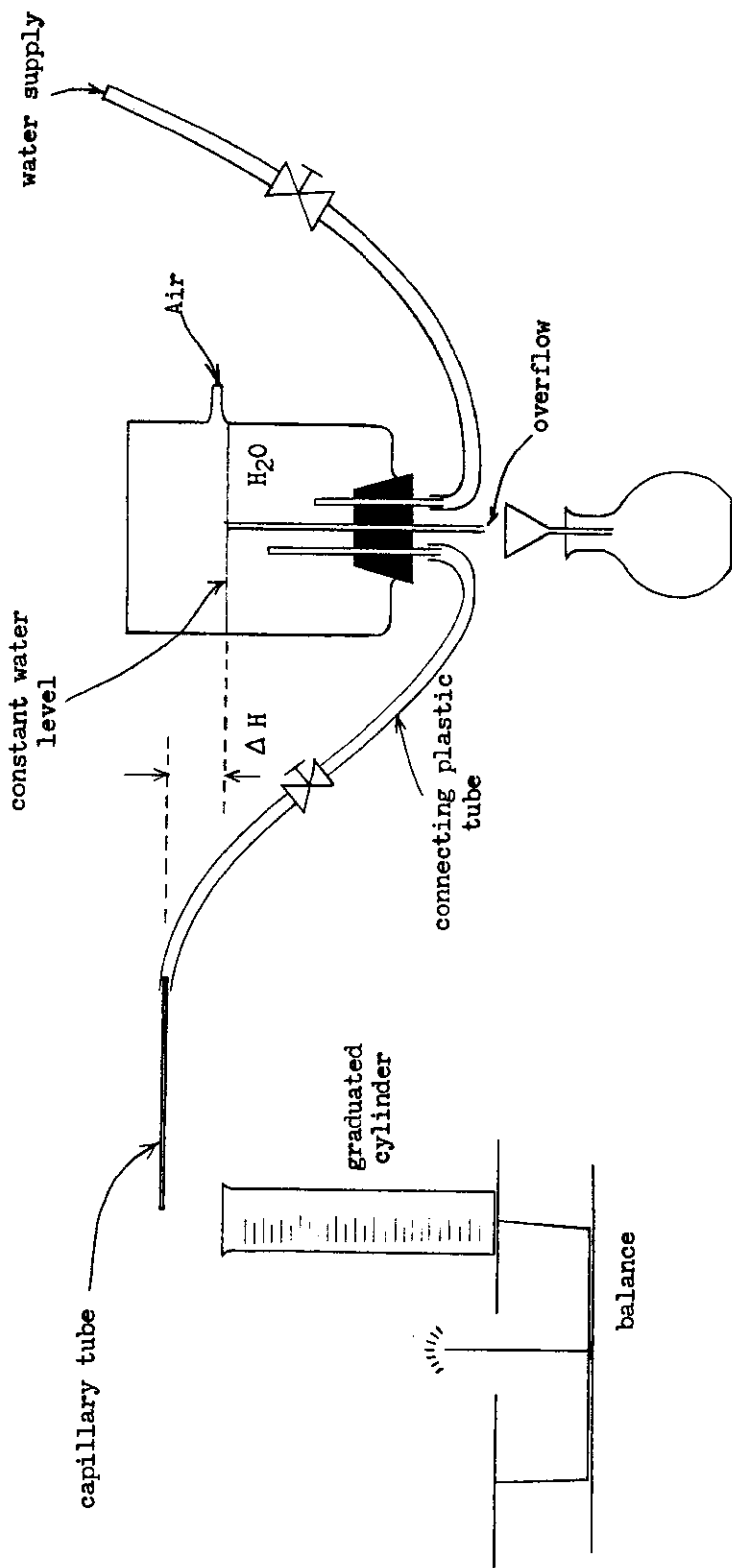
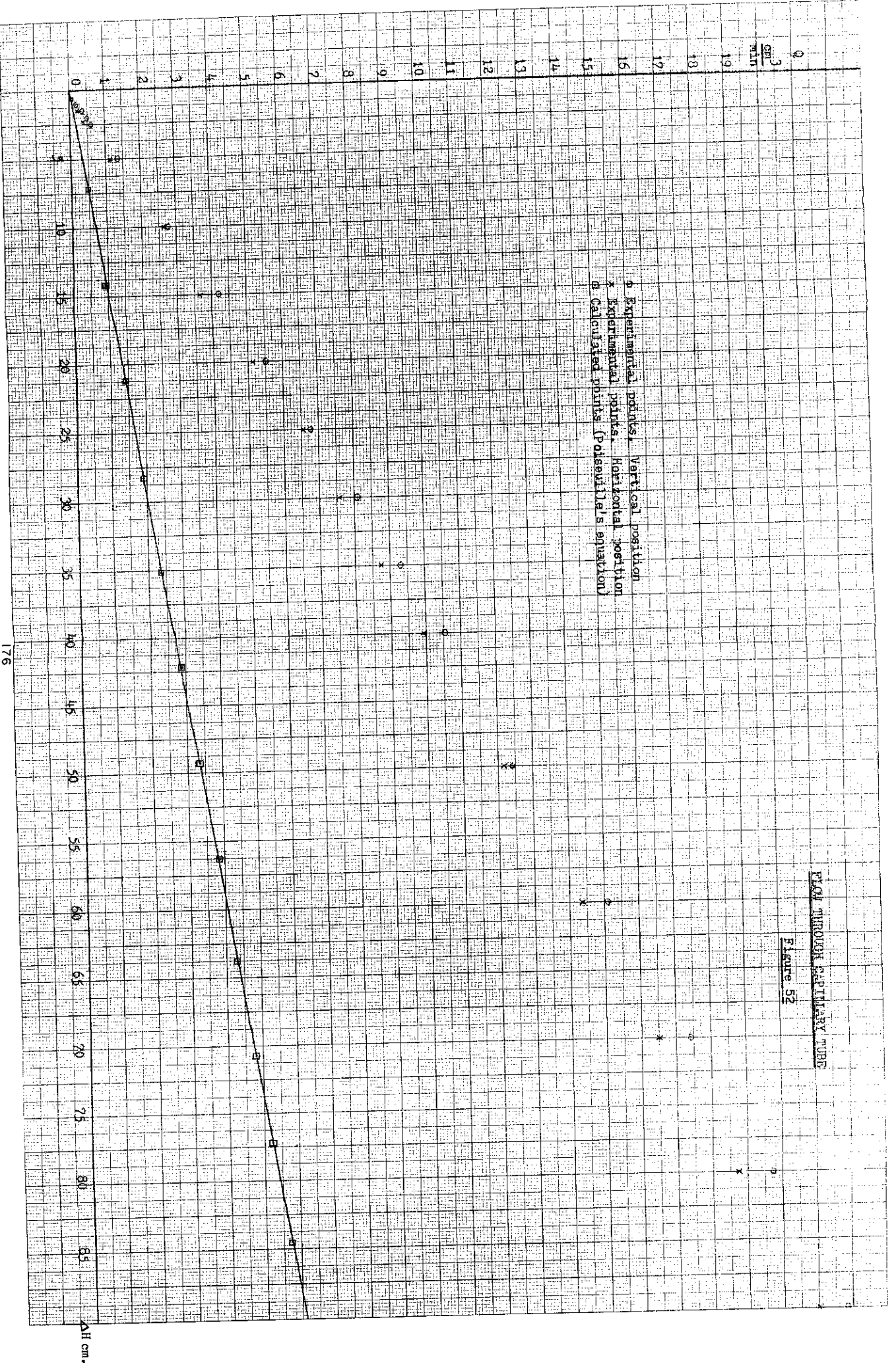
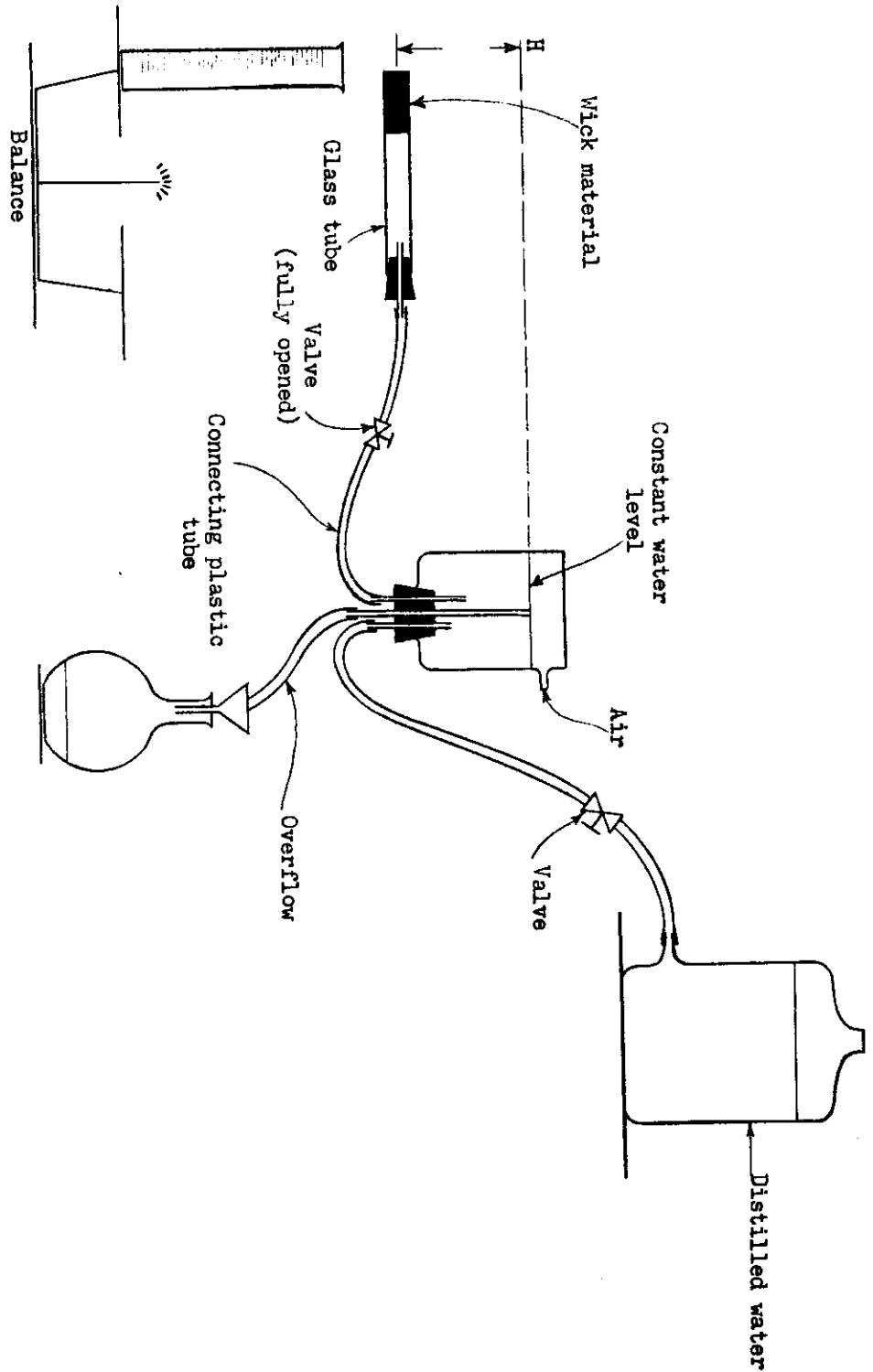


FIGURE 51: SCHEMATIC OF APPARATUS TO TEST CAPILLARY FLOW

WADD TR 60-776



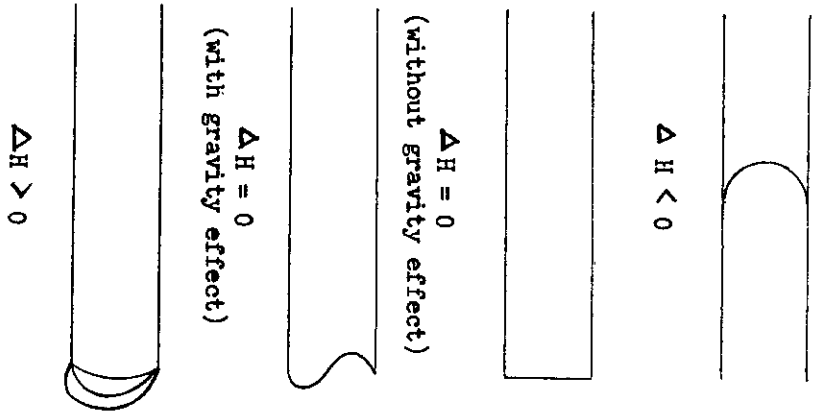
176



SCHEMATIC OF APPARATUS TO TEST CAPILLARY FLOW IN WICK MATERIALS

Figure 54

(a) Change in Meniscus Shape with Pressure Head



(b) Flow Rate vs Pressure Head

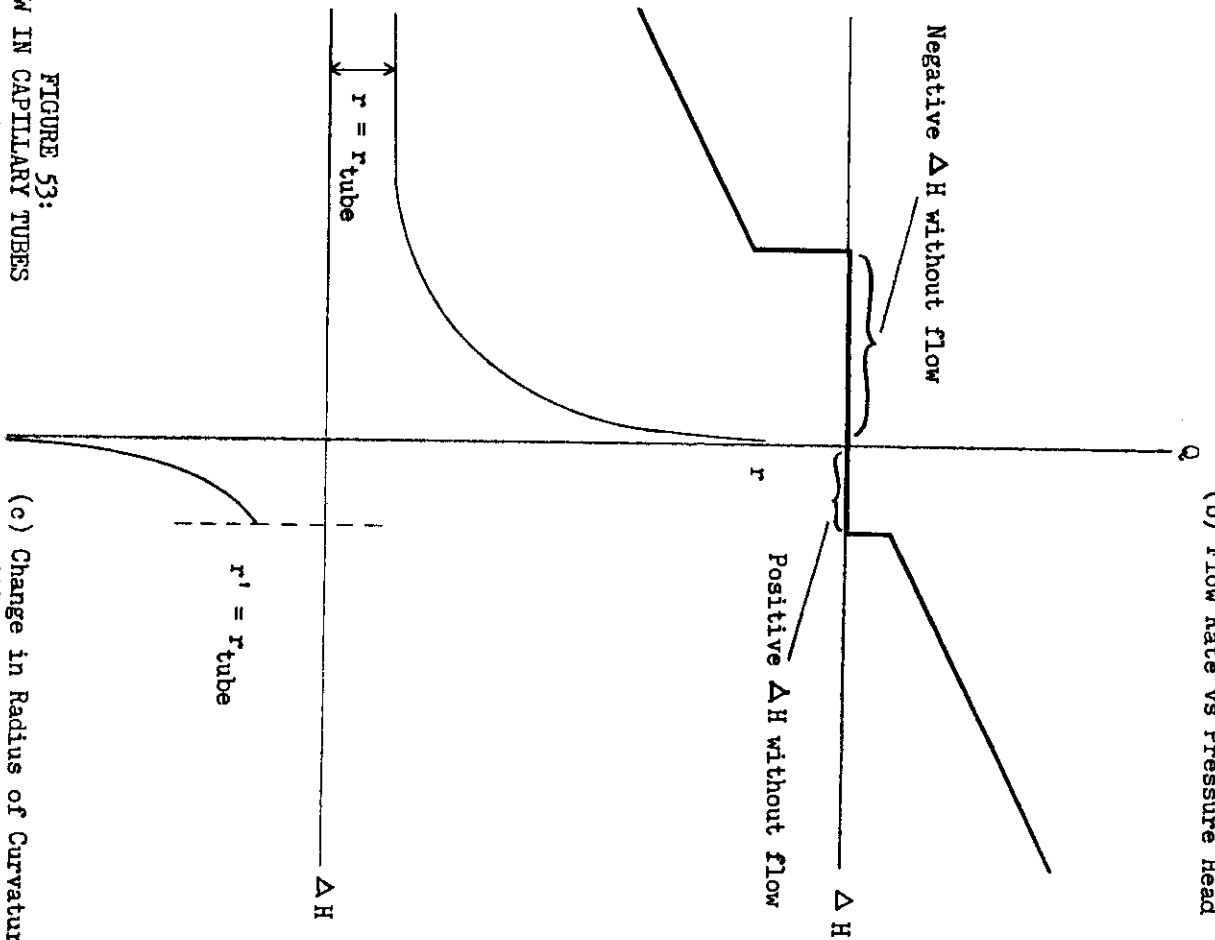


FIGURE 53:
FLOW IN CAPILLARY TUBES
177

(c) Change in Radius of Curvature with Pressure Head

WADD TR 60-776

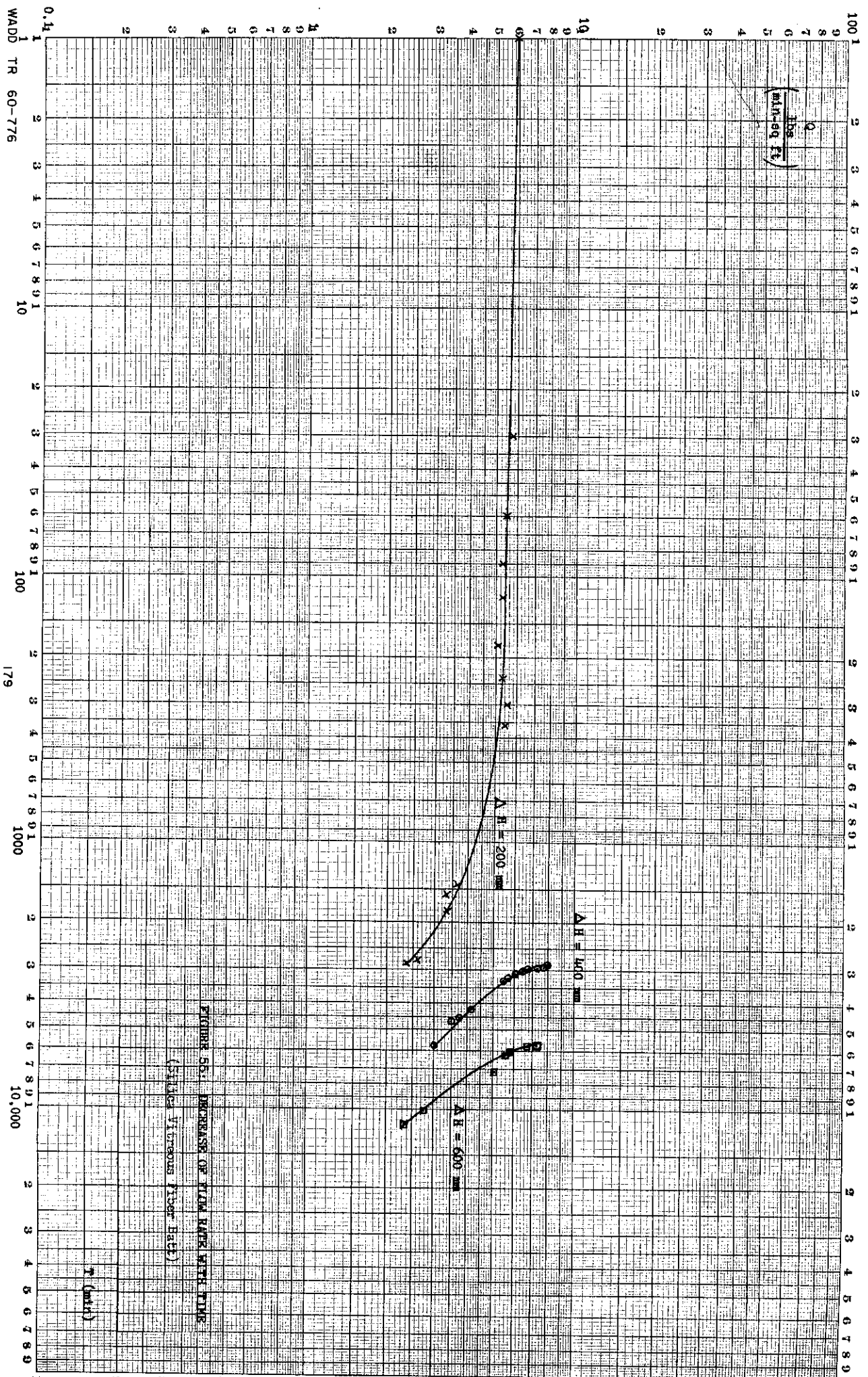


FIGURE 5B1. INCREASE OF FLOW RATE WITH TIME
(SHOULD VARIOUS FIBER HATS)

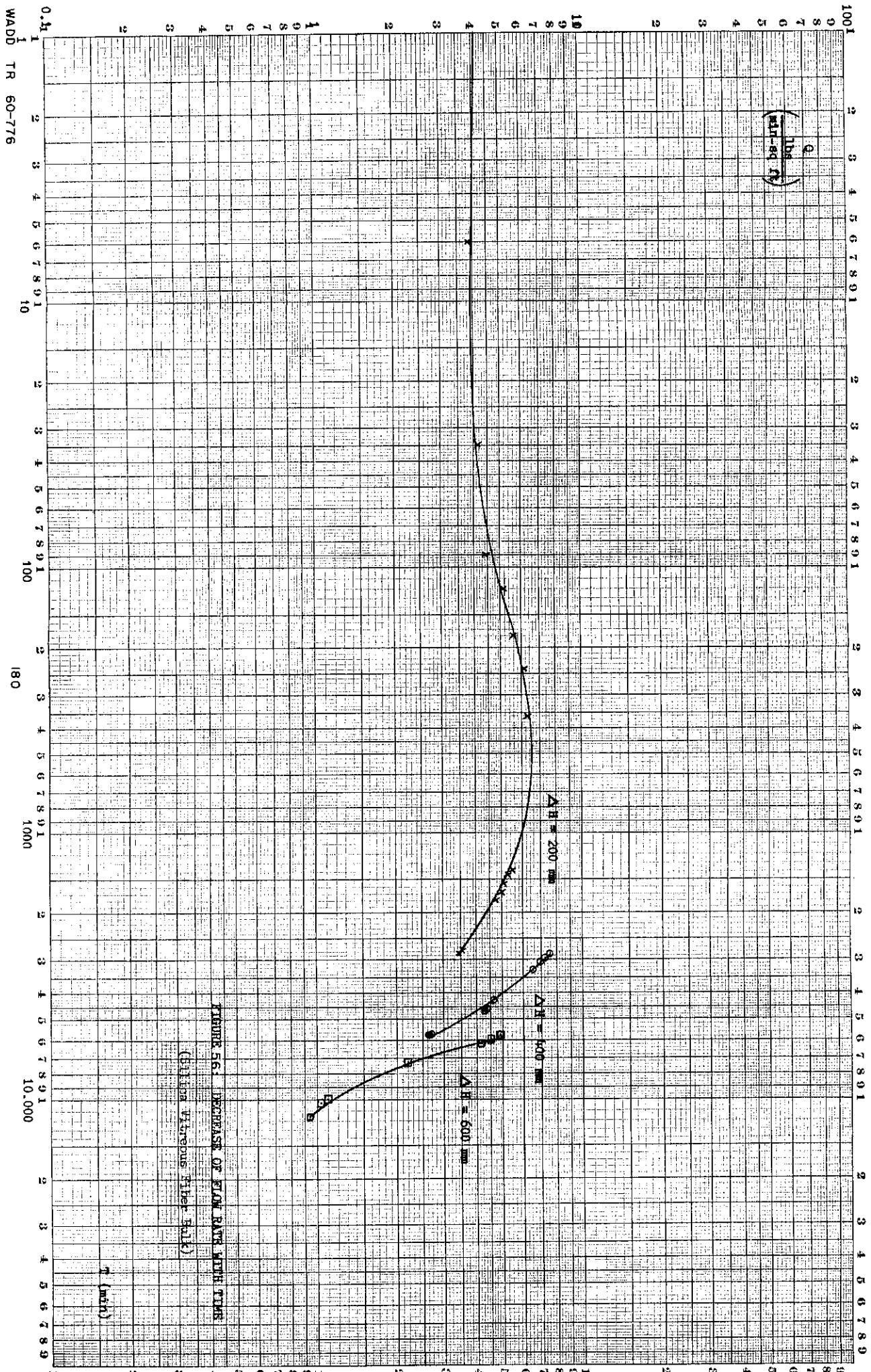
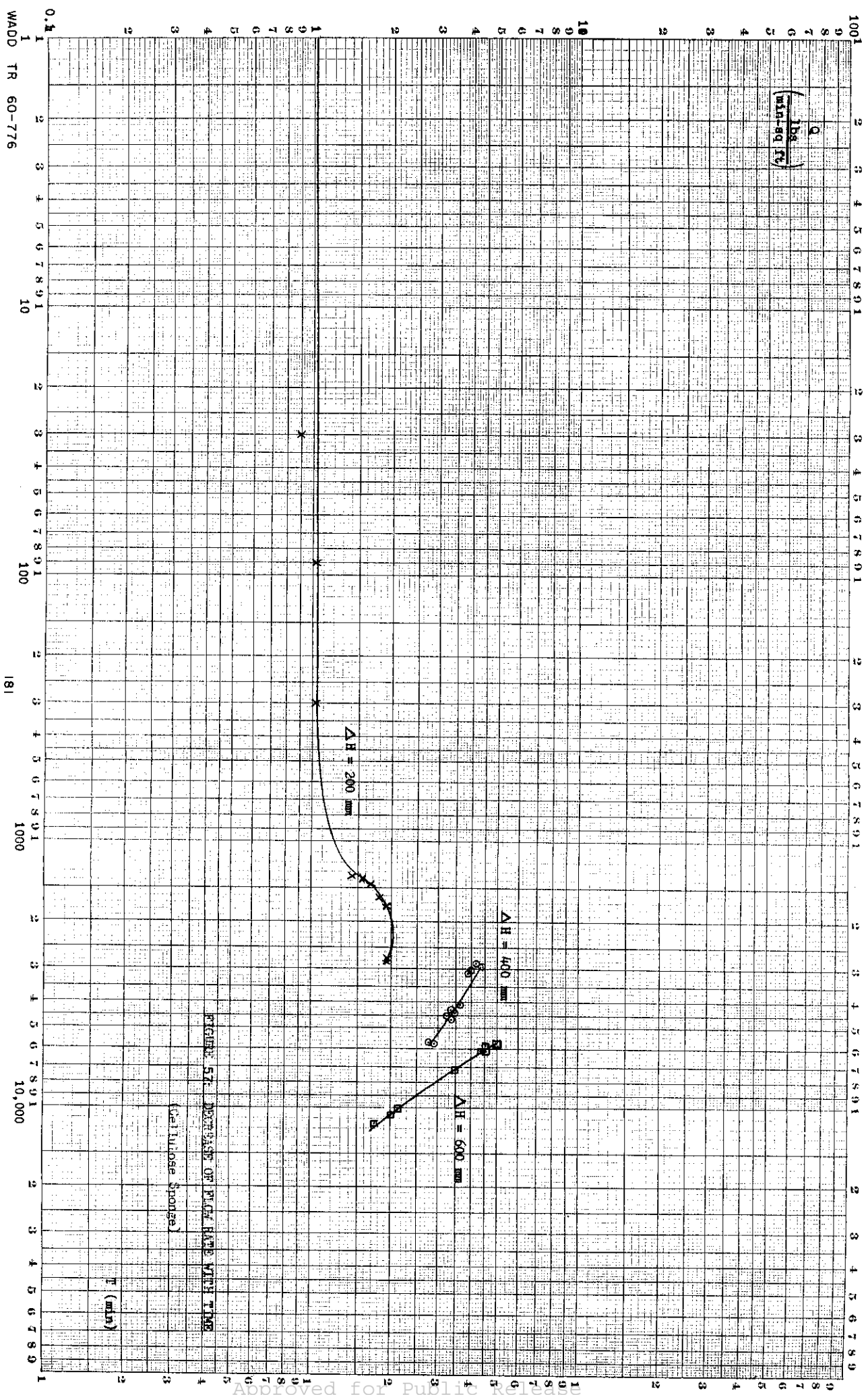


FIGURE 56. DECREASE OF FLOW RATE WITH TIME
(Biller Vitroneous Fiber Ball)

WADD TR 60-776



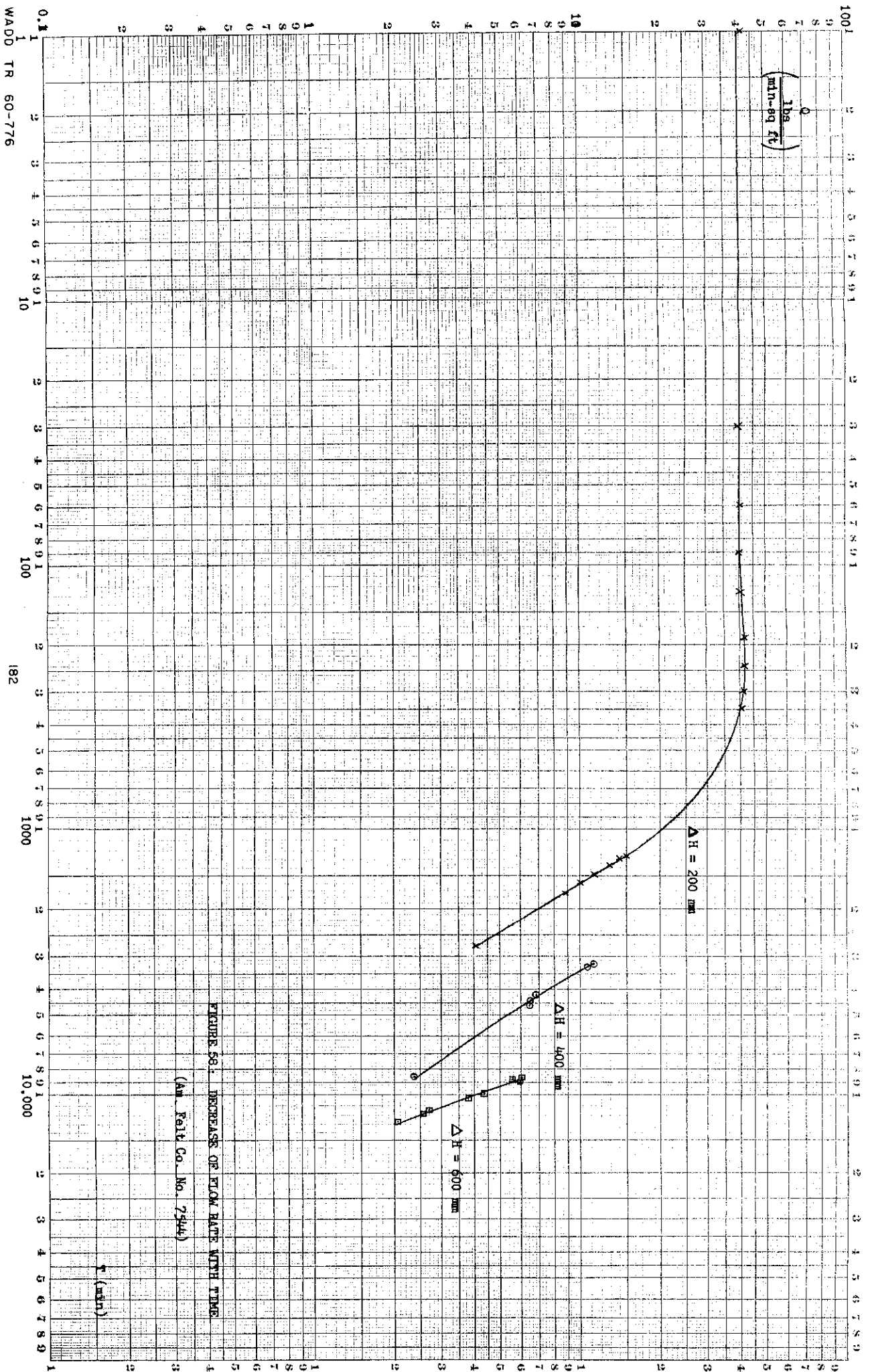
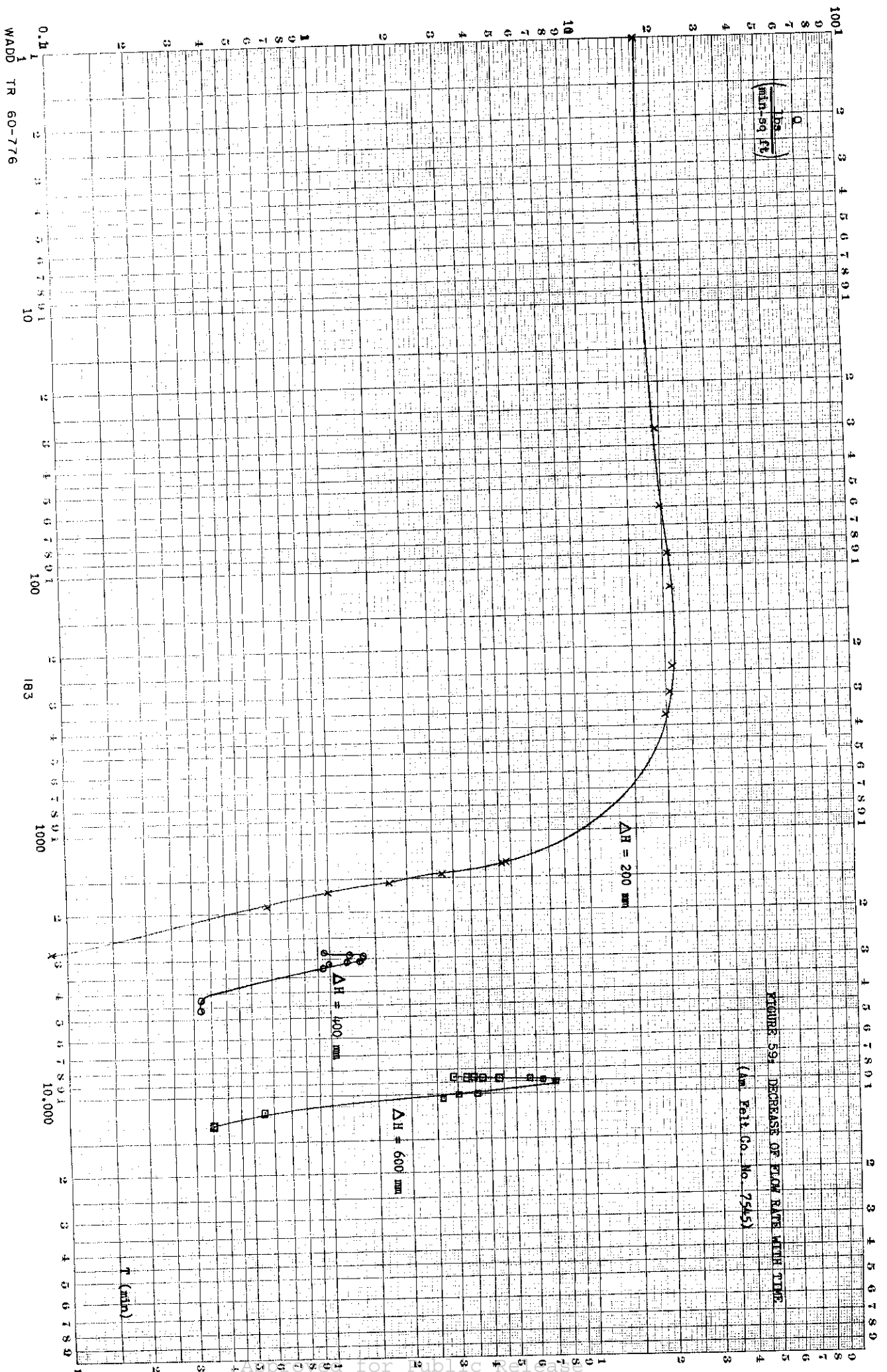


FIGURE 56. INCREASE OF FLOW RATE WITH TIME.
(Am. Felt Co. No. 7544)

WAADO TR 60-776

182



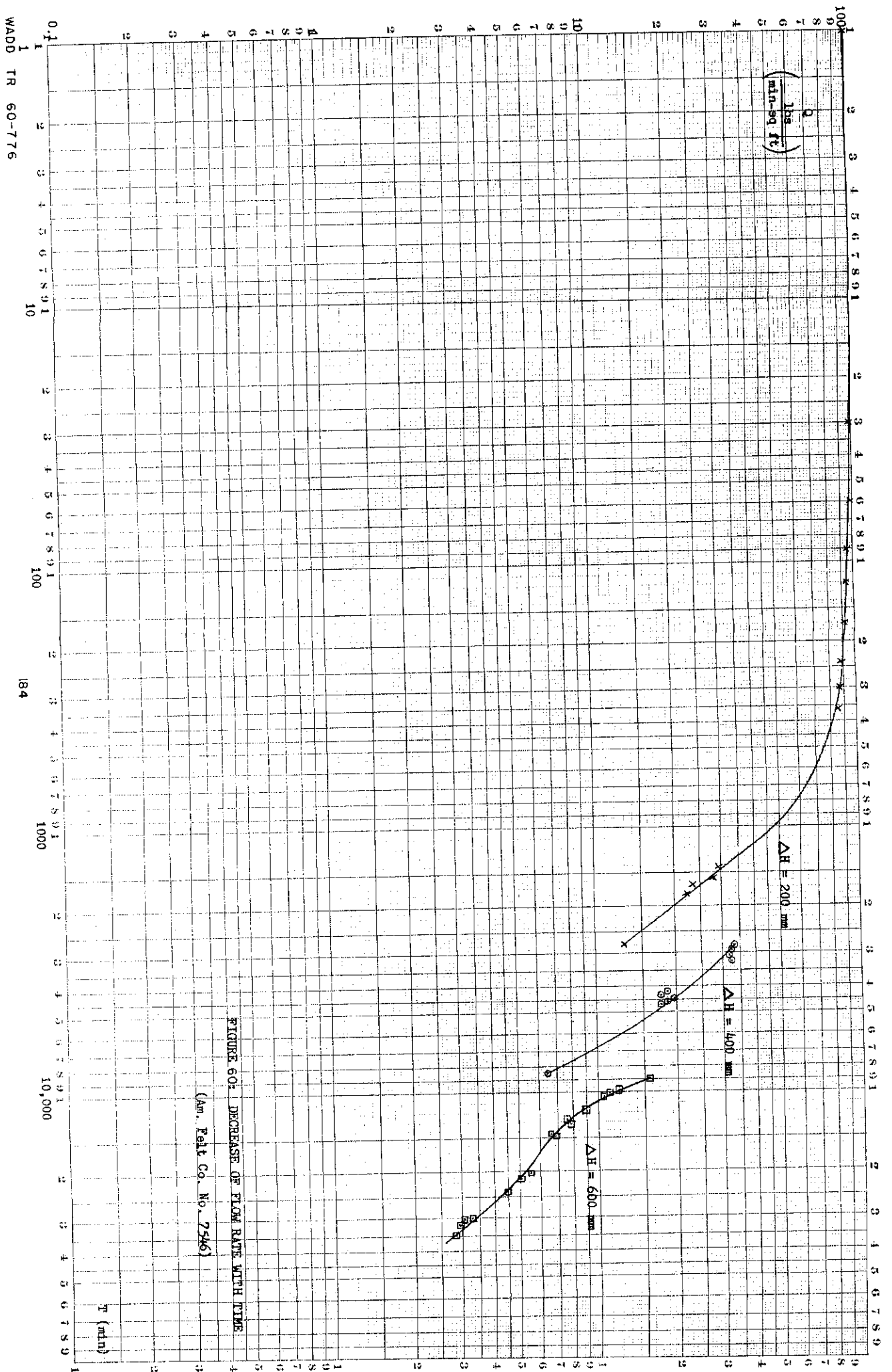


FIGURE 60: DECREASE OF FLOW RATE WITH TIME
(Am. Felt Co. No. 7546)

WADD TR 60-776

184

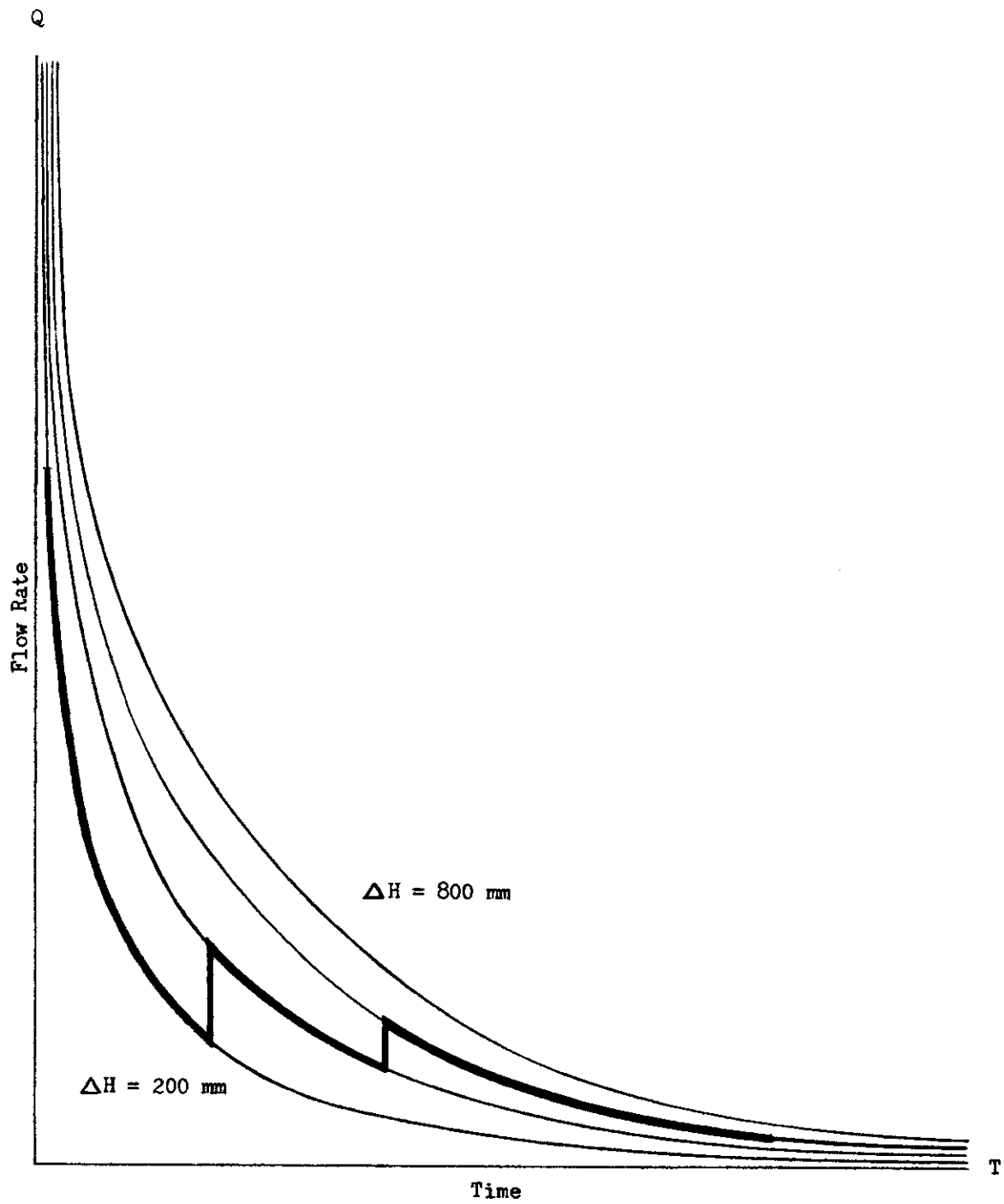


FIGURE 61:
ACTUAL FLOW RATE DROP IN WICK MATERIALS

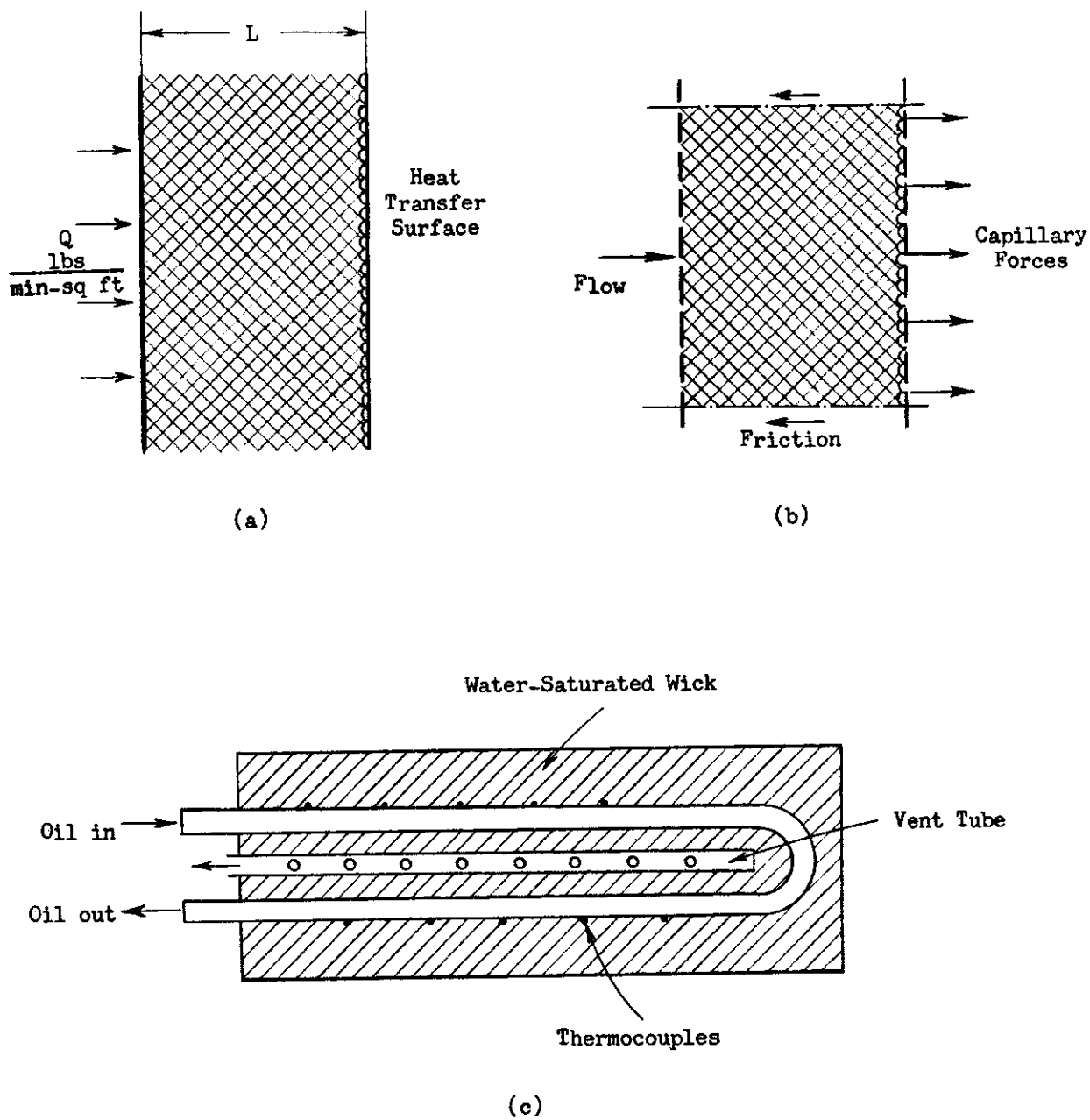


FIGURE 62: SCHEMATIC OF WICK HEAT EXCHANGER (REFERENCE 7)

Contrails

SECTION XI

COMPRESSOR STUDY

This section considers some of the factors which influence compressor selection for this application. No major effort was expended in this direction because of the extent of the effort spent on the previous studies.

An investigation of the physical phenomena occurring in mechanical compressors reveals that the absence of gravity does not appreciably affect the design of compressors. The energy equation for the compression process is derived from the first law of thermodynamics, and is written as follows:

$$\text{Power} = w \left(J h_2 + \frac{c_2^2}{2 g_c} + \frac{g}{g_c} z_2 - J h_1 - \frac{c_1^2}{2 g_c} - \frac{g}{g_c} z_1 + J Q_1 \right) \quad (124)$$

The momentum relation for a radial compressor is

$$\frac{H_2 - H_1}{u_2^2 / g_c} = \eta \left(\frac{c_{02}}{u_2} - \left(\frac{r_1}{r_2} \right)^2 \frac{c_{01}}{u_1} \right) \quad (125)$$

where

$$H = \frac{p}{\rho} + \frac{g}{g_c} z + \frac{c^2}{2 g_c}$$

In the zero-gravity case, the elevation terms with the factor z will be omitted. However, in actual compressor design for a gravitational case, these terms are of negligible magnitude and are usually omitted. An analysis of other compressor characteristics, such as pressure ratio, inlet circulation, centrifugal action, stability, and surging, choking, shock waves, slip factor, and separation (back flow), reveals no influence of gravity. To a very small degree, gravity influences bearing load design due to the weight of the bearings themselves.

It was stated in a previous section that, due to the effects of zero-gravity on heat transfer in the evaporator, there exists the possibility of some entrained liquid droplets entering the compressor with the vapor stream. The literature was investigated to study the effects of wet compression and the extent to which it may be tolerated. Hamrick (4) has reported excessive pitting of aluminum alloy blades when the entering air stream contained water droplets with a diameter greater than 20 microns. The effects of wet compression vary with the percent of liquid in the inlet vapor stream, with the size of the entrained liquid droplets, and with the pressure ratio. The presence of liquid usually decreases the cycle efficiency. Wet compression does not appear feasible for reliable vapor cycle operation, and it is necessary to ensure that no liquid enters the compressor.

Contrails

The problem of optimum specific speed and its influence on both compressor and refrigerant selection has been discussed in Section II. A range of recommended optimum specific speeds (taken from Reference 1) has been presented in Table 4. Axial and mixed flow compressors may be eliminated from consideration due to the high specific speeds required. The problems in compressor application for the vapor cycle considered here arise not so much from the zero-gravity environment in which the compressor must operate, but from the range of conditions under which the compressor must operate. These problems would exist regardless of whether the cycle were operating under a zero-gravity or earth-bound environment. The evaporator heat load in this study varies from 400 to 4000 BTU/min. At the lower value of the evaporator capacity, the refrigerant flow rate is quite small. For a centrifugal machine operating between 40 degrees F and 250 degrees F, an extremely high shaft speed is required to satisfy the minimum value of the optimum specific speed range. Centrifugal compressors capable of operating at the required speeds are not currently available, and some effort to develop high-speed centrifugal compressors for vapor cycle applications such as the one considered here appears worth while.

Centrifugal compressors are well suited for application to space vehicle vapor cycle systems. They are compact and light in weight. The main bearings are the only major rubbing surfaces, and, since the only moving parts are rotating, balancing is better than that for reciprocating machines. Centrifugal compressors provide uniform vapor flow and do not produce excessive pressures, so that bleed-off is not necessary. Lubrication is less of a problem for centrifugal compressors than for displacement compressors. In cases where oil becomes mixed with the refrigerant, oil separators are necessary for proper compressor operation in both gravitational and zero-gravity environments. In zero-gravity operation, where normal density differences between oil and refrigerant may not be utilized for separation, special separators would be required. Fortunately, the lubrication problem for a hermetically-sealed centrifugal compressor is not an acute one, since there is no mixing of oil and refrigerant. As stated before, the main problem in the use of a centrifugal compressor for this application is the high shaft speeds required to operate the compressor at low refrigerant flow rates. Current accepted practice limits compressor speeds to about 30,000 rpm. A centrifugal compressor capable of operating at almost 90,000 rpm (3) has been reported. More development work is needed in this direction. The development of centrifugal compressors capable of even higher shaft speeds is possible, and depends on the amount of effort and resources which can be directed towards the problem. Assuming an upper limit of shaft speed of 80,000 rpm fixes the lower limit of evaporator capacity using Freon 11 at about 1600 BTU/min. Freon 113 may be used with a centrifugal compressor over almost the entire range, but with a lower coefficient of performance. It is believed that the higher coefficient of performance and the advantages of using centrifugal compressors in vapor cycles makes the effort to develop higher-speed centrifugal compressors attractive. The only other solution is to use other types of compressors in the lower capacity ranges.

Rotary (positive-displacement) compressors stand between centrifugal and reciprocating compressors as far as the range of optimum specific speed is concerned. Rotary compressors are compact and light in weight, but give low pressure ratios per stage and have low efficiencies. Freon 21 and Freon 114 appear to be the most suitable refrigerants for rotary compressors, but suffer from the standpoint of coefficient of performance. Three types of rotary compressors are available; the vane, roller, and Heli-Rotor types. As in the case

Contrails

of centrifugal compressors, several stages are necessary when the pressure ratio is large. The Heli-Rotor compressor consists of a pair of intermeshing rotors surrounded by a housing. Power is supplied to the male rotor of the compressor through the rotor shaft. The female rotor is driven by timing gears and acts as a rotary seal. There is no contact between either the rotors themselves or rotors and housing. It is claimed that speeds of 40,000 to 50,000 rpm are practical for the compressor. Only the bearing and timing gears require lubrication, and Freon lubrication has been used successfully in refrigeration. The rotors themselves require no lubrication so that oil is not contained in the exit vapor, which is a serious problem with other rotary-type compressors. Usually, in rotary compressors, due to high mechanical friction, lubrication is very important, and both oil and refrigerant must circulate through the compressor to avoid damage. An oil separator is then required at the compressor exit to remove the large amount of oil in the exit stream. The Heli-Rotor unit avoids this difficulty.

The Heli-Rotor is currently available with rotor diameters of 54 mm, 63 mm, 125 mm, and 200 mm. Some information was obtained (2) on the applicability of the Heli-Rotor unit to the current problem using Freon 11 as the refrigerant. For a 40 degree F evaporator temperature and a 250 degree F condenser temperature, a single-stage Heli-Rotor is not suitable, since the pressure ratio is excessive. A two-stage Heli-Rotor may be used at the higher capacity (4000 BTU/min). At the lower capacity (400 BTU/min), the speed requirement would still be excessive, and although the unit may be used for the first stage, the next stage would have to use a reciprocating machine. There appears to have been little work done on the use of rotary compressors for refrigeration applications.

The only remaining choice for the low capacity range is the reciprocating compressor. These units have high efficiency, but are not vibration free or light in weight. Some weight reduction has been achieved for airborne application; any further decrease can be obtained only by increasing compressor speed. The optimum specific speed range for reciprocating units is low, from 0.001 to 0.005. Unfortunately, the more volatile refrigerants (which give the higher refrigerant effect per unit volume at the compressor entrance) such as Freon 12 and Freon 22, which are suitable for application to reciprocating compressors, were eliminated (see Section II) due to other considerations. Hence, some compromise would be necessary, and Freon 21 would probably have to be used in a reciprocating unit at the lower capacity. Reciprocating units require internal lubrication, so that the exit vapor would contain some oil requiring a separator.

In summary, centrifugal compressors are ideally suited to the higher capacity ranges. At the lower capacity, a centrifugal unit using Freon 113 may be applicable, but some development work on the compressor would still be necessary. A reciprocating unit at the lower capacity would have to use Freon 21 due to temperature considerations. A conventional (vane or roller) rotary compressor using Freon 21 in the low capacity range would require a specially designed oil separator for the zero-gravity case. The current development of the Heli-Rotor does not permit its use at the lower capacity, high pressure ratio condition.

Contrails

LIST OF SYMBOLS

C	ft/sec	Velocity of fluid
C_0	ft/sec	Tangential velocity of fluid
g	ft/sec ²	Local gravitational acceleration
g_c	32.17 lbm-ft/lbf-sec ²	Dimensional constant
h	BTU/lb	Enthalpy of fluid
H	ft-lbf/lbm	Total head
J	778 ft-lbf/BTU	Mechanical equivalent of heat
Q	BTU/lb	Heat loss from fluid per unit mass
r	ft	Radius
u	ft/sec	Tangential velocity of wheel
w	lbs/sec	Flow rate
z	ft	Elevation
p	lbs/sq ft	Pressure
ρ	lbs/cu ft	Density

Contrails

REFERENCES

1. Mason, J. L., Burriss, W. L., and Connolly, T. J., Vapor Cycle Cooling for Aircraft, WADC TR-53 338, October 1953
2. Borzilleri, Richard, Stratos Division of Fairchild Engine and Airplane Corporation, Personal Communication
3. Palmatier, E. P., "Centrifugal Refrigeration Compressor for Aircraft," 53rd Annual Meeting of A.S.R.E., Miami Beach, June 1957
4. Hamrich, J. T., "Some Investigations with Wet Compression," Trans. ASME, April 1953, p. 409
5. Kaye, J. and Rivas, M. A., "Experimental and Analytical Study of Two Component Two Phase Flow in an Ejector with Condensation Shocks," ASME-A.I.Ch.E. Heat Transfer Conference, University Park, Pennsylvania, August 1957, ASME Paper No. 57-HP-35
6. Shapiro, A. H. and Taylor, E. S., Fluid Machinery Notes, Massachusetts Institute of Technology

Contrails

SECTION XII

CONCLUSIONS AND RECOMMENDATIONS

On the basis of the previous study, it is concluded that the heat transfer performance of specific vapor cycle components would be seriously affected by the zero-gravity environment. Conventional evaporators and condensers would become inoperable; the compressor and throttle valve are affected indirectly by the performance of the evaporator and condenser. The zero-gravity environment requires special design of the heat transfer equipment to solve the vapor-liquid separation problem. The vortex evaporator and the spiral condenser represent two such solutions. An additional concept--the flash evaporator--was not analyzed in this study, but it may result in a simple lightweight concept for zero-gravity application.

From the work that has been performed, the following conclusions have been drawn:

1. The search for new refrigerants did not reveal any new compounds whose optimum thermodynamic and zero-gravity performance exceeded that of the known refrigerants. One difficulty in such a search is that thermodynamic data are readily available for only the more common organic compounds.
2. The most promising fluid properties to use for vapor-liquid separation appear to be density and surface tension.
3. A vortex evaporator operating under zero-gravity compares quite favorably with a plate-fin evaporator operating under one g, for the same cycle conditions. Its volume is smaller than that of a plate fin unit, and its weight is somewhat larger.
4. The fixed weight of a rotating condenser is quite large, but substantial reductions in weight should be possible by lowering the thicknesses of the materials used.
5. The spiral condenser is believed to be more feasible than the rotating condenser, since the former has no moving parts. Nevertheless, the spiral condenser, operating under zero-gravity, has a volume several times larger than that of a small-diameter tube-fin unit operating under one-g.
6. For the large temperature differences between evaporator and condenser that are encountered in space vehicle vapor cycles, a work-producing expansion machine, which replaces the throttle valve between the condenser and the evaporator, gives a significant theoretical improvement in the coefficient of performance.
7. Wick materials are suitable for use in zero-gravity evaporators, but further work is required before generalized correlations regarding the fluid mechanics and heat transfer behavior of these materials may be derived.

Contrails

The data currently available for the design of zero-gravity heat transfer equipment is insufficient, and reliable experimental data is required in the following areas. One concept not covered in this study appears to offer a promising solution to zero-gravity evaporator design. This is the flash boiler study discussed below.

Vortex Evaporator - Heat transfer data for boiling Freon in tubes with twisted tapes are required to provide reliable data for the design of vortex-evaporators in a zero-gravity environment. The work that has been done so far in this field has been directed specifically toward extending the burnout point for fuel elements in nuclear reactors, and not toward the nucleate boiling regime itself.

Spiral Condenser - Experimental data on condensation of Freon vapor in curved channels will provide accurate heat transfer performance data for the spiral condenser. Since condensation experiments in a single curved channel are not feasible, a facsimile of a spiral condenser must be used. Although the diameter of the test unit should be comparable to the proposed zero-gravity unit, the length of the test unit may be reduced. The tests should be performed for complete condensation of Freon 11 vapor at the temperatures, pressures, and scaled-down flow rates encountered in the zero-gravity vapor cycle.

Flash Boiler - In a flash boiler, the vapor-liquid separation problem is avoided by restricting the amount of liquid in the vicinity of the heat transfer surface so that the vapor formed by boiling does not have to travel through a bulk liquid phase. In the scheme suggested here, the throttling process is replaced by one in which the high pressure refrigerant from the condenser is atomized by a number of small nozzles in the flash boiler. The refrigerant leaves the nozzles as a fine spray and impinges on heated plates or staggered tubes and flashes into vapor. The vapor exit must be oriented to prevent liquid droplets from leaving the evaporator directly. High heat transfer coefficients should be obtained, since the droplets are small and the vapor velocity may be controlled to give a small pressure drop in the evaporator. Such a boiler is insensitive to gravity, but there appears to be no data available to provide the basis for a design.

Wick Materials - To provide a systematic approach to the use of wick materials in zero-gravity evaporators and condensers, fluid mechanics tests should be conducted with Freon refrigerants and boiling heat transfer coefficients should be measured.

Turbine Expander - It has been shown previously that for a vapor cycle operating between an evaporator temperature of 40 degrees F and a condenser temperature of 250 degrees F, the coefficient of performance may be improved by 30 per cent if the throttle valve is replaced with a turbine which has a 60 per cent adiabatic efficiency. The refrigeration flow rate is reduced about 15 per cent, so that other system components are reduced in volume. Although this substitution is not connected with the zero-gravity environment, it does improve the performance of space vehicle vapor cycles. The construction of a turbine expander where the liquid refrigerant enters

Contrails

the turbine nozzles in the saturated liquid state and leaves the nozzles as a mixture with high liquid fraction is suggested. Such a unit would be tested under actual cycle conditions, and the results would be directly applicable to a vapor cycle system design.

Contrails

APPENDIX I

EVAPORATOR DESIGN METHODS AND CALCULATIONS

A. GENERAL DISCUSSION ON HEAT TRANSFER

The over-all heat transfer rate equation may be written

$$\frac{d Q}{d A} = U (T_h - T_c) \quad (126)$$

$d Q/d A$ is the heat flux per unit transfer area at a section within the heat exchanger where the temperature difference is $(T_h - T_c)$, and U is the over-all thermal conductance, or over-all heat transfer coefficient, based on a temperature potential, $(T_h - T_c)$, and a unit transfer area.

The reciprocal of U , the thermal resistance, is made up of many components, involving the heat transfer coefficients of the heat exchanger fluids, the thermal conductivity and thickness of the heat exchanger walls, and fouling or scaling coefficients. Disregarding the fouling and wall conductivities,

$$\frac{1}{U} = \frac{1}{h_h} + \frac{1}{h_c} \quad (127)$$

The use of finned, or extended, surfaces introduces another factor into the calculation. Since temperature gradients exist along fins, the over-all "temperature effectiveness" of the surface is reduced. The total surface effectiveness is a weighted average of the fin effectiveness corresponding to the actual prime and extended heat transfer areas, so that

$$\begin{aligned} \eta_o A &= (A - A_F) + \eta_F A_F \\ \eta_o &= 1 - \frac{A_F}{A} (1 - \eta_F) \end{aligned} \quad (128)$$

Introducing η_o to Equation 127, we have

$$\frac{1}{U} = \frac{1}{h_h \eta_{oh}} + \frac{1}{h_c \eta_{oc}} \quad (129)$$

Using the unit heat transfer area dealing with the definition of U , we obtain

$$\frac{1}{U A} = \frac{1}{h_h \eta_{oh} A_h} + \frac{1}{h_c \eta_{oc} A_c} \quad (130)$$

B. HEAT EXCHANGER DESIGN METHODS

1. General Relations

The method usually used is based upon nondimensional parameters which

Contrails

allow ease of design without the use of algebraic solutions. Solutions of energy and heat transfer rate equations are no longer necessary. The variables involved in these equations are grouped in the following manner:

a. Capacity Rate Ratio

$$\frac{C_{\min}}{C_{\max}} = \frac{(w c_p)_{\min}}{(w c_p)_{\max}} \quad (131)$$

b. Exchanger Heat Transfer Effectiveness

$$\epsilon = \frac{C_h}{C_{\min}} \frac{(T_{h \text{ in}} - T_{h \text{ out}})}{(T_{h \text{ in}} - T_{c \text{ in}})} = \frac{C_c}{C_{\min}} \frac{(T_{c \text{ out}} - T_{c \text{ in}})}{(T_{h \text{ in}} - T_{c \text{ in}})} \quad (132)$$

This effectiveness is the ratio of the actual heat transfer rate,

$$C_h (T_{h \text{ in}} - T_{h \text{ out}}) = C_c (T_{c \text{ out}} - T_{c \text{ in}}), \quad (133)$$

to the maximum possible heat transfer rate. This thermodynamic maximum can be achieved only in a counterflow heat exchanger with infinite transfer area.

c. Number of Exchanger Heat Transfer Units

$$(\text{NTU}) = \frac{A U_{\text{ave}}}{C_{\min}} \quad (134)$$

Relationships for the three parameters have been derived for all types of "mixed" and "unmixed" flow cases, including multi-pass arrangements. Direct solutions of these exponential equations are available only when C_{\min}/C_{\max} equals 0 or 1. Therefore, many figures of plots of ϵ versus (NTU) with C_{\min}/C_{\max} values as parameters have been made available. Note that for evaporators and condensers, $C_{\min}/C_{\max} = 0$, since C_{\max} is infinite.

Knowledge of the three temperatures and the capacity rates shown in Equation (131) is sufficient to determine ϵ . An assumed value of ϵ diminishes the number of known temperature values to two. Eventually, $U A$ is determined by C_{\min} and (NTU). Multiplying Equation (130) by the total volume of the heat exchanger, V_T , we obtain the general form of the design equations,

$$\frac{V_T}{U A} = \frac{V_T}{h_h \eta_{oh} A_h} + \frac{V_T}{h_c \eta_{oc} A_c} \quad (135)$$

$V_T/\eta_o A$ is a function of the core geometry chosen for the heat exchanger. The determinations of h 's, the heat transfer coefficients which are used in this report, are included in the general descriptions in the following

sections.

2. Forced Convection

Heat transfer coefficient functions for single-phase flow are generally determined by certain nondimensional relationships pertaining to a particular heat exchanger core geometry. The basic correlations used for heat transfer and flow friction are $(N_{St}) (N_{Pr})^{2/3}$ as a function of N_{Re} , and f as a function of N_{Re} .

When dealing with gas flow, the great effect of temperature variation on thermodynamic properties introduces the need of some absolute temperature ratio function, usually involving mean and wall temperatures. This additional function, however, especially when the gas is being cooled, has negligible effect when gas temperature differences are relatively small, and is omitted from the analysis.

The Colburn modulus, which is the product of the Stanton number and the Prandtl number raised to the $2/3$ power, $(N_{St}) (N_{Pr})^{2/3}$, is briefly denoted as "j". The j versus N_{Re} functions are easily represented in the form,

$$j = a (N_{Re})^b \quad (136)$$

Three such functions may be needed for complete representation of the core geometry. These functions may represent the laminar, transient, and turbulent flow regions

$$\left(\frac{h}{G_{free} c_p} \right) \left(\frac{c_p \mu}{k} \right)^{2/3} = a \left(\frac{G_{free} d_h}{\mu} \right)^b \quad (136a)$$

Solving for h,

$$h = a \frac{c_p}{\left(\frac{c_p \mu}{k} \right)^{2/3}} \left(\frac{d_h}{\mu} \right)^b (G_{free})^{1+b} \quad (137)$$

To get a truer picture of the total exchanger volume, G_{face} is substituted for G_{free} and is multiplied by the number of passes, NP, of the fluid so that the face area designated is that of a complete side of the heat exchanger.

$$\frac{G_{face}}{G_{free}} = \frac{A_{free}}{A_{face}} \quad (138)$$

Contrails

$$h = a \frac{c_p}{\left(\frac{c_p \mu}{k}\right)^{2/3}} \left(\frac{d_h}{\mu}\right)^b \frac{(NPG_{face})^{1+b}}{(A_{free}/A_{face})^{1+b}} \quad (139)$$

Some correlations, such as those for liquid metals (used here for NaK) make use of N_{Mu} , the Nusselt number, N_{Re} , and N_{Pr} . The product $(N_{Re})(N_{Pr})$ is often used.

$$(N_{Re})(N_{Pr}) = N_{Pe}$$

where N_{Pe} is the Peclet number. Conversions from one form to the other are as follows:

$$\left(\frac{h}{G c_p}\right) (N_{Pr})^{2/3} = a (N_{Re})^b$$

$$\rightarrow \left(\frac{h d_h}{k}\right) = a (N_{Re})^{1+b} (N_{Pr})^{1/3} \quad (140a)$$

$$\left(\frac{h d_h}{k}\right) = m (N_{Re})^n (N_{Pr})^c$$

$$\rightarrow \left(\frac{h}{G c_p}\right) (N_{Pr})^{2/3} = m (N_{Re})^{n-1} (N_{Pr})^{c-1/3} \quad (140b)$$

Equation (139) represents a functional relationship between h and NPG_{face} , all of the other terms being known. If both sides of the equation are multiplied by the term $A \eta_o / V_T$, we obtain

$$\frac{h A \eta_o}{V} = K_H (NPG_{face})^H \quad (141)$$

Further modifications of this equation will allow more independent variables to be inserted as inputs and give a more complete solution. These additions necessitate the use of the friction factor relationship from which an evaluation of pressure drop per unit length, $\Delta P/NPL$, versus mass flux per unit face area, NPG_{face} may be obtained.

$$\frac{\Delta P}{NPL} = \frac{2 f (NPG_{free})^2}{g \rho d_h} \quad (142)$$

Contrails

where L is the heat exchanger length parallel to the fluid flow. If

$$f = s (N_{Re})^t \quad (143)$$

$$\frac{\Delta P}{NPL} = \frac{2 s}{g \rho d_h} \left(\frac{d_h}{\mu} \right)^t (NPG_{free})^{2+t} \quad (144)$$

$$= \frac{2 s}{g \rho} \frac{(d_h)^{t-1}}{\mu^t} \frac{(NPG_{face})^{2+t}}{(A_{free}/A_{face})^{2+t}} \quad (145)$$

Since the basic units used here are (lb) - (min) - (ft), and ΔP is usually expressed in psi, and g in ft/sec², the factor (144 x 3600) should be introduced into the denominator. Multiplying by ρ / ρ_{std} establishes a "standard temperature" relationship

$$\frac{\Delta P}{NPL} = \frac{2 s}{g \rho_{std}} \frac{(d_h)^{t-1}}{\mu^t} \frac{(NPG_{face})^{2+t}}{(A_{free}/A_{face})^{2+t}} \quad (146)$$

If the difference between the problem temperature and derivation temperature is great and the value of t is large, a correction of μ/μ_d may be needed.

We now have

$$\frac{\rho}{\rho_{std}} \frac{\Delta P}{NPL} = K_P (NPG_{face})^P \quad (147)$$

The derivation of the single-phase flow side portion of the volume equation using NPG_{face} as a parameter will be found in section 5.

3. Evaporation

The volume equation form used here is easily explained. Due to the lack of the experimental data correlated in similar forms and the absence of a generally accepted, universal theory, the expression used is simply

$$\frac{h A \eta_o}{v} = K_B \left(\frac{Q}{v} \right)^B \quad (148)$$

This is established in many ways. If experimental relations show

$$h = K_E [\Delta T]^E \quad (149)$$

where $\Delta T = T_w - T_{sat}$, a simple transformation is performed:

Contrails

$$T = \frac{Q}{A h}$$

$$h = K_E \left(\frac{Q}{A h} \right)^E$$

$$\text{or } h = \left(\frac{1}{K_E} \right)^{1+E} \left(\frac{Q}{A} \right)^{E/1+E}$$

Multiplying by A/V,

$$\frac{h A}{V} = \left(\frac{K_E A}{V} \right)^{1/1+E} \left(\frac{Q}{V} \right)^{E/1+E} \quad (150)$$

The previous example has also demonstrated the change of original data in the general form of

$$h = K_E \left(\frac{Q}{A} \right)^E \quad (149a)$$

Pressure drop functions are not included in this phase of the analysis. Since most heat exchangers are of the cross-flow type, the face area of one fluid includes the flow length of the other. The interdependent qualities plus the use of pressure drop as an independent variable produce a realistic, physically limited solution. Two-phase flow pressure drops, needing complex solutions, are computed separately after the flow lengths and heat transfer distribution have been determined. The same attitude is taken toward counter-flow exchangers, although a direct pressure drop relationship between the two fluids is possible because the individual flow lengths will differ only if the number of individual flow passes differ.

4. Condensation

The volume equation form used for condensation is equal to that used for evaporation.

$$\frac{h A \eta_c}{V} = K_C \left(\frac{Q}{V} \right)^C \quad (151)$$

This form is usually established from Nusselt's equation for laminar film condensation.

$$h = K \sqrt[4]{\frac{k_1^3 \rho_1 g_c h_{fg}}{L \mu_1 [T_{sat} - T_w]}} \quad (152)$$

Contrails

$$h = K_L [T_{\text{sat}} - T_w]^{-\frac{1}{4}} = K_L [\Delta T]^{-\frac{1}{4}}$$

From Equations and

$$\begin{aligned} \frac{h A}{V} &= \left(K_L \frac{A}{V} \right)^{1/1 - \frac{1}{4}} \left(\frac{Q}{V} \right)^{-\frac{1/4}{1 - \frac{1}{4}}} \\ &= \left(K_L \frac{A}{V} \right)^{4/3} \left(\frac{Q}{V} \right)^{-1/3} \end{aligned} \quad (151a)$$

$$K_C = \left(K_L \frac{A}{V} \right)^{4/3} ; \quad C = -1/3$$

Pressure drop functions are omitted here for the same reasons described in section 3.

5. Final Equation Derivations

To generalize the derivations, we assume a heat exchange process with a single-phase process on one side of the heat exchanger and a two-phase process on the other. Let the subscripts 1 and 2 refer to the single-phase and double-phase sides, respectively.

In shell-tube heat exchangers, A_1/V_T and A_2/V_T are directly interdependent. In plate-fin heat exchangers where the configurations on the two flow sides are independent of each other, the heat transfer and pressure drop functions are calculated separately. Individual expressions of (A/V) are used, and the total volume equation must make corrections for this.

The following equation will be derived on a plate-fin basis. The same solution without the terms used for individual-total volume correction is true for the shell-tube heat exchangers. The terms η_o and ρ/ρ_{std} shall be omitted here.

$$\frac{V_T}{U A} = \left(\frac{V}{h A} \right)_1 + \left(\frac{V}{h A} \right)_2 \quad (135)$$

$$\alpha = \frac{V_1}{V_2} ; \quad V_1 + V_2 = V_T$$

$$V_1 = V_T \left(\frac{\alpha}{\alpha + 1} \right) ; \quad V_2 = \left(\frac{1}{1 + \alpha} \right) V_T$$

Contrails

$$\frac{V_T}{U A} = \left(\frac{\alpha}{\alpha + 1} \right) \frac{V_T}{(h A)_1} + \left(\frac{1}{1 + \alpha} \right) \frac{V_T}{(h A)_2}$$

$$\frac{(h A)_2}{V_2} = K_B \left(\frac{Q}{V_2} \right)^B = K_B \left(\frac{Q}{V_T \left(\frac{1}{1 + \alpha} \right)} \right)^B \quad (148)$$

$$= K_B \left(\frac{Q}{V_T} \right)^B (1 + \alpha)^B$$

$$\frac{(h A)_2}{V_T} = \frac{(h A)_2}{V_2} \left(\frac{1}{1 + \alpha} \right)$$

$$\frac{(h A)_2}{V_T} = K_B \left(\frac{Q}{V_T} \right)^B \frac{(1 + \alpha)^B}{(1 + \alpha)}$$

$$= K_B \left(\frac{Q}{V_T} \right)^B \left(\frac{1}{1 + \alpha} \right)^{1 - B}$$

$$NPG_1 = \left(\frac{\Delta P_1}{K_{P_1} NPL_1} \right)^{1/P_1} \quad (147)$$

$$NPG_1 = \left(\frac{w_1 NPL_1}{V_T \left(\frac{\alpha}{\alpha + 1} \right)} \right)$$

$$\left(\frac{w_1 NPL_1}{V_T \left(\frac{\alpha}{\alpha + 1} \right)} \right) = \left(\frac{1}{K_{P_1} NPL_1} \frac{\Delta P_1}{NPL_1} \right)^{1/P_1}$$

Contrails

$$[NPL_1]^{1 + P_1/P_1} = \left(\frac{\Delta P_1}{K_{P_1}} \right)^{1/P_1} \left(\frac{V_T \left(\frac{\alpha}{\alpha+1} \right)}{w_1} \right)$$

$$NPL_1 = \left(\frac{V_T \left(\frac{\alpha}{\alpha+1} \right)}{w_1} \right)^{P_1/1 + P_1} \left(\frac{\Delta P_1}{K_{P_1}} \right)^{1/1 + P_1}$$

$$K_T (NPG_1)^{H_1} = \frac{K_{H_1}}{[K_{P_1}]^{H_1/1 + P_1}} \left(\frac{w_1 \Delta P_1}{V_T} \right)^{H_1/1 + P_1} \left(\frac{\alpha+1}{\alpha} \right)^{H_1/1 + P_1}$$

$$\frac{(h A)_1}{V_T} = \frac{(h A)_1}{V_1} \left(\frac{\alpha}{\alpha+1} \right); \quad \frac{V_T}{(h A)_1} = \frac{V_1}{(h A)_1} \left(\frac{\alpha+1}{\alpha} \right)$$

$$\frac{V_T}{(P A)_1} = \frac{[K_{P_1}]^{H_1/1 + P_1}}{K_{H_1}} \left(\frac{V_T}{w_1 \Delta P_1} \right)^{H_1/1 + P_1} \left(\frac{\left(\frac{\alpha+1}{\alpha} \right)}{\left(\frac{\alpha+1}{\alpha} \right)^{H_1/1 + P_1}} \right)$$

$$= \frac{[K_{P_1}]^{H_1/1 + P_1}}{K_{H_1}} \left(\frac{V_T}{w_1 \Delta P_1} \right)^{H_1/1 + P_1} \left(\frac{\alpha+1}{\alpha} \right)^{1 - H_1/1 + P_1/1 + P_1}$$

$$\frac{V_T}{(h A)_2} = \frac{1}{K_B} \left(\frac{V_T}{Q} \right)^B [\alpha+1]^{1-B}$$

$$\frac{V_T}{U A} = \left(\frac{\alpha+1}{\alpha} \right)^{\frac{1 - H_1 + P_1}{1 + P_1}} \frac{[K_{P_1}]^{\frac{H_1}{1 + P_1}}}{K_{H_1}} \left(\frac{V_T}{w_1 \Delta P_1} \right)^{\frac{H_1}{1 + P_1}}$$

Contrails

$$+ [\alpha + 1]^{1 - B} \frac{1}{K_B} \left(\frac{V_T}{Q} \right)^B$$

This exponential equation cannot be solved algebraically because a sum of two V_T terms exists on one side. An iterative method with successive approximations of V_T is used. Familiarity with an individual equation usually produces a solution within three iterative steps.

C. SAMPLE CALCULATIONS

1. Plate-Fin Evaporator

Evaporator temperature (Freon 11)	= 40 degF
Air inlet temperature	= 85 degF
Air outlet temperature	= 60 degF
Air flow rate	= 667 lbs/min
Air side pressure drop	= 0.3 psia

Air side parameters (for average temperature of 70 degF):

$$K_H = 23.8$$

$$H = 0.486$$

$$K_P = 1.36 \times 10^{-4}$$

$$P = 1.57$$

$$\rho/\rho_{std} = 0.981$$

$$\frac{K_P}{\rho/\rho_{std}} = 1.387 \times 10^{-4}$$

Freon 11 side parameters

$$K_B = 1.805$$

$$B = 0.667$$

$$\frac{V_{air}}{V_{Freon}} = 4.07$$

$$\epsilon = \frac{85 - 60}{85 - 40} = 0.556$$

$$\text{For } \frac{c_{min}}{c_{max}} = 0 \quad ; \quad \epsilon = 0.556 \quad ; \quad NTU = 0.811$$

Contrails

$$C_{\min} = w c_p = \frac{Q}{\Delta T} = 160 \text{ BTU/min-degF}$$

$$U A = 0.811 (160) = 130 \text{ BTU/min-degF}$$

$$\frac{V_T}{U A} = 0.00344 V_T^{0.189} + 0.00374 V_T^{0.667}$$

or $V_T = 0.446 V_T^{0.189} + 0.486 V_T^{0.667}$

Assume $V_T = 0.9 \text{ cu ft}$

$$\begin{aligned} V_T &= 0.446 (0.9)^{0.189} + 0.486 (0.9)^{0.667} \\ &= 0.891 \text{ cu ft} \end{aligned}$$

Assume $V_T = 0.88 \text{ cu ft}$

$$V_T = 0.446 (0.88)^{0.189} + 0.486 (0.88)^{0.667} = 0.88 \text{ cu ft}$$

2. Vortex Evaporator

$$\begin{aligned} y &= 3.5 \\ V_{\text{exit}} &= 50 \text{ ft/sec} \\ V_{\text{ave}} &= \frac{V_{\text{exit}}}{3} \end{aligned}$$

For high values of $\omega^2 r/g$,

$$\left(1 + \left(\frac{\omega^2 r}{g} \right)^{0.6} \right)^{1/6} \approx \left(\frac{\omega^2 r}{g} \right)^{0.1}$$

The Rohsenow correlation may then be written as

$$h = K \left(\frac{\omega^2 r}{g} \right)^{0.1} \left(\frac{Q}{A} \right)^{2/3}$$

where the constant K groups together all the properties of the fluid.

Then
$$\frac{h A}{V} = K \left(\frac{\omega^2 r}{g} \right)^{0.1} \left(\frac{A}{V} \right)^{1/3} \left(\frac{Q}{V} \right)^{2/3}$$

Contrails

$$\frac{V}{h A} = \frac{1}{K} \left(\frac{1}{\left(\frac{\omega^2 r}{g} \right)^{0.1}} \left(\frac{V}{A} \right)^{1/3} \left(\frac{V}{g} \right)^{2/3} \right)$$

Without twisted tapes (plain tube),

$$V_T = 0.395 V_T^{0.214} + 0.706 V_T^{2/3}$$

With twisted tapes (vortex tube),

$$V_T = 0.395 V_T^{0.214} + 0.424 V_T^{2/3}$$

APPENDIX 2

DESIGN METHODS AND CALCULATION PROCEDURES FOR THE ROTATING CONDENSER

A. DESIGN PROCEDURE FOR A ROTATING CONDENSER

The calculation procedure for a rotating condenser is presented below. The following assumptions will be made:

All assumptions which were made during the derivation of the basic equations (1-6).

The superheated vapor coming from the compressor enters the condenser, and this superheat will be subtracted in the condenser.

Subcooling, if necessary, will be done in a separate subcooler.

The condenser shaft is insulated; i.e., there is no condensation in the shaft.

The heat transfer coefficient is the same on both sides of the discs.

There is no interaction between discs.

Most characteristics of the system are found to be primarily dependent on the Prandtl number and on the dimensionless group

$$Y = \frac{c_p \Delta T}{h_{fg}} \quad (153)$$

both of which are functions of the given refrigerant and of the condensation pressure only. The most important independent variables, however, are the angular velocity, the number of discs necessary, and the duration of the flight. The calculation procedure consists of the determination of the optimum values for the angular velocity and number of discs to which the minimum penalty belongs. A step-by-step design method is presented so that an actual condenser may easily be designed by following the procedure. An example of the numerical calculation of a rotating condenser is given in a later section.

1. Angular Velocity

The angular velocity is one of the independent variables. Several values have to be assumed, and the calculation has to be carried out for each of these values. After comparing the resulting penalties, the optimum value for the angular velocity may be determined.

2. Temperature Difference

This is the difference between the saturation temperature of the condensing refrigerant and the wall temperature of the disc. It may be calculated from

$$\Delta T^{1/4} - A \Delta T^{-3/4} + B\omega^{0.425} = 0 \quad (154)$$

The derivation of this equation and of the values of A and B are given later.

3. Dimensionless Parameter

Together with the Prandtl number, a dimensionless parameter appears in the expressions of most heat transfer characteristics. It is

$$Y = \frac{c_p \Delta T}{h_{fg}} \quad (153)$$

where c_p and h_{fg} depend on the refrigerant and condensation pressure, while ΔT is defined by (2) above.

4. Heat Transfer Coefficient

Sparrow and Gregg (1) derive the following correlation for the heat transfer coefficient (which is also presented in Figures 2 and 3 of Reference 1):

$$\frac{h \left(\frac{\nu}{\omega} \right)^{\frac{1}{2}}}{k} = 0.904 \left(\frac{Pr}{Y} \right)^{\frac{1}{4}} \quad (155)$$

The heat transfer coefficients calculated from this equation differ from measured values (3) by approximately 25 per cent.

Nandapurkar (3) gives an empirical equation for h . His measured results (except for liquid metals) well agree with the values calculated from his equation. Therefore, the use of this equation is recommended. The equation is

$$h = 1.716 \frac{k}{\sqrt{\nu}} \left(\frac{Pr}{Y} \right)^{\frac{1}{4}} \omega^{0.425} \quad (156)$$

Y and ω are known from (1) and (3) above; the other values are functions of the applied refrigerant and the condensation pressure only. (All properties are those of the liquid refrigerant.)

5. Over-all Heat Transfer Coefficient

The expression for the over-all heat transfer coefficient is

$$U = \frac{1}{\frac{1}{h} + \frac{s}{k_w} + \frac{1}{h_c}} \quad (157)$$

where h is calculated from (4) above, s is the wall thickness of the disc, k_w is the conductivity of the wall, and h_c is the heat transfer coefficient on the coolant side.

6. Total Heat Transfer Area

The total surface necessary to transfer the required heat under the given condition is

$$A = \frac{Q}{U \Delta T_{LM}} \quad (158)$$

where Q is the total heat to be subtracted in the condenser, U is known from (5) above, and ΔT_{LM} is the logarithmic mean temperature difference between the refrigerant and the coolant in the condenser.

7. Number of Discs

The number of discs is the second independent variable or input. Several values for N have to be assumed and the calculations have to be carried out for all values of N for each angular velocity. The optimum N will be the one to which the minimum penalty belongs.

8. Disc Radius

The outside radius of the disc can be determined from

$$A = 2 N \pi (r_o^2 - r_s^2) \quad (159)$$

where A is known from (6) above, N is the number of discs, and the coefficient 2 indicates that both sides of each disc are utilized, while r_s is the outside radius of the shaft which has to be determined by the coolant pressure drop and stress considerations. Finally,

$$r_o = \sqrt{r_s^2 + \frac{A}{2 N \pi}} \quad (160)$$

9. Condensate Layer Thickness

Sparrow and Gregg (1) give the following correlation:

$$\delta = 1.107 \sqrt{\nu} \left(\frac{Y}{Pr} \right)^{\frac{1}{4}} \omega^{-\frac{1}{2}} \quad (161)$$

Also Diagrams 4 and 5 (1) can be used.

10. Boundary Layer Thickness

Extrapolating the results of References 4 and 5, boundary layer thickness is determined by

$$\sigma = 4.6 \sqrt{\frac{\nu}{\omega}} \quad (52)$$

11. Spacing of Discs

It was mentioned before that it is necessary that

$$Z > 2 (\sigma + \delta)$$

or

$$Z = 2 (\sigma + \delta) + K \quad (162)$$

where the value of K has to be determined by structural considerations, considering that there must be enough space for the vapor supply nozzles. On the other hand, a small value for K is desirable for weight penalty reasons.

12. Torque

Sparrow and Gregg (1) give the following correlation for the torque (Diagram 10 of Reference 1 can be used):

$$\frac{2M}{r_o^4 \pi \rho (\nu \omega^3)^{1/2}} = 0.666 \left[\delta \left(\frac{\omega}{\nu} \right)^{1/2} \right]^3 \quad (163)$$

Later (6) this correlation was revised to show that when drag between vapor and liquid is taken into account, the torque is approximately twice that calculated from the correlation above. Considering that

$$\delta \left(\frac{\omega}{\nu} \right)^{1/2} = 1.107 \left(\frac{Y}{Pr} \right)^{1/4} \quad (155a)$$

the torque will be

$$M = 0.903 r_o^4 \pi \rho (\nu \omega^3)^{1/2} \left(\frac{Y}{Pr} \right)^{3/4} \quad (164)$$

where M is the torque required to rotate one disc if condensation takes place on one side of the disc only.

13. Power to Condenser

The power required to rotate the condenser shaft will be

$$P_1 = \frac{2 N M \omega}{3600 \times \eta_{tr} \times \eta_b \times 550} \quad \text{HP} \quad (165)$$

where 3600 and 550 are conversion factors, N M and ω are known from (1), (7), and (12) above, and η_{tr} and η_b are the transmission and bearing efficiencies.

14. Coolant Side

The coolant to be used and the inlet and outlet temperatures are

Contrails

assumed to be given. The flow rate can be determined by

$$W_c = \frac{Q}{c_{pc} (t_{co} - t_{ci})} \quad (166)$$

The log mean temperature for the condenser is

$$\Delta T_{LM} = \frac{(T_c - t_{ci}) - (T_c - t_{co})}{\ln \frac{T_c - t_{ci}}{T_c - t_{co}}} \quad (167)$$

and the condenser effectiveness (considering temperature effectiveness) is

$$\epsilon = \frac{t_{co} - t_{ci}}{T_c - t_{ci}} \quad (168)$$

The pressure drop on the coolant side will be

$$H = H_{shaft} + \sum_{n=1}^{n=N} H_{disc} \quad (169)$$

Here,

$$H_{shaft} = f \frac{L}{D} \frac{V^2}{2g_o} \quad (170)$$

where $f = f(N_{Re})$ is the friction factor

$D = 2 r_i$ is the inside diameter of the shaft

$L = (N + 1) Z$ is the length of the shaft (see Figure 29)

The pressure drop in the discs can be approximated in several ways. One method will be shown in the numerical calculations. Exact results may be obtained by experiments only. The power required to drive the coolant pump will be

$$P_2 = \frac{W_c H}{550 \times \eta_p \times 60} \quad (171)$$

15. Total Power Required

The total power required to operate the rotating condenser will be the sum of the power requirements for the condenser shaft and the coolant pump;

i.e., $P = P_1 + P_2$.

(172)

16. Condenser Weight

The condenser dead weight is the sum of the weights of the components listed previously. The calculation of the dead weight can be carried out after the type of condenser to be used is decided upon. The weight calculation for the type of condenser shown in Figure 25 will be shown in the numerical calculations.

B. DERIVATION OF $\Delta T^{1/4} - A \Delta T^{-3/4} + B \omega^{0.425} = 0$

The above equation was used in the numerical calculations of rotating condensers to determine $\Delta T = T_{sat} - T_{wall}$. The derivation of the above equation is given below.

Basic Equations:

$$(1) \quad Q = A h \Delta T$$

$$(2) \quad Q = A U \Delta T_{LM}$$

$$(3) \quad U = \frac{1}{\frac{1}{h} + \frac{s}{k_w} + \frac{1}{h_c}}$$

$$(4) \quad h = 1.716 \frac{k}{\sqrt{v}} \left(\frac{Pr}{Y} \right)^{\frac{1}{4}} \omega^{0.425}$$

$$(5) \quad Y = \frac{c_p}{h_{fg}} \Delta T$$

The following substitutions in the above equations will be made:

$$\Delta T_{LM} = a$$

$$\left(\frac{s}{k_w} + \frac{1}{h_c} \right) = b$$

$$1.716 \frac{k}{\sqrt{v}} Pr^{\frac{1}{4}} = c$$

$$\frac{c_p}{h_{fg}} = d$$

Then the new forms of the equations will be:

Contrails

$$(1a) \quad \Delta T = \frac{Q}{A h}$$

$$(2a) \quad A = \frac{Q}{a U}$$

$$(3a) \quad U = \frac{1}{\frac{1}{h} + b}$$

$$(4a) \quad h = c Y^{-\frac{1}{4}} \omega^{0.425}$$

$$(5a) \quad Y = d \Delta T$$

Substituting (2a) into (1a):

$$(6) \quad \Delta T = \frac{Q}{A h} = \frac{Q}{h \left(\frac{Q}{a U} \right)} = \frac{a U}{h}$$

Substituting (3a) into (6):

$$(7) \quad \Delta T = \frac{a U}{h} = \frac{a}{h \left(\frac{1}{\frac{1}{h} + b} \right)} = \frac{a}{1 + b h}$$

Substituting (4a) into (7):

$$(8) \quad \Delta T = \frac{a}{1 + b h} = \frac{a}{1 + b c Y^{-\frac{1}{4}} \omega^{0.425}}$$

Substituting (5a) into (8):

$$(9) \quad \Delta T = \frac{a}{1 + \frac{b c}{d^{\frac{1}{4}}} \Delta T^{-\frac{1}{4}} \omega^{0.425}} = \frac{a \Delta T^{\frac{1}{4}}}{\Delta T^{\frac{1}{4}} + \frac{b c}{d^{\frac{1}{4}}} \omega^{0.425}}$$

$$\text{and } \Delta T \left[\Delta T^{\frac{1}{4}} + \frac{b c}{d^{\frac{1}{4}}} \omega^{0.425} \right] = a \Delta T^{\frac{1}{4}}$$

$$\text{or } \Delta T^{\frac{1}{4}} + \frac{b c}{d^{\frac{1}{4}}} \omega^{0.425} = a \Delta T^{-3/4}$$

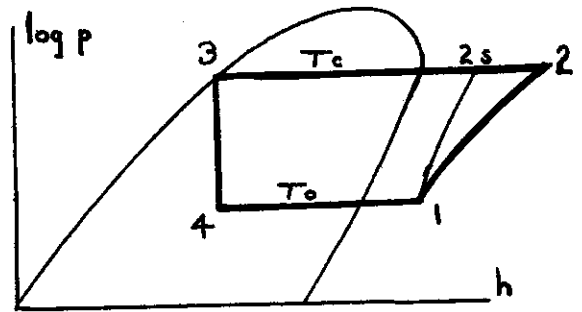
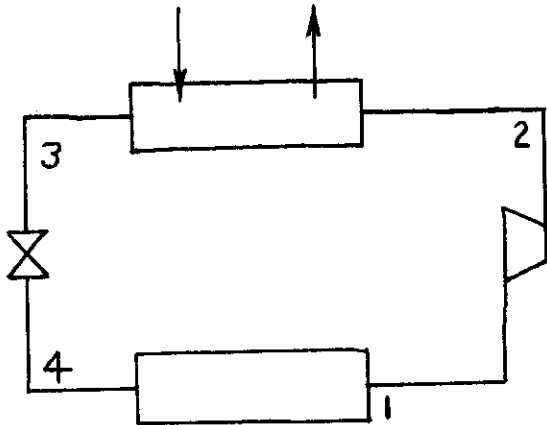
$$\text{finally } \Delta T^{\frac{1}{4}} - A \Delta T^{-3/4} + B \omega^{0.425} = 0$$

Contrails

where $A = a = \Delta T_{LM}$

$$B = \frac{b c}{d^{\frac{1}{4}}} = 1.716 \left(\frac{s}{k_w} + \frac{1}{h_c} \right) \frac{k}{\sqrt{V}} \left(\frac{Pr h_{fg}}{c_p} \right)^{\frac{1}{4}}$$

C. NUMERICAL CALCULATION OF A ROTATING CONDENSER



Vapor Cycle Data

Given:

$$Q_o = 2000 \text{ BTU/min}$$

$$T_o = 40 \text{ deg F}$$

$$T_c = 250 \text{ deg F}$$

Refrigerant: Freon 11

$$\eta_{\text{comp}} = 60\%$$

Coolant: Dowtherm A

$$t_{ci} = 225 \text{ deg F}$$

Contrails

$$t_{co} = 245 \text{ deg F}$$

$$t_1 - t_0 = 20 \text{ deg F (superheat)}$$

From Tables or Charts:

$$t_1 = 60 \text{ deg F}$$

$$h_2 = 145 \text{ BTU/lb}$$

$$h_1 = 100 \text{ BTU/lb}$$

$$t_2 = 390.8 \text{ deg F}$$

$$v_1 = 5.7 \text{ cu ft/lb}$$

$$h_3 = 62.5 \text{ BTU/lb}$$

$$h_{2s} = 127 \text{ BTU/lb}$$

$$h_4 = 62.5 \text{ BTU/lb}$$

Refrigerant Data:

$$k = 0.040 \text{ BTU/hr-degF-ft}$$

$$\mu = 0.224 \text{ centipoises}$$

$$c_p = 0.209 \text{ BTU/lb-degF}$$

$$\rho = 75.1 \text{ lbs/cu ft}$$

$$\nu = 0.0072 \text{ sq ft/hr}$$

$$h_{fg} = 58.1 \text{ BTU/lb}$$

$$Pr = 2.84$$

Refrigerating Effect Per Pound:

$$q_o = h_1 - h_4 = 37.5 \text{ BTU/lb}$$

Condensation Heat Per Pound:

$$q = h_2 - h_3 = 82.5 \text{ BTU/lb}$$

Refrigerant Flow Rate:

$$w_r = \frac{Q_o}{q_o} = 53.3 \text{ lbs/min}$$

Heat to be Rejected in Condenser:

$$Q = w_r q = 4397.2 \text{ BTU/min}$$

Contrails

Heat Exchanger Effectiveness:

$$\epsilon = \frac{t_{co} - t_{ci}}{T_c - t_{ci}} = 0.8$$

Coolant Flow Rate:

$$W_c = \frac{Q}{c_p (t_{co} - t_{ci})} = 488 \text{ lbs/min}$$

Log Mean Temperature Difference:

$$\Delta T_{LM} = \frac{(T_c - t_{ci}) - (T_c - t_{co})}{\ln \frac{t_c - t_{ci}}{T_c - t_{co}}} = 12.4 \text{ deg F}$$

Condenser Calculation

Angular Velocity:

$$\text{Chosen: } \omega = 37600 \text{ /hr}$$

Temperature Difference:

$$\Delta T^{\frac{1}{4}} - 12.402 \Delta T^{-3/4} + 0.0144 \omega^{0.425} = 0$$
$$\Delta T = 6.968 \text{ deg F}$$

Dimensionless Parameter:

$$Y = \frac{c_p \Delta T}{h_{fg}} = 3.59 \times 10^{-3} \Delta T = 0.025$$

Heat Transfer Coefficient:

$$h = 1.716 \frac{k}{\sqrt{D}} \left(\frac{Pr}{Y} \right)^{\frac{1}{4}} \omega^{0.425} = 1.050 \omega^{0.425} Y^{-\frac{1}{4}} = 232.3 \text{ BTU/hr-degF-sq ft}$$

Over-all Heat Transfer Coefficient:

$$U = \frac{1}{\frac{1}{h} + \frac{s}{k_w} + \frac{1}{h_c}} = 129.5 \text{ BTU/hr-sq ft-degF}$$

Contrails

$s = 3/64$ in
Aluminum
 $k_w = 120$ BTU/hr-degF-ft
 $h_c = 300$ BTU/hr-degF-sq ft

Total Heat Transfer Area:

$$A = \frac{Q}{U \Delta T_{LM}} = \frac{21273}{U} = 164.3 \text{ sq ft}$$

Condensate Layer Thickness:

$$\delta = 1.107 \sqrt{\frac{\nu}{\omega}} \left(\frac{Y}{Pr} \right)^{\frac{1}{4}} = 0.0725 Y^{\frac{1}{4}} \omega^{-\frac{1}{2}} = 0.00014 \text{ ft}$$

Boundary Layer Thickness:

$$\sigma = 4.6 \sqrt{\frac{\nu}{\omega}} = 0.390 \omega^{-\frac{1}{2}} = 0.00201 \text{ ft}$$

Spacing of Discs:

$$Z = 2 (\delta + \sigma) + K = 0.1083 \text{ ft}$$

$K = 0.104$ ft for constructional reasons

Number of Discs:

Chosen: $N = 5$

Disc Radius:

$$r_o = \sqrt{r_s^2 + \frac{A}{2 N \pi}} = \sqrt{0.00695 + 0.16 \frac{A}{N}} = 2.294 \text{ ft}$$

$r_s = 1$ in (shaft outside radius)

$r_i = 7/8$ in (shaft inside radius)

Torque:

$$M = 0.903 r_o^4 \pi \rho (\nu \omega^3)^{\frac{1}{2}} \left(\frac{Y}{Pr} \right)^{\frac{3}{4}}$$
$$= 1.979 \times 10^{-8} Y^{\frac{3}{4}} \omega^{\frac{3}{2}} r_o^4 = 0.250 \text{ ft lb}$$

Contrails

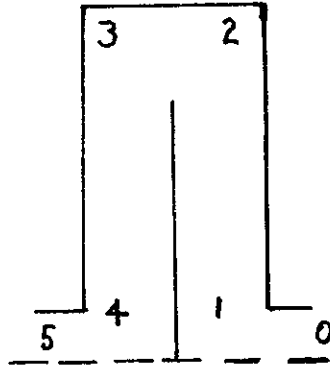
Power to Condenser:

$$P_1 = \frac{2 \text{ N M } \omega}{3600 \eta_{tr} \eta_b 550} = 1.12 \times 10^{-6} \text{ N M } \omega = 0.0527 \text{ HP}$$

assuming: $\eta_{tr} = \eta_b = 0.95$

Coolant Side Pressure Drop:

Disc (Approximation)



$$\begin{aligned} \Delta P = P_0 - P_5 &= (\Delta P_{turn})_0^1 + (\Delta P_{friction} - \Delta P_{diffuser})_1^2 \\ &- (\Delta P_{centrifugal})_1^2 + (\Delta P_{turn})_2^3 + (\Delta P_{friction} + \Delta P_{conv.})_3^4 \\ &+ (\Delta P_{centrifugal})_3^4 + (\Delta P_{turn})_4^5 \end{aligned}$$

$$\text{assuming: } (\Delta P_{centrifugal})_1^2 = (\Delta P_{centrifugal})_3^4$$

$$(\Delta P_{fr.} - \Delta P_{diffuser})_1^2 = -0.79 \rho \frac{v_1^2 - v_2^2}{2 g_0}$$

$$(\Delta P_{fr.} + \Delta P_{conv.})_3^4 = 1.18 \rho \frac{v_1^2 - v_2^2}{2 g_0}$$

$$\sum \Delta P_{turn} = 0.52 \rho \frac{v_1^2 - v_2^2}{2 g_0}$$

Contrails

$$\Delta P = \rho \frac{v_1^2 - v_2^2}{2 g_o}$$

$$v_1 = \frac{W_c}{60 \rho r_i^2 \pi} = 7.95 \text{ ft/sec}$$

$$b = \frac{W_c}{2 r_s \pi \rho v_1} = 0.03125 \text{ ft} = 3/8 \text{ in}$$

$$v_2 = \frac{W_c}{2 r_o \pi \rho b} = \frac{0.668}{r_o}$$

$$H_{\text{discs}} = N \frac{v_1^2 - v_2^2}{2 g_o} = N (0.982 - 0.0069 r_o^{-2})$$

Shaft

$$H_s = f \frac{L}{D_i} \frac{v^2}{2 g_o} = 0.135 (N + 1) Z$$

$$L = (N + 1) Z, \quad f = 0.02, \quad v = 7.95 \text{ ft/sec}$$

and the total pressure drop

$$H = H_d + H_s = N (0.982 - 0.0069 r_o^{-2}) + 0.135 (N + 1) Z = 4.99 \text{ ft}$$

Pumping Power:

$$P_2 = \frac{W_c H}{550 \eta_p 60} = 0.0988 \text{ HP}$$

$$\eta_p = 0.75$$

Contrails

Total Power Requirement:

$$P = P_1 + P_2 = 0.1515 \text{ HP}$$

Condenser Weight (See Figure):

Shaft

$$W_a = [(N + 1) Z] (r_s^2 - r_i^2) \pi \rho_{st}$$

Discs

$$W_b = N [2 (r_o^2 - r_s^2) \pi s + (r_o - b)^2 \pi s \\ + 2 r_o \pi s (2 b + 3 s)] \rho_{al}$$

Housing

$$W_c = (2 r_o + \frac{3}{12}) \pi s \rho_{al} [(N + 1) Z + (2 b + 3 s) N] \\ + 2 [(r_o + \frac{3}{24})^2 - r_s^2] \pi s \rho_{al}$$

Base

$$W_d = 2 r_o [(N + 1) Z + N (2 b + 3 s)] s \rho_{al}$$

Condenser Motor

$$W_e = 5 + 1.5 P_1$$

Coolant Pump and Motor

$$W_f = 8 + 3 P_2$$

Coolant

$$W_g = [N r_o^2 \pi 2 b + (N + 1) Z r_i^2 \pi] \rho_c$$

The weights of the bearings, joining piping, and refrigerant are neglected.

After adding the weights given by the expressions above and substituting the known values,

Contrails

$$\begin{aligned}W_d &= (N + 1) Z [12.559 r_o + 4.208] \\&+ N [18.347 r_o^2 + 1.106 r_o + 0.025] + 5.518 r_o^2 \\&+ 1.379 r_o + 1.5 P_1 + 3 P_2 + 13.018 = 562.7 \text{ lbs}\end{aligned}$$

Contrails

APPENDIX 3

DESIGN PROCEDURE AND SAMPLE CALCULATION FOR SPIRAL CONDENSERS

A. COUNTERFLOW SPIRAL CONDENSER CALCULATION PROCEDURE

Condenser temperature = 250 degF
 Evaporator temperature = 40 degF
 Evaporator heat load = 4000 BTU/min

From two-phase fluid (isenthalpic flow from saturated liquid at condenser exit)

To vapor at 20 degF superheat

$$\Delta h = 100 - 62.5 = 37.5 \text{ BTU/lb}$$

$$\text{Freon 11 flow rate} = \frac{4000 \text{ BTU/min}}{37.5 \text{ BTU/lb}} = 106.7 \text{ lbs/min}$$

Freon 11 Compressor Conditions

Compressor efficiency (assumed) = 0.60

$$h = \frac{127 - 100}{0.60} = 45 \text{ BTU/lb}$$

Freon 11 Condenser Conditions

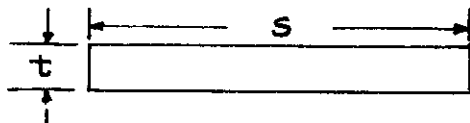
From superheated vapor (at compressor exit)

To saturated liquid

$$h'_{fgC} \text{ (including superheat)} = (100 + 45) - 62.5 = 82.5 \text{ BTU/lb}$$

$$(w_{F-11}) (h'_{fgC}) = Q_C = (106.7) (82.5) = 8803 \text{ BTU/min}$$

The flow in the spiral condenser is considered as flow between parallel plates or flow in rectangular tubes with a high value of s/t



Assumptions

- (1) $\epsilon = 0.75$
- (2) $\Delta T_{NaK} = 40 \text{ degF}$

Contrails

$$T_{\text{NaK}_2} = 236.7 \text{ degF} \approx 237 \text{ degF}$$

$$T_{\text{NaK}_1} = 197 \text{ degF}$$

- (3) The relationship for the Freon 11 heat transfer coefficient is

$$h_{\text{F-11}} = 0.065 \left(\frac{c_{p1} \rho_1}{2 \mu_1 \rho_v} k_1 f \right)^{\frac{1}{2}} G_{\text{mv}} \quad (62)$$

(Reference 3, Section VII)

f is the Fanning friction factor pertaining to complete vapor flow, and

G_{mv} is the mean vapor mass flux

$$G_{\text{mv}} = 0.58 G_m \quad (173)$$

where G_m is the total mean mass flux when all vapor has been condensed.

- (4) The relationship* for the NaK heat transfer coefficient is

$$h_{\text{NaK}} = \frac{k}{d_h} \left(5.0 + 0.025 \left\{ (N_{\text{Re}}) (N_{\text{Pr}}) \right\}^{0.8} \right) \quad (174)$$

- (5) The Freon 11 pressure drop will be calculated by using the Lockhart-Martinelli method applied to pipe flow.

- (6) The relationship** used for the NaK friction factor is

$$f = 0.0481 (N_{\text{Re}})^{-0.205} \quad (175)$$

$$\Delta P = \left(\frac{L}{d_h} \right) \frac{2 f \rho v_{\text{NaK}}^2}{g (144)} \quad (176)$$

*Seban-Shimazaki equation for low N_{Pr} fluids in turbulent flow at constant wall temperature. This equation seems closest to actual cases which operate between constant heat input and constant wall temperature.

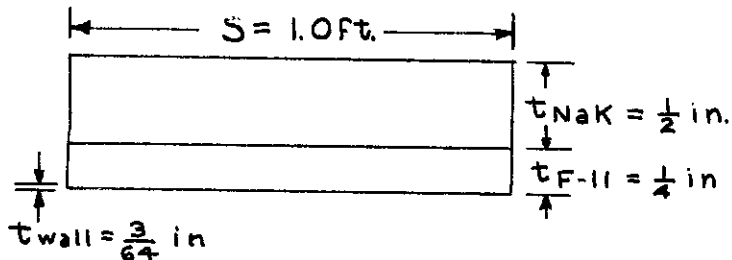
**Kays and London, Compact Heat Exchangers, Figure 40, Liquid Flow in Tubes - turbulent region.

Contrails

(7) The relationship* used for the Freon 11 vapor friction factor is

$$f = 0.0474 (N_{Re})^{-0.216} \quad (177)$$

(8) The basic geometry to be used is



thermodynamic Properties

Freon 11 at 250 degF

$$k_1 = 0.040 \text{ BTU/hr-ft-degF}$$

$$\mu_1 = 0.55 \text{ lbs/hr-ft}$$

$$\mu_v = 0.0329 \text{ lbs/hr-ft}$$

$$\rho_1 = 75.1 \text{ lbs/cu ft}$$

$$\rho_v = 4.17 \text{ lbs/cu ft}$$

$$c_{p1} = 0.216 \text{ BTU/lb-degF}$$

NaK at 220 degF

$$k = 14.15 \text{ BTU/hr-ft-degF}$$

$$\mu = 1.15 \text{ lbs/hr-ft}$$

$$\rho = 52.5 \text{ lbs/cu ft}$$

$$c_p = 0.226 \text{ BTU/lb-degF}$$

$$N_{Pr} = (c_p / k) = 0.0184$$

Freon 11 Side

Free Flow Area

$$A_{\text{free}} = (s) (t_{\text{F-11}}) = (1 \text{ ft}) (1/4 \text{ in}) (1/12 \text{ in/ft}) = 1/48 \text{ sq ft} \quad (178)$$

Hydraulic Diameter

$$d_h = 4 \frac{\text{Free Flow Area}}{\text{Wetted Perimeter}} = 4 \left(\frac{(s) (t)}{2s + 2t} \right)$$

Kays and London, Compact Heat Exchangers, Figure 32, Gas Flow in Rectangular Tubes - turbulent region; $L/D = \infty$; $s/t = 8.00$.

Contrails

Since $s \gg t$, consider

$$d_h = 4 \left(\frac{(s)(t)}{2s} \right) = 2t = \frac{1}{2} \text{ in} \quad (179)$$

Initial Vapor Velocity

$$v_v = \frac{w}{\rho A_{\text{free}}} = \frac{106.7 \text{ lbs/min}}{(4.17 \text{ lbs/cu ft}) (1/48 \text{ sq ft}) (60 \text{ sec/min})} \quad (180)$$
$$= 20.45 \text{ ft/sec}$$

Initial Vapor Reynolds Number

$$N_{\text{Re}_v} = \frac{\rho v_v d_h}{\mu_v} \quad (181)$$
$$= \frac{(4.17 \text{ lbs/cu ft}) (20.45 \text{ ft/sec}) (3600 \text{ sec/hr})}{0.0329 \text{ lbs/hr-ft}}$$
$$= 389,000$$

Initial Vapor Friction Factor

$$f = 0.0474 (389,000)^{-0.215}$$
$$= 0.00297$$

This seems to be an extremely low value. The data from which the equation was derived seems to be directly pertinent to $N_{\text{Re}} < 100,000$

$$\text{at } N_{\text{Re}} = 100,000, \quad f = 0.0040$$

0.0040 shall be the minimum value used.

Total Mean Mass Flux When All Vapor Has Been Condensed

$$G_m = \frac{Q_c}{h'_{fgC} A_{\text{free}}} = \frac{8803 \text{ BTU/min}}{(82.5 \text{ BTU/lb}) (1/48 \text{ sq ft})} \quad (182)$$
$$= 5120 \text{ lbs/min-sq ft}$$

Mean Vapor Mass Flux

$$G_{mv} = 0.58 G_m$$
$$= 0.58 (5120)$$
$$= 2970 \text{ lbs/min-sq ft}$$

Contrails

Freon 11 Heat Transfer Coefficient

$$\begin{aligned}h_{F-11} &= 0.065 \left(\frac{c_{p1} \rho_1}{2 \mu_1 \rho_v} k_1 f \right)^{\frac{1}{2}} G_{mv} \\&= 0.065 \left(\frac{(0.216) (75.1)}{2 (0.55) (4.17)} (0.040) (0.004) \right)^{\frac{1}{2}} 2970 \\&= 4.59 \text{ BTU/min-sq ft-degF}\end{aligned}$$

NaK Side

Free Flow Area

$$A_{\text{free}} = (s) (t_{F-11}) = (1 \text{ ft}) (1/2 \text{ in}) (1/12 \text{ in/ft}) = 1/24 \text{ sq ft}$$

Hydraulic Diameter

$$\begin{aligned}d_h &= 4 \left(\frac{(s) (t)}{2 s} \right) \\&= 2 t = 1 \text{ in}\end{aligned}$$

Mass Flux

$$\begin{aligned}G_{\text{NaK}} &= \frac{Q_c}{A_{\text{free}} c_p \Delta T_{\text{NaK}}} \quad (183) \\&= \frac{8803 \text{ BTU/min}}{(1/24 \text{ sq ft}) (0.226 \text{ BTU/lb-degF}) (40 \text{ deg F})} \\&= 23,400 \text{ lbs/min-sq ft}\end{aligned}$$

NaK Velocity

$$\begin{aligned}v_{\text{NaK}} &= \frac{G_{\text{NaK}}}{\rho} = \frac{23,400 \text{ lbs/min-sq ft}}{(52.5 \text{ lbs/cu ft}) (60 \text{ sec/min})} \quad (184) \\&= 7.43 \text{ ft/sec}\end{aligned}$$

Reynolds Number

$$N_{\text{Re}_{\text{NaK}}} = \frac{G_{\text{NaK}} d_h}{\mu} \quad (136a)$$

Contrails

$$= \frac{(23,400 \text{ lbs/min}) (60 \text{ min/hr}) (1/12 \text{ ft})}{1.15 \text{ lbs/hr-ft}}$$
$$= 101,800$$

Friction Factor

$$f = 0.0481 (101,800)^{-0.205} = 0.00454$$

NaK Heat Transfer Coefficient

$$h_{\text{NaK}} = \frac{k}{d_h} \left(5.0 + 0.025 \left\{ (N_{\text{Re}}) (N_{\text{Pr}}) \right\}^{0.8} \right)$$
$$= \frac{14.15 \text{ hr-ft-degF}}{60 \text{ min/hr}} \cdot 12 \text{ 1/ft} \left(5.0 + 0.025 \left\{ (101,800) (0.0184) \right\}^{0.8} \right)$$
$$= \frac{(14.15) (12)}{60} (5.0 + 10.4)$$
$$= 43.6 \text{ BTU/min-sq ft-degF}$$

Wall Heat Transfer Coefficient

$$h = \frac{k}{t}$$

$$k = k_{\text{Al}} \cdot 120 \text{ BTU/hr-ft-degF}$$

$$h_{\text{wall}} = \frac{120 \text{ BTU/hr-ft-degF}}{(3/64 \text{ in}) (60 \text{ min/hr})} (12 \text{ in/ft}) = 512 \text{ BTU/min-sq ft-degF}$$

Over-all Heat Transfer Coefficient

$$U = \frac{1}{1/h_{\text{F-11}} + 1/h_{\text{NaK}} + 1/h_{\text{wall}}}$$
$$= \frac{1}{1/4.59 + 1/43.6 + 1/512}$$
$$= \frac{1}{0.218 + 0.02295 + 0.00195}$$

Contrails

$$= \frac{1}{0.243} = 4.11 \text{ BTU/min-sq ft-degF}$$

Log Mean Temperature Difference

$$\Delta T_{lm} = \frac{[250 - 197] - [250 - 237]}{\ln \left(\frac{250 - 197}{250 - 237} \right)} = \frac{53 - 13}{\ln \left(\frac{53}{13} \right)} = \frac{40}{1.407} = 28.4 \text{ degF}$$

Heat Transfer Area

$$A = \frac{Q}{U \Delta T_{lm}} = \frac{8803 \text{ BTU/min}}{(4.11 \text{ BTU/min-sq ft-degF}) (28.4 \text{ degF})} = 75.3 \text{ sq ft}$$

Condenser Length

This length is the circumferential length of the spiral condenser. The heat transfer area is the sum of the surface area on both sides of the heat exchanger walls.

$$A = L s \quad (185)$$

$$L = \frac{A}{s} = \frac{75.3 \text{ sq ft}}{1 \text{ ft}} = 75.3 \text{ ft}$$

Condenser Volume

Assume an initial condenser radius of $t_{F-11} + t_{NaK}$

Initial radius = $3/4$ in

$$V_T = \frac{\pi}{144 \text{ sq in/sq ft}} (3/4)^2 + ((L) (s) [(t_{F-11} + t_{NaK} + 2 (t_{wall}))]) \quad (186)$$

$$= 0.0123 + (75.3) (1) \left(\frac{27}{(32) (12)} \right) = 5.30 \text{ cu ft}$$

Maximum Diameter

$$D_{max} = 2 \sqrt{\frac{V_T}{\pi}} + t_{F-11} + t_{NaK} + 2 (t_{wall}) \quad (187)$$

$$= 2 \sqrt{\frac{5.30}{3.14}} + 0.0703 = 2.67 \text{ ft}$$

Contrails

The volume solution used here is of the same form as

$$\frac{V_T}{U A} = \frac{V_T}{[h A]_h} + \frac{V_T}{[h A]_c}$$

Since unfinned plates are being used, and $s \gg t$,

$$A_h = A_c$$

$$A = A_h = A_c$$

$$\frac{V_T}{U A} = \frac{V_T}{A_h} \left(\frac{1}{h_h} + \frac{1}{h_c} \right)$$

This is also true with regard to the cross-counter flow spiral condenser.

NaK Pressure Drop

$$\Delta P_{\text{NaK}} = \left(\frac{L}{d_h} \right) \frac{2 f \rho (v_{\text{NaK}})^2}{g (144)}$$

$$= \left(\frac{75.3}{1/12} \right) \frac{2 (0.00454) (52.5 \text{ lbs/cu ft}) 7.43 \text{ sq ft/sec}^2}{(32.2 \text{ ft/sec}^2) (144 \text{ sq in/sq ft})} = 5.13 \text{ psia}$$

Freon 11 Pressure Drop

If the flow continued in the vapor state,

$$P_{\text{F-11}} = \left(\frac{75.3}{1/12} \right) \frac{2 (0.004) (4.17) (20.45)^2}{(32.2) (144)} = 2.73 \text{ psia}$$

$$X^2 = \frac{\rho_v}{\rho_l} = \frac{4.17}{75.1} = 0.0555 \quad (188)$$

$$X = 0.236$$

Considering the flow to be completely turbulent, we find, dependent on X,

*Lockhart and Martinelli, "Proposed Correlation of Two-Phase Two-Component Flow in Pipes," Chem. Eng. Progress, vol. 45, 1949, p. 39

Contrails

$$\phi_{v_{tt}}^2 = \frac{\Delta P_{\text{two-phase}}}{\Delta P_{\text{vapor}}} = 5.0 \quad (189)$$

Since $P \sim \rho_{\text{mix}} v_{\text{mix}}^2$ and $\rho_{\text{mix}} v_{\text{mix}}$ may be considered constant,

$$\Delta P_{\text{ave}} \sim v_{\text{mix,ave}}$$

Assuming a constant heat input which implies a linear variation of v_{mix} ,

$$\Delta P_{\text{ave}} \approx \frac{\Delta P_V}{2} \quad (190)$$

Due to shear,

$$\Delta P_{F-11} = (2.73) (5) \left(\frac{1}{2}\right) = 6.82 \text{ psia}$$

Due to momentum change,

$$\Delta P \approx \frac{(v_V - v_1) v_1 (\rho_1 - \rho_V)}{g} = \frac{(19.3) (1.135) (70.9)}{(32.2) (144)} = 0.34 \text{ psia} \quad (191)$$

$$\Delta P_{F-11} = 6.82 + 0.34 = 7.16 \text{ psia}$$

In this pressure, temperature region,

ΔT_{sat} of 10 deg^F corresponds to ΔP_{sat} of 18 psia

$$\Delta T_{F-11} = 7.16 \text{ psia} \frac{10 \text{ deg}^F}{18 \text{ psia}} = 3.98 \text{ deg}^F$$

$$\Delta T_{\text{ave}_{F-11}} \approx 2 \text{ deg}^F$$

B. CROSSFLOW SPIRAL CONDENSER CALCULATION PROCEDURE

The crossflow condenser has Freon 11 flowing in the spiral passage with NaK flowing across the spiral. The NaK has a much smaller flow length in this case than in the completely counterflow condenser.

The calculations performed here will be for the same thermodynamic conditions as in the counterflow spiral condenser calculation procedure. The geometric conditions for this example are the same except that $t_{\text{NaK}} = \frac{1}{4}$ in.

The calculation method, which involves an iterative process, uses the

Contrails

numerical conclusions of the geometrically similar counterflow case. These are:

$$V_T = 3.56 \text{ cu ft} \qquad N_{Re_{NaK}} = 101,800$$

$$D_{o_{max}} = 2.17 \text{ ft} \qquad A = 71.7 \text{ sq ft}$$

$$\Delta P_{NaK} = 39.1 \text{ psia}$$

$$A_{face} = \frac{V_T}{s} = \frac{3.56 \text{ cu ft}}{1.0 \text{ ft}} = 3.56 \text{ sq ft}$$

$$A_{face_{NaK}} = \frac{8}{19} (A_{face}) = \frac{8}{19} (3.56) = 1.50 \text{ sq ft}$$

In rectangular tubes, A_{face} is linear with reference to d_h .

$$\begin{aligned} N_{Re_{NaK}} &= 101,800 \frac{1/48 \text{ sq ft}}{1.50 \text{ sq ft}} \\ &= 101,800 \frac{0.02083}{1.50} = \frac{101,800}{72} = 1,410 \end{aligned}$$

At this value,* flow is in the laminar region. Even though some experiments have noted entrance to the turbulent region at Reynolds numbers below 1000 under unsteady flow and/or rough pipe conditions, we have chosen the conservative laminar friction factor value (viz. 0.013).

Iteration Step No. 1

Since the Freon 11 conditions are the same as those in the counterflow case, only the NaK side needs to be investigated here.

NaK Heat Transfer Coefficient

$$\begin{aligned} h_{NaK} &= \frac{(14.15)(24)}{60} \left(5.0 + 0.025 \cdot \left\{ (0.0184)(1,410) \right\}^{0.8} \right) \\ &= \frac{(14.15)(24)}{60} \left(5.0 + 0.025 (25.9)^{0.8} \right) = \frac{(14.15)(24)}{60} (5.0 + 0.3375)** \\ &= 30.2 \text{ BTU/min-sq ft-degF} \end{aligned}$$

*Kays and London, Compact Heat Exchangers, Figure 40

**It should be noted here that changes in N_{Pe} , Peclet number, especially when N_{Pe} is small, have little effect on the NaK heat transfer coefficient; $5.0 \gg 0.338$. Therefore, one additional iteration step will suffice for solution.

Contrails

Over-all Heat Transfer Coefficient

$$U = \frac{1}{1/h_{F-11} + 1/h_{NaK} + 1/h_{wall}} = \frac{1}{0.218 + 0.0331 + 0.00195}$$
$$= \frac{1}{0.2531} = 3.95 \text{ BTU/min-sq ft-degF}$$

Heat Transfer Area

$$A = \frac{8803}{(3.95)(28.4)} = 78.5 \text{ sq ft}$$
$$78.5 \text{ sq ft} \neq 71.1 \text{ sq ft}$$

Since

- (1) $A_{free} = (L) (t_{NaK})$.
- (2) $L = A/s = A$,
- (3) $G \sim 1/A_{free}$,
- (4) and $N_{Re} \sim G$,

we have sufficient information for the following iteration step.

Iteration Step No. 2

NaK Reynolds Number

$$N_{Re_{NaK}} = 1,410 \frac{71.7}{78.5} = 1,290$$

NaK Heat Transfer Coefficient

$$h_{NaK} = \frac{(14.15)(24)}{60} \left(5.0 + 0.025 \left\{ (0.0184)(1,290) \right\}^{0.8} \right)$$
$$= (14.15)(0.4)(5.315) = 30.1 \text{ BTU/min-sq ft-degF}$$

Over-all Heat Transfer Coefficient

$$U = \frac{1}{0.218 + 0.0332 + 0.00195} = \frac{1}{0.2532} = 3.95$$

Contrails

Heat Transfer Area

$$A = \frac{8803}{(3.95)(28.4)} = 78.5 \text{ sq ft}$$

Condenser Length (L_{F-11} ; $L_{NaK} = 1.0 \text{ ft}$)

$$L = \frac{A}{s} = 78.5 \text{ ft}$$

Condenser Volume

$$V_T = 0.005 + (78.5)(0.0495) = 3.89 \text{ cu ft}$$

NaK Pressure Drop

The laminar region friction factor, f , mentioned earlier, is 0.013.

$$A_{\text{face}_{NaK}} = \frac{8}{19} \left(\frac{3.89 \text{ cu ft}}{1 \text{ ft}} \right) = 1.64 \text{ sq ft}$$

Using values comparable with the counterflow case,

$$\begin{aligned} \Delta P_{NaK} &= \left(\frac{0.02083}{1.64} \right)^2 \left(\frac{0.013}{0.00454} \right) \left(\frac{1.0}{71.7} \right) 39.1 \text{ psia} \\ &\quad \begin{array}{l} 1/A_{\text{free}} \text{ and} \\ v_{NaK} \text{ ratio} \end{array} \quad \begin{array}{l} f \text{ ratio} \\ L \text{ ratio} \end{array} \\ &= (0.0127)^2 \left(\frac{0.013}{0.00454} \right) \left(\frac{1.0}{71.7} \right) 39.1 = 0.000252 \text{ psia} \end{aligned}$$

This is a negligible pressure loss. In the comparable counterflow condenser,

$$V_T = 3.56 \text{ cu ft} \quad \Delta P_{NaK} = 39.1 \text{ psi}$$

In the cross-counterflow case,

$$V_T = 3.89 \text{ cu ft} \quad \Delta P_{NaK} = 0.00025 \text{ psi}$$

For equivalent NaK pressure loss, it is obvious that a cross-counterflow spiral condenser will be of lower volume.

Assuming that NaK parting plate spacing (t_{NaK}) of 1/8 inch is minimum for cleaning purposes, a final design may have the following dimensions:

Contrails

$$s = 1.0 \text{ ft}$$

$$t_{F-11} = 1/4 \text{ in}$$

$$t_{NaK} = 1/8 \text{ in}$$

$$t_{\text{wall}} = 3/64 \text{ in}$$

s may be varied. If s is smaller, the Freon 11 pressure drop would increase, but total volume would decrease. The use of 1 foot in this example produces a well-balanced geometric structure.

Final Design

Iteration Step No. 1

$$A_{\text{face}_{NaK}} = A_{\text{face}} (4/15)$$

Assuming A_{face} will be smaller than in the previous example,

$$A_{\text{face}_{NaK}} < \frac{(4/15)}{(8/19)} (1.64 \text{ sq ft}) < \frac{1}{2}(19/15) (1.64 \text{ sq ft}) < 1.04 \text{ sq ft}$$

$$\text{Assume } A_{\text{face}_{NaK}} = 1.04 \text{ sq ft}$$

NaK Reynolds Number

$$N_{Re_{NaK}} = 101,800 \frac{0.02083 \text{ sq ft}}{1.04 \text{ sq ft}} = 2,040$$

NaK Heat Transfer Coefficient

$$h_{NaK} = \frac{(14.15)(48)}{60} \left(5.0 + 0.025 \left\{ (0.0184)(2,040) \right\}^{0.8} \right)$$
$$= (14.15)(0.8)(5.452) = 61.7 \text{ BTU/min-sq ft-degF}$$

Over-all Heat Transfer Coefficient

$$U = \frac{1}{0.218 + 0.0162 + 0.00195}$$

Contrails

$$U = \frac{1}{0.2362} = 4.23 \text{ BTU/min-sq ft-degF}$$

Heat Transfer Area

$$A = \frac{8803}{(4.23)(28.4)} = 73.3 \text{ sq ft}$$

$$73.3 \neq 78.5$$

Iteration Step No. 2

NaK Reynolds Number

$$N_{Re_{NaK}} = 2,040 \frac{78.5}{73.3} = 2,185$$

NaK Heat Transfer Coefficient

$$h_{NaK} = \frac{(14.15)(48)}{60} \left(5.0 + \left\{ (0.0184)(2,185) \right\}^{0.8} \right)$$

$$= (14.15)(0.8) [5.482] = 62.05 \text{ BTU/min-sq ft-degF}$$

Over-all Heat Transfer Coefficient

$$U = \frac{1}{0.218 + 0.0161 + 0.00195}$$

$$U = \frac{1}{0.236} = 4.24 \text{ BTU/min-sq ft-degF}$$

Heat Transfer Area

$$A = \frac{8803}{(4.24)(28.4)} = 73.1 \text{ sq ft}$$

Condenser Length (L_{F-11} ; $L_{NaK} = 1.0 \text{ ft}$)

$$L = A/S = 73.1 \text{ ft}$$

Condenser Volume

$$V_T = \frac{\pi}{144} (3/8)^2 + (73.1)(1) \left(\frac{15}{(32)(12)} \right)$$
$$= 0.003 + (73.1)(0.03906) = 2.86 \text{ cu ft}$$

Contrails

NaK Pressure Drop

$$f = 0.087$$

$$A_{\text{face, NaK}} = (4/15) \frac{2.86 \text{ cu ft}}{1 \text{ ft}} = 0.763 \text{ sq ft}$$

$$\begin{aligned} \Delta P_{\text{NaK}} &= \left(\frac{0.02083}{0.763} \right)^2 \left(\frac{(0.0087) (1.0) (48)}{(0.00454) (35.85) (24)} \right) 39.1 \text{ psia} \\ &= (.000745) \left(\frac{(0.0087) (1.0)}{(0.00454) (35.85)} \right) (2) 39.1 = 0.00312 \text{ psia} \end{aligned}$$

Contrails

Contrails

APPENDIX 4

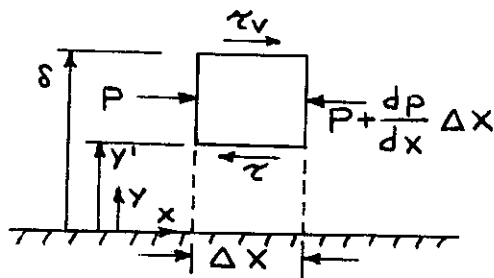
DERIVATION OF EQUATIONS FOR FILM CONDENSATION UNDER ZERO GRAVITY

DERIVATION OF THE CONDENSATE FILM VELOCITY DISTRIBUTION

The assumption is made that inertia effects are negligible in the condensate flow and therefore the condensate layer is in force equilibrium. This assumption is common to all approximate analyses of the condensation process and has been shown to be a reasonable assumption for a wide range of conditions.

Consider a small element of the condensate layer; with negligible inertia effects; Newton's Law becomes

$$\tau_v = \tau + \left(\frac{dp}{dx}\right)(\delta - y) \quad (192)$$



For the shear stress within the liquid film, we may write

$$\tau = \mu \left(\frac{du}{dy}\right) \quad (193)$$

and the velocity distribution is determined by

$$\mu \left(\frac{du}{dy}\right) = \tau_v - \frac{dp}{dx} (\delta - y) \quad (194)$$

Integrating, with the condition that $u = 0$ at $y = 0$, we obtain

$$u = \frac{\tau_v}{\mu} y - \frac{1}{\mu} \frac{dp}{dx} y \left(\delta - \frac{y}{2}\right) \quad (195)$$

The average velocity within the condensate layer is obtained by integration

$$u_{ave} = \frac{\tau_v \delta}{2\mu} - \frac{1}{3\mu} \left(\frac{dp}{dx}\right) \delta^2 \quad (196)$$

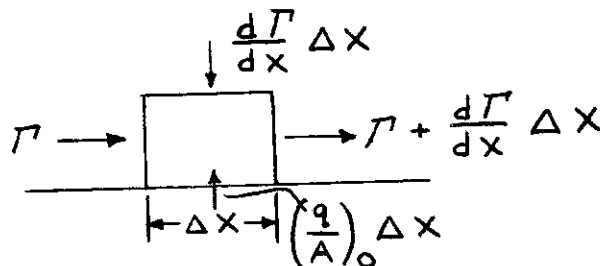
Contrails

The condensate flow per unit width of duct, Γ , is

$$\Gamma = \rho \delta u_{ave} = \frac{\rho \delta^2}{\mu} \left(\frac{\gamma_v}{2} - \frac{\delta}{3} \frac{dp}{dx} \right) \quad (197)$$

DERIVATION OF THE ENERGY EQUATION

The heat transfer rate at the wall of the duct is set equal to the net enthalpy flux through a control surface surrounding the condensate layer, neglecting the effect of liquid subcooling.



$$\left(\frac{q}{A} \right)_0 = - \frac{d\Gamma}{dx} h_{fg} \quad (198)$$

We assume a temperature distribution which satisfies the following conditions:

$$\begin{aligned} y = 0 & \quad T = T_w \\ y = \delta & \quad T = T_{sat} \end{aligned}$$

That is

$$\frac{T - T_w}{T_{sat} - T_w} = \frac{y}{\delta} \quad (199)$$

The heat transfer at the wall may be computed in terms of the temperature gradient at the wall;

$$\left(\frac{q}{A} \right)_0 = - \frac{k [T_{sat} - T_w]}{\delta}$$

Substituting this expression for wall heat transfer rate into the Energy Equation, we obtain

Contrails

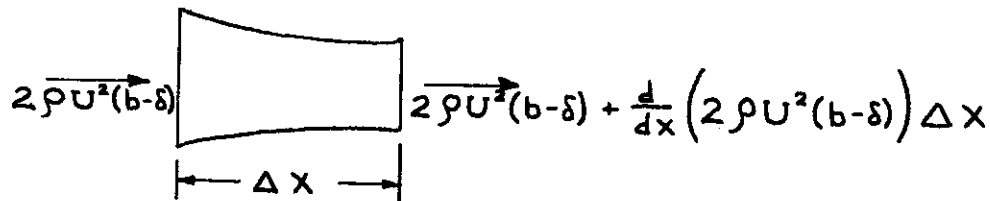
$$\frac{k [T_{\text{sat}} - T_w]}{\delta} = h_{fg} \frac{d\Gamma}{dx} \quad (200)$$

Further, if the expression for condensate flow is substituted into the above equation, we obtain

$$\frac{k(T_{\text{sat}} - T_w)}{\delta} = h_{fg} \frac{d}{dx} \left\{ \frac{\rho \delta^2}{\mu} \left(\frac{\gamma_v}{2} - \frac{\delta}{3} \left(\frac{d\rho}{dx} \right) \right) \right\} \quad (201)$$

DERIVATION OF THE MOMENTUM EQUATION FOR THE GAS FLOW

Consider a control surface about a portion of the gas core of length Δx .



The momentum flux into the control surface at the left-hand face is

$$2\rho U^2(b-\delta)$$

The momentum flux out of the control surface at the right-hand face is

$$2\rho U^2(b-\delta) + \frac{d}{dx}(2\rho U^2(b-\delta))\Delta x$$

In this analysis, the momentum transfer across the liquid-vapor interface will be assumed to be negligible, so that the net momentum transfer out of the control surface in the x-direction is

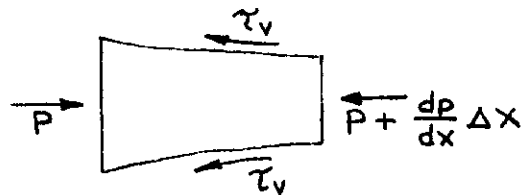
$$\frac{d}{dx}(2\rho U^2(b-\delta))\Delta x$$

The net forces acting on the control surface in the positive x-direction are due to shear stresses at the liquid-vapor interfaces and pressure forces.

Contrails

The force exerted by the shear stresses is

$$-2\tau_v \Delta x$$



The net force exerted by the pressure is

$$2p(b-\delta) - 2p(b-\delta) - \frac{d}{dx}(2p(b-\delta))\Delta x - 2\left(p + \frac{1}{2} \frac{dp}{dx} \Delta x\right) \frac{d\delta}{dx} \Delta x \quad (202)$$

Neglecting quantities of second order, this expression reduces to

$$-2(b-\delta) \frac{dp}{dx} \Delta x$$

Setting the net force on the control surface in the positive x-direction equal to the net momentum flux out of the control surface in this direction, we obtain the momentum equation for the gas flow,

$$-2(b-\delta) \frac{dp}{dx} \Delta x - 2\tau_v \Delta x = \frac{d}{dx}(\rho U^2 (b-\delta)) \Delta x ,$$

$$-(b-\delta) \frac{dp}{dx} - \tau_v = \frac{d}{dx}(\rho U^2 (b-\delta)) \quad (203)$$

TABLE 19
SUMMARY OF NUMERICAL RESULTS

$$A = 1.62 \times 10^{-5} \quad B = 4.76 \times 10^4 \quad C = 1.57 \times 10^5$$

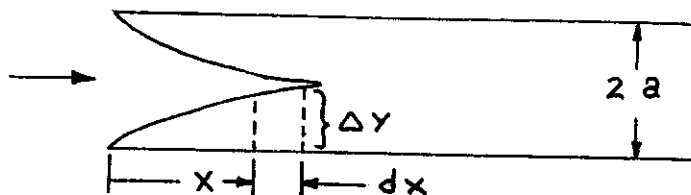
\bar{x}	$\bar{\delta}$	\bar{T}	\bar{U}	$\bar{\tau}_v$	$d\bar{p}/dx$
50	.028	.042	.985	.00434	-.00258
75	.033	.056	.977	.00426	-.00278
100	.036	.067	.967	.00418	-.00276
125	.040	.078	.960	.00412	-.00287
150	.042	.088	.952	.00413	-.00296
175	.044	.097	.944	.00406	-.00299
200	.047	.106	.938	.00401	-.00303
300	.054	.138	.911	.00384	-.00305
400	.061	.167	.887	.00367	-.00301
500	.066	.192	.865	.00352	-.00296
600	.0718	.216	.845	.00339	-.00290
700	.0766	.238	.826	.00326	-.00284
800	.0812	.258	.807	.00314	-.00278

Contrails

APPENDIX 5

MINIMUM CONDENSATION HEAT TRANSFER COEFFICIENT ANALYSIS

Consider the flow of a condensing fluid between two parallel plates, separated by the distance $2a$. The heat conducted (per unit depth) through the



liquid film at any section x along the plates can be expressed by the Fourier law of conduction,

$$dq = 2 k dx \frac{\Delta T}{\Delta y} \quad (204)$$

where k is the liquid conductivity and $\Delta T / \Delta y$ is the temperature gradient across the film. Similarly, the application of Newton's law of cooling to the liquid boundary layer at this same section x results in

$$dq = 2 h_c dx \Delta T \quad (205)$$

where h_c is the condensing film coefficient of heat transfer. Comparing these two equations, it is immediately obvious that

$$h_c = \frac{k}{\Delta y} \quad (206)$$

It is also obvious that the minimum value of the condensing film coefficient of heat transfer is

$$(h_c)_{\min} = \lim_{\Delta y \rightarrow a} \frac{k}{\Delta y} = \frac{k}{a} \quad (207)$$

The equivalent hydraulic diameter of the case under consideration can be shown to be

$$D_h = 4a$$

Thus the minimum value of the condensing film coefficient of heat transfer, in terms of the hydraulic diameter, is

$$(h_c)_{\min} = \frac{4k}{D_h} \quad (208)$$

Contrails